Atmospheric Dispersion Modelling Liaison Committee

Annual Report 2002/2003

INCLUDING

Sources of meteorological data for use in dispersion modelling

Uncertainty in deriving dispersion parameters from meteorological data

Dispersion from accidental releases in urban areas

AND

Effect on atmospheric dispersion of changing land use around Heathrow

National Radiological Protection Board
Chilton
Didcot
Oxon OX11 0RQ

Publication date: April 2004
ISBN 0 85951 525 7

PREFACE

In 1977 a meeting of representatives of government departments, utilities and research organisations was held to discuss methods of calculation of atmospheric dispersion for radioactive releases. Those present agreed on the need for a review of recent developments in atmospheric dispersion modelling, and a Working Group was formed. Those present at the meeting formed an informal Steering Committee, that subsequently became the UK Atmospheric Dispersion Modelling Liaison Committee. That Committee operated for a number of years. Members of the Working Group worked voluntarily and produced a series of reports. A workshop on dispersion at low wind speeds was also held, but its proceedings were never published.

The Committee has been reorganised and has adopted terms of reference. The organisations represented on the Committee, and the terms of reference adopted, are given in this report. The organisations represented on the Committee pay a small annual subscription. The money thus raised is used to fund reviews on topics agreed by the Committee, and to support in part its secretariat, provided by NRPB. The new arrangements came into place for the start of the 1995/96 financial year. This report describes the eighth year in which the Committee has operated under the new arrangements, and during which it placed four contracts. These covered a review of possible sources of meteorological data for use in dispersion modelling, uncertainty in deriving dispersion parameters from meteorological data, dispersion following accidental releases in urban areas and the effect on atmospheric dispersion of changing land use. The technical specifications for the contracts are given in this report, and the contract reports are attached as annexes to this report. The Committee funded twelve studies in previous years; they are described in its earlier annual reports.

The Committee intends to place further contracts in future years and would like to hear from those interested in tendering for such contracts. They should contact the Secretary:

Mr J G Smith
National Radiological Protection Board
Chilton
Didcot
Oxon OX11 0RQ

E-mail: ADMLC@nrpb.org.uk

CONTENTS

1 ORGANISATIONS REPRESENTED ON THE COMMITTEE

The organisations on the committee during the year covered by this report were:

Amersham plc - now a GE Healthcare company

Atomic Weapons Establishment, Aldermaston

British Nuclear Fuels plc

BNFL Magnox Generation

Defence Science and Technology Laboratory

Department of the Environment Northern Ireland

Environment Agency

Health and Safety Executive

- Methodology and Standards Development Unit, Hazardous Installations Directorate
- Nuclear Installations Inspectorate

Ministry of Agriculture, Fisheries and Food

Meteorological Office

National Nuclear Corporation

National Radiological Protection Board

Nuclear Department, HMS Sultan

Rolls Royce Power Engineering plc

Scottish Environment Protection Agency

Westlakes Research Institute

The Chairman and Secretary are provided by NRPB.

2 TERMS OF REFERENCE

The terms of reference of the committee during the year covered by this report were:

1 To review current understanding of atmospheric dispersion and related phenomena and to identify suitable models for application primarily in authorisation or licensing, in the context of discharges to atmosphere resulting from nuclear industry activities.

2 The Committee shall consist of representatives of government departments, government agencies and primarily the nuclear industry. Each organisation represented on the Committee shall pay an annual membership fee of £1000.

3 The Committee will consider selected topics. These should be selected following discussion and provisional agreement at meetings of the Committee, followed by confirmation after the meeting. Where possible, it will produce reports describing suitable models for that topic. These will reflect either the views of an Expert Working Group appointed by the Committee or the outcome of a workshop organised on behalf of the Committee. The Working Group will determine who should be invited to speak at workshops, and will subsequently review their outcome and identify suitable models.

4 The money raised from membership fees and registration fees for the workshops will be used to support the Working Group, the drafting of reports, and any other matters which the Committee may decide.

3 WORK FUNDED DURING THE YEAR

3.1 Sources of meteorological data for use in dispersion modelling

ADMLC has previously funded studies by the Met Office into various topics relating to the most appropriate meteorological data to use in dispersion calculations. Following discussions between ADMLC and the Met Office, the following work programme was agreed.

Traditionally the dispersion modelling community has used meteorological data recorded at observing sites as input to their prediction models. However, the increased automation of weather observing (and the consequent absence of some variables formerly observed by eye) has prompted consideration of alternative approaches which might provide suitably representative data for dispersion studies. These alternatives include data derived from the analysis fields of the Met Office's Numerical Weather Prediction (NWP) model, the use of Laser Cloud Base Recorder (LCBR) cloud amount and the application of a site-specific model to NWP data to provide truly local data. Following discussions with ADMLC, the Met Office undertook work to describe the following:

a Met Observations, how they are made and the quality control applied to them.

b The representivity, both temporally and spatially, of observed met data.

c Available data in Met Office archives suitable for ADMS or R91 type dispersion models and how data are processed for input to ADMS.
d The NWP Process.
e The Site Specific model.
f The NWP Archive.
g Deriving ADMS datasets from NWP data and Site Specific Model.
h Pre-processing met. data to reduce the calculation burden.
i The provision of met. data and/or dispersion calculations in real time.

The report on this work is published as ADMLC/2002/1.

3.2 Uncertainty in deriving dispersion parameters from meteorological data

The calculation of concentrations of material released to atmosphere is achieved using models of the dispersion process. Such models use estimates of the relationship between plume growth and indicators of atmospheric turbulence, with the indicators of turbulence being derived from measurements of the state of the atmosphere. Older models define the state of the atmosphere in terms of a small number of stability categories, while more recent models use continuously varying quantities, such as the Monin-Obukhov length and the depth of the boundary layer.

There are several sources of uncertainty in deriving estimates of plume growth from measurements of the atmospheric conditions. The Atmospheric Dispersion Modelling Liaison Committee is interested in a review of the uncertainty in predicted plume growth arising from uncertainty in

a Describing the atmospheric conditions
b Deriving a description of the atmospheric boundary layer (quantities such as Monin-Obukhov length and the depth of the boundary layer) in the measured conditions.

The review should address questions such as what parameters should be used, how accurately can they be known (including the difference between spot measurements and averages over longer periods), how well do they represent conditions through the boundary layer, and the importance of quantities that are not routinely measured but for which a value is required when characterising the boundary layer.

The review should also address the time variation of quantities, such as the Monin-Obukhov length and the depth of the boundary layer, and the effect changes in such parameters might have on predicted concentration. Situations when these, and other parameters, might change rapidly should be identified. Comments should be made on the growth of the boundary layer depth during a typical day, and the likely difference in predicted concentrations for the same

surface conditions in the morning and the evening, reflecting the differences in the boundary layer depth.

The contractor should consider in particular the methods used in ADMS and AERMOD, identifying the general weaknesses and strengths of the models and commenting on the meteorological situations when the two models might produce substantial differences in predicted concentration derived from the same meteorological conditions.

ADMLC requires comments on the reasons for the different predictions, guidance on the most appropriate method and comments on whether the use of particular stability indicators would lead to lower uncertainty in the final predicted concentration, rather than simply a comparison between the two programs. This could include comments on whether the same process for deriving stability indicators for meteorological data is appropriate for different users, with different needs. The contractor should address the problems of selecting parameters suitable for a range of different releases for example releases at a constant rate over periods of months and short duration releases.

The contractor should recognise who the report will be used by (industry, regulators, model users), and identify their needs and in what way the results will be used.

The report on this work is published as ADMLC/2002/2.

3.3 Dispersion from accidental releases in urban areas

Prof. J C R Hunt (University College London and Cambridge Environmental Consultants) suggested to ADMLC that a review of dispersion following accidental in urban areas was required, and that ADMLC may be the most appropriate body to oversee the work. ADMLC accepted this suggestion and the following work programme was agreed.

Scientific Overview

Key Problems

The range of possible scenarios is very large so therefore not all problems or possible scenarios can be covered in detail. The main considerations in this review are as follows:

Airflow and thermal conditions in various types, and scale, of urban area, (including open spaces and also closed spaces such as tunnels) and different meteorological conditions inside and outside the urban areas. The effects of mesoscale influences such as nearby mountains and coasts will be considered. The main emphasis will be on the UK, but with some reference to complex conditions abroad. Spatial scales will include local effects and city wide impacts.

Different types of accidental release including buoyant, neutral and dense gases over different periods/areas/elevations, and also liquid spills.

Dispersion and deposition in urban areas (including sources just outside and just inside - eg airports), over short to long time scales (i.e. seconds to hours) considerations of spatial averaging (street scale to city wide), limited discussion of chemical transformations. The study will consider outdoor rather than indoor impacts.

Research progress

Theoretical concepts including parameterisations beyond roughness length, flow zones (canopies), release and dispersion processes etc. Review of recent field and lab experiments and concepts/contradictions that have emerged (eg US experiments). New approaches to numerical simulation in urban areas including random flight and approximate simulation of boundary conditions/physics etc.

Practical Modelling Approaches

c Discussion of principles and operating features of models (data requirements, run times, computer capacity), user sophistication/verification.

d Reviews of US and European mesoscale approaches; local scale eddy viscosity modelling (e.g. CFD codes); computed flows plus diffusion (eg modified FLOWSTAR, plus diffusion formulae (as in ADMS) or plus random flight simulation); plume/box modelling formulae (Gaussian and non-Gaussian) with special urban parameters (e.g. ADMS adaptation; Met Office approach of D Middleton); explicit consideration of the model developed at Porton.

e Tests done so far against data (eg on local and urban wide scales) in laboratory and field studies.

f Discussion of sensitivity of models to input parameters including release location. Estimates will be given of where current research indicates significant errors from using current practical methods.

g Codes currently available (or under development)

Recommendations for Action

h Validation exercises (how they should be done for various purposes) with prioritisation based on results of d above.

i Need for new data/experiments (requirement that they can be compared with models).

j Suggestions for collaborations and ‘harmonisation’ exercises for comparison experiments and codes, use of current/developing programmes (eg UWERN, Cost Action ... etc).

The report on this work is published as ADMLC/2002/3.

3.4 Effect on atmospheric dispersion of changing land use around Heathrow

Dr D Harvey (ADM Ltd) approached ADMLC with comments on an earlier ADMLC study ('Options for the Most Appropriate Meteorological Data for Use in Short Range Dispersion Modelling' published in the Annual report for 2000/2001). Dr Harvey felt that the grid size used in that study may not have been adequate, and suggested that further work should be carried out to check the original results. Following discussions, ADMLC accepted the following proposal.

The proposed study is intended to complement the work carried out by the Meteorological Office for the ADMLC Annual Report 2000/2001 publication W3 title 'Options for the Most Appropriate Meteorological Data for Use in Short Range Dispersion Modelling'. This study investigated how representative the use of historic meteorological data is by using meteorological data sets from the 1950's onwards. The study concluded that the urbanization around Heathrow has affected both the measured met data and resulting predictions of ground level concentrations. Concern has however been raised that the stack height and grid size used have reduced the confidence in the findings of the study as the grid resolution was not sufficient to capture the maximum ground level concentrations.

This study will repeat some of the previous work using two sources and a grid size that ensures the maximum concentrations are captured. In addition, predictions will be made to see if the urbanization of the region surrounding Heathrow can be replicated in the modelling.

ADMS 3.1 dispersion modelling will be undertaken using two point sources;

a 40 m stack; no buoyancy
b 150 m stack; with buoyancy

The use of two stacks heights will enable assessment of whether there is any difference in the trend in predicted ground level concentrations with time for two source heights. The sources selected will also be more representative of typical sources than that selected in the previous study which was a 10 m stack with no building downwash. The two sources selected will be identical to those modelled in the Environment Agency's October 2000 Intercomparison study and subsequent papers. This will facilitate cross referencing of the predicted concentrations with other work.

Predictions will be made for each of the 12 separate years of met data (from the years 1950 to 2000) giving a total of approximately 24 separate ADMS runs.

Predictions will be made for a range of statistics including annual average, 100th, 99.9th, 99.8th, 99.7th 99th and 98th percentile of hourly means.

The concentrations predicted by this set of predictions will be analysed and the results of this analysis compared to the previous study.

If this studies findings are similar to those of the previous work and show a trend in predicted concentrations with the age of the meteorological data a further series of predictions will be undertaken using ADMS 3.1 to see if the trend in predicted concentrations can be replicated and hence explained by changing the surface characteristics used in the modelling (eg roughness length, minimum Monin-Obukhov length, albedo and Priestly-Taylor parameter).

The report on this work is published as ADMLC/2002/4.

An Assessment of Alternative Sources of Met Data for Use in Dispersion Modelling

A report prepared for ADMLC by

N Nelson, A K Mirza, K N Weaver

Met Office

MetO ref: M/SCG/P64

This study was funded by the UK Atmospheric Dispersion Modelling Liaison Committee.

London Road
Bracknell
Berkshire RG12 2SY

Publication date: June 2003

EXECUTIVE SUMMARY

Traditionally the dispersion modelling community has used meteorological data recorded at observing sites as input to their prediction models (more so for short rather than long range modelling). However, the increased automation of weather observing (and the consequent absence of some variables formerly observed by eye) has prompted consideration of alternative approaches which might provide suitably representative data for dispersion studies.

These alternatives include data derived from the analysis fields of the Met Office's Numerical Weather Prediction (NWP) model, the use of Laser Cloud Base Recorder (LCBR) cloud amount and the application of a site-specific model to NWP data to provide truly local data.

This report assesses some of the alternatives available, highlighting their relative strengths and weaknesses, and identifying gaps in our current knowledge that might hinder the use of these techniques.

CONTENTS

1 METEOROLOGICAL OBSERVATIONS

1.1 Introduction

The weather forecasting process requires the input of current weather information to initialise Numerical Weather Prediction (NWP) models (see section 4). Consequently it is necessary for the Met Office to organise the measurement and collection of weather data on a national scale, and, because the weather in the UK is obviously affected by global conditions, to liaise with other national weather services to acquire data from overseas. A real-time Global Telecommunication System (GTS) allows dissemination of these data for use by the international meteorological community.

Data are collected from a wide variety of sources including:

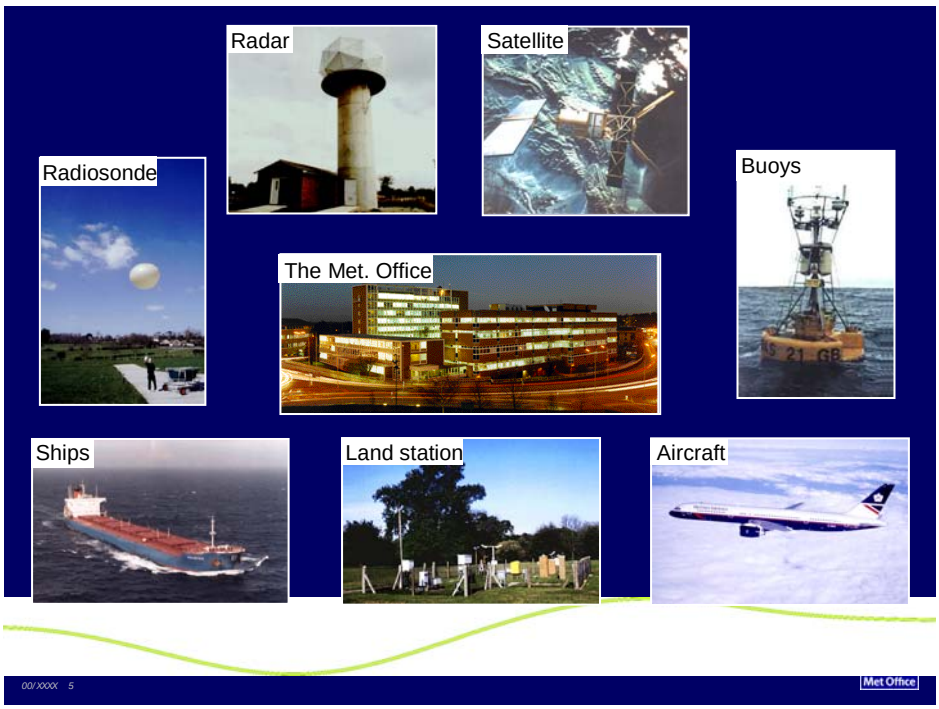

Figure 1.1: **Sources of Weather Observations**

- radiosonde ascents – wind speed and direction, temperature and humidity versus height at fixed locations,
- radar – detailed space/time coverage of precipitation,
- satellites – remote sensing from both geostationary and polar-orbiting systems,
- ships – winds, waves, pressures and temperatures across the oceans,

- floating buoys – marine data where there are no regular human observations,
- civil aircraft – winds and temperatures along routes in troposphere and stratosphere,
- land stations – relevant surface variables from both manned and automatic locations.

Data collection suitable for dispersion modelling however tends to originate from mainly land based stations in the observing network.

Over the past 25 years or so the meteorological observing network has undergone considerable change, in both instrumentation and coverage. In 1970 the synoptic network consisted of about 100 stations, mostly reporting hourly. The collection, coding and transmission of data were all very labour-intensive processes, and the network coverage was very uneven nationally, with poor coverage especially in upland and low-population areas.

To fill gaps in the observing network, the decision was taken in 1980 to adopt the use of automatic weather stations. Forty-three Enhanced Synoptic Automatic Weather Stations (ESAWS) were installed initially in the data-sparse regions of the Scottish Highlands, Wales and N Ireland, and then throughout the UK (see Fig 1.2). Measurement, coding and transmission of the weather variables were computerised, resulting in clear cost savings. Also, over time, a computer-based automatic weather station - the Semi-Automatic Met Observing System (SAMOS) - was introduced at manned stations. (see Fig 1.2) SAMOS supplements the work of the observers, by providing 90% of the observation if the observer is absent for any length of time (eg, overnight or weekends). This instrument was only semi-automatic, as human involvement was still required to record variables such as visibility and cloud base height and amount.

Further enhancements were made to the SAMOS in 1995 when the visiometer and laser cloud base recorder (LCBR) were introduced to the suite of instrumentation used on these sites. The LCBR could provide good cloud height information and total cloud amount data. The SAMOS and ESAWS stations could then record:

- wind speed and direction,
- dry-bulb and wet bulb (air) temperature,
- visibility,
- cloud base height and cloud amount,
- barometric pressure and
- rain amount

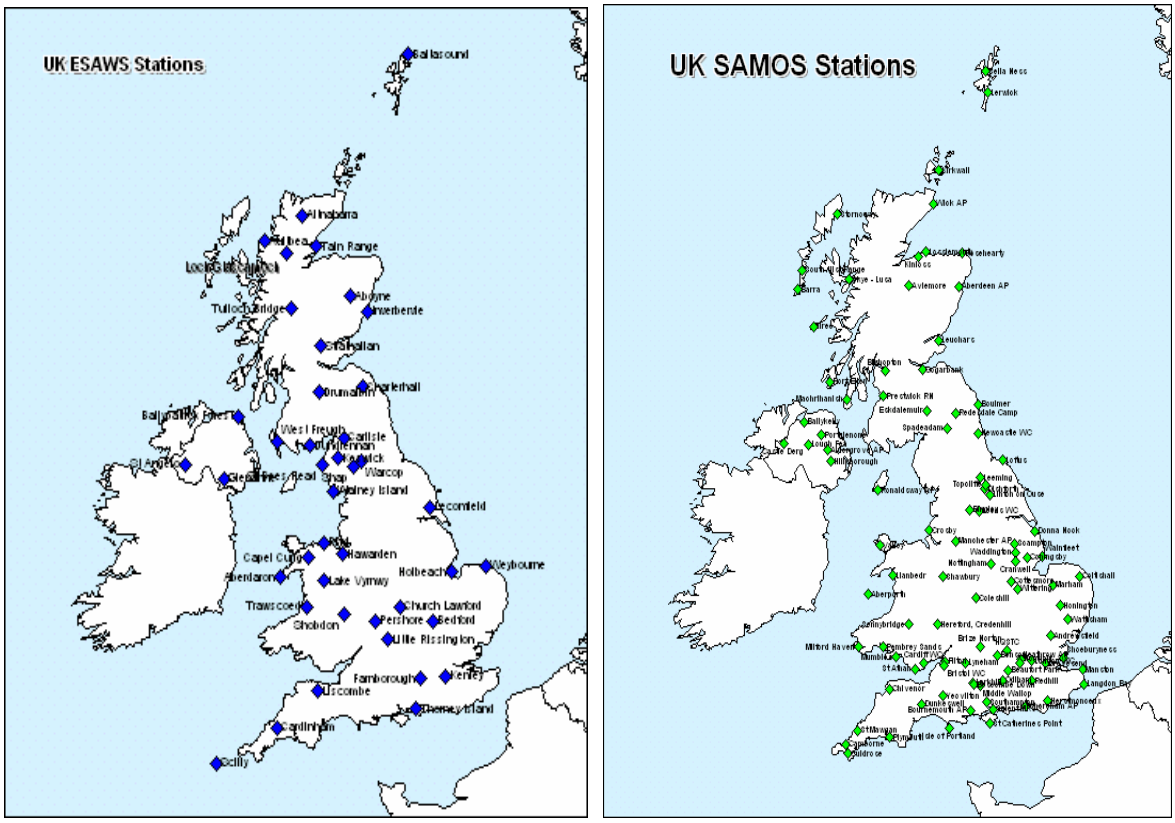

Figure 1.2**: UK ESAWS and SAMOS Stations**

More recent developments have increased the number of met parameters recorded by SAMOS, to include solar radiation, soil and ground surface temperatures. Currently there are 103 SAMOS sites in the UK.

1.2 Measurements

Winds. Surface wind is the horizontal movement of air relative to the rotating surface of the earth. Turbulence near the earth's surface (the lowest 1000 m) caused by terrain, topography, buildings, trees, etc, often produces convection and rapid, irregular, short lived fluctuations in both speed and direction - a feature known as gustiness**.** Thus, an adequate description of the wind requires speed and direction of the mean wind plus a maximum gust speed to be specified. Where possible the surface wind is determined by an anemometer, but if this is not available, rough estimation is usually possible using the Beaufort Scale.

In order to obtain comparable observations from different locations it has been decided that the surface wind should refer to the wind at a standard height of 10 metres above the ground over open and level terrain. Ideally this means no obstructions within 300 m, or the distance between the instrument and any obstruction should be at least ten times the height of the obstruction. The effect of any obstruction within 300 m will depend on its dimensions and its distance

from the anemometer. For example, a decrease of 20 to 30% in wind speed can be expected up to 200 m directly downwind from a copse of trees 10 m tall. In the UK wind speed is measured in knots, where 10 knots = 11.5 (statute) miles/hour = 5.1 m/s = 18.5 km/hour.

The wind direction is specified as that direction from which the wind is blowing and is expressed in tens of degrees measured clockwise from true north, or in terms of the points of the compass (see Figure 1.3 below).

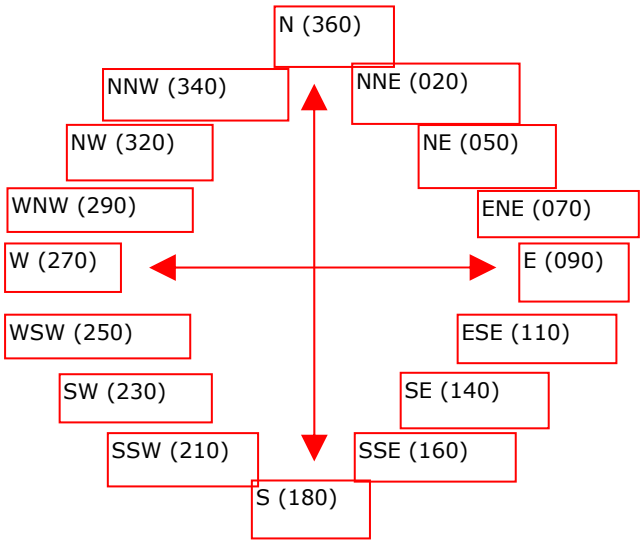

Figure 1.3: **The 16 main compass points & their degree equivalents**

The wind report for synoptic purposes (ie, relevant to the branch of meteorology describing current weather as represented on a geographical chart and applied to the prediction of its future development) is normally taken as the 10-minute mean immediately preceding the nominal time of the observation. This is known as the "spot" wind, to distinguish it from the hourly mean speed. Generally speaking it is the hourly averaged wind speed that is used for dispersion modelling, as most models will assume a constant meteorological state over an hour.

At stations where anemometers are installed at heights differing substantially from 10 metres above ground level, the mean speeds are not strictly comparable with those recorded at sites with a standard exposure. For synoptic reporting purposes, the estimated corrections in Table 1 are then applied to values of the mean wind speed (Observer's Handbook 1982).

Table 1.1: **Correction necessary to readings to achieve 'standard' 10 m wind speeds**

Height of anemometer (metres)	Correction to achieve 'standard' 10 metre wind speed
1-2	add 30%
3-4	add 20%
5-7	add 10%
8-13	no correction
14-22	subtract 10%
23-42	subtract 20%
43-93	subtract 30%

The most common instrument used for measuring wind speed is the Cup Generator Anemometer. Three cups, roughly conical in cross-section, are mounted symmetrically on arms set at right angles to a vertical spindle. The rotation of the cups is used to drive an electrical generator. The voltage generated increases with the speed of the wind and this voltage is indicated on a dial graduated directly in knots. The start-up wind speed for these instruments has improved with time. Some early instruments had start-up speeds of up to 6 knots, but design improvements over the years have led to a currently achievable start up speed of 2 knots. As long as the recording instrumentation is working correctly for every hour of the year there will be 8760 readings taken. Exceptions to this occur when there is only enough wind to move the wind vane (so recording a wind direction) but not to register a wind speed on the anemometer (usually because the wind speed is below the start up speed of the anemometer). This situation is recorded by the observers as a 'variable' wind condition. The intention is to replace older anemometers with the most up-to-date systems. In the past anemometer readings were recorded to paper (on an anemograph) and hourly means hand calculated. Modern systems electronically record wind information and derive hourly means and gusts. Although sonic anemometers have been briefly investigated, there are no plans at present to introduce them to the network.

The continuous remote indication of wind direction is provided by a wind vane, which drives a transmitting device through gear wheels and a countershaft, or through magnetic fields. The movement of the vane is electrically transmitted to a receiver and the changes in direction indicated on a dial graduated in tens of degrees from true north. On occasions when there is not enough wind to move the wind vane (or the anemometer), the observers will record the conditions as being 'calm'. This event is obviously very important for dispersion modelling as they can often lead to elevated ground level pollution episodes. This information is therefore given in the literature accompanying the input met dataset for ADMS, or can be found along with the wind rose diagrams.

Air Temperature. The thermometers used for the measurement of air temperatures (dry-bulb, wet-bulb, maximum and minimum temperatures) should be exposed in a Stevenson-pattern wooden thermometer screen. This

has double-louvred sides (ie, slatted walls on four sides, the cross-section of the slats being an inverted V), a double roof and a floor made of three partially overlapping boards separated by an air space. The screen must be painted white inside and out, and must be set on a stand so that the thermometer sensors are 1.25 m above the ground (for most standard screens this means that the base of the screen is 1.10 m above the ground). The screen door should face north (or slightly east of north). Platinum resistance thermometers have now largely superseded mercury-in-glass thermometers manufactured to meet British Standards Specification BS692. All Met Office thermometers are made to this specification and are identifiable by an engraved serial number. They must be certified by either the Met Office or a recognised calibration laboratory (such as the British Standards Institution).

Soil Temperature. Soil temperatures are required mainly for agricultural applications, and can be measured at a number of standard depths - 5, 10, 20, 30, 50 and 100 cm.

Humidity. The humidity of the air is not normally measured directly. Instead, dry-bulb and wet-bulb temperatures are observed and the humidity is calculated from these readings using look-up tables. The wet-bulb thermometer is a similar thermometer to the dry-bulb, with the sensor surrounded by a muslin wick, which is kept wet from a reservoir of distilled water nearby. The wet-bulb cools by evaporation and should normally read lower than the dry-bulb, although in some conditions of high humidity it can read the same. The wick should be replaced regularly and care taken to ensure that the reservoir is kept topped up to prevent the wick drying out.

Rainfall. The rain gauge is usually made of copper with a knife-edged brass rim of 127 mm (5") diameter and a deep funnel, to minimise out-splash. The rim should be set exactly level and at a height of 30 cm above the ground. Daily totals are read using a graduated glass measure, but hourly rainfalls are nowadays measured electronically using a tipping-bucket device, which sends a signal at each tip signifying 0.2 mm.

Sunshine and Radiation. For many decades, the Campbell–Stokes pattern sunshine recorder was used to record duration of bright sunshine. The glass sphere focuses the sun's rays and a trace burned onto a record card, allowing sunshine duration to be measured. The readings cannot be converted into standard physical units, and the instrument cannot be readily automated. Therefore, radiation sensors are now superseding the Campbell-Stokes device, and will provide a better scientific standard for the future, although continuity with past records does present difficulties. The modern instruments will distinguish between duration above a specific threshold of 120 $W.m^{-2}$ ('sun hours') and quantity of radiation.

Cloud Cover. Laser cloud base recorders (LCBRs) measure the height of the cloud base in a single narrow column directly above the instrument. If the cloud cover is not changing significantly, a timeseries of these results describes the sky on a line downwind of the station. By suitable averaging, Sky Condition

Algorithms (SCAs) allow the computation of cloud amount from this timeseries. Although the technique has some limitations, cloud amounts correlate quite well with those recorded by an observer.

All SCAs working from LCBR single point output have the same weaknesses. The most important is that the vertically pointing sensor may not see significant cloud. In an initially-clear sky, with a continuous sheet of cloud approaching the station, the SCA output must be zero while the cloud is upwind and 8 oktas (eighths of the sky) as soon as the cloud edge passes over. The increase from zero to eight oktas would happen gradually with time rather than a stepped increase from zero to eight. However, a human observer would report 1 okta as soon as the cloud is visible, and his reports would rise to 4 oktas when the cloud edge is overhead, and continue to increase steadily to 8 oktas. A fundamental limitation of all LCBR SCAs is that none will be able to report cloud that is upwind of the station.

Internationally, there are two SCAs in use, the Met Office Exponential Decay Algorithm (EDA) (Farmer 1992) and the Larsson algorithm. In tests by KNMI (Wauben 2001), the Larsson algorithm and the EDA gave results that were similar, with cloud amount being provided slightly better by the Larsson, and cloud height analysis better by the EDA. The Larsson SCA is widely accepted in Europe, and is incorporated in the Vaisala CT25K model. Currently, there are plans to perform another in-depth comparison of the two SCAs against human-observed cloud amounts and heights.

Other weather elements may be measured depending on the resources available or interest at the station.

1.3 Site and exposure

Readings of most weather variables depend on the exposure of the instruments used and, if observations made at different stations are to be comparable, it is necessary to ensure that instruments are set up under uniform conditions. The site of the instruments, known generally as the instrument enclosure, should ideally be on level ground covered with short grass or, where grass does not grow, the natural surface of the area. The enclosure, may be surrounded by open fencing or palings to exclude animals or unauthorised persons. It should measure about 10 by 7 m (see Figure 1.4) but 7 by 6 m for a basic climatological station and should be away from the immediate influence of trees, buildings, hedges, fences and other obstacles. No obstruction should be nearer to the rain gauge than a distance equal to twice the height of the obstruction above the rim of the gauge. Trees or buildings should not unduly shade the screen and any thermometers on or in the ground.

Conversely, the site should not be unduly exposed to the sweep of the wind, especially that of the rain gauge. However, unavoidably exposed sites, such as on moorland or near the coast, can often be made acceptable by the construction of a turf wall around the rain gauge or by use of a ground-level pit

gauge. In general, a site should be representative of the surrounding area; when in a town, a site near the centre (if an acceptable exposure can be found, ie – not on the roof of a building) is preferred. A station should not be on, or close to, steep slopes, ridges, cliffs or hollows, although it is acknowledged that such conditions may be difficult to avoid altogether in mountainous and hilly areas.

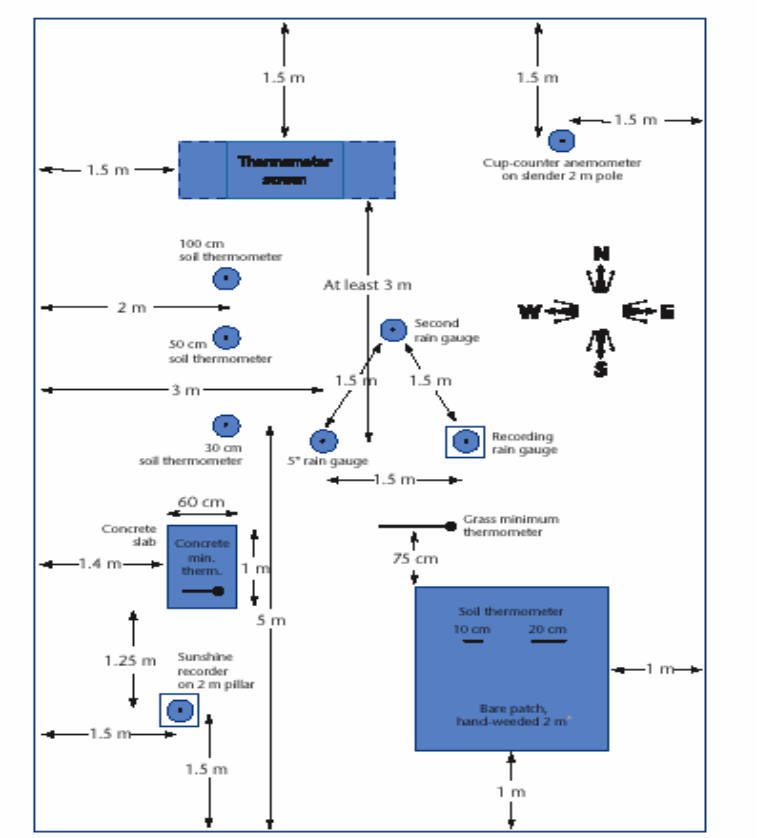

Figure 1.4: **Recommended layout of meteorological enclosure**

1.4 Upper air data

The Met Office also operates radiosonde stations that are specifically responsible for obtaining quasi-vertical soundings through the atmosphere up to 20 km or so. These data provide valuable input to the analysis of the state of the atmosphere in three dimensions at the start of each run of the operational forecasting models. Some dispersion models (eg, AERMOD, SCIPUFF) are able to accommodate these upper-air data as input to the met pre-processor section. This allows these models to better estimate changes in certain atmospheric parameters with height. Other models such as ADMS will use basic assumptions about the vertical profile of the atmosphere. The variables recorded are wind speed, wind direction, temperature and humidity, normally at 00 and 12UTC.

Network reviews in recent years have resulted in changes to the upper-air network – see Figure 1.5. The coverage is adequate to represent variations on the synoptic space-scale for forecasting purposes, but clearly cannot provide local detail of boundary-layer conditions, for example.

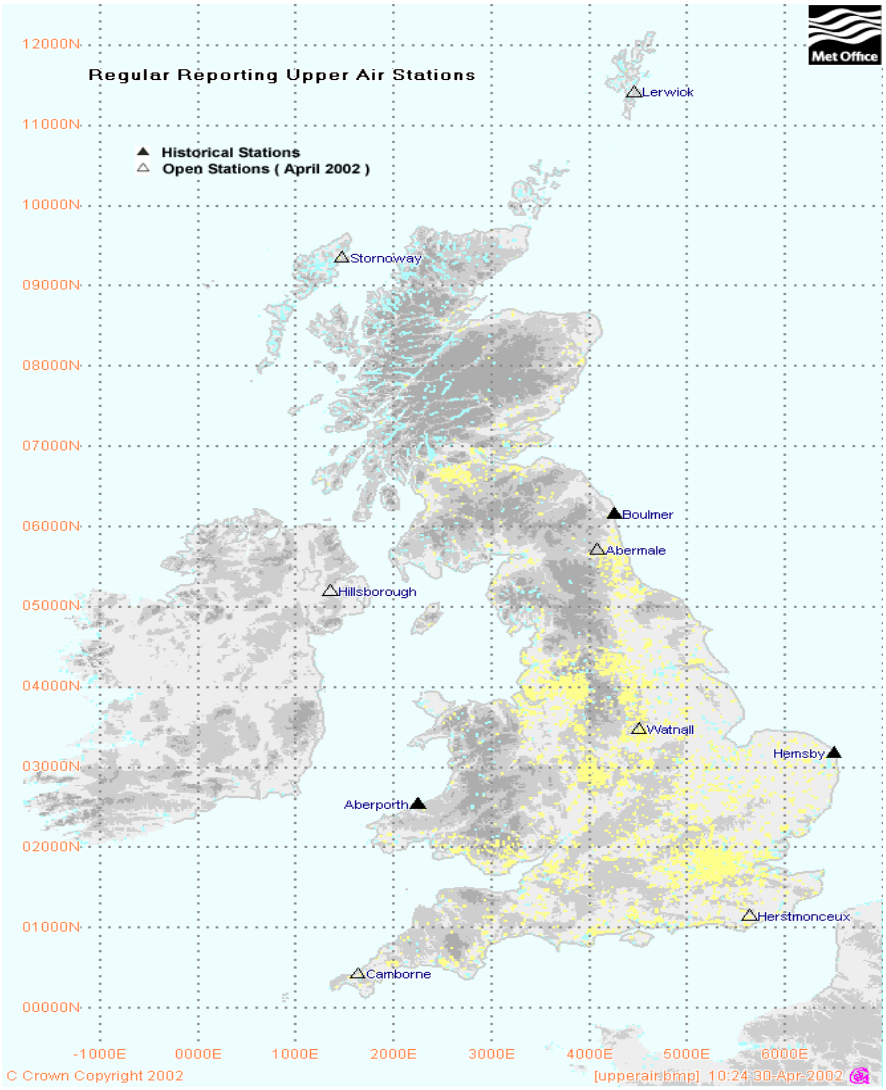

Figure 1.5: **Upper Air Stations with regular reports**

To provide more spatial detail, supplementary sonde sites (including autosondes) undertake ascents when necessary rather than routinely, and wind profilers have been introduced at sites where there may be a particular need for data. At airports, aircraft Meteorological Data and Reporting (AMDAR) provides essentially the same parameters as are recorded by radiosondes (wind speed, wind direction and air temperature currently with humidity to follow in the future). The data are processed by software fitted into the aircraft avionics

system and transmitted to ground sites via VHF transmission. The system can work up to a height of 15 km (although limited by cruise altitudes which rarely exceed ~12 km). Generally the system produces one observation every 7 mins in level flight (above 500 hPa) and observation at selected pressure levels in ascent (10 at 10 hPa intervals initially then every 50 hPa up to 500 hPa) and descent (every 50 hPa below 500 hPa and every 10 hPa below 700 hPa).

These developments have greatly improved the national coverage of information through the atmosphere – see Figure 1.6. The network shown below was designed with the European requirements for upper air soundings in mind. This requested that there should not be more than 250 km spacing between any two recording stations. In an ideal world the circles drawn on the figure below would just touch each other. However some larger gaps could not be avoided (eg, between Stornoway and Lerwick).

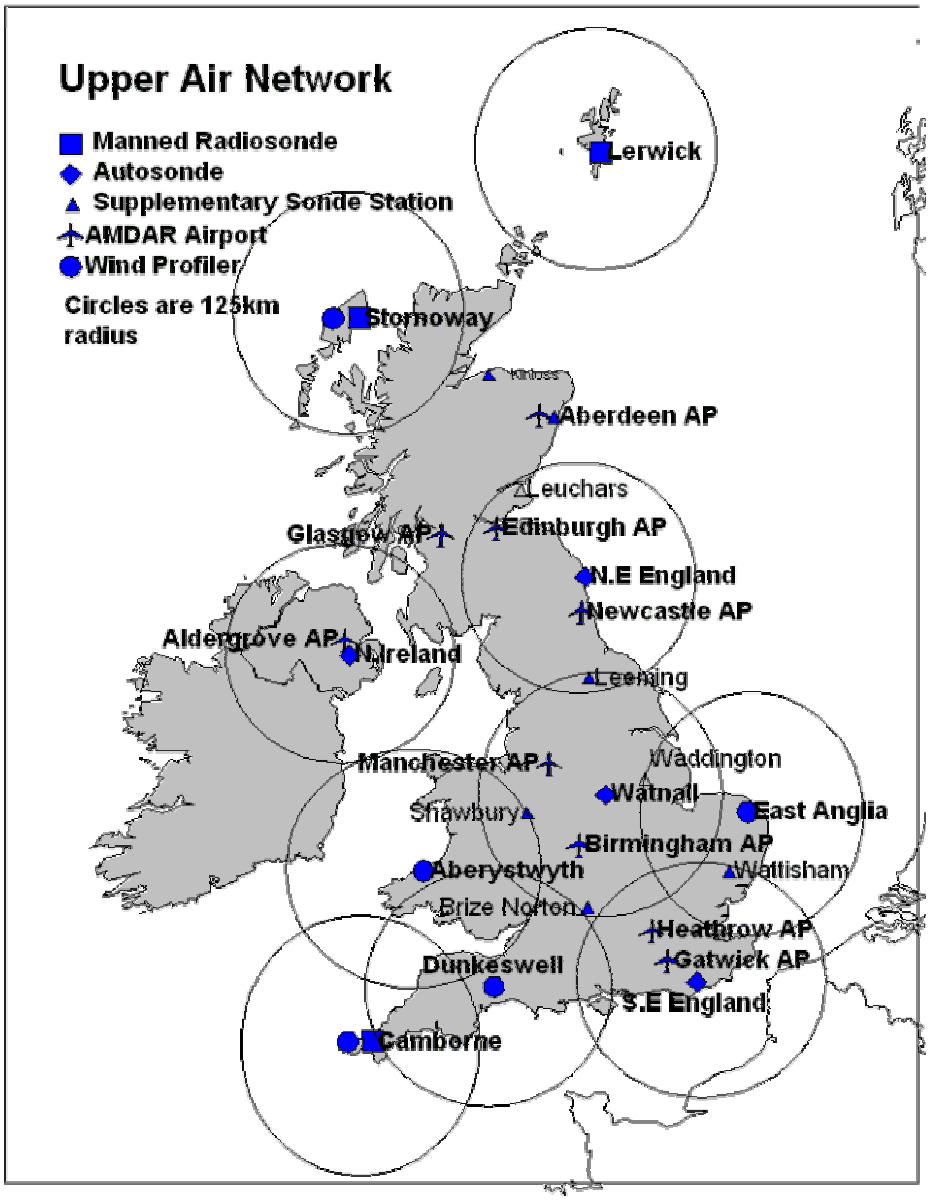

Figure 1.6**: Upper Air Stations including non-regular reports**

1.5 Quality control

The Met Office has considerable experience of archiving large amounts of data. It is clearly important that the data retained is of the highest quality, and so the data undergo a series of quality-control checks between the observation stage and the final archiving.

At the point of observation, basic checks are made to assist detection of simple coding and internal consistency errors. At manned stations, trained observers undertook this task, but nowadays software utility applies a range of checks to all reported variables.

As the data are entered in the main database, further tests on permitted range, self-consistency and time-sequence are applied, and consistency in space is also analysed by comparing against values recorded at nearby stations.

When the checks indicate a possible error, trained meteorological quality-control staff is alerted, and corrections are made only after subjective scrutiny. Missing values may also be estimated, where possible. After this correction process, a final sweep through the archived values is made in order to flag any remaining gross errors.

The following data are archived in MIDAS (The Met Office Integrated Data Archive System):

- Surface observations over land areas of the UK as far back as the digital record extends
- A selection of global surface observations for the last 20 years
- Global surface marine observations from national and international sources as far back as the digital record extends
- Radiosonde observations over the UK, and at overseas stations operated by the Met. Office, as far back as the digital record extends
- A selection of global radiosonde observations for the last 10 years

1.6 The future network

Due to a variety of reasons, the national observing network has undergone major changes over the last 20 years or so and will continue to do so. The drive to maintain an ever-efficient network has resulted in the employment of automatic weather stations. This has been particularly useful in locations such as military sites where the number of forecasters has been reduced or deemed not

necessary. Additionally, in cases where observations could only be made at irregular intervals (or not at weekends for example), the automatic station has provided continuous measurement and recording of the various weather parameters.

The long-term intention regarding the network will include the improvement of the network coverage throughout the country using automatic stations. Not only will the density of stations increase but so too will the number of stations found in traditionally troublesome locations for modelling (complex terrain, coastal, etc). In the past, dispersion modellers have requested that new stations be situated in areas where pollution events regularly occur, or certainly near heavily industrialised locations. Unfortunately the siting of met stations is quite a complex process, which, in addition to the considerations mentioned in Section 1.3, need to be aware of;

- security (vandalism has become an ever increasing problem),
- meteorological relevance (of the site) and
- potential for change in the immediate area (possible urbanisation for example).

It is considered that in the next 5 years, a 'nowcasting' system, comprising automated observing, high resolution numerical models and information display could remove the need for manual augmentation by Met Office staff for any observed element. The number of human operated stations therefore seems set to be reduced. The loss of human observed cloud cover appears to be the main problem for dispersion modellers (certainly in the short term). While there seems to be limitations regarding the use of the automatic cloud cover instruments (see Section 1.2), the techniques employed will no doubt be improved and refined with time. Ultimately the question has to be asked whether in the long term dispersion modellers should become less reliant on cloud cover and more accepting of heat flux measurements or maybe modelled Boundary Layer Depth.

The Met Office must ensure that all future systems are reliable, require minimal manual maintenance and deliver homogeneous records for a variety of purposes. Remote analysis and correction of faults will be an important factor in efficient management of automated systems.

1.7 References

Farmer SFG (1992). Verification of two methods of estimating cloud cover heights and amounts derived from the output of a Belfort LCBR. Met Office OP Branch memo no 126.

Karkkainen A-M (1997). Sky Condition Algorithms: Report on comparison studies at Vaisala. Vaisala News No 142.

Mazee AN (2000). Cloud Algorithms. Internal KNMI report (in Dutch) - figures and tables are clear.

Observer's Handbook (1982). HMSO Publication ISBN 0 11 400329 7.

Swedish Met & Hydro Instit (1995). The CT12K cloud cover upgrade (1995-03-14 PN) and Cloud cover algorithm (Io-BN 1995-01-11).

Wauben W (2001). Analysis of Cloud algorithms. Internal KNMI report (in Dutch) - figures and tables are clear.

2 THE REPRESENTIVITY OF OBSERVED METEOROLOGICAL DATA

2.1 Introduction

In dispersion modelling there is uncertainty regarding the most appropriate value for each input parameter. While there is a recognition that meteorological data is a critical input to dispersion modelling and that any inadequacy in it contributes to uncertainty in the final results, most research directed at improving predictions has been directed at the mathematics of the models themselves. There is agreement that meteorological data must be representative, but little useful guidance exists on determining whether it is or not. This is still largely a matter of expert opinion.

Meteorological input to dispersion models is generally a source of uncertainty because:

- it will generally originate from a distant site so may not represent conditions at the study site
- it will contain some measurement error
- even if it is measured at the location of the pollutant source itself, it will not necessarily represent conditions throughout the modelled area
- many modelling studies attempt to predict future impacts, but historical records may not represent the future period during which the modelled source will be operating.

The longer the period covered by a data set, the more likely it is that the full range of possibilities will be captured. Five years is normally considered a minimum period to cover an adequate range of conditions, although in recent times, ten years was thought to be necessary to comprehensively cover all eventualities. The decision to use ten years was perhaps as much based on practical considerations as it was on statistical good sense. According to WMO practice the meteorological means and extremes are calculated over a thirty years period. In the past many met stations would not have had this many years of data and so ten years would have seemed a reasonable practical option. Certainly the work undertaken by Davies and Thomson (1997) showed that five years was adequate for most circumstances.

To be sufficiently accurate for dispersion modelling purposes, data must provide a reasonable representation of the meteorological conditions likely to be experienced over the area under investigation. Detailed historical records from one or more nearby sites can normally be taken as representative of conditions in the study area, but differences in latitude, topography, land use and proximity to the sea (or even smaller bodies of water) will all affect the climate of specific locations to some degree. A number of studies have investigated the level of agreement between climatological records from different sites (eg, Hough and Nelson, 2000; Hopkins, 1977; Singleton & Spackman, 1984). While they do quantify to some extent how agreement diminishes with distance, such studies also show clearly that factors other than separation distance are important. Topographical features may significantly alter climatic conditions over quite short distances, so that even data from the nearest available site may not be truly representative of the study area.

Some assessment needs to be made of the degree to which climate data is representative of the site under investigation, otherwise dispersion model outputs will be suspect at best and possibly quite misleading.

2.2 Met Office work on representivity

The issue of station spacing for climatological purposes has been considered at some length (Met Office, 2001). Ideally (using limited resources), the climatological observing site network should provide just enough data to permit the climate of any given area to be defined within specific limits. The objective is to have enough data to perform the job, but too much data would not add additional value and could prove to be costly. The density of observations to meet this requirement has always been a matter of subjective judgement. The World Meteorological Organisation "Guide to Climatological Practices" (WMO100, 1983) discusses in qualitative terms the considerations to be taken into account when planning the distribution of land surface stations in a climatological network. It states that "*care must be taken to ensure that all the types of terrain in the country are satisfactorily represented and that the demand for information should be taken into account*". So, for example, a greater density of stations may be required in or near urban areas. Ideally, the number of stations at which any particular climatic element is observed should be large enough to permit a complete analysis to be made of the geographical distribution of mean values, frequencies, extremes and other characteristics of the element. This means that the ideal density depends very much on the element in question and on the geographical features of the area. A sparse network may be sufficient for the study of surface pressure reduced to sea level but, on the other hand, a fairly dense network is required for the study of the wind regime and maximum temperatures, while a very dense network is needed for the study of precipitation.

WMO100 does not quantify what is meant by "sparse", "fairly dense" and "very dense". Table 1 gives the Met Office's best estimate of required station spacing

for selected variables. The only specific guidance given by WMO is that "where the geographical conditions are fairly uniform, one ordinary climatological station per 1,000 km^2 (~30 km spacing) would normally be sufficient for most climatological purposes". The total area of the United Kingdom is some 241,000 km^2 and this, therefore, implies a minimum of around 240 climatological stations, assuming "fairly uniform" geography.

Table 2.1 **Recommended station spacing and minimum number of sites required to provide an adequate representation of the UK climate for selected variables. Information taken from the UKON2 requirements document, Met Office (2001)**

Element to be measured	Period	Station spacing (km)	Minimum number of stations needed in UK
Wind speed and direction	Hourly	50	100
Air temperature	Hourly	50	100
Global radiation	Hourly	75	40
Rainfall	Hourly	30	270

As a result of several studies within the Met Office, a set of pragmatic rules for determining the density of the climatological network and representivity has been developed and these are summarised as follows:

Distance criteria. For climatological purposes a station is normally taken to represent a circular area of radius 30 km. (In flat terrain this is circular inland but near the coast is elliptical based on the proportion of sea within 15 km, the major axis of 40 km being parallel to the coast and the minor axis 10 km).

Terrain Height Criteria. A low-level station cannot represent high level areas even within 30 km. For temperatures, stations below 200 m can represent sites within an altitude range of +83 m. This is equivalent to specifying a temperature criterion of +0.5ºC assuming a standard lapse rate of 6ºC per 1000 m. Above 200 m, the upper height criterion increases logarithmically so that for a station at 1000 metres, sites up to 1333 m and down to 833 m can be represented. These height differences are equivalent to temperature criteria of +2ºC and -1ºC respectively. (Different criteria will apply for other variables.)

Land use classes. Stations are classified as 'urban' or 'rural' if 30% or more of the land within either 1 km or 2.5 km is of that type. So if 30% or more of the land within the specified distance is urban the site is assigned as urban and similarly for rural. An urban site is not representative of rural areas and vice versa.

Using these criteria, Figure 2.1 shows climatological stations reporting in 1998 and the areas for which they are deemed representative. (Red circles are urban, black circles are rural, black ellipses are coastal and the pink represent high level.) While this diagram suggests relatively good coverage of Wales and northwest England there are only 21 sites within that area for which historical data are available in sufficient time detail for use in dispersion modelling, and only 4 of those sites (*) are still fully manned.

Leeming	Coningsby	Leeds Weather Centre	Finningley
Bedford	Wittering	Marham	Wyton
Stansted	Waddington*	Aughton	Speke
Squires Gate	Aberporth	Valley	Shawbury
Elmdon	Watnall	Ringway*	Brize Norton*
			Ronaldsway*

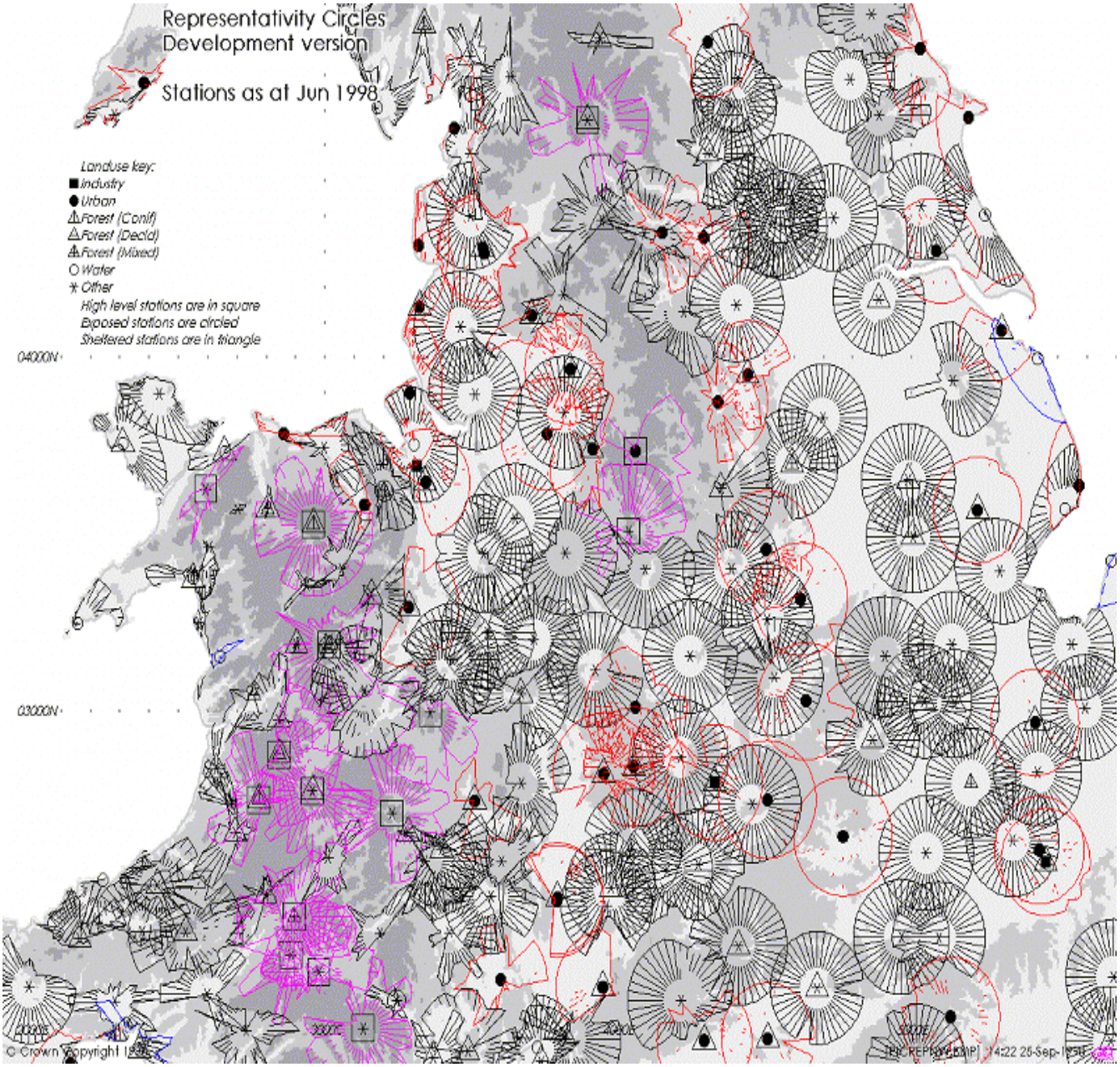

Figure 2.1 **Representivity circles for central England and north Wales (Stations at June 1998)**

Work is continuing on the mapping of representivity, to indicate areas around climatological stations where estimated averages for specified variables lie within specified tolerances. Also, a project is under way to compute synthetic climatologies at unobserved locations (Sheffield and Hopwood, 2001).

2.3 Other research on representivity

Svensson (1996) emphasised the importance of understanding how errors and uncertainties relating to meteorological inputs affect the results of air quality modelling. Murphy and Ohr (1985) concluded that "uncertainties of as much as a factor of 2 may be due [to uncertainties in] characterising past climate and to year on year variation in climatology for a given location".

Al-Wali and Samson (1996) undertook an analysis of model sensitivity to near-surface wind measurements. They recognised that their "control" case was not a true control, since even the best meteorological datasets contain errors and omissions. Results may be particularly sensitive to choice of wind data but other factors will certainly have an impact.

Fox (1984) acknowledged that representivity of meteorological data is a major difficulty in air quality modelling and concluded that data should represent conditions at the study site both spatially and temporally. This should be demonstrated by showing a positive correlation between variables measured on and off-site. However there is still uncertainty about

- how representative a record has to be,
- how good a correlation is required, in order to be good enough for dispersion modelling and
- how to determine objectively the degree of representivity of a record for a site where few or no meteorological measurements have been made.

Weaver (2002) found correlations in wind direction frequencies, for two pairs of sites, of 0.29 (Heathrow and Southampton) and 0.56 (Finningley and Scunthorpe). The poor correlation between Heathrow and Southampton is to be expected for two widely separated and dissimilar locations. A relatively poor correlation between Finningley and Scunthorpe, separated as they are by only 27 km, may indicate a significant influence from local topographical differences. Spatial correlations in wind speeds were studied by Smith (1982), who found that, correlations were unlikely to exceed 0.8, even over short distances over uniform terrain.

Different variables have inherently different spatial coherence. Hopkins (1977) found that winter daily minimum temperatures at good-quality open sites in uniform terrain (East Anglia) could achieve a likely upper correlation limit of 0.94, even at 100 km separation. However, local topography influencing cold air drainage would certainly degrade correlations and hence representivity. Rainfall is well known to be highly variable over very short distances even with no

influence from terrain, and so comparing frequency distributions from the surrounding area rather than simply correlating simultaneous records should assess the representivity of a good-quality rainfall dataset.

Whether a given dataset is sufficiently representative depends to some extent on the application. For long-term studies, the magnitude of representivity errors is considered to be well within the level of uncertainty inherent in dispersion models, but for short-term studies, especially for specific locations, the additional error can be more significant.

Hough and Nelson (2000) suggested that annual mean wind strength was a reasonable indicator of representivity. This does not provide a useful means of testing whether a given data-set is representative of a site for which there is no long term climatic record, unless of course there is knowledge of the site's annual mean wind strength for comparison. (But see Section 2.2 above). Monthly means for a variety of met parameters have been generated within the Met Office, based on a 5 km grid. These datasets could be used to generate more long-term mean values. Using only annual mean wind strength as an indicator would probably not be reliable in an area of complex terrain because of the effects of topography on both wind speed and direction. Also, using mean wind strength as an indicator of representivity says nothing about other meteorological parameters that are equally important in dispersion modelling. However, for that study, mean wind strengths would have been the most significant factor over flat uncomplicated terrain.

The view expressed by Pielke and Uliasz (1998) that more sophisticated models are questionable without good quality data, applies to meteorological data as well as to source characteristics or background levels. Thus, in general, the more sophisticated a simulation, the better the quality of input data required. Consequently, dispersion models in current use have a greater need for reliable climatic data that is truly representative of the area and period of interest. Svensson (1996) highlighted the importance of understanding how errors in meteorological inputs affect modelling results since those errors can be relatively large compared to other uncertainties. There is little point in expending time and money on highly sophisticated modelling techniques to give an answer that, at face value, appears to be definitive but is misleading in reality because it is based on unrepresentative climatic data.

Ultimately, the errors due to representivity may or may not be large in comparison to the inherent uncertainty – depending on model sophistication and modelled parameter (ie, long-term means, short-term fluctuations or percentiles). The modelling community still needs a better understanding of how and when meteorological uncertainty is important.

Vawda (1999), in a review of dispersion modelling, reported that there is a relatively small number of sites within the UK for which suitable climatological records are available. Full climatological records suitable for use in ADMS, are available from only 49 sites in the UK, and of those 25 have closed or reduced their manned hours in recent years. Manual observations of cloud amount

constitute a key input for ADMS, but manning of meteorological stations at weekends and overnight is becoming the exception. The UK is less advanced with its automation programme than several other European countries, but automatic weather stations are now significantly more common and more evenly distributed across the country than manned stations. Very much more data would become available for dispersion modelling if methods could be developed to allow data from automated sites to be used; the main problem to be overcome being a substitute for manual cloud observations. The automatic cloud cover instruments (the LCBR – see Section 1.2) are capable of providing cloud cover measurements for most conditions but do suffer some limitations.

If the available meteorological data are not considered to be representative, then current guidance (Hester & Harrison, 1994; World Bank, 1991) suggests that meteorological measurements must be made at the site in order to generate a representative data set. Compiling a climatological dataset in this way can be expensive, particularly in terms of the time required. At least 1 year of data is needed to quantify seasonal variation, but even having gone to the expense of collecting data for a year, representivity of the data-set over the longer term is uncertain, although comparisons with other nearby sites may help in this respect.

In an earlier report for ADMLC (Smith, 2000), it was concluded that climatological records may have a "shelf life" due to local changes such as urbanisation or other land use changes. In the longer term, global climate change may render older records unrepresentative although this was not evident in data covering the period 1950 to 1999. This may cast some doubts on long term use of older data particularly in view of the gradual reduction in the number of sites that have kept continuous records up to the present. Robinson (1999) found that "*changes in instrumentation, procedures and local site conditions as well as climate change, contributed to apparent long term changes in parameters describing the climate of a site*". To some extent this can be accommodated by taking into account effects of known changes and this is routinely done in order to standardise the long-term record when studying climate change. Robinson concluded that meteorological datasets should be used with circumspection. However, Smith found that changes over time in data from Heathrow airport could not be linked with changes in instrumentation or procedures. It was surmised that urbanisation of the surrounding area is probably related to an increase in the frequency of light winds and an increase in average temperatures, a conclusion supported by Harvey (2002).

2.4 Further research

Increasing availability of climatic data interpolated to regular gridpoints across the country will offer greater opportunity to assess spatial variability and hence representivity close to nominated sites. Averages of the main weather variables are becoming available on a 5 km grid, and these can be used to define spatial domains within which variables of interest lie within defined limits, as indicated

in para 2.10 above. Gridding of daily or even hourly values over long periods is clearly a much more daunting task, but the techniques and computing power are becoming available.

2.5 References

Al-Wali KI and Samson PJ (1996). Preliminary sensitivity analysis of urban airshed model simulations to temporal and spatial availability of boundary layer wind measurements. *Atmospheric Environment*, **30**, 2027-2042.

Fox DG (1984). Uncertainty in air quality modelling. *Bull Am Met Soc*, **65**, 27-36.

Harvey D (2002). Effect on atmospheric dispersion of changing land use around Heathrow. NRPB Report P0217.

Hester RE and Harrison RM (eds) (1994) .Waste Incineration and the Environment. Issues in Environmental Science and Technology 2. Royal Soc of Chemistry, Letchworth, Herts.

Hopkins JS (1977). The spatial variability of daily temperatures and sunshine over uniform terrain. *Met Mag*, **106**, 278-292.

Hough MN and Nelson N (2000). Portability of weather data for dispersion calculations. Met Office report for the Atmospheric Dispersion Modelling Liaison Committee (ADMLC). ADMLC report for 1997/98 – NRPB-R316.

Met Office (2001). A Network of Surface Climatological Observing Stations for the UK. United Kingdom Observing Networks strategy – UKON 2.

Murphy BD and Ohr SY (1985). The limitations of atmospheric dispersion data and their contribution to uncertainties in dose assessment. Proc DOE/AMS Air Pollution Model Evaluation Workshop, Kiawah SC, 23-26 October 1984, NTIS DP-1701-1, paper No 2-5.

Pielke RA and Uliasz M (1998). Use of meteorological models as input to regional and mesoscale air quality models - limitations and strengths. *Atmospheric Environment*, **32** (8), 1455-1466.

Robinson M (1999). The consistency of long-term climate datasets: Two examples of the need for caution. *Weather*, **54** (1), 2-8.

Sheffield PM and Hopwood WP (2001). Generation of synthetic climatologies for unobserved locations using predictor observations - the impact of predictor site distance.

Met Office Forecasting Research Technical Report, No 366.

Singleton F and Spackman EA (1984). Climatological network design. *Met Mag*, **113** (1341), 77-89.

Smith J (2000) Option for the most appropriate meteorological data for use in short range dispersion modelling. Met Office report for the Atmospheric Dispersion Modelling Liaison Committee (ADMLC). ADMLC annual report for 2002 – NRPB-W3.

Smith SG (1982). Root-mean-square interpolation errors for wind speeds in the United Kingdom. Met Office, Met O 3 Tech Note No 20.

Svensson G (1996). A numerical model for chemical and meteorological processes in the atmospheric boundary layer. Part II: A case study of the air quality situation in Athens, Greece. *J App Met*, **35**, 95-973.

Vawda Y (1999). Predicting air quality - use of meteorological data in atmospheric dispersion models. *Weather*, **54** (6), 189-194.

Weaver KN (2002). An investigation of accuracy and uncertainty in numerical modelling used for the assessment of impacts from airborne pollution. Dissertation for an MSc in Integrated Environmental Management, University of Bath.

World Bank (1991). Guidelines for Environmental Assessment of Energy and Industry Projects. Environmental Assessment Sourcebook Vol III. World Bank Technical Paper No 154, Washington DC.

World Meteorological Organisation (1983). Guide to Climatological Practices, second edition; WMO100, Geneva.

3 AVAILABLE DATA IN ARCHIVES SUITABLE FOR DISPERSION MODELLING

3.1 Introduction

Automation of stations has taken place over a period of about 20 years, and has been implemented in order to improve the efficiency of data-gathering for day-to-day weather prediction. However, it is recognised that changes in the observational network have implications for the dispersion modelling community. Over the same period, new challenges have arisen due to considerable changes in air quality legislation, and more sophisticated dispersion models (eg, ADMS, AERMOD) have been designed, capable of accepting a wider range of meteorological variables as input.

The first generation dispersion models (eg, R91) used the Pasquill Stability categories to determine the relative importance of mechanical and thermal effects, but problems were experienced since they did not characterise the change in turbulence with height. In the boundary layer, turbulence can arise from two main sources – wind shear driving mechanical mixing effects and convective mixing due to heating of the earth's surface. For dispersion modelling purposes it is useful to understand the relative importance of the thermally- and mechanically-generated forms of turbulence. These simple models required wind speed, cloud cover, temperature (recorded routinely by the manned observing network) and Pasquill Stability (easily derived from the observed variables) as input to the process. More recent dispersion models like ADMS can accept new variables such as boundary layer height, surface heat flux and Monin-Obukhov length. However, because of the difficulty in either measuring or deriving some of these additional parameters, many model users preferred to continue with the list of variables traditionally recorded by the Met Office.

The gradual automation of the observing network has resulted in a lack of human-observed cloud cover. Although the cloud base recorder replaced the human observer, the measurements taken were not without their perceived problems and were not considered to be as reliable. Consequently the coverage of met stations providing full ADMS datasets (ie, including human-observed cloud cover) has diminished, with large gaps already in the overall coverage.

Figure 3.1 shows that, although the coverage for historical full ADMS datasets is reasonable (manual cloud cover data available for previous years), the number of stations currently providing human-observed cloud cover is much smaller. It is clear that this problem needs to be addressed. The Met Office is currently investigating possible options to accommodate both its meteorological responsibilities and the wishes of the dispersion modelling community. Cloud cover is used in dispersion models together with temperature and time of year and day to estimate surface heat flux and so estimate boundary layer height. One possible solution would be to estimate heat flux directly. Another solution might be to provide interpolated data from the Met Office Numerical Weather Prediction model (see section 4). It can be argued that sequential met data from a ground-based point source (observing station) represent conditions only at that point. Model data have the advantage of being spatially-representative and so possibly more suitable for dispersion modelling applications.

3.2 Observational datasets

The availability of ADMS datasets is subject to customer demand. At present these datasets are not prepared routinely due to the costs of production and quality control. Table 3.1 lists stations available for direct use in ADMS. Some data before 1990 are available at a few sites.

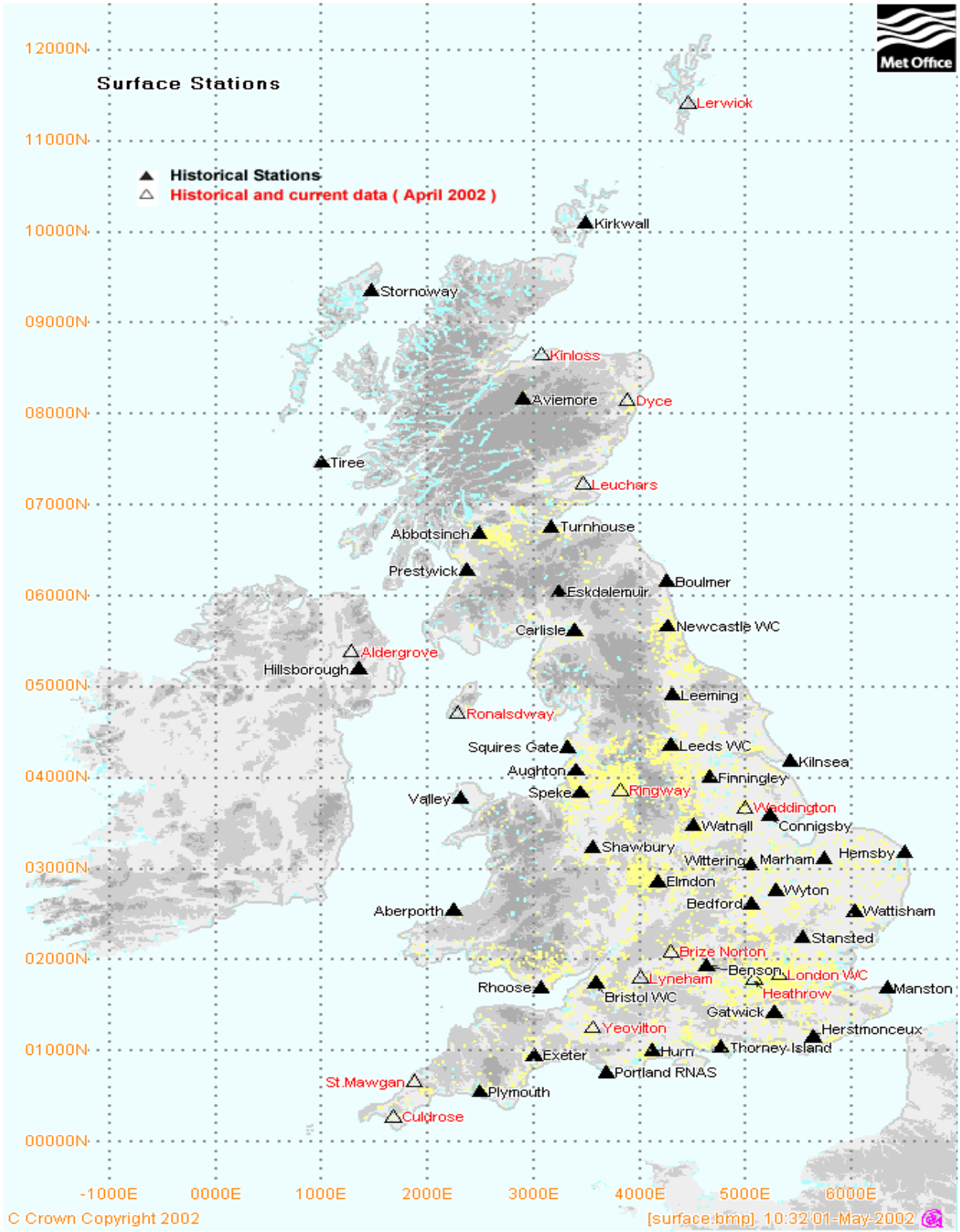

Figure 3.1: **Stations currently used for ADMS datasets**

Some years ago, there was a demand for ten-year statistical datasets, which could provide more efficient input than detailed sequential data to some dispersion models. With recent increases in computing power, the requirement for such summary datasets has decreased, and so they have not been updated since 1996 or 1997. Statistical datasets can still be produced on request, but clearly require the basic sequential data to be available.

At the present time, it is Met Office policy that observational data for air dispersion use will be retained indefinitely. However, it is possible that this policy maybe reviewed at some future date; level of demand for data will be taken into account at any review.

Most data for ADMS are available for download from the Met Office website at http://www.metoffice.com/environment.

Data for other air dispersion models are also available, although to a more limited extent than for ADMS. ISCSTv3 and ISC-AERMOD formats can be provided.

Hourly reports covering the traditional full range of weather variables are available only from manned observational stations. Most manned stations are now being replaced by semi-automatic weather stations (SAWS), which will have a better national coverage. (see topic 1). Quality control of data from SAWS is also to be automated.

Relevant observational data retrieved from the main Met Office archive undergoes a very simple re-formatting procedure to achieve the dataset suitable for an ADMS sequential input. The statistical datasets are described in topic 8. For other dispersion models such as the ISCST or early R91 that input Pasquill Stability Categories, further consideration may be needed.

Station	1990	1991	1992	1993	1994	1995	1996	1997	1998	1999	2000	2001	2002	Statistical
Abbotsinch	✓	✓	✓	✓	✓	✓	✓	✓	✓	×	×	×	×	1988-1997
Aldergrove	×	×	✓	✓	✓	✓	✓	✓	✓	✓	✓	×	×	1987-1996
Aughton	×	×	✓	✓	✓	✓	×	×	×	×	×	×	×	None
Aviemore	×	×	✓	✓	✓	✓	✓	✓	✓	✓	✓	×	×	None
Boulmer	✓	✓	✓	✓	✓	✓	✓	✓	✓	✓	✓	×	×	1988-1997
Brize Norton	✓	✓	✓	✓	✓	✓	✓	✓	✓	✓	✓	✓	×	None
Culdrose	×	×	×	✓	✓	✓	✓	✓	✓	✓	✓	×	×	1987-1996
Dyce	✓	✓	✓	✓	✓	✓	✓	✓	✓	✓	×	×	×	1988-1997
Elmdon	✓	✓	✓	✓	✓	✓	✓	✓	×	×	×	×	×	1987-1996
Finningley	✓	✓	✓	✓	✓	×	×	×	×	×	×	×	×	1985-1994
Aberporth	×	×	×	×	×	×	✓	✓	✓	✓	✓	×	×	1987-1996
Gatwick	×	×	×	✓	✓	✓	✓	✓	×	×	×	×	×	1988-1997
Heathrow	✓	✓	✓	✓	✓	✓	✓	✓	✓	✓	✓	×	×	1988-1997
Hemsby	✓	✓	✓	✓	✓	✓	✓	✓	✓	✓	✓	×	×	1987-1996
Herstmonceux	✓	×	×	×	✓	✓	✓	✓	✓	✓	✓	×	×	1982-1991
Hurn	✓	✓	✓	✓	✓	✓	✓	✓	✓	✓	✓	✓	×	1988-1997
Kinloss	×	×	×	×	✓	✓	✓	✓	✓	✓	✓	×	×	1987-1996
Kirkwall	×	×	×	×	✓	✓	✓	✓	×	×	×	×	×	1987-1996
Leeds WC	✓	✓	✓	✓	✓	✓	✓	✓	✓	✓	✓	×	×	1988-1997
Leeming	×	×	×	×	✓	✓	✓	✓	✓	✓	✓	×	×	1987-1996
Lerwick	×	×	×	✓	✓	✓	✓	✓	✓	✓	✓	×	×	1988-1997
Leuchars	×	×	✓	✓	✓	✓	✓	✓	✓	✓	✓	×	×	1987-1996
London WC	×	×	×	✓	✓	✓	✓	✓	✓	✓	✓	×	×	1982-1991
Lyneham	×	×	✓	✓	✓	✓	✓	✓	✓	✓	✓	×	×	1982-1991
Manston	✓	✓	✓	✓	✓	✓	✓	✓	✓	✓	×	✓	×	1988-1997
Marham	✓	✓	✓	✓	×	×	×	×	×	×	×	×	×	1984-1993
Newcastle WC	×	×	×	×	✓	✓	✓	✓	✓	✓	✓	×	×	None
Nottingham	✓	✓	✓	✓	✓	×	×	×	×	×	×	×	×	1985-1994
Plymouth	✓	✓	✓	✓	✓	×	×	×	×	×	×	×	×	1982-1991
Prestwick	✓	✓	✓	×	×	×	×	×	✓	✓	✓	×	×	1983-1992
Rhoose	✓	✓	✓	✓	✓	✓	✓	✓	×	×	×	×	×	None
Ringway	✓	✓	✓	✓	✓	✓	✓	✓	✓	✓	✓	✓	×	1988-1997
Shawbury	✓	✓	✓	✓	✓	✓	✓	✓	✓	✓	✓	✓	×	1987-1996
St.Mawgan	✓	✓	✓	✓	✓	✓	✓	✓	✓	✓	✓	✓	×	1987-1996
Stansted	✓	✓	✓	✓	✓	✓	✓	×	×	×	×	×	×	1987-1996
Tiree	×	×	×	×	×	×	✓	✓	✓	✓	✓	×	×	None
Turnhouse	✓	✓	✓	✓	✓	✓	✓	✓	✓	×	×	×	×	1987-1996
Valley	✓	✓	✓	✓	✓	✓	✓	✓	✓	✓	✓	✓	×	1987-1996
Waddington	✓	✓	✓	✓	✓	✓	✓	✓	✓	✓	✓	✓	×	1987-1996
Wattisham	×	×	×	×	✓	✓	✓	✓	✓	✓	✓	✓	×	1987-1996
Wittering	×	×	×	×	×	×	✓	✓	✓	✓	✓	×	×	None
Wyton	✓	✓	✓	✓	✓	×	×	×	×	×	×	×	×	1985-1994
Yeovilton	×	×	×	✓	✓	✓	✓	✓	✓	✓	✓	✓	×	None

Table 3.1 **Availability of ADMS datasets (WC = Weather Centre, ie, Leeds WC)**

3.3 Specially-formatted datasets

ADMS datasets are relatively straightforward as they contain mainly directly-observed variables with the exception of relative humidity, which is calculated using dew point temperature. (Thomson, 1992) – see Section 3.3.

ISCST datasets require estimates of solar radiation (Neilson et al, 1981; Michalsky, 1988), stability (Pasquill, 1981) – derived from observed cloud cover - and boundary layer depths (Farmer, 1984) – derived from temperature, cloud and wind speeds. These values are obtained using algorithms outlined in the user documentation for this model, which is available on the EPA website at http://www.epa.gov/scram001/.

AERMOD, which is the next generation of dispersion models developed by the EPA, requires vertical profiles of temperature and wind in addition to surface observations.

Availability of upper air data is determined by the available network and recording practices. (see topic 1) At present data for years 1997, 1998 and 1999 are available in the required format for AERMOD. Non-trivial effort would be needed to make other years available, since they are archived on tape and would require extraction, quality checks and reformatting.

3.4 References

Nielson LB et al (1981). Net Incoming Radiation Estimated from Hourly Global Radiation and/or Cloud Observations. *Journal of Climat*, **1**, 255-272.

Michalsky J (1988). The Astronomical Almanac's Algorithm for approximate solar position (1950-2050). *Solar Energy*, **40** (3), 227-235.

Farmer SFG (1984). A Comparison of methods of estimating stability category and boundary layer depth using routine surface observations. Met Office Special Investigations Technical Note No 37.

Pasquill F (1961). The estimation of the dispersion of windborne material. *Met Mag*, **90** (1),063, 33-49.

Thomson DJ et al (1992). Provision of Climatological Met Data for the UK Atmospheric Dispersion Modelling System. Met Office Internal Memorandum No 26.

4 NUMERICAL WEATHER PREDICTION PROCESS

4.1 Introduction

Numerical Weather Prediction (NWP) underpins modern weather forecasting. It is the process by which an objective forecast of the future state of the atmosphere is produced, by solving the dynamic and thermodynamic equations that describe the evolution of the atmosphere. The variables modelled are

pressure, temperature, wind velocity and specific humidity. The primary purpose of NWP is therefore to predict the state of the atmosphere at specified future times. NWP has advanced significantly over the last 25 years or so as improvements in supercomputers have allowed operational use of higher resolution forecasting models incorporating increasingly-complex representations of atmospheric processes. It should be stressed that operational models will continue to improve in complexity and accuracy, as computing technology develops further; this has implications for homogeneity of datasets over time.

In the current UK Met Office system, global and regional (mesoscale) models are essentially different configurations of the Unified Model (UM), using the same set of governing equations. The models differ in the following respects: area covered, spatial and temporal resolution, the approximations and assumptions made in the application of the equations, the observational data that are used to define initial conditions, and the representation or parameterisation of small scale physical processes. (Atmospheric processes that operate on scales smaller than those resolved by the model resolution must be parameterised to account for their effect on the large-scale flow.)

The physical processes represented in the model include:

- Atmospheric radiation allowing for the effects of clouds, water vapour, ozone, carbon dioxide and a number of trace gases.
- Large-scale precipitation determined from the water or ice content of a cloud.
- Land surface processes including a multi-layer soil temperature and moisture prediction scheme.
- Vertical turbulent transport within the boundary layer.
- The effects of convection through a scheme based on the initial buoyancy flux of a parcel of air. It includes entrainment, detrainment and the evaporation of falling precipitation. An explicit treatment of downdraughts is included.
- A treatment of the form drag due to the sub-grid scale variations in orography.
- The effects of the drag caused by vertically propagating gravity waves is modelled using the sub-grid scale orography and known absorption properties of gravity waves.

4.2 Assimilation

The NWP process begins with an analysis of the current state of the atmosphere. To produce an accurate weather forecast, precise knowledge of the initial conditions is needed. This is achieved by "assimilating" observations into the model (see Section 1).

Before observational data can be assimilated they are quality controlled, to exclude likely erroneous reports from the analysis. The data assimilation process adjusts a forecast from a previous model run (the model background field) to correspond as closely as possible to the new data received from the observations, so that the best estimate of the current state of the atmosphere is obtained.

Many thousands of observations are received each day from a variety of sources: satellites, aircraft, ships, buoys, radiosondes and stations on land (both human and automatic – see Section 1.1). Even so, there are never enough observations available at any one time to determine the true global state of the atmosphere. In order to get a more complete and detailed picture, additional information is needed. Knowledge of the behaviour and structure of the atmosphere provides some of this information. For instance, knowing the typical structure of a frontal depression or an anticyclone, enables a more complete picture to be inferred from scattered observations. This knowledge of the behaviour and structure of the atmosphere is embodied in a numerical model. Data assimilation is a fully automated and objective process of defining the numerical representation of the state of the atmosphere that is most consistent with the observations and the known behaviour of the atmosphere.

The data assimilation method currently used by the Met Office is known as the 3-Dimensional Variational Analysis (3DVAR) data assimilation scheme, introduced operationally in 1999 (Lorenc et al, 2000). Its purpose is to produce the best possible description of the state of the atmosphere at a given time. This description is provided by the mathematical best fit to all available data taking into account likely errors in the data, so that each category of data is allocated a certain weight relative to other types.

It is important that the model should be of sufficiently high resolution, with physically realistic detail, to adequately represent assimilated information. In the Global Model the only variable assimilated from land surface observations is pressure. Surface wind is also assimilated over the sea but not over land because local topography may affect winds and reduce their spatial representivity.

The higher resolution Mesoscale Model is intended to provide more detailed forecasts of cloud, precipitation and humidity for the UK and surrounding areas, and so it assimilates much more data. Screen-level relative humidity observations help define areas of fog; cloud top temperature data from infrared satellite imagery are combined with surface cloud reports to produce a 3-dimensional cloud analysis, and rain-rate data are assimilated from the Weather Radar Network.

The assimilated analyses are obviously used to initialise the numerical model forecast runs, but they can also be archived to generate synthetic climatological "data" which could be useful for air quality modelling. These NWP-derived data have the advantages of possessing excellent space and time continuity, whilst

incorporating a wide variety of available data in a consistent and objective fashion.

4.3 Operational models

Operationally, the Met Office runs two configurations of its Unified Model. The global model (GM) encompasses the entire globe at a horizontal resolution of approximately 60 km (0.83° longitude and 0.55° latitude) with 30 vertical levels. The first 4 vertical levels follow the model terrain but there is a gradual change to constant pressure surfaces in the upper atmosphere. This allows for realistic boundary conditions without serious distortion of co-ordinate surfaces at high levels. The horizontal resolution is approximately 60 km in mid-latitudes. See Figures 4.1 and 4.2.

The mesoscale model (MM) has a domain centred on the United Kingdom that extends across much of France and the low countries. Northern Italy, Denmark and much of the southern half of Norway and Sweden are also covered. It runs as a nested model within the GM, so that boundary conditions for the MM are taken from the GM (Fig 4.1). The MM has a horizontal resolution of approximately 11 km (0.11° latitude and longitude) with 38 vertical levels (Fig 4.2). These are the same as the GM in the free troposphere but at a finer resolution in the lowest two kilometres. This enables the MM to represent more complex boundary layer structures.

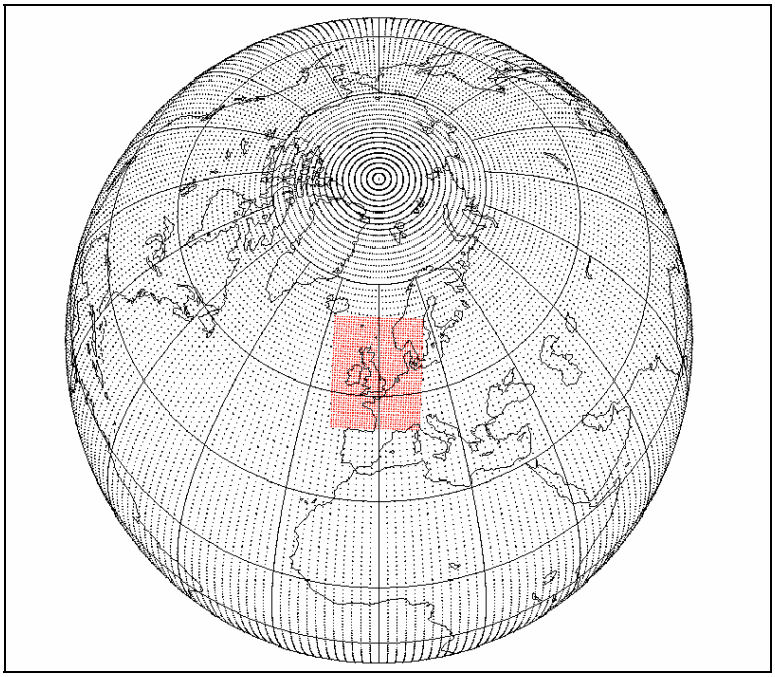

Figure 4.1: **The grids used by the Met Office Global and Mesoscale forecast models**

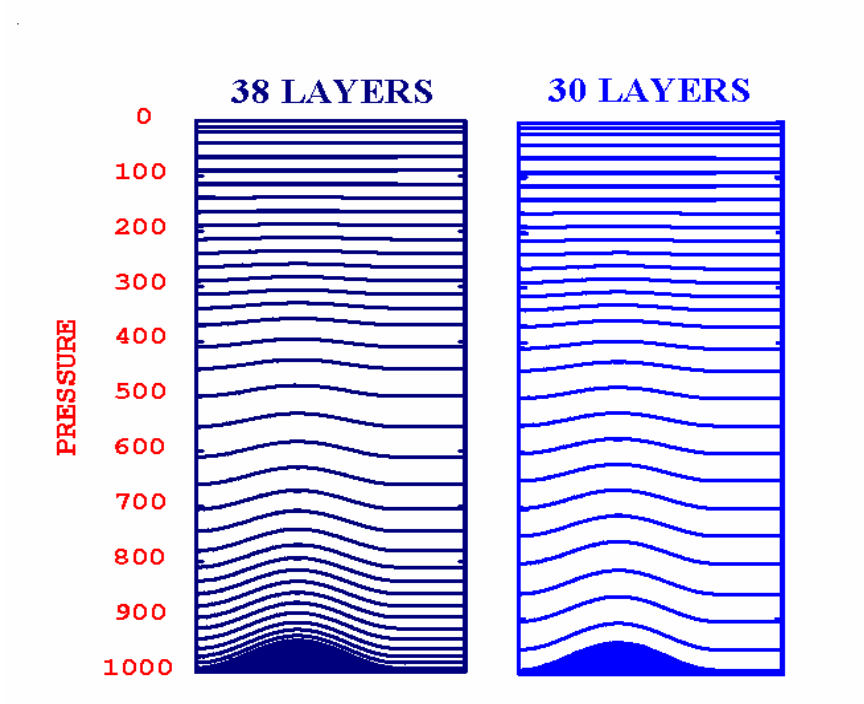

Figure 4.2: **The distribution of levels used in the Mesoscale (left) and Global (right) configurations**

In both models, the variables are arranged in the same fashion. In the horizontal, an Arakawa C grid is used (Arakawa & Lamb, 1977), with the co-ordinates for wind offset with respect to those for temperature. The u wind components are east-west staggered and the v wind components are north-south staggered from the temperature points.

Following assimilation, the NWP models are run to produce forecasts of the expected state of the atmosphere at specified future times. The global model is run twice each day to produce forecasts for up to 6 days (144 hours) ahead, initialised with data valid at 00 and 12 UTC. The main runs of the mesoscale model are at data times of 00, 06, 12 and 18 UTC.

4.4 Model verification

For many years Met Office global forecasts have been verified by comparing forecast variables with corresponding actuals to calculate indices which quantify forecast accuracy. One long-running index is the root mean square (RMS) error of mean sea-level pressure forecasts over the North Atlantic/Western Europe area. The reduction in errors over time shows that forecasts have improved steadily since the 1980s, to the extent that a three-day pressure field forecast is more accurate on average today than a one-day forecast was 20 years ago.

Forecast accuracy varies with time of day, season, locality and with weather type, since some situations are inherently more predictable than others. Assimilation and the quality of the analysis will depend on the coverage of observational data over the area in question and will be better for some variables than others.

Since the main purpose of verification is to monitor the results of changes made to the NWP models, ongoing verification work does not specifically address the impact of model improvements on dispersion prediction. However, improvements in data assimilation and analysis will clearly benefit the meteorological data used as input to dispersion modelling. Sensitivity studies to assess the impact on dispersion predictions of errors in the various inputs could be addressed without the need for concentration measurements.

Dispersion models have traditionally used observed cloud cover to help quantify the description of the boundary layer. Since the NWP process derives boundary layer and heat flux information, it may be argued that these data could now be used directly as input to dispersion models. With improved vertical and spatial resolutions, models are now capable of providing better descriptions of boundary layer conditions, and these should lead to improved and more scientifically-defensible dispersion predictions. Some limited validations of the model's treatment of low cloud have been undertaken (Bush, 2002).

It should not be assumed that differences between dispersion predictions based on NWP data and those based on observations necessarily indicate that the NWP-based predictions are poorer. In some areas of complex terrain, it is quite likely that NWP data may provide a better representation of the climate over the area of interest than do observations from a single site subject to very local characteristics. Essentially, such a comparison would not be comparing like with like. The modelled data would represent an area and time averaged estimation of the atmospheric characteristics, whereas the observations would account for those characteristics at a specific time and place.

Almost 20 years ago, Fox (1984) reported a consensus view that NWP data would be likely to represent the climate of a specific site better than data from a distant, possibly unrepresentative, meteorological observing station, and so would bring benefits outweighing possible lack of accuracy. Even much more recently, Pielke and Uliaz (1998) regretted that US regulatory agencies have generally failed to take advantage of NWP-generated wind fields. It was suggested that – for real-time applications such as emergency response predictions - the limits of accuracy of the forecasting models could set an upper limit to the skill of air quality models. Whether that is the case could be determined by comparing results from different meteorological data sets, and by comparing predictions based on the alternative data sources with the results of pollution monitoring in the field.

A small-scale case study of Port Talbot steelworks (Weaver, 2002) showed that NWP data gave results that were closer to reality than those based on

observations, but the differences between the two predictions were small in comparison with the differences between predictions and measured values.

To verify the quality of NWP-derived data for dispersion modelling, it would be valuable to undertake a comparison with data from an independent observation site, whose met records were not normally input to the NWP analysis process. One such site exists at the Met Office Research Unit at Cardington, Bedfordshire (Fig 4.3 shows location). Here, the parameters relevant to dispersion modelling are routinely recorded. It would be a relatively straightforward task to obtain several years of Cardington data to compare with NWP data interpolated to Cardington's location. Parameters for comparison could include:

- Wind speed
- Wind direction
- Surface temperature
- Surface radiation
- Cloud amount
- Observation-derived Boundary layer depth.

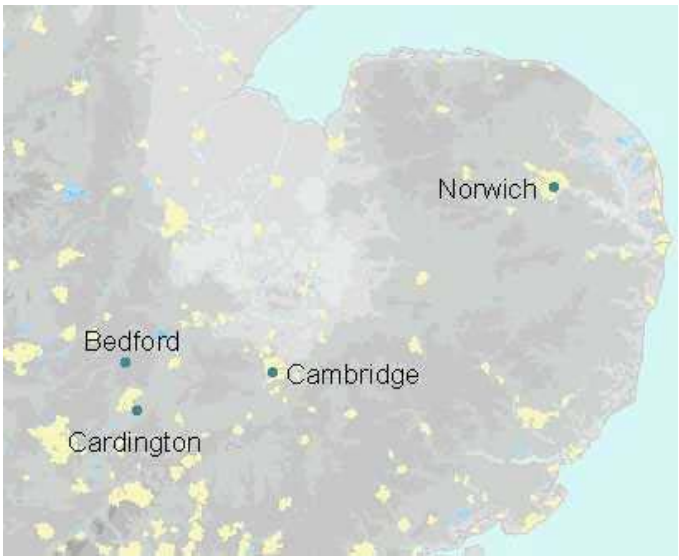

Figure 4.3**: Location of the Met Office Research Unit at Cardington**

Although a comparison with Cardington observations would demonstrate how well the NWP data compare in an area of uniform terrain, it would not indicate the model's performance over areas of more complex topography, coastal environments, or urban areas. Ideally, dispersion applications require the local meteorological input to capture these effects; as NWP models increase their spatial resolutions, representation of these effects is improving all the time. However, at the present time, some differences may be expected between NWP

data and conventional observations; whether these differences are significant in the context of dispersion modelling can only be assessed in the light of results from real case studies.

4.5 New dynamics

In August 2002, the Met Office introduced a completely new formulation of the fundamental equations - the operational model's dynamical core, referred to as 'the New Dynamics'. Fewer approximations are now made in solving the equations, in particular vertical accelerations are now taken into account, making the UM fully non-hydrostatic. There were also many enhancements to physical parameterisations.

This new dynamical formulation provides the scientific foundation for very high resolution modelling, which is a key element of the long-term strategy for improving weather forecasts over the UK. The New Dynamics formulation provides, for the first time, the capability to run models at very high horizontal resolutions of around 1 km or less. This facilitates more accurate representation and development of small-scale features and opens up the possibility of significantly improving predictions of severe weather over the UK, something that was not possible with the old numerical integration scheme.

A number of improved parameterisations have been developed and form part of the New Dynamics implementation in the global forecast configuration, including:

- an improved radiation scheme, incorporating a more consistent treatment of the interaction of clouds with both long-wave and short-wave radiation*
- an improved mixed-phase, cloud microphysics scheme, including the facility to define the amount of water present as ice*
- an improved boundary-layer turbulent-mixing scheme - including non-local mixing in unstable conditions and an entrainment parameterisation. An additional eight vertical levels in the boundary layer for the global model*
- improvements to convection, including a shallow convection scheme and new parameterisation of convective momentum transports**
- revised definition of cloud coverage, accounting for anvil cirrus clouds and cloud fractional variations in the vertical**
- improved representation of orography, including use of new global 1 km terrain data to generate the orography fields replacing the previous 20 km resolution data**, smoothed orography fields to remove numerically undesirable gridscale and near gridscale forcing**, and a new sub-gridscale orography scheme that is both simpler and more robust than the existing scheme***

Some of the above developments (*) were already in use in the mesoscale configuration of the UM, some (**) are used only in its global configuration and others (***) are newly implemented in the UK mesoscale configuration.

Trials of the new scheme carried out during 2000/01 showed the following:

- Root-mean-square errors are reduced by as much as 5% in the northern hemisphere in all seasons.
- Negative bias in wind speeds is reduced in all seasons.
- Systematic biases in temperatures are reduced - notably in the stratosphere but also at 1.5 m.
- There is improved handling of some extreme cyclogenesis events.
- Modelling of radiation balance at the surface is improved.

In addition to the new improvements mentioned above, the UK regional model will benefit from utilising parameterisations of sub-gridscale orography and cumulus momentum transport for the first time. Trials of the new system have exhibited improvements for the prediction of the following:

- Near-surface wind speed (reduction in the systematic bias),
- Temperature and humidity (both at 1.5m) – also a reduction in systematic bias,
- Visibility and temperature (overall improvement in forecast accuracy).

These benefits imply that NWP analyses and forecasts are becoming increasingly realistic, and their wider use for dispersion modelling demands serious consideration.

4.6 References

Met Office website pages are given where relevant, but these may change over time.

A new data assimilation scheme for the global model. NWP Gazette (Sep 1999) - available on Met Office web site http://www.metoffice.com

A new Unified Model. NWP Gazette (June 2002) - available on Met Office web site http://www.metoffice.com

Improved resolution global and mesoscale models. NWP Gazette (Sep 1999) - available on Met Office web site http://www.metoffice.com

Operational Numerical Modelling - available on Met Office web site http://www.metoffice.com/research/nwp/numerical/index.html

New Dynamics in the Unified Model - available on Met Office web site http://www.metoffice.com/research/nwp/numerical/unified_model/new_dynamics.html

Arakawa A and Lamb VR (1977). Computational design of the basic dynamical processes of the UCLA general circulation model. *Methods in Computational Physics*, **17**, Academic Press, 174–265, 337 pp.

Bush M (2002). Validation of the mesoscale model during periods of observed low cloud using data from the Cardington balloon facility. Met Office Forecasting Research Technical Report No 382.

Fox DG (1984). Uncertainty in air quality modelling. *Bull Am Met Soc*, **65**, 27-36.

Lorenc AC, Ballard SP, Bell RS, Ingleby NB, Andrews PLF, Barker DM, Bray JR, Clayton AM, Dalby T, Li D, Payne TJ and Saunders FW (2000). The Met Office Global 3-Dimensional Variational Data Assimilation scheme. *QJRMetSoc*, **126**, 2991-3012.

Lorenc AC (1995) . Atmospheric data assimilation. Met Office Forecasting Research Division Scientific Paper No 34. Available on Met Office website http://www.metoffice.com/research/nwp/analysis/da_intro.pdf

Macpherson B, Wright BJ, Hand WH and Maycock AJ (1995). The Meteorological Office mesoscale data assimilation scheme. Available on Met Office website http://www.metoffice.com/research/nwp/analysis/mesoscale/mes_assim.pdf

Pielke RA, Uliasz M (1998). Use of meteorological models as input to regional and mesoscale air quality models - limitations and strengths. *Atmospheric Environment*, **32** (8), 1455-1466.

Weaver KN (2002). An investigation of accuracy and uncertainty in numerical modelling used for the assessment of impacts from airborne pollution. Dissertation for an MSc in Integrated Environmental Management, University of Bath.

5 THE SITE SPECIFIC FORECAST MODEL

5.1 Introduction

The resolution of operational Numerical Weather Prediction (NWP) models has improved steadily over time (see section 4), to the extent that horizontal resolution of about 10x10 km is now achievable. However, spatial resolution improved even further by a factor of 2 would be insufficient to resolve small urban areas or the variations that tend to occur within heterogeneous landscapes. Until sufficient computer power becomes available, alternative methods are required for operational local forecasting. Furthermore, for some applications, such as forecasting road surface conditions, it is questionable whether full 3D modelling will ever be appropriate, since the immediate local environment can be very dominant. Therefore, a new forecasting model has been developed to add site-specific forecast skill to NWP products. It is called the Site Specific Forecast Model (SSFM).

5.2 The models

5.2.1 Site specific model

While some features of local meteorology require solution of the 3D problem, the broader features of the local boundary layer can be described using a 1D vertical

model; indeed, many routinely- applied air quality models require only 1D information, as they assume local horizontal homogeneity. The 1D version of the Unified Model (UM - see section 4) is dynamically forced from 3D NWP data and modified in a simple way to take some account of local orography. Extensive modifications have been made to the surface exchange scheme to provide better surface layer simulations, based upon a coupled multiple tile/source area approach driven by detailed land-use (25 m ITE data) and orography data (100 m). Care has been taken to represent the component surface 'tiles' realistically, both in terms of drag and heat and moisture exchange. It is run at higher resolution in the boundary layer than the UM in order to improve resolution of stable layers and radiative exchanges. (Hopwood, 1998)

The model includes parameterisations of the full range of diabatic processes, including a full long-wave and short-wave radiation scheme, layer and convective cloud and precipitation processes, boundary layer transport and surface exchange. In practice the convection scheme has been used in a 'diagnostic' mode, to provide input to the radiation and hydrology schemes, but not allowed to impact the prognostic variables as convection is regarded as a process occurring on a scale larger than the model. A new soil surface scheme called the Met Office Surface Exchange Scheme (MOSES) (Cox et al, 1999) has been used which includes a sophisticated treatment of plant physiology to predict surface resistance to evaporation, multi-layer soil hydrology and thermal model including soil-moisture freezing. A radiative canopy treatment has been added to this to improve the treatment of heat exchange over vegetative surfaces and an urban canopy. Surface exchange is treated using Monin-Obukhov similarity theory.

The boundary layer is treated using a purely local scheme, though a new non-local scheme has been developed and will be tested in future versions of the model. It incorporates a first-order scheme which models fluxes between layers in terms of mixing lengths, the vertical gradient of wind velocity and the local stability measured in terms of local bulk Richardson number. Mixing lengths are taken to be functions of height, surface roughness length and asymptotic neutral mixing lengths proportional to the boundary layer depth (except in very shallow boundary layers). The boundary layer scheme is run with four times the vertical resolution of the operational NWP models (ie, 53 levels below about 2.2 km with the lowest model level at 2.5 m), primarily to improve treatment of fog and cloud processes.

5.2.2 The unified model

The UM surface scheme is typical of NWP and General Circulation Models and is relatively simple. It uses a Louis type explicit surface exchange parameterisation (Louis 1979), the surface being represented by a fixed roughness, vegetation fraction, surface resistance to evaporation, albedo etc. The sub-surface is represented using a 4-layer heat transport scheme and single-layer hydrology. This surface and sub-surface scheme has been completely replaced in the SSFM.

The UM physics have been used to minimise development and maintenance costs and maintain compatibility with the driving model. In this respect the approach is very similar to that of Gollvik and Olsson (1995), who use a high vertical resolution 1D version of the High Resolution Limited-Area Model (HIRLAM). However, the approach to forcing the model and surface exchange is somewhat different. It has been argued that, in practice, local meteorology is generally dominated by two factors - local orography and the surface characteristics of the upwind fetch. It is very difficult to correct for local orography in a 1D model. A simple system has been implemented which assumes that the 'zeroth' order impact of orography is through surface pressure perturbations.

5.3 Forcing and local orography

To force the SSFM, extraction of surface pressure and height and vertical profiles of wind, temperature and total water from NWP output, together with their horizontal gradients are performed. From these the hydrostatic pressure gradient and large-scale vertical velocity are derived. A full description can be found in Clark and Dunlop (1997). The NWP model levels are assumed to be perturbed by local orography as follows. First, the maximum upwind elevation (out to a range of 10 km) relative to the orography in the forcing model is used to estimate whether any flow blocking is likely. A (conservative) estimate of a 'dividing streamline height', H, is derived from U/N where U is the average wind speed in the layer and N the average buoyancy frequency.

5.4 Local surface exchange

Results from the UM single surface exchange scheme have been compared with observational data recorded at the Met Research Unit at Cardington. Initial results were typical of a concrete slab rather than a vegetative surface, with indications that some surface cooling was being prevented. Experimental results have shown road (or bare soil) surface temperatures to be 1-2 degrees below screen level temperatures on a clear sky night. Grass surface temperatures can be as much as 5-10 degrees below this value. Various modifications were made to the scheme, which included the introduction of a vegetation canopy scheme. The impact on the soil temperatures can be seen in Figures 5.1a and b below (the acronym SCUM denotes Surface Canopy Unified Model). The inclusion of the canopy scheme (Fig 5.1b) shows an improvement to the grass surface temperatures. However, for the case without the canopy (Fig 5.1a), results for air and surface temperature shows good agreement (which we know should not be true from experiments – there should be an appreciable temperature difference). The introduction of the canopy scheme allows the atmosphere to be buffered from the effects of the heat stored in the soil and therefore allows the surface temperature to drop well below the air temperature (as observations show).

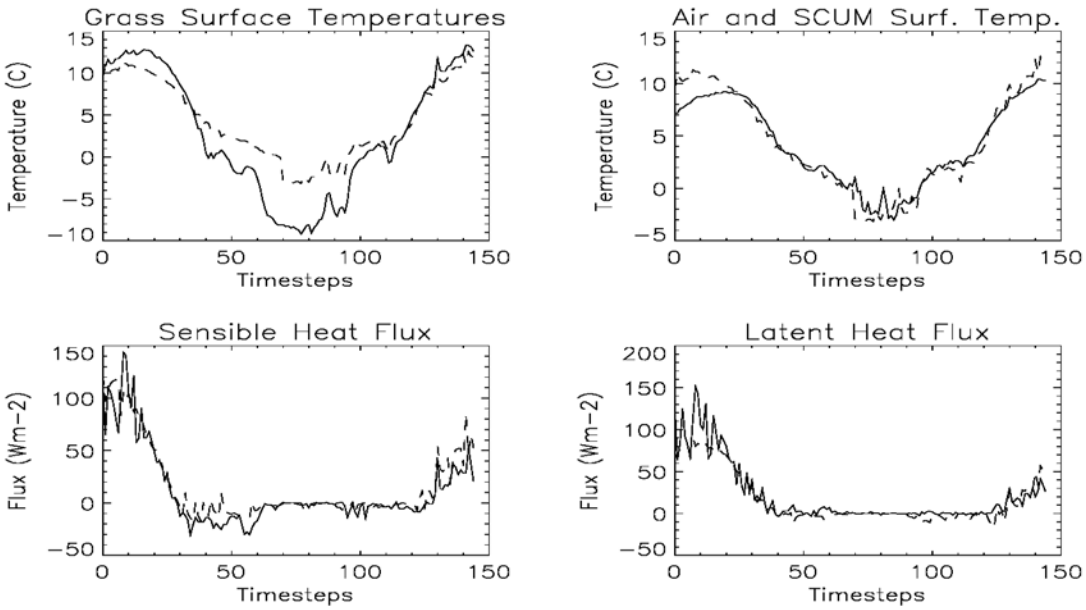

Figure 5.1 a**: Comparison of model output with UM surface parameterisation (dashed) against observed for surface temperature, air temperature, sensible heat flux and latent heat flux**

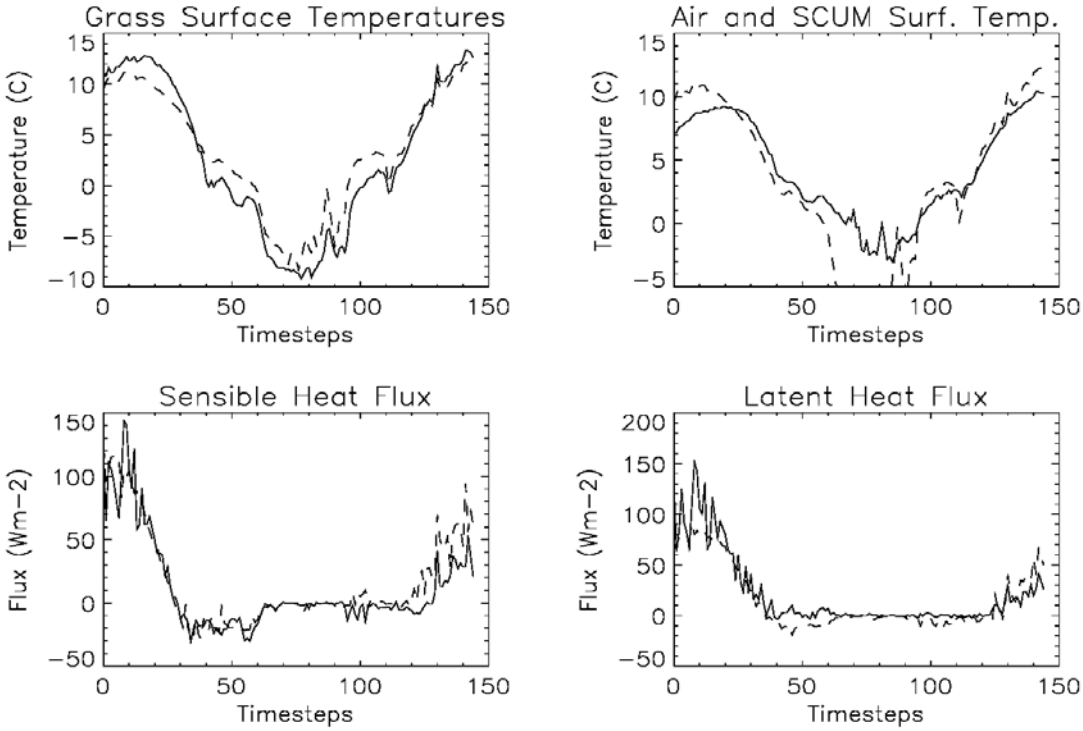

Figure 5.1b: **Comparison of model output with canopy scheme (dashed) against observed for surface temperature, air temperature, sensible heat flux and latent heat flux**

Continued development will take place on this model, in three particular respects:

- screen temperature and dewpoint to provide improved input to soil moisture calculations,
- synoptic reports to constrain anomalous local surface fluxes arising from errors in landuse and/or topography and
- cloud diagnosis from the NIMROD nowcasting system to improve the performance of the surface exchange model.

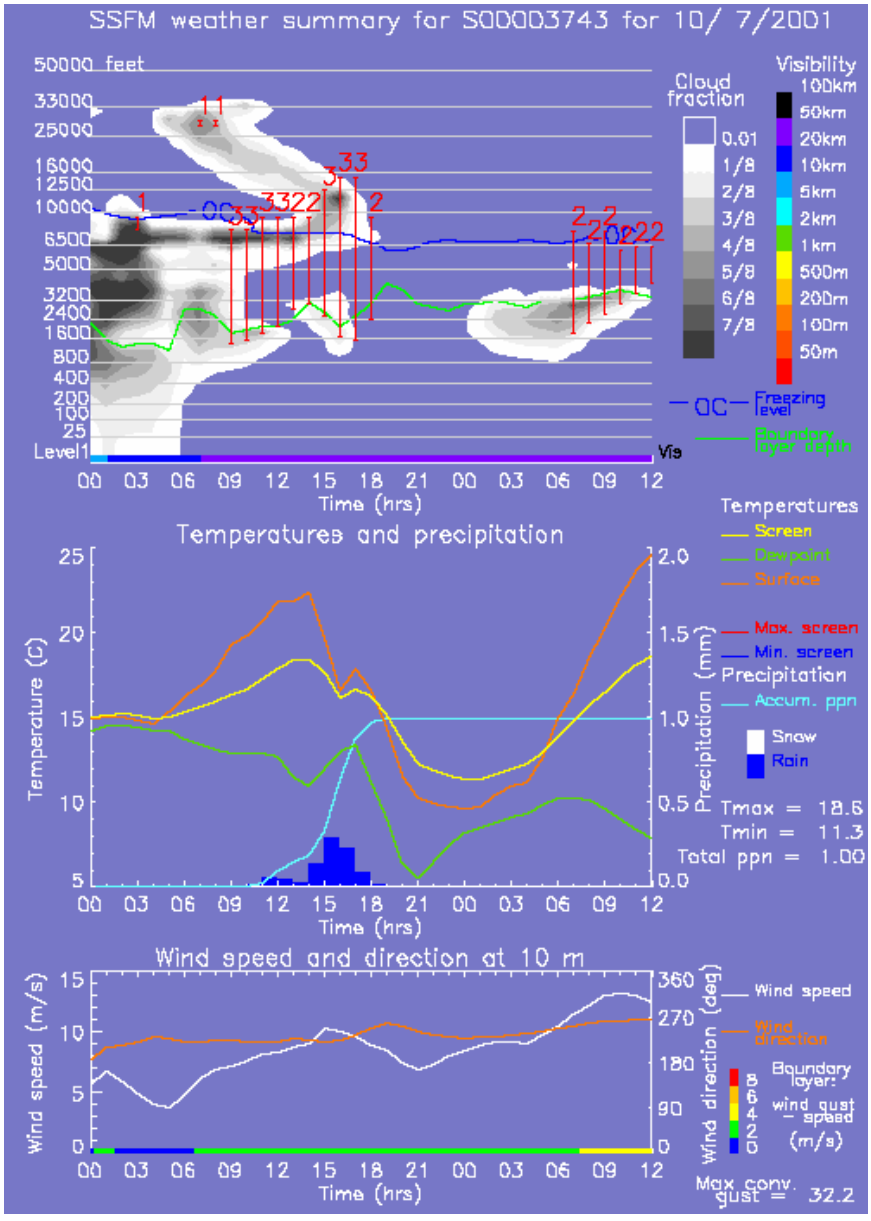

Figure 5.2: **Example of Site Specific Forecast Model Output**

The existing system is used to produce several products, which are disseminated to users. The example (Figure 5.2) shows information versus time in three plots – cloud (at the top), temperature/precipitation (in the middle) and wind speed/direction. Information on the plot includes:

Cloud

- Layer cloud
- Freezing level
- Convective cloud amount and depth
- Boundary layer top
- Visibility bar.

Temperature/precipitation

- Screen and Surface Temperature
- Precipitation accumulation
- Hourly precipitation
- Dewpoint temperature
- Maximum and minimum temperature and total precipitation during period.

Wind

- Wind direction and speed and wind gusts above mean.

In areas of flat terrain with uniform roughness length, the SSFM will bring minimal improvement over results obtainable from the UM. However in areas which are typically difficult to forecast (within or near complex orography, near coasts), the SSFM has improved the predictions of surface heat flux, wind speeds, air temperatures and humidities, with consequent benefits to the estimation of boundary layer depth. Estimates of cloud cover do not show significant improvements, since cloud derives from the larger- scale forcing rather than immediately local conditions. The SSFM is mainly used at present to provide improvement to the prediction of road temperatures, and the infrastructure to allow its routine use for dispersion modelling does not yet exist.

5.5 References

Best MJ and Hopwood WP (2001). Modelling the local surface exchange over a grass-field site under stable conditions. *Quar J R Met Soc*, **127** (576), 2033-2052.

Clark PA, Hopwood WP, Best MJ, Dunlop CC and Maisey PE (1997). Assessment of the single-column UM for use as a local forecasting tool – suitability and recommended configuration. Met Office Forecasting Research Technical Report, No 203.

Cox PM, Betts RA, Bunton CB, Essery RLH, Rowntree PR and Smith J (1999). The impact of new land surface physics on the GCM simulation of climate and climate sensitivity. *Climate Dynamics*, **15**, 183–203.

Gollvik S and Olsson E (1995). A one-dimensional interpretation model for detailed short-range forecasting. *Met. Apps*, **2**, 209-216.

Hopwood WP (1998). The implementation of local surface characteristics within a site-specific model for short range forecasting. Proc 16th conference on weather analysis, 11-16 Jan 1998, Phoenix, Arizona, pp487-489.

Louis JF (1979). A parametric model of vertical eddy fluxes in the atmosphere. *Boundary - Layer Meteorology*, **17**.

Sheffield PM and Hopwood WP (2001). Sensitivity of Site-specific forecast model performance to vertical resolution, model timestep and forcing data. Met Office Forecasting Research Technical Report, No 367.

6 THE NWP ARCHIVE

Operational forecast data are stored in two ways: variables on the (hybrid) eta-level surfaces (model levels), and variables interpolated to the standard pressure levels.

NWP data that are currently held in archive is given in table 6.1, which presents the data by calendar year and the percentage of data currently available for that year. Shortfalls in 1998 and 2002 are due to (a) data for 1998 expiring from the archive in line with current 5-year retention policy and (b) 2002 still being added to the archive.

QMxx Operational 48 hour Forecast Files UK Mesoscale starting at T = 00, 06, 12, 18Z

QGxx Operational 120 hour Forecast Files Global starting at T = 00, 12Z

Table 6.1: **Availability of archived Unified NWP model data**

Model Level Data - % complete

Year	QM00	QM06	QM12	QM18	QG00	QG12
1998	56	56	56	56	92	92
1999	100	100	100	100	100	100
2000	100	100	100	100	100	100
2001	100	100	100	100	100	100
2002	73	73	73	73	86	86

Standard Pressure Level Data - % complete

Year	QM00	QM06	QM12	QM18	QG00	QG12
1998	56	56	56	56	92	92
1999	100	100	100	100	100	100
2000	100	100	100	100	100	100
2001	100	100	100	100	100	100
2002	73	73	73	73	87	87

It should be emphasised that the Unified Model is under continuous development, and so new operational versions are introduced from time to time. For the archived data presented in table 6.1, the UM has undergone three upgrades, incorporating various improvements, with most of these being consolidated into the latest operational version. The principal change to the UM v4 was the increase in resolution of the global and mesoscale grids.

Table 6.2: **Resolution of Model Grids**

UM version	Data Period	Resolution global*	Resolution mesoscale
4.2	01-01-1998 to 29-01-1998	90 km	17 km
4.3	30-01-1998 to 14-04-1998	90 km	17 km
4.4	15-04-1998 to 06-08-2002	60 km	12 km
5.2	07-08-2002 to present	60 km	12 km

* Resolution is for mid-latitudes

6.1 Archive Policy

The Met Office data retention policy is based on the following principles:

- to meet Met Office obligations under the Public Records Act for the retention of historical records,
- to maintain the nation's memory of the weather for the needs of today's customers - commerce & industry, government bodies, the general public, educational and research institutions

- to meet the likely needs of future generations
- to fulfil international commitments for the collection and archiving of meteorological data
- to meet Met Office internal requirements
- to account for Met Office actions to Parliament, to our owner and to our customers.

All UK observational data are retained permanently, and a selection of global data is retained for 10 years. However, there is a potential difficulty with numerical model output, since space and time resolutions have increased substantially in recent years, resulting in a significant increase in data volumes being generated from each forecast run. Each day produces on average 6000 MB of data that accumulates to approx. 2,200 GB annually, and this figure is expected to increase further as computing power increases. All data archiving has associated costs, which clearly increase as data holdings increase. A review of NWP data retention practice is currently under way.

Present retention practice for NWP data:

- Retain permanently:
  - analyses and forecasts (Global and UK) for every 10th year, starting in 1960.
- Retain for a period of not less than five years (with periodic review):
  - ***global atmospheric model analyses (Standard Pressure levels)
  - ***mesoscale atmospheric model analyses (Standard Pressure levels)
  - global atmospheric model forecasts
  - mesoscale atmospheric model forecasts
    - global atmospheric model analyses (model levels)
    - mesoscale atmospheric model analyses (model levels)

* Extension to 10 years is under consideration.

7 DERIVING ADMS DATASETS FROM NWP DATA & SITE SPECIFIC FORECAST MODEL

Supply of atmospheric model data is not advertised as being generally available, although it is well known within the dispersion community that the Met Office will supply such data if requested. This lack of promotion is because no official Met Office studies have yet been completed to assess the applicability of model

data to dispersion modelling. However, model data have been supplied to a number of customers for them to undertake their own assessment.

Any numerical model that processes variables on a rectangular grid can clearly not represent spatial variability on a scale smaller than the grid spacing. Thus, data at one grid point can be considered to be broadly representative of an area of dimension equivalent to the grid spacing (eg, 12 x 12 km for the mesoscale model). Topographic influences on airflow will be represented according to the model's physics, bearing in mind that the model topography will be a version of reality which is smoothed on the scale of the model grid.

Since wind is probably the most important field for dispersion modelling, the extraction routine uses the wind grid (see topic 2) as a starting point. For a point location expressed in geographic co-ordinates, the nearest four grid points on the vector grid are located. All five points are then projected onto a map of the area using a geographic information system, eg, MapInfo. This provides a facility to view the model grid points within the context of the local surroundings and topography. The customer is sent a graphical (bitmap) image of the area and asked to select the most suitable grid point. As with observational station data, the customer can seek advice from the data consultants. The selected grid point's location is then entered via a user-interface into the software package MADE – Model Atmosphere Data Extraction. MADE then converts this location to a grid point on the vector grid and a corresponding point on the scalar grid.

The model field files, each containing a subset of the data used for general weather forecasting, are currently stored in compressed format. For retrieval, each file is decompressed and the relevant meteorological fields are sought. From each field, the appropriate grid point is extracted and stored in a temporary file. When the period required has been extracted, the temporary file is reformatted for use within a spreadsheet package. At present the extraction program can process only a single point at one time, although multiple point extraction may be introduced in future. The extracted dataset is then post-processed within Excel, to convert the field data into primary meteorological variables, and to format for use within an air dispersion model. Because of the way in which the files are currently organised, this whole process is rather labour-intensive.

The extracted field data are:

- 10 metre zonal (latitudinal) wind component (m s^{-1})
- 10 metre meridional (longitudinal) wind component (m s^{-1})
- 1.5 m Screen Temperature (deg Kelvin)
- Relative humidity at the surface (%)
- Low cloud amount (fraction)
- Medium cloud amount (fraction)

- High cloud amount (fraction)
- Dynamic rainfall rate (kg m^{-2} s^{-1})
- Convective rainfall rate (kg m^{-2} s^{-1})
- Dynamic snowfall rate (kg m^{-2} s^{-1})
- Convective snowfall rate (kg m^{-2} s^{-1})
- Boundary layer height (m)
- Surface heat flux (watts m^{-2})

The following variables are then derived from these quantities to correspond with the observed variables to produce a file format suitable for use with ADMS:

- Wind speed (m s^{-1}) at 10 m
- Wind direction (degrees true) at 10 m
- Surface Temperature (deg C) at 1.5 m
- Total Precipitation rate (mm/hr)
- Total Cloud Cover (oktas)
- Surface Relative Humidity (%)

Boundary layer heights and surface heat fluxes are available within the model files, and it is recognised that these can be input as variables to ADMS. However, for the present, the approach has been to present model data in the same format as observed data, to meet customer expectations. It is envisaged that boundary layer heights and surface heat fluxes will be made available in ADMS format in due course, as resources allow.

The main strengths of NWP-derived data are:

- representative hourly data are available for areas of the UK that have little or limited observed data,
- data incorporate information from a wide variety of sources, and not just surface observations,
- heat exchanges and albedo are allowed to vary dynamically on a day-to-day or even hour-to-hour basis, rather than being treated as constant or with given seasonal variation and
- data may be presented to emulate conventional observational data, if this is required by the user.

The main weaknesses of NWP-derived data are:

- changes in model formulation over time can give rise to step changes in data quality and grid resolution,

- current methods of extraction are time consuming and labour intensive,
- appropriate research on data usage has not yet taken place, and so there is uncertainty on applicability, especially for short-range/medium-term air dispersion modelling and
- no studies have yet been undertaken on the quality of output at coastal locations.

7.1 The future

Since the development of the model data extraction routines, the first stage of the Met Office's Archive Storage System (MASS) has been completed. MASS will allow more efficient retrieval of time-series for multiple locations from the weather forecast field files. Also, further experience with the Site-specific model (topic 5) will allow decisions to be made on the value, archiving and wider usage of this type of data. These developments will be dependent upon further verification work on the use of model data for dispersion modelling, and upon the commercial demand for such products.

8 PRE-PROCESSING METEOROLOGICAL DATA

The pre-processing of met data is an important and necessary step in the preparation of data used within a dispersion model. This process usually allows the 'raw' met data to be checked and processed in such a way as to make it suitable for the dispersion calculations to be undertaken. In models such as ADMS the met pre-processor will ensure that the received met file contains data that are sensible and will alert the user to inappropriate values or missing data. In some models this pre-processor will also calculate other derived parameters such as surface sensible heat flux or boundary layer depth which cannot be easily measured directly. Often a balance must be attained between collecting enough information for the model to make useful and accurate dispersion calculations, and allowing these calculations to be completed in a reasonable timeframe. There are three main types of dispersion modelling applications:

- emergency response, eg, Chernobyl, foot and mouth, etc
- air quality episode forecasting, eg, for urban episodes, etc
- environmental impact assessments, eg, for impact studies used for regulatory purposes.

The following restricts itself to the impact assessment scenario.

The aim of an impact study is to investigate how a proposed source of atmospheric pollution will impact on the surrounding environment. To establish this, two main values are useful. The long-term average concentration in the

surrounding area (or receptor sensitive area) and the extreme event concentration usually captured by one of the higher percentile values, eg, 95th or 98th percentile. For the long-term average value, one would require met data that truly represent the main variations in the weather of the region under consideration. To be certain of capturing the extreme concentration, one would wish to have hourly data over several years. In the past it was considered that ten years of representative data would be needed to capture the year on year variability (see paragraph 2.3 above). However, Davies and Thomson (1997) showed that five and three year analyses gave good results for long-term mean and high percentile concentrations when compared to a ten-year analysis. One year was considered insufficient. The computing time required to analyse ten or even five years of hourly met data is quite considerable, so a technique for statistically representing the variations in met parameters has been developed which reduces computing time considerably.

Modern dispersion models can perform calculations on both hourly sequential or statistically binned data to give long-term impact assessments of pollutant concentrations and depositions. The hourly sequential data allow dispersion calculations to be made for each hourly set of met data, and quantities such as the long-term mean and/or various concentration percentiles are calculated in much the same way as they would be calculated for long-term sequences of observed concentrations.

Statistically binned met data provide a set of representative meteorological conditions, each with a frequency of occurrence associated with it. These frequencies are used to 'weight' the results in calculating long-term averages or percentiles. The statistical data are usually produced from sequential data by grouping the hourly values into classes or bins, and counting the number of cases in each bin. The use of statistical data therefore reduces the number of occasions that have to be considered and hence the computational costs associated with the dispersion calculations.

Sequential datasets offer an hour by hour record of specific parameters as measured at observing sites. The sequential data includes:

- year
- Julian Day Number
- hour of the day
- near-surface air temperature
- wind speed
- wind direction
- precipitation rate
- cloud amount
- relative humidity.

The values for cloud amount, surface temperature, hour and date are used to estimate the surface sensible heat flux from which boundary layer heights can be calculated.

The statistical datasets are constructed using a standard procedure that effectively reduces the input parameters to five, as shown in table 8.1. For each hour, these five variables are retained and the rest are discarded. Categories or 'bins' are then defined for each of the five variables.

Table 8.1 **Variables used in statistical datasets**

Variable	No of classes	Upper limits to classes
Wind Speed (knots)	5	3 6 10 16 ∞
Wind Direction (deg)	12	15 45 75 105 35 65 95 225 255 285 315 345
Heat Flux ($W.m^{-2}$)	7	-30 -10 0 50 100 150 ∞
Boundary Layer Height (m)	7	100 200 300 500 800 1200 ∞
Precipitation (tenths of mm)	3	0 6 ∞

Each hour of met data is then assigned to one of the (5x12x7x7x3=) 8820 categories, and the number of hours falling into each of the categories is computed. Essentially the model develops a 5-dimensional frequency table. The met input file is constructed by specifying a representative set of met data for each of the 8820 categories and associating the corresponding occurrence frequency. When the dataset is used by ADMS, dispersion is calculated for each of the 8820 sets of data and the frequency information is used to weight the results in calculating long-term means and percentiles. In practice there are fewer than 8820 cases because some of these will be empty, eg, stable cases with light winds and deep boundary layers, or strong winds with shallow boundary layers.

For each of the parameter bins, the representative value is chosen as the mean value of all the cases falling in that bin, except for wind direction, where the representative value is chosen to be the mid-point of each bin. A possible way to improve the binning scheme (without specifying more bins) is to use, for example, a different value of wind speed for each of the 8820 combination of bins based on the average wind speed for all the cases falling in that combination of bins. However that would mean ADMS would have to calculate each case from scratch which would reduce the computational advantage provided by the statistical approach. A typical ten-year statistical dataset contains about 2000 representative hours of met data compared with the max possible of 87600 (over ten years). This is significantly less than the number of hours in a year (8760) and so statistical binning reduces the computing time significantly even if just a single year is being considered. In addition, if the terrain is uniform with no buildings etc considered, a model like ADMS will not need to calculate everything for each case. For example if only wind direction and precipitation change, this will only affect the direction of the plume and the wet deposition calculations.

As shown above, the raw sequential data are used to generate heat flux and boundary layer values. Since knowledge of the recent history of met conditions is crucial for the estimation of boundary layer height, the sequential data allow the boundary layer characteristics to evolve over time. For the statistical datasets, values for these two parameters are pre-calculated for each hour before being prepared for direct input to the model, and no information exists to allow a time evolution of boundary layer height. If (as is the case for the sequential dataset) time of day and year were input as additional variables, this would increase the multi-dimensional frequency table to 7 dimensions. The result would be an increase in computation, and therefore a reduction in the running time advantage attained by using statistical over sequential datasets.

8.1 References

Davies BM and Thomson DJ (1997). Investigating the importance of pre-processing in estimating dispersion climatology. *Int J Environment and Pollution*, **8**, (3-6).

9 PROVISION OF METEOROLOGICAL DATA AND/OR DISPERSION CALCULATIONS IN REAL TIME

Numerical Weather Prediction forecast data can be extracted and distributed, normally within two hours of the availability of the forecast field files. The Met Office already supplies forecast products to a number of customers for use within their own dispersion models.

Basic weather variables - the following are automated services that provide a range of forecast variables that are used for air dispersion or episode analysis studies:

- an automated service that provides a 24 hour hindcast and 24 hour forecast, at hourly intervals, of wind speed, wind direction and surface temperature. These data can be provided twice daily for any location in the United Kingdom. The locations are specified by submitting a request file via the internet.
- an automated service that provides a 24 hour hindcast and 120 hour forecast, at three hourly intervals, of vertical profiles for wind speed, wind direction and atmospheric temperature. This data can be provided for any number of locations. The forecast data file is formatted for input to the Airviro dispersion model.

Forecasts including derived parameters:

- an automated service that provides a forecast out to 48 hours, at hourly intervals. A number of parameters are supplied including wind speed, wind direction, Monin-Obukhov length, boundary layer height, wind stress and

surface temperature. These data can be provided for any number of locations in the UK. The forecast data file is formatted for input to the Airviro dispersion model.

- a forecast out to 48-hours at hourly intervals for the atmospheric pollutants: SO2, NO2, CO2, CO and PM10 (Ozone forecasts are expected to become available during 2003).

Given adequate notice, the distributed files can be supplied in any desired format suitable for direct input into air dispersion models. However, it should be noted that there are a limited number of basic and derived parameters available, and real-time supply assumes minimal post-processing of the forecast data to obtain the correct format. Post-processing to include parameters not normally available within the forecast data files (to apply statistical analysis or categorisation of the data) would require development effort. The data products can be delivered either by electronic mail (email) or by file transfer protocol (FTP). The file format is normally supplied as ASCII text. Costs will depend on the customer's requirements for data volume and level of service resilience.

The real-time routine supply of dispersion calculations is possible but, since most dispersion models require interactive input, costs would reflect the significant effort needed to set up such a service. At present, the Met Office supplies routine dispersion data from the NAME model as part of the National Air Quality Forecasting Service.

Alternatively, real time dispersion calculations could be supplied by subscription to the Met Office's CHEMET service (see Section 9.2). This service provides response to six on-demand calls to the EMARC desk.

9.1 EMARC

EMARC is the Environment Monitoring And Response Centre, one of the production units within the National Met Centre. This unit was set up in 1999 to centralise short-notice specialist forecasts and manage demands from the UK emergency services and other government departments, as well as from the international community. EMARC is manned by a duty forecaster 24 hours a day for 365 days a year, enabling the Met Office to provide a quick response to customers requiring forecast information to help them deal with a variety of environmental incidents.

EMARC use data from the Met Office's suite of computer models to deduce expected localised weather conditions. Local variations in expected wind speed and direction are the most important elements. Rain at the scene can wash the chemical out of the atmosphere, leading to higher concentrations on the ground. The vertical temperature profile of the atmosphere affects the stability of the air, and this determines how high the plume is likely to rise, which subsequently effects the distance it might travel and its behaviour close to hills. A forecast supplied in these cases is called a CHEMET.

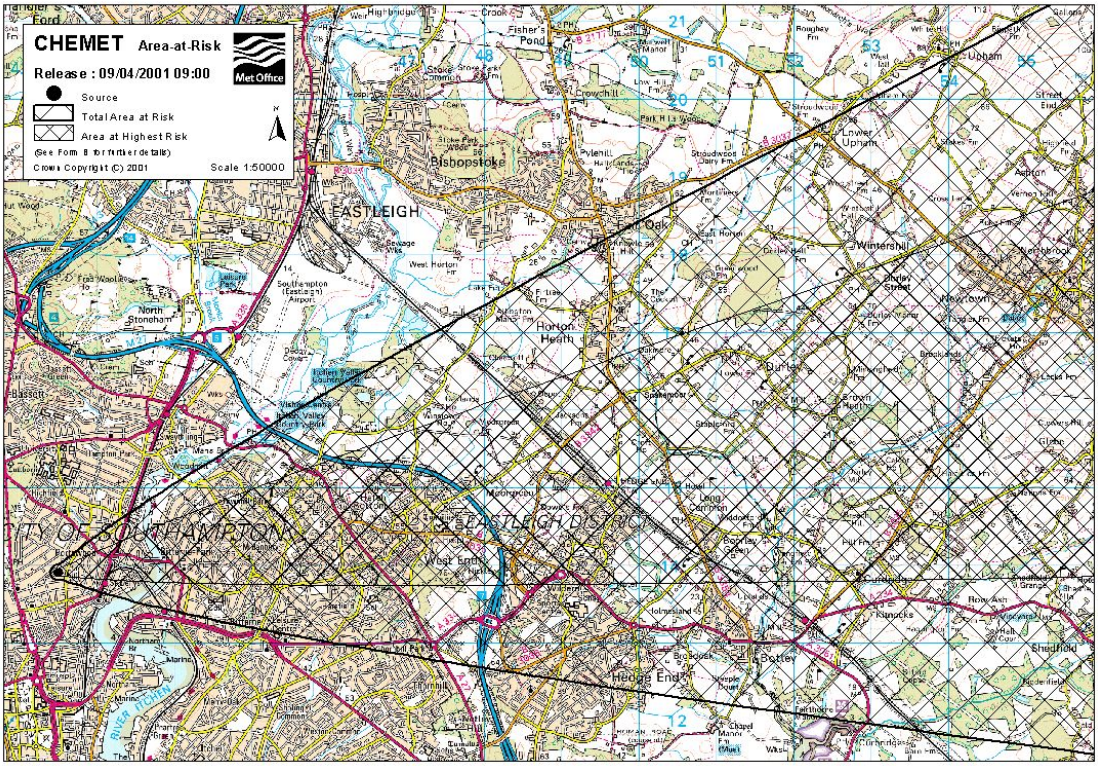

Figure 9.1 **Example of a CHEMET "area at risk" forecast**

9.2 CHEMET

The CHEMET service uses the ADMS model to provide dispersion output based upon information provided by the customer. This output can be delivered electronically in picture format after post-processing with a geographic information system (GIS).

In the event of an incident involving hazardous chemicals, local police and fire services can contact the Met Office via EMARC's dedicated emergency phone line. Typical scenarios include a spillage or fire at a chemical plant, or a road traffic accident in which a hazardous substance has escaped or been ignited. Police and fire services have specific procedures for dealing with accidents involving listed hazardous substances, and they need to know how the chemicals will behave once released into the atmosphere, to assess risk and determine operational tactics for evacuation or clean-up.

CHEMET forecasts consist of a brief document giving details of relevant meteorological parameters, together with an Ordnance Survey map with an overlay showing the main area at risk. The map is produced by running the ADMS (Atmospheric Dispersion Modelling System) model that produces the overlay and map in a GIS environment. The CHEMET is faxed to the relevant emergency service typically 10-15 minutes after the initial request. Figure 9.1 shows an example of an 'Area at Risk' map.

9.3 Nuclear incidents

EMARC will provide weather forecasts to various outside agencies following the release of radioactive materials into the environment. All the UK's civil nuclear power stations, both active and decommissioned, have set procedures to follow in the event of accidents of all scales. Nuclear sites have their own anemometers to enable them to pass EMARC detailed information about current wind on site.

A 'small scale' incident would be the loss of small amounts of radioactive material, either at a fixed nuclear site or from nuclear products in transit, and unlikely to have an effect on a large geographical area. Following such an incident, the response of EMARC would be similar to that for a chemical incident, so a map showing the area most at risk and a brief document giving other relevant meteorological details would be supplied. The forecast information, part of the PACRAM national response plan (Procedures And Communications following Release of radioactive Material), is sent to the site in question or to an off-site emergency room, as well as to the nuclear industry's Central Emergency Support Centre.

Larger nuclear accidents require a different response. In 1986 an accident at the nuclear plant in Chernobyl in the Ukraine led to the release to the environment of 8 tonnes of fuel, which contained plutonium, caesium and other radioactive fission products. The Chernobyl incident changed the public perception of nuclear safety, and led to massive reviews of procedures in the management of nuclear materials. As part of this international response, the Met Office developed a new computer model - NAME (Nuclear Accident Model). NAME draws on meteorological and radiological data to predict the movement, deposition and dispersal of large plumes of material over several days.

On notification of an accident, EMARC staff input all known information about the release and run the NAME simulation. Output from the model is an animated graphic to show plume movement. Output is dispatched automatically via a dedicated closed network to the various government authorities involved in co-ordinating the national response to larger accidents. These include the Department of the Environment, Food, and Rural Affairs, as well as the Department of Trade and Industry, the Ministry of Defence, and the National Radiological Protection Board. A member of the EMARC team could be detached to London to brief ministers and other representatives of these departments to advise on the interpretation and implications of the forecast.

9.4 International commitments

As well as responding to incidents within the UK and to incidents abroad which are likely to affect the UK, the Met Office has additional international responsibility in its role as one of the 8 Regional Specialised Meteorological Centres (RSMC). In this guise, EMARC has responsibility for running the NAME model for all incidents occurring anywhere within Europe or Africa, regardless of their direct impact on the UK.

Notification of an incident would usually come from the International Atomic Energy Authority in Vienna. In these instances, the Met Office senior forecasters are responsible for liaising with the French national meteorological service, to produce a joint statement outlining the expected behaviour of the resultant plume. These forecasts are dispatched to the international community at large.

10 SUMMARY

This report has investigated the potential alternative sources of meteorological data that could be used for dispersion modelling purposes. Particular attention has been given to the land-based observing network, Numerical Weather Prediction products and the Site Specific Forecast Model. Where possible indications have been given to how current and future operations in these areas might benefit dispersion modelling work. The report also explains how much data is readily available for dispersion modelling and how raw data is transformed for inclusion as input datasets. The report does not comment on the financial considerations regarding the sales of alternative data as this would not be appropriate for this report and would require a pricing policy to be proposed and agreed within the Met Office first.

11 CONCLUSIONS

It is clear that the Met Office has prioritised the management of its data to benefit weather prediction which has always been its main focus regarding core activity. In the past, this data was still considered suitable for dispersion modelling work. With the changes made to the observing network regarding automation and the increased level of sophistication of recent dispersion models, traditional data readily available for dispersion modelling has reduced. The Met Office is committed to increasing the density of automatic weather stations throughout the country paying particular attention to locations that are notoriously difficult to model (coastal and hilly areas for example).

The alternative sources are in the main computer generated and as such require a certain amount of validation before they are seen to be acceptable by the dispersion modelling community. However, because the dispersion modelling community has developed only knowing manually recorded weather data, many questions regarding the suitability and accuracy of this data has perhaps been overlooked. For example, it is possible for small mistakes made by trained human observers to be missed by quality control procedures. In particular, consistency between human observers regarding estimations of cloud height or amount. Also the effect of possible waning concentration as an observer approaches the end of a shift. Ground based point source weather data is perhaps not as suitable for dispersion modelling as area averaged data

(providing it was possible to account for localised effects). The alternative sources have already provided benefits with regard to weather forecasting. Although it is perhaps too early to comment categorically on which data source is most suitable, it is the opinion of the authors that in time the alternative sources will also provide benefits to the dispersion modelling community.

12 FURTHER WORK

Much of the possible work that could come out of this report is associated with the acceptance of alternative sources of met data. Demonstrating that alternative sources of the met data are as good as, or better than that currently available, would be useful.

In the short term, an analysis of how sensitive dispersion calculations are to manually observed and LCBR calculated cloud amounts would be useful (see Section 1.2). Developing a better understanding of the NWP data products obtained from the model would also be very useful. A comparison of appropriate met parameters obtained from the model and recorded at a site (who's results are not normally input to the model) could help us understand how big the discrepancies are, and whether they are significant in dispersion modelling terms (see Sections 4.1).

Uncertainty in deriving dispersion parameters from meteorological data

A report prepared for ADMLC by

V Auld, R Hill, T J Taylor

Westlakes Scientific Consulting

This study was funded by the UK Atmospheric Dispersion Modelling Liaison Committee.

Publication date: June 2003
Westlakes Science & Technology Parl
Moor Row
Cumbria CA24 3LN

EXECUTIVE SUMMARY

Atmospheric dispersion models are frequently used for assessing the dispersion of pollutants in order to determine concentrations at local sensitive receptors. The models are used by both emergency planners, to determine under what conditions to implement accident plans, and by environmental assessors and regulators, to quantify the impact of proposed or current emissions. The uncertainty associated with deterministic model predictions of long and short term concentrations is an issue of concern to all users. This study was funded by ADMLC, the Atmospheric Dispersion Modelling Liaison Committee, to investigate the uncertainty in model predictions due to meteorological data input and the subsequent treatment of that input within Gaussian models.

The report briefly reviews the measurement techniques and instrument accuracies associated with meteorological data most frequently used by the modelling community. It discusses issues of representativity of the measured and estimated boundary layer parameters input by the model user, such as roughness length, albedo and Bowen ratio. The treatment of the meteorological data within ADMS and AERMOD is discussed in detail, the relevant differences between the model's meteorological pre-processors are identified and their influences on boundary layer structure and plume dispersion calculations are considered.

The use of alternative meteorological data sources, such as flux profile measurements, sonic anemometers and the use of NWP (numerical weather prediction) data are evaluated. The review aimed to establish whether there are viable alternatives to the current dependence upon the model pre-processors to estimate boundary layer stability parameters. In the absence of representative site measurements, the use of NWP data is recommended after encouraging comparisons with site data. Potential improvements to the current NWP dataset provided by the Met Office are suggested and further feasibility studies recommended. Specific conditions where meteorological input to ADMS and AERMOD result in disparate predictions are identified and investigated, and the results of a probabilistic assessment of uncertainty associated with meteorological input to ADMS are discussed.

This study illustrates that the accuracy of meteorological systems measuring standard parameters such as wind speed, direction and temperature contribute little towards the overall uncertainty of the model predictions. The main factors considered when discussing the 'representativity' of meteorological data include distance between the measurement site and industrial site, the matching of surface characteristics at each site (particularly roughness length), and the local terrain (including coastal influences). Results from several sections of the report identify roughness length as a parameter whose contribution to overall model uncertainty was significant. A concerted attempt to provide the model with realistic input of this parameter for both the meteorological site and within the chosen model domain should reduce the uncertainty associated with predictions.

Peak concentrations often occur during periods of low wind speeds, and agreement between models under these conditions is poor. Poor agreement is also found during dusk periods and periods where there is rapid change in cloud cover. If the model user is particularly concerned with modelling these conditions, or where results are close to benchmark concentrations, they are recommended to consider obtaining predictions from more than one model. The results of the study concentrate on a 40 m stack release scenario and further investigation of meteorological uncertainty for releases at different stack heights is proposed. Throughout the report, the authors have intended to highlight findings of relevance to the model users, with the main guidance summarised in the final section.

CONTENTS

1 INTRODUCTION

Dispersion modelling tools are used to support emergency response decision making in the event of accidental or otherwise unscheduled discharges. They are also used to assess the environmental impacts of atmospheric releases with regard to the granting of planning permission and authorisation of site operation licenses. Whether using a simple robust and efficient R91 (Clark, 1979) based Gaussian model, or a more advanced commercial Gaussian-like model such as ADMS (Carruthers et al, 1994; CERC, 2001) or AERMOD (Cimorelli et al, 2002), all model users are required to consider the uncertainty attached to the model's deterministic predictions. There continues to be a dissociation between the models estimated ranges of certainty and the increasing accuracy of prediction required to fulfil the needs of the decision makers and regulators.

Regulators are often required to make planning and discharge authorisation decisions on the basis of model predictions alone, in the absence of detailed site specific measurements. The impact of emissions is routinely assessed against air quality standards based on either the annual average concentration of a pollutant or on a certain percentile of the annual distribution of air concentrations, averaged over a particular time period. For example, nitrogen dioxide air concentrations are regulated as both annual average (40 $\mu g\ m^{-3}$) and the 99.8^{th} percentile of the hourly concentration distribution for a given year. An alternative way of interpreting the 99.8^{th} percentile of hourly averaged air concentrations is the 18^{th} highest hourly air concentration value over the full period of a year.

Emergency decision makers rely on a dispersion modelling assessment to provide a rapid, robust and potentially conservative (maximum) estimate of short term concentrations downwind of an emission source. All model users would benefit from knowledge of the likely range of uncertainty associated with the single value provided for their purpose, and also from an understanding of which parameters are the dominant contributors towards this ambiguity.

This study concentrates on the uncertainties associated with the user's choice and model's treatment of meteorological data. It is recognised that further ambiguities are associated with confidence in the inputs of emission rates, stack characteristics, the model's treatment of terrain and buildings, and the user's choice of input parameters and output format. Beyond the dispersion modelling of pollutants are additional uncertainties such as obtaining a true 'background' concentration against which to analyse the contribution of a site's proposed emissions. Perhaps the largest uncertainty of all within an environmental assessment is that associated with the final outcome, ie, the level of exposure and relative risk that each pollutant of concern might pose to the health of members of the public.

Both the AERMOD system and ADMS contain meteorological pre-processors that are used to derive boundary layer parameters from commonly measured

meteorological data. For the UK, the primary data used as input to these models are surface wind speeds, wind direction, temperature and cloud cover estimates. AERMOD and ADMS use similar basic meteorological and dispersion assumptions, yet comparisons of their predictions for matched input data can occasionally be significantly different. Hall et al (2000) concluded in their model inter-comparison study that the large differences they observed in predicted concentrations might be due to the different treatment of meteorological data within the met pre-processors. Within this study we have aimed to identify, describe and understand such possible disparities between the models.

The report briefly reviews the measurement techniques and instrument accuracies associated with meteorological data most frequently used by the modelling community. This is followed by a discussion on the representativity of the measured parameters and that of the boundary layer and surface parameters which are input directly and/or estimated within the model pre-processors.

The model's treatment of the meteorological data is discussed in detail, identifying relevant differences between the pre-processors and their influences on boundary layer structure and plume dispersion calculations. Three meteorological data sources are evaluated to establish whether there are viable alternatives to the current dependence upon the meteorological pre-processors to estimate boundary layer stability parameters. The first two alternatives are site specific flux profile and sonic anemometer measurements, the last is the use of numerical weather prediction (NWP) data from the Met Office. Analytical techniques were employed to identify and investigate specific conditions in which the uncertainties introduced through both user discretion and model treatment of meteorological inputs, result in ADMS and AERMOD producing disparate predictions. These events may lead to situations where contradictory conclusions could be presented by different model users, leading to wider implications such as the implementation of emergency action plans or granting of a planning consent. This is followed by a probabilistic assessment, using Monte Carlo methods, to determine the range of uncertainty of long and short term ADMS predictions attributed to individual meteorological parameters.

Finally, the last section of the report summarises the main findings of the study with specific attendance to the needs of the model user community. Where possible, methods of best practice for modelling assessments are identified and ideas for further consideration are provided.

2 MEASUREMENT METHODS AND ACCURACY OF METEOROLOGICAL PARAMETERS

Dispersion predictions depend upon the input and treatment of air flow and atmospheric turbulence within the model. Air flow is typically parameterised by measurements of wind speed and direction at 10 m height. Turbulence (the variance of fluctuations in velocity components) is more difficult to parameterise,

with older models such as R91 (Clark, 1979), assigning conditions into one of seven different Pasquill Gifford (PG) stability categories. ADMS and AERMOD offer more continuous coverage of conditions using parameters such as the boundary layer height, h, Monin-Obukhov length, L_{MO}, sensible heat flux, $F_{\theta 0}$, and friction velocity, u_*.

Meteorological data required for emergency prediction purposes may simply be continuous and current site measurements of wind speed and direction, and instantaneous observations of cloud cover. Currently, the UK Environment Agency Air Quality Modelling Assessment Unit (AQMAU) recommend using 5 years of representative hourly sequential meteorological records (Shi & Ng, 2002) for dispersion model assessments for annual licensing purposes. This is considered a practical period with which to assess the influence of local climatology and inter-annual variability on predictions of annual averages and peak hourly concentrations.

Climatological records can be manipulated for input to ADMS or AERMOD. The Met Office provide datasets from UK airports, military airfield sites and Met Office Regional Centres as well as smaller observing sites, which comprise of hourly averages from automatic instruments with additional hourly observations of cloud cover. Similar datasets are provided by ADM Ltd, the UK suppliers of Breeze meteorological data which can be supplied in AERMOD or ADMS format upon request. These records may be spot measurements on the hour, averages over the hour, or a mixture of both. Further information regarding the dataset can be requested at the time of purchase.

The measurement methods and accuracy of parameters are considered in the following sections. The accuracy of an instrument measurement is considered to be the amount by which a recorded value deviates from an accepted standard value. Values can be quoted for the individual parameter sensors (ie, a cup anemometer) or as a measurement system accuracy allowing for the limitations of the signal processing and datalogging systems. The US Environmental Protection Agency (US EPA) have reviewed and approved a meteorological monitoring guide (www.webmet.com) recommending system accuracies for in-situ meteorological measurements for general use in air quality models based on digital recording systems and standard averaging times of nominally 1 hour (see Table 1). It is expected that these system accuracies are typically obtained by the systems used to collate Met Office and ADM Ltd datasets and also by well managed independent measurement sites. The authors are unaware of any equivalent document designed for UK air quality modellers, however the Met Office provide recommendations for the minimum instrument specifications required for a UK climatological station (www.metoffice.gov.uk) and the World Meteorological Office publish a Guide to Meteorological Instruments and Methods of Observation detailing the basic standards of instruments and observing practices. In addition, British Standards exist for the specification of meteorological thermometers and aspirated hygrometers (BS 692:1990, BS 5248:1990) as do guidelines for the acquisition and management of meteorological precipitation data (BS 7843:1996).

2.1 Ringway 2000 meteorological data

Data from Ringway, Manchester for the year 2000 has been used frequently within this study to demonstrate the effects of uncertainty of meteorological data treatment within ADMS and AERMOD. A preliminary review of this dataset highlighted a number of interesting issues which may influence model predictions.

The data was purchased via the Met Office web site in hourly sequential ADMS format, and contained Julian day, time of day, near surface air temperature, wind speed and wind direction at 10 m, precipitation, observed total cloud cover and relative humidity. It was noted that the wind speeds increased in steps of 1 knot/sec (approximately 0.5 m/s), hence records jump discontinuously from 0.5, 1, 1.5, 2.1, 2.6, 3.1, 3.6, 4.1, 4.6, 5.2, 5.7, 6.2, 6.7 m/s and onwards. This is presumably due to the Met Office storing climatological records of wind speed to the nearest knot, however this resolution is well outside the system accuracy of 0.1 m/s quoted by the US EPA, and it is expected that the majority of recently upgraded Met Office sites routinely measure wind speed with a greater resolution than 0.5 m/s. Wind directions are provided to the nearest 10° sector, again, the standard for climatological purposes, this is comparable to the ±5° system accuracy in Table 1. Temperature is reported to the nearest 0.1ºC and relative humidity to the nearest 0.1%, these resolutions are high in contrast to the expected system accuracy for these measurements as might be expected from expert siting. A higher than expected frequency of very stable conditions (13% PG category G) was observed, which was also apparent in several other statistically binned ADMS meteorological files provided to WSC by the Met Office. Table 2 also displays boundary layer heights for Category A that are lower (average height of 542 m) than less unstable categories (average height of 687 m for Category C), perhaps due to lighter winds occurring in these extremely unstable conditions.

2.2 Wind field

The wind field is commonly measured as scalar components of speed and direction. These are used within dispersion models to determine the speed and direction in which a plume travels. They are also used to estimate boundary layer parameters, such as friction velocity, and provide the basis for vertical profiling of parameters in ADMS and AERMET (the meteorological pre-processor used in the AERMOD system).

Low wind speeds give rise to additional uncertainty, both due to their effect on the dispersion of a plume but also resulting from their treatment within the dispersion model. The US-EPA recommend that wind speed sensors used for dispersion modelling assessments should have a maximum start up threshold of 0.5 m/s, and an accuracy of ±0.25 m/s at low wind speeds such as 1 m/s (www.webmet.com/met_monitoring). Most modern cup anemometers qualify within these bounds with a typical measurement accuracy of 0.1 m/s. Data

provided by the Met Office typically includes wind speeds down to 0.5 m/s (1 kt), although it is expected that data provided from sites with older instruments may be limited to 1 m/s (2 kts) and above. Wind direction, typically measured with a potentiometer wind vane, is generally reported in dispersion model datasets to the nearest 10°, while instrument accuracy might typically be ±2° and system accuracy of ±5°. Use of wind speed measurements at release height and the input of measured standard deviation of the wind direction (σ_θ) can improve model predictions of lateral dispersion, particularly for users of R91 type model codes (Hill et al, 2001).

2.3 Temperature and relative humidity

It is assumed that resistance temperature detectors (RTDs) are used to provide input to the ADM Ltd and Met Office datasets, these typically have an instrument resolution of 0.1°C and accuracy of ±0.1 to 0.3°C. System accuracy is likely to be poorer than instrument accuracy due to variation of air flow and shading influences associated with different sites and systems, however careful siting and shielding can ensure accuaracies with the US-EPA recommendation of ±0.5°C(Table 1).

Relative humidity (RH) sensors provide a balance of actual vapour density to saturation vapour density at the same temperature. Measurement of temperature and RH together allow the determination of vapour density which can be employed within the model pre-processors. The standard reference heights of measurements of RH and temperature are assumed to be sufficiently similar (within 1 m) within different models such that they will contribute little uncertainty to model formulations of profiles and predictions.

Temperature and humidity values influence plume rise, plume visibility, and to a lesser extent, mixing height and boundary layer parameter calculations. Temperatures are reported in met datasets to the nearest 0.1°C, RH to the nearest 0.1%, however system accuracies are expected to be poorer. Despite this, the overall influence of temperature and humidity inputs on dispersion predictions is expected to be low compared to the stronger influences of other input parameters. One condition where ambient temperature might strongly influence predictions is when emission temperatures fall below ambient temperatures and plume sinkage may occur.

2.4 Precipitation

Deposition of soluble pollutants will be strongly influenced by the frequency and strength of precipitation. Tipping bucket rain gauges are typically used to obtain rainfall records, these usually have a measurement resolution of between 0.1 to 0.2 mm/hr. The accuracy of the instrument is somewhat dependent upon its placement, and it is assumed that climatological records are obtained from sites

suitably positioned to be protected from strong winds in order to avoid spurious tipping.

2.5 Cloud cover

Total cloud cover is recorded in oktas (eighths of sky covered) by the Met Office weather observers as part of the standard observing routine. The requirement to discretely band the amount of cloud can lead to bias in the records, for example the frequency of records giving 1 and 7 oktas may be enhanced due to the observers caution in recording totally clear and totally overcast skies as per their observing instructions. This is apparent in the analysis of cloud records from Ringway in 2000 (see Figure 1). It is unavoidable that observations of cloud cover in the hours of darkness contain an additional uncertainty due to the limitations of the human eye, and typical accuracy of ±1 okta in day time may increase to ±2 to 3 oktas overnight.

Cloud observations are gradually being replaced with cloud measurements as the UK Met Office weather stations become increasingly automated. Time series data from laser cloud base recorders (LCBRs) can be processed to provide measurements of cloud height and cloud amount using Sky Condition Algorithms (SCAs). Although these measurements are less susceptible to reduced accuracy during night time conditions, this cloud data also has its limitations. The instrument is designed to view only the zenith of the sky, and does not detect the presence of an invading cloud bank until it reaches overhead. Other developing methods for measuring cloud cover digitally (and then processing into oktas of cloud) include the routine processing of images from an all sky camera. It is possible that these developing methods of cloud cover measurement may supersede manual observations in the future, however, at present we are left with reducing coverage of cloud observations over the UK and no immediate alternative measurement routinely available.

ADMS datasets include values of total cloud cover and do not provide information detailing cloud level. It is possible that a record of 7 oktas cloud corresponds to 7 oktas high level fine cirrus cloud which might exert a lesser influence on surface fluxes than 7 oktas of dense low level stratocumulus. Models such as the Danish dispersion model, OML (Olesen & Brown, 1992), which sits in the same class of models as ADMS and AERMOD, use a heat flux scheme described in Bercowicz & Prahm (1982) and Nielsen (1981) that calculates heat flux allowing for cloud height.

2.6 Solar radiation

Solar radiation can be used within ADMS as an alternative or in addition to cloud cover, although solar radiation measurements from Met Office sites are not routinely included in datasets provided to dispersion modellers. World Meteorological Office second class standard pyranometers are typically adequate

for measuring solar radiation for dispersion modelling purposes (matching the 5% system accuracy acceptable to the US EPA). These are more affordable instruments (~£500) than those matching more exacting standards, and they are regularly included within a standard automatic weather station instrument suite. Solar radiation data is of no use during periods of darkness, instead ADMS reverts to using a default cloud cover value of 5 oktas within its algorithms during these conditions.

3 REPRESENTATIVITY OF METEOROLOGICAL PARAMETERS

The temporal and spatial representativity of meteorological input data is an issue often overlooked by the dispersion model user when considering the uncertainty of overall model predictions. Purchasers of met data for model use can usually obtain a certificate of representativity from the supplier upon request, determining the dataset as the 'most representative' for the emission site in question. A more appropriate label might be 'best available' dataset, as due to limited appropriately measured and formatted data, the closest meteorological sites can be significant distances from the emission site of interest.

This chapter reviews the meteorological input routinely used by modellers and aims to highlight their limitations and inaccuracies. There are obvious difficulties in setting objective criteria to determine whether a met site is representative of an emission site. Distance from the emission site is arguably the most important factor, in order to match the timing of similar air flow over both sites. Length of a data period, local terrain and surface characteristics, coastal influences, and the 'age' of the supplied data are all issues that should be considered on a site by site basis. In reality, wind fields and atmospheric stability will vary with height, location and time due to the localised influences, synoptic weather patterns and stochastic variability. The amount of variation will depend, in part, on the averaging time of the recorded value.

The length of the data period used in a dispersion model assessment should be considered as fit for purpose by the user. Guidance on this decision is available from regulators, for example, the US EPA recommend the use of 5 years of National Weather Service (NWS) data or at least one year of site-specific data within modelling assessments. The AQMAU (UK Environment Agency Air Quality Modelling Assessment Unit) consider 5 years of hourly sequential data to be appropriate for assessments of industrial releases. This period is deemed sufficient to represent the temporal uncertainty associated with annual average and peak concentrations predicted for a point source emission. A recent release of new technical guidance for local authorities regarding air quality management (LAQM TG03, 2002) reviews a variety of studies regarding inter-annual variability and summarises with the suggestion that the use of 2 different met years should give no more than a 30% difference in model predictions of both annual and short-term percentiles. Site specific meteorological data is used

infrequently by the UK Gaussian dispersion modelling community due to industrial monitoring sites generally lacking a sufficient instrumentation to provide a full input dataset. The best practice for statistical binning of meteorological data and its portability have also been subjects of ADMLC research (Smith, 2000).

There is a continuous development of flow and turbulence characteristics during the passage of air over an emission site as the influence of previous land surfaces and topography takes effect. Air flow is also subject to the sometimes abrupt force of synoptic weather systems such as depressions and associated frontal activity. Emission sites located within the influence of a local coastline might also be likely to experience rapid and frequent changes in wind field and stability on both a vertical and horizontal scale. The magnitude of this variability will not be constant, changing on both a spatial and temporal scale. The most rapid changes will be associated with frontal systems that might alter wind direction and speed rapidly within a one hour period, however, for most synoptic conditions the passage of weather systems is sufficiently slow such that their contribution to the uncertainty of model predictions is limited.

The issue of representativity of parameters throughout the vertical height of the boundary layer has been addressed to a limited extent within AERMET. AERMET was designed to accept upper air measurements of temperature, wind speed and direction from radiosondes as well as hourly NWS data and/or site specific data, thus increasing the spatial representativity of input data. Currently, upper air data for the UK is not available for routine use in AERMET, hence providers of AERMOD user interfaces within the UK have incorporated an estimation tool into their model interface that calculates boundary layer parameters using Monin-Obukhov similarity theory. ADMS relies on the calculation of stability corrected vertical profiles using surface based measurements only, whilst R91 recommends using 10 m wind speed or correcting winds to 10 m values using a power law approximation for on axis calculations and does not account for the vertical variation in turbulence. Ideally, meteorological data should be recorded and stored as 10 minute average data for emergency purposes, such that the latest trends are identified prior to running model scenarios. Model users attempting to determine implications of emergency scenarios might also benefit from considering shorter model averaging times, of the order of 10 minutes, to capture these infrequent but significant events. Users of R91 based codes should carefully consider the vertical representativity of wind speed input as Lowles (2002) observed significantly improved performance when using wind speed at release height rather than the default 10 m input. Sites with elevated stacks (significantly above the standard wind speed measurement height of 10 m) may be subject to increased uncertainty than those with lower emissions, particularly in conditions where the stack height is significant compared to the boundary layer height, or where the boundary layer structure is stratified.

In reality, stratified flow is a common phenomena, and stack emissions may be exposed to multiple influences from weak jets and elevated minor inversion layers. These conditions cannot be resolved from surface measurements, neither

can remote radiosonde measurements resolve locally induced irregularities in boundary layer behaviour, highlighting a major limitation of Gaussian steady-state models. The use of dynamic modelling may present less modelling constraints, however, the uncertainty of the predictions may remain similar where the stochastic nature of turbulence is the dominant contributor to overall uncertainty.

The degree of representativity of met data from a remote location for use at an emission site is dependent upon the distance between locations, the similarity in terrain and the surface roughness of the surrounding area. Within the US-EPA guidance, the complexity of the terrain is considered with regard to stack top and plume height. Terrain is classed as 'simple' if below the stack top height, 'intermediate' if between the stack top and plume height and 'complex' if above the plume height. The UK Environment Agency guidance leaves the decision to consider the significance of terrain to the modeller, requiring a justification of the choice of modelling scenario. CERC (2001) recommend using terrain grid files in ADMS where the local gradients exceed 10%. Where the emission site is located in complex terrain, a terrain file can be incorporated into the models to assess flow fields over the model domain, which will in turn influence local meteorological parameters. Where terrain is sufficiently complex, and meteorological datasets sufficiently sparse, it might be most appropriate, where practicable, to set up a tower to record measurements close to the emission source at plume height. In reality, siting of instrumentation is usually a compromise between practicality and usefulness. A site evaluation should be undertaken to consider the most appropriate placement of equipment if that option is to be pursued. Alternatively, dynamic modelling may be required to create diagnostic wind fields over the area of interest.

3.1 Low wind speeds and calm conditions

Peak concentration events are often predicted to occur in light wind speed conditions. Treatment of light wind conditions within models should therefore be as realistic as possible to account for these occasions. Models typically have a limiting value of wind speed below which dispersion calculations are not completed. ADMS does not predict downwind concentrations for any hour in which the wind speed is below 0.75 m/s. AERMET uses a threshold of $2^{1/2}\sigma_{v\_min}$, equivalent to 0.28 m/s, below which no dispersion calculations will be performed (EPA, 1998). AERMET was designed to receive NWS met data as hourly input, in which the lowest reported wind speed is 1 m/s. This is in contrast to the Met Office datasets supplied in ADMS format, which include minimum values of 0.5 m/s. ADMS datasets can be converted within Lake's AERMET user interface to SAMSON format (similar to that of NWS) hourly data. Predictions using this data will be completed for all available datapoints unless wind speeds read below 0.28 m/s.

Using Ringway 2000 data as an example, ADMS will not predict concentrations for 413 hours of data (3 data gaps, 208 calm measurements where u=0, and

202 hours where wind speed records are 0.5 m/s). AERMOD will not calculate concentrations for the 3 data gaps and 208 hours of calm measurements, but will predict for hours where wind speeds are 0.5 m/s. Where site specific meteorological data are input to AERMET, a minimum threshold value of wind speed can be set, this should match the threshold start up speed of the site anemometer. The frequency of calms and the different treatment of low wind speeds between models highlight the issue that model assessments, for both standard and emergency purposes, should cautiously consider the treatment of low wind speed data and its impact on the reported predictions.

3.2 Data gaps

Data purchased from the Met Office and ADM Ltd is normally provided with greater than 99% coverage, with typically 2-3% calm conditions. The user is provided with no information regarding any data filling procedures (eg, interpolation between hours or concatenation of data from two sites) that may have been carried out prior to purchase. The US EPA recommend that meteorological datasets should be a minimum of 90% complete, allowing a maximum of 10% data to be substituted for use in the dispersion model. They recommend filling single hour gaps using persistence or interpolation techniques, and suggest that using these techniques for longer periods will result in 'moderate probable error', as will substituting data from a similar (surface-specific) site. 'High probable error' is expected from using a close but dissimilar location, monthly average, simulated or 'dummy' data. If met data is obtained on site, careful processing following current guidelines should be completed. When calculating peak percentile values the model's treatment of missing data should be acknowledged. For example, the 99.7^{th} percentile value might be taken as the 26^{th} highest value for a full year of data (8760 hrs) but would be the 25^{th} highest hour for 8300 hrs of data.

3.3 Atmospheric stability

R91 based Gaussian models use time of day, cloud cover and wind speed parameters to determine the influence of stability on dispersion using the simple discrete PG stability category scheme where Category A is extremely unstable and Category G is most stable. Environmental assessors required to determine the impacts of an accidental release can use nomograms from Clarke (1979) to estimate a stability category. A typical daytime accuracy of ±1 okta can result in predicted stability differing by ±1 stability category, although in low wind speeds and during night-time periods, situations may occur where predictions differ by ±2 categories.

Cloud cover is the most typical input used to calculate further boundary layer parameters in more modern Gaussian models such as ADMS and AERMOD, hence the models are similarly susceptible to the inaccuracies of cloud observations.

Friction velocity, u_*(m/s), represents the turbulent eddy velocity, and sensible heat flux, $F_{\theta 0}$ (W/m^2), represents the exchange of sensible heat over the ground surface, positive values representing net output from the ground, ie, typical in convective conditions. The Monin-Obukhov length, $L_{MO,}$ (m) represents the height at which equal magnitudes of turbulent kinetic energy are generated (or consumed) by convective and mechanical forces; this is dependent upon $-u_*^3/F_{\theta 0}$. In convective or unstable conditions L_{MO} is negative, with its magnitude being a measure of the height above the surface at which thermally induced turbulence, the convective motion, is more important than mechanical turbulence generated by friction at the surface. In stable conditions, L_{MO} is positive and gives a measure of the height above the surface where vertical turbulent motion is greatly inhibited by stratification. Steady state Gaussian models assume a single value of u_*^3, $F_{\theta 0}$ and L_{MO} as representative over the surface model domain for the length of averaging time (typically one hour). In reality, these parameters and vertical profiles of temperature, wind speed and direction will evolve continuously over space and time as they react to surface and synoptic influences.

3.4 Surface energy balance parameters

The net radiation balance at the surface is determined in part by the fraction of radiation reflected from the surface. This reflection coefficient, or albedo (r), is dependent upon surface characteristics and changes on a daily and seasonal scale. ADMS defaults to a constant value of 0.23 for albedo throughout the year, although it is possible to input hourly values where they are known. Using this default value may result in under-estimating the frequency and magnitude of stable conditions for sites that have significant periods of snow cover. The surface radiation balance is also strongly influenced by the latent heat flux which is dependent upon the amount of moisture present at the surface. The availability of moisture at the surface will alter significantly over space and time depending upon surface characteristics and the intermittency of precipitation. This will contribute to uncertainty in partitioning of heat flux between latent and sensible flux and will therefore add to uncertainties in sensible heat flux estimates. Although the influence of meteorological uncertainty on deposition predictions has not been considered in detail within this report, it is noted that the inherently large spatial and temporal variation of rainfall will lead to large uncertainty on deposition predictions over a model domain when using a spot measurement of precipitation.

ADMS uses the modified Priestley-Taylor parameter (α) to represent the fraction of surface moisture available for evaporation. This is defined by

$$\alpha = \frac{1 + \gamma/s}{1 + \beta}$$ **Equation 1**

where the psychrometric constant, $\gamma=c_p/\lambda$, with λ being the specific latent heat of vaporisation of water, c_p the specific heat capacity of water, s the rate of change of saturation specific humidity with temperature, and β is the Bowen ratio, the ratio of sensible to latent heat flux. A default value of $\alpha=1$ ($\beta=0.6$), typical for moist grassland, is used within ADMS which may under-estimate moisture availability over nearby bodies of water or after prolonged periods of precipitation (particularly over areas susceptible to flooding) and over-estimate availability during dry conditions. This could lead to corresponding significant over and under prediction of sensible heat flux. The AERMET user is requested to specify a surface characteristic for the emission site, eg, cultivated grassland, for which seasonal values of albedo, Bowen ratio and surface roughness, z_0 are then provided. Surface characteristics can be input on a sector based level, increasing the spatial resolution of these parameters beyond that of single input default values in ADMS. The influence of albedo and surface moisture balance on dispersion predictions is investigated within sections 6 and 7 of the report.

3.5 Surface roughness

Roughness length, z_0, represents the aerodynamic effects of surface friction and is physically defined as the height at which the extrapolated surface layer formula (eg, log law in neutral) goes to zero. This value is an important parameter used by meteorological pre-processors to interpret the vertical profile of wind speed and estimate friction velocities which are in turn used to define heat fluxes and turbulence level. Typically a single value of z_0 is input to represent the emission site in ADMS and R91 models, with ADMS offering the option of inputting an additional value for the met site where it is considered 'non-representative' of the emission site in question. It is also possible to create a z_0 grid over the ADMS model domain, although it is believed that few users utilise this capability for routine assessments. Use of a z_0 grid has the additional advantage of determining the influence of surface roughness on boundary layer structure both up and downwind of the source. Seasonal and sectoral values are assigned to the emission site within AERMET based upon the user's choice of surface characteristics. Roughness length at the meteorological data site is determined from flagging the site as 'urban' or 'rural'. It is also possible to input hourly values of z_0 to AERMET through the meteorological data file.

Roughness length will vary in space and time during the passage of a plume from an emission point, depending upon the fetch over which the air has previously travelled. A detailed study to quantify the influence of using single value z_0, sector specific or grid level values is beyond the scope of this document, however interested readers are directed towards Hanna & Britter (2002) for further recommendations on appropriate roughness lengths for complex locations. More complex treatment of roughness length could potentially add significant financial and time constraints to assessments, if for example, a roughness length grid was deemed necessary. In practice, individual sites will need to determine whether or not this is necessary for their requirements.

4 TREATMENT OF METEOROLOGICAL INPUT WITHIN ADMS AND AERMOD

4.1 Meteorology

One of the major advances of ADMS and AERMOD, compared to the models they were developed to replace (R91, ISC3), is in the treatment of the Planetary Boundary Layer (PBL). The growth and structure of the PBL is driven by fluxes of heat and momentum, which in turn depend upon local surface effects such as the surface roughness, reflectivity and moisture levels.

ISC3 and similar 'older generation' Gaussian models, such as R91, are based on Pasquill-Gifford stability categories. The stability of the atmosphere is divided into generally seven discrete regions (Pasquill-Gifford stability categories A to G) dependent upon wind speed and surface heat flux. Dispersion characteristics are then defined for each category. Thus, a slight variation in meteorological conditions can result in a change in stability category and consequently significant variation in model concentration predictions.

The so-called 'new generation' models, such as AERMOD and ADMS, characterise the boundary layer structure using continuous parameters such as the boundary layer height, h, and the Monin-Obukhov length scale, L_{MO}. Similarity profile relationships are used to calculate the boundary layer structure in terms of two variables, z/L_{MO} and z/h, where z is vertical height. This allows for the variation of boundary layer properties with height, a crucial difference from the Pasquill-Gifford formulation in which boundary layer properties only vary discretely with stability category. It is difficult to make exact comparison between the two schemes, as the Pasquill-Gifford categories are not a simple function of z/L_{MO}, particularly under stable meteorological conditions (CERC, 2001).

While AERMOD and ADMS both use equivalent concepts derived from the same meteorological research base in determining the stability characteristics of the PBL flow, the methods and parameterisations used do vary. Hall et al (2000) reported significant variations, factor of 2 or 3, in the predicted L_{MO} and h between the ADMS and AERMOD meteorological pre-processors using selected single meteorological conditions from hourly sequential meteorological data collected at Lyneham, UK, during 1995.

The estimation of the sensible heat flux, $F_{\theta 0,}$ is critical in determining both L_{MO} and h. In both models the boundary layer depth in unstable conditions is determined from the boundary layer's past history, growing as a result of the daytime sensible heat flux. However, the prediction of $F_{\theta 0}$ can have a large uncertainty resulting from the estimation of variables in its formulation, primarily from the estimation of the available surface moisture which determines the partitioning between latent and sensible heat flux. Thus, both L_{MO} and h depend upon variables that are not routinely determined, and are therefore susceptible to higher uncertainty.

Generally, the differences are not as serious as might be first thought, with the 'new generation' models being a significant improvement on the 'older generation' models due to their ability to incorporate variations in PBL characteristics with height. However, for elevated or buoyant sources estimation of the boundary layer height can be critical, with both the new and older generation models using h to determine how much of a plume penetrates the boundary layer and how much remains within the boundary layer, in addition to placing a limit on the vertical spread.

In their response to the report by Hall et al (2000) the developers of ADMS commented in relation to these variations: "In our view the differences are not surprising and reflect real uncertainties in predicting surface heat flux and boundary layer depth." (Carruthers et al, 2001). While reducing the uncertainty in predicting such critical parameters would be desirable, a degree of uncertainty exists in the data used for developing the models as well as in the estimation of the model input parameters. Thus uncertainty in these parameters is unlikely to reduce below certain levels.

It is not the intention of the authors to determine whether one model outperforms the other. Even an extremely rigorous investigation into the performance of the meteorological pre-processors of both ADMS and AERMOD is unlikely to determine most realistic performance as it would probably be impossible to obtain a suitably extensive and reliable data set on which to base such work. Thus, in looking at the processes of both models it is currently only possible to investigate the disparity between the models and the resulting differences in the final dispersion predictions. In doing this we consider Version 3.1 of ADMS (CERC, 2001) and Version 02222 of AERMOD (Cimorelli et al, 2002). It should be noted that as this latter document was not available until well after the commencement of this project, an earlier document (Cimorelli et al, 1998) was relied upon for much of the model technical detail. Discussions and conclusions within this report are not altered by the publication of the more recent AERMOD user guide.

4.2 Meteorological pre-processors

Both AERMOD and ADMS employ meteorological pre-processors whose role is to determine meteorological parameters necessary for estimating profiles of wind, turbulence and temperature from standard meteorological measurements. The standard meteorological parameters taken as input do differ, although both pre-processors currently require a minimum of:

- wind velocity at a reference height, u_z,
- wind direction at a reference height, ϕ_z,
- temperature (Dry Bulb) at a reference height, T_z, (required in AERMOD but not essential in ADMS) and

- cloud cover, Cl, (or solar radiation, $F_{\theta 0}$, or $1/L_{MO}$ can be used as alternatives within ADMS).

The meteorological pre-processors also require surface parameters such as surface roughness, z_0, albedo and either a Bowen ratio or a modified Priestley-Taylor parameter in conjunction with location and time information. Originally, AERMET, also required a pre-dawn upper air sounding. However, due to the limited availability of such data, except in North America, a boundary layer height estimation method is now incorporated into the proprietary user interfaces developed to enhance the operation of AERMOD. The interface used in this project was that developed by Lakes Environmental (Thé et al, 2000) which in unstable conditions uses a boundary layer height estimation technique adapted from Thomson (1992, 2000) which was developed for ADMS (Thé et al, 2001).

The surface parameters provided by the meteorological pre-processors, to the boundary layer structure algorithms, also differ, although the main boundary layer parameters, listed below, are common to both pre-processors:

- Monin Obukhov Length, L_{MO},
- Friction velocity, u_*,
- Surface roughness length, z_0, (input directly)
- Sensible heat flux, $F_{\theta 0,}$
- Convective velocity scale, w_*. and
- Boundary layer heights, h,

(**NB**: AERMET outputs estimates of both the convective, $h_{ic,}$ and mechanical, $h_{im,}$ mixed layer heights).

The ADMS meteorological pre-processor output includes all measured inputs, plus additional near surface parameters of specific humidity and latent heat flux. The maximum turning of the wind with height, the temperature step across the elevated inversion and the buoyancy frequency and relative humidity lapse rate above the boundary layer are also estimated by the ADMS meteorological pre-processor.

Assuming the minimum meteorological input data listed above (ie, u_z, ϕ_z, T_z and Cl), which are generally standard in UK, the overall approach taken by the two pre-processors in parameterising the boundary layer is broadly similar, although, as with the input and output data there are subtle differences. Both use the solar angle, determined from time of day and time of year, cloud cover and albedo, to estimate the net radiation. If the net radiation is positive, the PBL is defined as convective, with both using energy balance principles to estimate the sensible heat flux, however, the equations for estimating $F_{\theta 0}$ do differ slightly. AERMET uses the equation of Oke (1978) while ADMS uses the parameterisation of Holtslag and Van Ulden (1983). The parameterisations differ by the amount of

20α, where α is the modified Priestley-Taylor parameter used in ADMS. Using the ADMS default value of α=1, this suggests AERMET will give sensible heat flux estimates 20 W/m^2 higher than those predicted by ADMS. While this difference is generally of little significance, when the net radiation is low this amount can be a substantial proportion of the total sensible heat flux. The difference is likely to be most significant in the hours near dawn and dusk or highly overcast conditions when the sensible heat flux is low. It is possible one pre-processor may classify the stability as unstable while the other could give a stable classification.

Under convective conditions both models use the sensible heat flux ($F_{\theta 0}$) estimation to compute u_* and L_{MO}, based on the methods of Panofsky and Dutton (1984). As u_* and L_{MO} are interdependent this requires an iterative procedure. Both models also use $F_{\theta 0}$, in conjunction with the potential temperature gradient, to calculate the time evolution of the convective boundary layer throughout the day, and thus the estimation of the boundary layer height, h. AERMOD also calculates the boundary layer height due to mechanical turbulence, and when it is greater than that due to thermal convection (under weak convective conditions) it is used in preference. ADMS tries to incorporate the affect of mechanical turbulence directly into its boundary layer growth formulae.

The original AERMOD method for convective conditions is based on simple one-dimensional energy budget principles, which uses the early morning potential temperature sounding in conjunction with the time varying sensible heat flux. However, this method is not suitable for use in the UK as routinely measured potential temperature sounding data are not available. As mentioned above, to enable more global use, a boundary layer height estimation method is now incorporated into the proprietary user interfaces developed to enhance the operation of AERMOD. A comparison between the use of sounding data and the estimation method within the Lakes Environmental version of AERMOD (Thé et al, 2001) indicated the estimation method predicted the height of the boundary layer to be larger by nearly 50% on average. However, for stacks up to 60 m this was found to have only a minor influence on the mean and peak concentration predictions. For taller stacks and highly buoyant plumes that may rise to the top of the boundary layer or penetrate the elevated inversion, the differences may become more significant.

When the net radiation is negative the PBL is defined as stable. Under stable conditions neither model uses energy budget considerations, preferring instead to use semi-empirical methods for estimating u_* and L_{MO}. The eddy temperature θ_*, is estimated from the cloud cover following Van Ulden and Holtslag (1985). In stable and neutral boundary layers, in which only mechanically generated turbulence exists, both ADMS and AERMOD use u_*, L_{MO} and the Coriolis parameter, f, to estimate the boundary layer height (Nieuwstadt, 1981; Zilitinkevich, 1972; Venkatram, 1980). To prevent extreme values occurring, both models have upper limits of 4000 m on the boundary layer height, while ADMS also has a lower limit of 50 m.

4.3 Boundary layer structure calculations

Following the estimation of the primary boundary layer parameters within the meteorological pre-processors, as described above, both models then proceed to use similarity relationships, in conjunction with the boundary layer parameters, to compute vertical profiles of:

- mean wind speed, u(z),
- potential temperature, $\theta(z)$, and
- vertical and horizontal turbulence components, $\sigma_w(z)$ and $\sigma_v(z)$.

Both ADMS and AERMOD use forms of stability correction functions based on Panofsky and Dutton (1984) in convective conditions. In stable conditions AERMOD uses those of Van Ulden and Holtslag (1985) while ADMS uses Holtslag and de Bruin (1988). ADMS utilises three sets of turbulence parameterisation schemes as described in Hunt et al (1988) (an internal CERC report) depending upon h/L_{MO}. Changes in the parameterisations cause discontinuities at the boundaries of the defined stability regions, while AERMOD uses a continuous turbulence parameterisation scheme throughout the stability range (Cimorelli et al, 2002).

One of the primary differences between the two models in determining the structure of the boundary layer is the ability of AERMOD to consider on-site measurements in addition to the standard meteorological data. Although several UK industrial sectors have a growing requirement to obtain site specific meteorological data to fulfil environmental regulations, at present it is understood that these data are not routinely incorporated into dispersion model input, except for emergency purposes, perhaps due to data archiving and processing difficulties. Thus, the inclusion of site specific data is not the standard mode of operation in the UK, even for large industrial sites.

4.4 Plume dispersion

New generation atmospheric dispersion models, such as AERMOD and ADMS, are also often referred to as modified Gaussian models. Like the older generation models (ISC3 and R91) they generally use a simple Gaussian form to describe the plume spread and determine concentrations. However, the application of the Gaussian model and the determination of the dispersion coefficients is more sophisticated in the new generation models.

The older generation Gaussian dispersion models were very simplistic, not properly accounting for the physics of real atmospheric flows and dispersion phenomena. They assumed the plume travelled horizontally, with the lateral and vertical spread determined solely by the atmospheric stability class in a step function. Their only additional feature was the inclusion of the reflection term to account for the plume's interaction with the ground and inversion layer. Features

such as the variation of turbulence with height and within an atmospheric stability regime are not addressed in such models. More complicated processes such as the effect of complex terrain, the non-Gaussian nature of convective plumes, plume lofting and fumigation of elevated plumes within convective boundary layer (CBL) flows are not routinely considered within R91 based models.

An area in which the new generation atmospheric dispersion models vary significantly from the traditional Gaussian models, is in their approach to dispersion in the CBL. In the neutral and stable boundary layers (NBL and SBL) the distribution of the turbulent velocities is Gaussian in nature, ie, normally distributed about the mean, with, for the vertical velocity component, updrafts and downdrafts occurring for equivalent amounts of time. However, the vertical velocity distribution in a CBL is not Gaussian in nature. Downdrafts are more prevalent and with correspondingly weaker velocities than the less frequent updrafts of higher velocity to ensure mass continuity. In addition, convective circulations within the CBL fill the space available, with the dominant scale of the turbulence being of the order of the depth of the boundary layer. Thus large eddy time scales of the order 10 to 20 minutes are typical in strongly convective conditions.

This has a significant and unusual effect on the dispersion of plumes released into the CBL. The point of maximum concentration of a passive plume released close to the surface lifts from the ground and gives rise to an elevated locus of maximum concentration. In contrast the point of maximum concentration of a passive plume released from an elevated source will descend until it impinges on the ground, where it will remain for a considerable time before it ascends in a manner similar to a surface source. This behaviour is contrary to the traditional view of a Gaussian plume moving downwind and spreading vertically and laterally from a fixed height, and can produce significantly higher concentrations at the surface than predicted by standard Gaussian plume models. Another complication is that due to the large time scales of the convective motions, a mean hourly concentration, as generally predicted by atmospheric dispersion models, is often not an appropriate time scale to obtain a stationary average. In practice, under strongly convective conditions hourly average concentrations will vary significantly, with a minimum period of several hours required to obtain close to a stationary average.

AERMOD's dispersion algorithms for the CBL are based on Gifford's (1959) meandering plume concept in which a small 'instantaneous' plume wanders due to the large eddies in a turbulent flow. The instantaneous plume is assumed to have a Gaussian concentration distribution about its randomly varying centreline. The mean, or average, concentration is calculated by summing the concentrations due to all the random centreline displacements computed from the probability density functions (pdfs) of the vertical and lateral velocities.

Similarly ADMS uses a simple Gaussian formulation for stable and neutral boundary layer conditions. However, for the CBL, ADMS uses a non-Gaussian or skewed vertical concentration distribution, which ensures that for elevated

sources the locus of maximum concentration descends as the plume moves downwind. In a simple trial the locus of maximum concentration did not appear to rise again after it had reached the ground, although it is claimed it can within CERC (2001).

Like R91 and ISC, ADMS and AERMOD are steady-state plume models designed to apply to releases and meteorological conditions that can be assumed steady over individual modelling periods, generally 1 hour. However, within each period AERMOD can simulate five different plume types depending on the atmospheric stability and the location of the plume in and above the boundary layer as summarised below:

- **direct plume** –remains within the mixed layer initially.
- **indirect plume** – rises and tends to initially loft near the top of the mixed layer before mixing.
- **penetrated plume** – released into the mixed layer but rises to penetrate into the elevated inversion above the mixed layer.
- **injected plume** – where the release height is greater than the inversion height, with the plume released directly into the stable elevated inversion before being entrained into the mixed layer.
- **stable plume** – modelled with the familiar horizontal and vertical Gaussian distribution.

The first four refer to plumes released in unstable surface conditions, while the fifth, as it states, is for stable conditions.

ADMS generally only considers the direct and indirect plumes in the CBL, although if a penetrated plume is allowed to escape the boundary layer it is not re-entrained. Apart from in the specific coastline module, ADMS does not model the re-entrainment of releases that are injected or penetrate above the elevated inversion, back into the mixed layer under unstable atmospheric conditions. For very tall stacks and low boundary layer height convective conditions, this may result in AERMOD predicting higher ground level concentrations than ADMS.

4.4.1 Dispersion parameter estimation

In R91 the lateral and vertical dispersion parameters (σ_y and σ_z respectively) were related directly to the stability category of the atmosphere in a step function. No account of variations resulting from differing plume heights or turbulence levels within stability categories are taken, neither are local turbulence enhancements resulting from buildings or roughness variations considered in most older generation models. New generation models, such as ADMS and AERMOD, use more sophisticated routines for determining the concentration distributions. Dispersion is directly related to the turbulence level and scale of the flow field in which the plume is travelling.

AERMOD incorporates contributions from the individual sources of turbulence resulting from the atmospheric ambient turbulence, plume buoyancy induced turbulence and enhanced turbulence resulting from building wake effects. The total dispersion coefficients, σ_y and σ_z, are calculated from a general expression of the form (Pasquill and Smith, 1983):

$$\sigma^2_{y,z} = \sigma^2_{ya,za} + \sigma^2_{yb,zb} + \sigma^2_{yd,zd} \qquad \textbf{Equation 2}$$

where, $\sigma_{y,z}$ is the total dispersion in either the crosswind, y, or vertical, z, direction, and σ_a, σ_b and σ_d are the dispersion coefficient contributions from the ambient atmospheric turbulence, buoyancy induced turbulence and building downwash induced turbulence respectively. In the more recent version of AERMOD, which incorporates the PRIME buildings algorithms, building downwash induced turbulence is treated separately. Similar ideas of incorporating different individual contributions to dispersion are employed by ADMS, although, as with the models throughout, the methodologies differ in their more detailed application. Although none of the individual contributions to the total dispersion should be ignored, it seems more appropriate in the context of the current work to concentrate on the contributions that result from atmospheric flow and turbulence.

Turbulence levels within the atmospheric boundary layer are known to vary significantly with height, with the strongest variation near the earth's surface and under stable and neutral conditions. As a result, the dispersion induced by the ambient turbulence also varies with height. With the ability to estimate the vertical structure of the PBL, AERMOD and ADMS are able to utilise an applicable turbulence level at the plume height and atmospheric stability when estimating spread parameters for use in the dispersion equations. Calculation of the dispersion coefficients due to ambient atmospheric turbulence generally follows a statistical theory equation of the form:

$$\sigma_{y,z} = \sigma_{v,w} t(1+fn_{y,z}(t/T))^{-p} \qquad \textbf{Equation 3}$$

Here, $\sigma_{v,w}$ are the lateral and vertical turbulence, t $(=x/u)$ is the mean travel time, T a relevant time scale dependent upon the source and atmospheric conditions and p is generally equal to 0.5. This is a somewhat simplified general form of the equations used to calculate the dispersion parameters from the state of the atmosphere, particularly for vertical dispersion in the CBL where a bi-Gaussian approach further complicates the formulation.

The approach to determining applicable parameters, such as turbulence level, wind speed, etc, for use within the dispersion coefficient equations differs significantly between the two models. ADMS typically uses values estimated from the boundary layer structure parameterisation at the mean plume height.

AERMOD uses a more complicated approach based on the concept that the primary region of importance is the one through which the plume travels directly from the source to the receptor. Thus, effective values of the boundary layer parameters are determined by averaging over the region between the plume centroid height and the receptor height.

Under stable and neutral atmospheric conditions, ADMS and AERMOD both use parameterisations based on statistical theory to relate the lateral and vertical dispersion parameters (σ_y and σ_z) to atmosphere turbulence levels (σ_v and σ_w).

As was the case in R91, the ADMS parameterisation is based upon a lateral turbulence-induced dispersion component, σ_{yt}, and a wind direction unsteadiness component, σ_{yw}, following Moore (1976). Thus the total lateral dispersion due to atmospheric flow and turbulence is given by $\sigma_y^2 = \sigma_{yt}^2 + \sigma_{yw}^2$. The directional unsteadiness component, σ_{yw}, is proportional to σ_θ, the standard deviation of the horizontal wind direction. In principle, σ_θ should be determined from 3-minute average wind direction measurements over the modelling period of generally one hour in ADMS, although, typically σ_θ based on 10-minute averages or a parameterisation based on u_{10m} is used. The use of σ_θ based on a 10-minute average would be expected to give slightly lower σ_{yw} and thus dispersion than σ_θ based on a 3-minute average.

Under stable conditions AERMOD includes the effect of the slow lateral plume shift due to shifting wind directions during the modelling period using a meandering plume model as opposed to a direct measurement or estimate of σ_θ.

In determining the turbulence-induced lateral dispersion component, σ_{yt}, from σ_v, both models use parameterisations based on interpolation forms of Taylor's (1921) small and large travel time dispersion relations. Again, the parameterisations differ slightly, with that used in AERMOD being empirically tuned with the full Prairie Grass (Barad, 1958) data set to overcome problems observed with the treatment of lateral dispersion for near surface releases. It is not immediately clear as to how the ADMS parameterisation has developed, with no attribution given in either the User Guide (CERC, 2001) or the Technical Specifications (Carruthers et al, 2000).

In estimating the vertical dispersion parameter, σ_z, under stable or neutral atmospheric conditions both AERMOD and ADMS use different solutions for surface (where shear plays a significant role) and elevated dispersion in conjunction with transitional smoothing functions. Although the basic approach is similar, the parameterisations used differ. For further information the reader is directed to Venkatram (1992), Weil (1985) and Hunt (1985).

In unstable conditions the turbulent component of lateral dispersion, σ_{yt}, is derived from combining both convectively and mechanically generated turbulence. In AERMOD both turbulence components are incorporated directly in the estimate of the lateral turbulence, σ_v, with the final form of the σ_y parameterisation obtained from an empirical fit to the Prairie Grass measurements. An empirical relation is also used to account for variations in release height from that of the Prairie Grass experiments. ADMS independently

calculates a convective dispersion parameter, based on the convective turbulence and the convective velocity and a mechanical dispersion parameter, based on shear-generated turbulence and the shear velocity. The final turbulent lateral dispersion parameter is determined from the combined influence.

In AERMOD the turbulent component of the vertical dispersion, σ_{zt}, during convective conditions is composed of an elevated and surface portion to distinguish between near surface and elevated releases. However, the surface portion, based on Venkatram (1992), contributes to only 10% of the boundary layer height. Thus, only the elevated portion of vertical turbulence is considered throughout the mixed layer region of the boundary layer. A bi-Gaussian pdf formulation, following Weil et al (1997), is used to account for the skewed nature of the vertical turbulence and thus dispersion in the CBL.

ADMS also uses a non-Gaussian pdf to describe the convective component of turbulent vertical dispersion in the CBL. The ADMS formulation is based on the vertical velocity distribution described by Hunt et al (1988). As the form of the ADMS Gaussian plume formulation for the convective boundary layer is not the same as that of the neutral or stable boundary layers, a transitional smoothing formulation is used between neutral and convective dispersion.

4.5 Summary

ADMS and AERMOD, the 'new generation' atmospheric dispersion models developed in the UK and US respectively, incorporate more up-to-date planetary boundary layer and dispersion concepts, with both models bringing improvements over older dispersion models such as R91 and ISC, particularly in relation to:

- the continuous characterisation of the planetary boundary layer through surface fluxes,
- the characterisation of the dispersion parameters in terms of the local turbulence,
- the use of convective scaling and bi-Gaussian vertical dispersion in unstable conditions.

The 'new generation' models were essentially developed from the same research and theory base, although the application of different parameterisations and assumptions results in a number of differences between them. This work has attempted to highlight both the similarities and differences in meteorological modelling approach together with the potential impact on dispersion calculations. The complexity of the model formulations makes it virtually impossible to quantify the impact of the subtle differences on every processed parameter without undertaking an extremely rigorous investigation. Appropriately reliable data enabling such an undertaking is scarce with much of what is available already used in the model development. Section 6 identifies specific occasions

where ADMS and AERMOD model predictions differ significantly due to critical assumptions and differences in model approach highlighted in this section.

5 EVALUATION OF ALTERNATIVE METHODS FOR ESTIMATING BOUNDARY LAYER PARAMETERS FOR DISPERSION MODELS

The majority of routine modelling assessments using ADMS or AERMOD are completed using meteorological data obtained from suppliers such as the Met Office and ADM Ltd. There are few independent sites at which suitable and sufficient measurements are recorded to be used as input to second generation dispersion models. Where on-site data are available, careful consideration should be made of the weather station position with respect to local obstructions to air flow such as buildings and changes in fetch and surface characteristics.

Where on site measurements are used to estimate boundary layer stability, cloud cover or solar radiation is most frequently used to estimate either Pasquill Gifford stability categories or boundary layer parameters such as Monin Obukhov length. Solar radiation measurements give an estimate of the total energy input into the surface energy balance. Assumptions can then be made (within the model pre-processors) of the partitioning between the various loss pathways to derive the emissions of radiation from the surface in the form of sensible heat. This method is of course of little use during overnight periods when the surface energy balance is no longer driven by solar inputs.

Alternative methods, that can be used to directly estimate friction velocities, sensible heat fluxes and therefore Monin-Obukhov lengths, include the use of eddy correlation techniques, using sonic anemometry, and the application of flux-gradient relationships to measured wind speed and temperature profiles. In order that the results of these measurements can be used in dispersion modelling, assumptions of homogeneity in the upwind (fluxes are constant across the upwind fetch) and vertical (measurements are made in a constant flux layer) must be made.

This section reviews the use and uncertainty of these alternative techniques for estimating boundary layer parameters. The issue of measurement uncertainty and uncertainty due to sensor configuration, when using flux-gradient methods is considered in detail. These uncertainties are propagated through the ADMS 3.1 atmospheric dispersion model to investigate their contribution to uncertainty in the prediction of air concentrations. Appendix A provides further background to the flux profile method that has been employed within this section. The use of NWP data as a further alternative data source is also evaluated in Section 5.3.

5.1 Eddy-correlation method

The eddy-correlation method estimates surface sensible heat fluxes directly from turbulent fluctuations in vertical wind speed (w') and the corresponding fluctuations in air temperature (T'). Turbulent fluctuations in the horizontal and lateral wind velocities are denoted as u' and v' and are used to calculate the friction velocity. The sensible heat flux and friction velocity can be determined from the time-averages of these correlated fluctuations.

$$F_{\theta 0} = \rho_a \, C_p \overline{w'T'} \quad , \quad u_* = [(\overline{u'w'})^2 + (\overline{v'w'})^2]^{1/4} \qquad \textbf{Equation 4, 5}$$

The validity of the above relationships depends on the correct alignment of the sonic anemometer and the selection of a suitably flat site to ensure that w_{mean} = 0. Tilt errors have been found by Dyer (1981) to cause an error of approximately 14 % in u_* per degree. In order to minimise the impact of these error terms 2 or 3 dimensional co-ordinate rotations are often performed. Zeller (1993) estimated that in ideal conditions the error in heat fluxes derived using sonic anemometers was of the order of 14 %. This compares with estimates of 20% uncertainty in the derivation of fluxes over extensive Kansas wheat fields by Haugen et al (1971).

5.2 Flux-gradient method

Friction velocities, sensible heat fluxes and thus Monin Obukhov lengths can also be estimated from measurements of air temperature and wind speed at a number of vertical heights using flux-gradient relationships. A commonly used set of equations are:

$$\text{Friction velocity} = u_* = k \frac{\partial \, u \, \{z - d\}}{\partial \, [\ln(z - d) + \Psi_M]} \qquad \textbf{Equation 6}$$

$$\text{Eddy temperature} = \theta_* = k \frac{\partial \, \theta \, \{z - d\}}{\partial \, [\ln(z - d) + \Psi_H]} \qquad \textbf{Equation 7}$$

$$\text{Sensible heat flux} = F_{\theta 0} = -\rho_a \, C_p u_* \, \theta_* \qquad \textbf{Equation 8}$$

$$\text{Monin Obukhov length} = L_{MO} = -\frac{\rho_a \, C_p (\theta + 273) \, {u_*}^3}{k \, g \, F_{\theta 0}} \qquad \textbf{Equation 9}$$

Where, θ is the potential temperature in degrees Celsius and d is the height of the aerodynamic zero plane.Ψ_H and Ψ_M are semi-empirical stability correction

factors for heat and momentum that have been integrated with respect to height. Errors in the estimation of surface fluxes using the flux-gradient method range between 10-30% (Baldocchi et al, 1988) and are largely due to the empiricism of the factors Ψ_H and Ψ_M. Consequently errors in the determination of boundary layer parameters using these methods are expected to be highest during periods of stability extremes.

A further limitation of the aerodynamic gradient method can occur due to the violation of the constant flux layer assumption. Horst and Wiel (1994) found that fetch to height ratios, representing the uniform upwind distance required for a constant flux layer to extend to a specific measurement height, can be 1000:1 during stable conditions (ie, a measurement at a height of 1 m requires a uniform upwind fetch of 1 km) and up to 200:1 for neutral conditions. As a result, Horst and Wiel (1994) showed that micrometeorological measurements of heat fluxes made using the rule-of-thumb fetch to height ratio of 100:1 could be in error by 20 % for neutral conditions and more than 50 % for stable conditions.

5.2.1 Assessment of the errors in applying flux gradient methods

Flux-gradient methods can be employed in a variety of different configurations, though must use at least two measurement heights of temperature. The accuracy of the estimates of heat flux may be expected to be greater when a larger number of sensors are used, due to the results being less sensitive to the errors in individual measurements. Furthermore, the measurement accuracy in the determination of wind speeds and temperatures also can have a significant influence on the predictions of the method. The accuracy of typical measurements of temperature and wind speed were discussed in Section 2.

Monte Carlo techniques enable the propagation of errors through sets of equations by randomly resampling input data that have been assigned probability distributions. In order to assess the errors that would be likely to occur when using flux-gradient techniques to interpret vertical profiles of wind speed and temperature, Monte Carlo methods were used to propagate errors in these scalars through a set of flux-gradient equations.

Four scenarios were used to assess errors due to sensor configuration and measurement uncertainty. The sensor configurations that were investigated represented the use of measurements at two heights (2 m and 10 m), as often used for providing data for atmospheric dispersion models; and also a more detailed four heights configuration (0.5 m, 0.75 m, 1.0 m & 2.0 m), as often used when conducting micrometeorological research.

The precision of the measurements of temperature and wind speed were defined as inputs to the Monte Carlo model using normal distributions with the mean set to the deterministic value and the range defined by the following error terms (expressed as the 95% confidence limits).

- Temperature: coarse +/- 0.1°C; fine +/- 0.02°C
- Wind speed: coarse +/- 5%; fine +/- 2%

Overall the four sensor precision and configuration scenarios that were used were:

- Scenario 1: Fine sensor precision, measurements made at 2 heights
- Scenario 2: Coarse sensor precision, measurements made at 2 heights
- Scenario 3: Fine sensor precision, measurements made at 4 heights
- Scenario 4: Coarse sensor precision, measurements made at 4 heights

As previously stated, the uncertainty in the estimation of heat fluxes and friction velocities using the flux gradient method was likely to vary with the prevailing meteorological conditions. Hence, wind speeds and temperatures at the above heights were reconstructed from values of $F_{\theta 0}$, u_* and θ_* for seven meteorological scenarios following the Pasquill stability classification system (A-G). These were determined from the Ringway meteorological dataset by processing the data through the meteorological pre-processor of ADMS 3.1 and banding the results into stability classes using the relationship between Monin Obukhov length and stability class derived by Golder (1972). The results of this analysis are shown in Table 2. The values of $F_{\theta 0}$ and u_* that were derived for each stability class, shown in Table 2, were determined as the arithmetic averages of the hourly results. Appendix A details the methods used to reconstruct temperatures and wind speeds from these data.

The Monte Carlo model was run with 5000 different sets of randomly sampled input data (temperatures and wind speeds) for each of the above scenarios. The results are shown in Table 3. Overall Table 3 shows that the flux gradient method provided reasonably consistent estimates of $F_{\theta 0}$ and u_* when comparing the different sensor precision and configuration scenarios. However, during strongly stable conditions (category G) the median friction velocities and heat fluxes output using the 2 point profiles were significantly different from the expected values from Table 2 or the more detailed 4 point profiles. This illustrates that users of the method should be aware that during strongly stable conditions the flux-gradient method can produce spurious results if insufficient data are available to resolve the variations in temperature and wind speed with height.

Table 3 also shows that friction velocities had narrower uncertainty bounds, as shown by the percentile ranges and the coefficients of variation, than the sensible heat fluxes. Sensible heat fluxes were mostly predicted to within 20 – 30% using the coarse precision instrumentation and to within 10% when fine precision instrumentation were simulated. The two stability classes where wider ranges were observed were categories D and G. The large range for category D reflects the very small values of heat flux, a good approximation of the limit of detection of the method, and the fact that fluxes could be either positive or negative in value. The range for category G, for the 4 point profiles, is likely to be due to the dominance of the stability correction terms for this class.

It should be noted that the above analysis only considered the error in estimating fluxes due to measurement uncertainty and did not consider other error terms that may be significant in a real-world situation. These errors may arise from sensor drift, from violations of the implicit assumptions of the method (such as the constant flux layer assumption), and from stochastic variability caused by turbulence in the atmosphere. An estimate of the overall errors in the determination of heat fluxes using on-site micrometeorological methods was made by Hill et al (2002). They compared eddy-correlation and flux-gradient measurements from a site close to the BNFL Sellafield complex. Overall, the coefficient of variation (CV), which is defined as the standard deviation divided by the mean, for the hourly sensible heat flux had a typical value of 0.4 (40%), much higher than observed in Table 3. This indicates that in a realistic situation measurement error may be only one of the contributors to the uncertainty in estimating boundary layer parameters.

An assessment was also made of the likely effect that the measurement errors in heat fluxes and friction velocities could have on the determination of air concentrations using the ADMS 3.1 dispersion model. The assessment was conducted for a 40 m high stack and evaluated air concentrations at 6 downwind distances. A set of 5000 probabilistic meteorological input data were run through the model, generated from the data discussed in the previous section. In order to reduce the duplication of data only data for the 4 point profiles are presented. The data for coarse precision instruments and fine precision instruments are shown in Tables 4 & 5 respectively.

The results in Table 4 show that the uncertainty in the model (expressed as the ratio of the 95^{th} percentile to the 5^{th} percentile) was relatively low for stability classes A-E at distances beyond 700 m downwind, ranging between 1.49 and 1.28. Uncertainties were higher at receptor positions close to the source for all stability classes except A. For category A the uncertainty in air concentrations was relatively constant with distance from the source. This was likely to be due to the plume being well mixed in the vertical in such convective conditions. Uncertainties were much larger for plumes released in Category F and G. This was likely to be due to the extreme sensitivity of ground level air concentrations on the vertical spread of the poorly mixed elevated plume.

The uncertainties in the predictions of the dispersion model, beyond 100 m, were much smaller when the measurement errors in the fine precision instrumentation were considered, being less than 1.10 (or 10%) for categories A-D beyond 100 m, as shown in Table 5. As found in Table 4, uncertainties were higher close to the stack, especially for stability categories D, E and F and for category G the plume was predicted to remain almost completely insulated from the surface. At distances of 700 m and beyond, the highest air concentrations (as the 50^{th} percentile) were associated with stability class E. The model predictions at 700 m downwind for class E also showed a relatively large uncertainty. The combination of high air concentrations and large uncertainty illustrates that particular care should be exercised when interpreting model predictions determined during such conditions.

5.3 Numerical weather prediction datasets

The use of on site meteorological measurements or representative observations from a remote location within dispersion models have been described in earlier sections. Output from a dynamic 3-D weather prediction model provides a further data source. Mirza et al (2002) reviewed the potential use of numerical weather prediction (NWP) datasets as input to dispersion models within their study completed for ADMLC. The Met Office continue to develop their Unified Model (UM) to predict global and regional (mesoscale) movement of weather systems in order to provide weather forecasts for a large range of customers. The mesoscale model assimilates observed data from around the UK, and includes the treatment of a number of important boundary layer processes. It has a horizontal grid resolution of 11 km and vertical resolution of 38 levels, with finer boundary layer resolution than the global configuration. Boundary layer parameters and vertical profiles of speed and temperature are derived within this NWP process.

Topographic forcing within the mesoscale model is limited by the grid scale, so that effects of topographic features on local surface flow may not be reproduced accurately. The NWP model was designed for forecasting over a much larger area than that typically considered within dispersion models and as such cannot be expected to exactly reproduce flow fields over local scale topography. It does, however, provide a representative picture of the average state of the atmosphere over the 11 km grid, rather that providing point specific data such as that from surface measurements.

At present, it is understood that the wind field, temperature, humidity, precipitation, cloud cover (at three heights), boundary layer height and surface heat flux are routinely extracted from the archive. These are processed to deliver an ADMS dataset including a total cloud cover value calculated using randomising overlap algorithms. The surface heat flux and boundary layer height are currently not provided to the customer. Other surface and boundary layer parameters and vertical profiles of wind and temperature are also output from the NWP process, however they are not routinely extracted from the archive. These include friction velocity, Monin Obukhov length, various roughness length scales and soil moisture values. The practicalities, time and expense of extracting all the desired parameters and profiles for dispersion modelling from the NWP archive systems would need to be determined by the Met Office themselves. If available, this data could be directly input to models such as ADMS and AERMOD potentially negating the requirement of the met pre-processors. It should be noted that this system would not be without problems of its own. Continual development of the NWP process by the Met Office will result in increasingly higher resolution of the grid, which may lead to difficulties in processing datasets from different grids to obtain the 5 years sequential data deemed sufficient for assessments by the Environment Agency in their guidance.

5.3.1 Comparison of NWP data and coastal site measurements and their impact on ADMS predictions

In order to promote further discussion on the validity and use of NWP data within dispersion models, Kidd (2002) compared meteorological measurements obtained at Sellafield, a West Cumbria coastal industrial site situated within the influence of Lake District fells to the East, with NWP data for the nearest grid location. The influence of these datasets on ADMS model predictions was then assessed. This study undertaken at Westlakes Research Institute identified that NWP data and site measurements of temperature, wind speed and precipitation displayed good agreement, both hour by hour and in distribution, with the observed data displaying more extreme conditions, eg, high wind speeds and precipitation events.

Figure 2 displays the windroses for the measured dataset, the dataset of the nearest NWP grid to the Sellafield site and Ringway data for 2000. Encouragingly, it can be seen in this instance that the NWP and site measured wind fields show fairly close agreement. The measured wind field displayed more variability in direction than that predicted by NWP, and the NWP did not reproduce the strong westerly conditions measured on site, thought to be due to the local coast influence, however the general trends are reproduced. Due to Sellafield's relatively remote location, Ringway, near Manchester, approximately 150 km from Sellafield is one of the closest Met Office sites from which data is available for use as dispersion model input. It is immediately apparent that the Ringway dataset does not represent local conditions around Sellafield as well as the NWP predictions. This is likely to be due to the large distance between sites and the influence of complex terrain and coastlines at the Sellafield site.

The choice of methods used to calculate boundary parameters (eg, using profile measurements to calculate values externally or inputting solar radiation or cloud cover and allowing ADMS to calculate values) led to significantly different estimates of boundary layer parameters.

Figure 3 displays the frequency of banded values of $F_{\theta 0}$ for a range of inputs. Comparisons of heat flux values estimated within the ADMS pre-processor using a variety of data sources (Ringway cloud cover, NWP cloud cover from two nearest sites, A and B, and site measured solar radiation data) show strong agreement between each other, particularly when compared to estimates calculated using the micro-meteorological flux profile method. Heat fluxes estimated by ADMS using site solar radiation measurements display an increased frequency in the –50 to –100 W/m^2 band (extremely stable conditions). This is thought to be associated with the limitations of using the solar radiation parameter during night time conditions, where the default value of 5 oktas cloud is assumed in the absence of cloud cover records.

The flux profile method calculates boundary layer parameters (eg, $F_{\theta 0}$ and L_{MO}) externally to ADMS. These can then be input to the ADMS pre-processor in a variety of configurations, to obtain estimates of further parameters such as boundary layer height, h. Sensible heat flux using direct estimates from the flux profile method results in more slightly stable conditions (negative $F_{\theta 0}$) than

slightly unstable, with the opposite effect predicted using L_{MO} as ADMS input to calculate sensible heat flux. Both the flux profile methods exhibit a significant increase in frequency of extreme unstable conditions. These results are consistent with boundary layer height estimates (Figure 4), where both flux profile input configurations ($F_{\theta 0}$ and L_{MO}) display a greater frequency of large h, associated with unstable conditions.

The effect on the overall predicted concentrations is more subtle, with the location of annual concentrations highly dependent upon the wind field (ie, independent of the met pre-processor but dependent upon the source of data). Short term concentrations and the magnitude of the annual concentration are highly influenced by wind speed and stability conditions, hence a mixture of effects from source data (wind speed) and processing of data (stability conditions) are combined.

5.4 Summary

Met Office sites providing sufficient (5 years hourly sequential) meteorological data for use in dispersion models are not able to fully represent locations over the whole of the UK. In particular coastal and mountainous areas are poorly represented and industrial sites at these locations, such as Sellafield, must resort to using remote data from a distant Met Office site (potentially non-representative), site observations (sensitive to choice of measurements and method used to estimate boundary layer parameters) or NWP data (complete UK coverage but unable to resolve small scale local topography effects).

Use of high precision instrumentation for the flux-gradient method should result in estimates of boundary layer parameters that would be comparable to the quality of data produced by sonic anemometers. Methodological problems can, however, limit the usefulness of flux-gradient relationships during periods of strong stability, particularly if the resolution of the vertical gradients (number of sensors) is low. The use of sonic anemometry for commercial purposes remains severely limited, however, we consider careful deployment and maintenance of equipment by competent personnel can provide data of a suitable quality for use in dispersion model assessments. NWP datasets appear to provide a promising alternative to the current situation of searching for the most 'representative' data available. Uncertainty attached to these datasets may actually reduce the overall uncertainty of the dispersion modelling process, if the NWP model output is considered to more closely represent real and model domain average boundary layer conditions than those output from the dispersion model meteorological pre-processors using spot measurements from one location.

Measurement error is likely to be often only a minor source of uncertainty as differences between processing methods and the likely violations of assumptions of stationarity, upwind homogeneity and a constant flux layer have been shown from field experiments at the Sellafield site to have more significant influences on model predictions.

Site measurements are likely to appeal to the emergency assessor who may need only to input a single accurate and immediate value of the current wind field and stability in order to fulfil his requirements. The option of obtaining hourly sequential NWP data is likely to be more appealing to the standard industry operator, who may regard the installation of a met station as excessive. Providing it is acceptable to the regulator, the operator is likely to consider the use of NWP in a similar manner to that of measured datasets, where the purchase of met data from either the Met Office or a WMO data supplier is routine for completing modelling assessments. The price of NWP data at present is similar to that of measured data, however, the effect on prices is unknown if further parameters are requested from the archive.

6 ADMS AND AERMOD DISPARITIES DUE TO TREATMENT OF METEOROLOGICAL INPUTS

This section reviews an inter-comparison between ADMS and AERMOD pre-processors and investigates the sensitivity of predicted concentrations upon pre-processor outputs. It also highlights differences associated with user input of roughness length, z_0, and energy budget parameters (Albedo, r, modified Priestley Taylor parameter used in ADMS, α, and the Bowen Ratio used in AERMOD, β). Differences in annual and short term peak concentrations are examined and where disparities are apparent, the causes are identified.

6.1 Methods

Meteorological data from Ringway was used as input to the ADMS and AERMET pre-processors for the single calendar year of 2000. The data that were supplied to the model were Julian day, time of day, near surface air temperature, wind speed, wind direction, precipitation, cloud cover and relative humidity. In addition to this dataset, further parameter inputs are required by both models.

ADMS defaults to using single values of albedo, r, and modified Priestley Taylor parameter, α, throughout the year, although hourly values can be input through the met file. Most users input surface roughness, z_0 as a single value for the emission site, although it is possible to input values for the met site and/or create a surface roughness grid for the model domain. It is not possible to change surface roughness on a seasonal basis.

The AERMET user selects a suitable site surface characteristic on a sector based level, which automatically assigns default seasonal values of albedo, r, Bowen ratio, β and surface roughness, z_0. For this modelling study, cultivated grassland (average moisture) was chosen as the surface characteristic. Associated values of r, β and z_0 are given in Table 6. CERC (2001) provide a temperature dependent values of γ/s (see equation 1) that allow simple transfer between the ADMS α parameter and the value of β used in AERMET. Hence it is possible to

set up ADMS and AERMET model configurations with equivalent surface moisture budget parameters (see ADMSseas and AMETseas below) assuming a constant γ/s value for 15°C.

Four meteorological inputs were created for further model testing, two from each pre-processor. The first (labelled **def** in details below) were created using single values of r, β and z_0, the second (labelled **seas** in details below) used seasonal values of r, β in both models and seasonal values of z_0 in AERMET. The following configurations of meteorological, surface energy budget and roughness length inputs were tested:

ADMSdef Output from the ADMS pre-processor using default conditions of r and α. z_0=0.1. This dataset represents a standard ADMS user input. Configuration tested on AERMET and the ADMS pre-processor.

ADMSseas Output from the ADMS pre-processor using seasonal values of r and α (Table 6) for average moisture cultivated grassland. z_0 remained at 0.1 m. Configuration tested on AERMET and the ADMS pre-processor.

AMETseas Output from the AERMET pre-processor using default conditions, ie, seasonal values of r, β and z_0 for average moisture cultivated grassland. This configuration is considered typical of a standard AERMOD user. Configuration tested on AERMET and the ADMS pre-processor.

AMETdef Output from the AERMET pre-processor was forced to use ADMS default values of r and equivalent β (Table 6). Configuration tested on AERMET and the ADMS pre-processor.

Estimated parameters such as boundary layer height, sensible heat flux, Monin-Obukhov length and friction velocity output from both models for each of these datasets were compared using graphs to display correlation and statistical analysis tables. The mean bias was used to illustrate the ensemble mean under or over estimation of friction velocity and boundary layer height from one dataset compared to another, given by the ratio of the ensemble mean of the model predictions over the ensemble mean of the measurements. The average difference between hourly values and the associated standard deviation are reported for all parameters, as is the correlation coefficient squared, R^2. The statistical factors F1.25 and F2 were used to represent the percentage of data from one dataset within a factor of 1.25 of 2 of the values from the dataset with which it was compared. Where parameter values can be negative (heat flux and Monin-Obukhov length) the F factors were calculated for conditions where both data points had positive values and where both data points had negative values. All other hours were excluded from the statistics and reported as the fraction excluded.

Following analysis of the pre-processors outputs, the four datasets were tested against a generic model scenario in both ADMS and AERMOD in order to determine the impact of each dataset on annual average and short term percentile concentrations. In order to incorporate AERMET output into ADMS, friction velocity (u*) replaced 10 m wind speed input, and boundary layer height,

heat flux and the reciprocal of Monin Obukhov length were added to the standard input parameters. To incorporate AERMETseas, seasonal values of albedo and equivalent Priestley Taylor parameter were used in the input file, however, a single value of 0.3 m was used for roughness length throughout the year.

A non-buoyant emission of SO_2 from a 40 m stack was created as a standard scenario with input parameters and output details provided in Table 7. The following model configurations were also created to test the sensitivity of predictions to urban emission site conditions, to buoyant releases, and to the inclusion (within AERMET) of low wind speed conditions:

Urban: Model configuration run through ADMS using ADMSdef input with z_0 increased to 1 m. Model configuration run through AERMOD using AMETseas input with urban values of r, β and z_0 in AERMET.

40m_b: Model configuration run through ADMS using ADMSdef input and AERMOD using AMETseas input. Exit temperature increased to 130°C and exit velocity increased to 25 m/s.

u0.75: Model configuration run through AERMOD using AMETseas input with minimum wind speed set to 0.75 m/s.

In order to identify disparities for individual hourly conditions, the pre-processor estimates of boundary layer parameters were compared on an hour by hour level using specific days chosen to represent a wide range of conditions throughout the year. Predicted concentrations for periods during these days were also obtained and compared to attempt to identify whether particular disparities in boundary layer parameters strongly influenced model predictions of location and magnitude of maximum concentrations.

6.2 Results

6.2.1 Correlation between yearly distributions of boundary layer parameters

Figure 5 displays the correlation of boundary layer parameters for the ADMSdef and the AMETseas datasets. These were chosen for display as they are the most likely datasets created from processing standard user input to each of the models. Tables 8 to 11 display the statistical analysis of differences in boundary layer parameters.

6.2.1.1 Boundary Layer Height

Although there is reasonable correlation between ADMSdef and AMETseas (Table 8), AERMET (using the UA estimation tool rather than upper air data) estimates higher boundary layers than both ADMS and those that might be typical for convective conditions in the UK. This reflects previous findings of Thé et al (2001), who identified that the UA Estimation Tool, written by Lakes Environmental to allow AERMET to process data without upper air soundings,

generally predicted higher boundary layers than those using upper air data. The influence of seasonal energy balance and roughness parameters did not significantly effect the agreement between the model met processor outputs, however AMET boundary layer heights displayed a larger sensitivity than ADMS (assumed to be due to changing values of roughness length). There is a large amount of scatter apparent in figure 5 indicating numerous hours where ADMS estimates boundary layer heights around or below 500 m while AERMET values range up to 3000 m. Figure 6 reveals the hourly and seasonal dependence associated with these large differences between AERMET and ADMS, showing the majority of these occasions occur during the hours of dusk.

Further seasonal analysis (Figure 7) highlights the tendency for ADMS values to be larger than those of AERMET during the winter months when boundary layers are low. This will be due in part to the lower limit of 50 m applied to ADMS values, while the lowest value in AMETseas is 4 m. Stable and complex stratified flows are associated with these low boundary layers and the ability of either model to predict accurate dispersion calculations is limited.

6.2.1.2 Friction velocity

Correlation of friction velocity between all datasets is strong (see Table 9). It is apparent that the friction velocity algorithms are dependent upon surface roughness, hence the appearance of 4 lines of strong correlation in Figure 5 where AMETseas is using seasonal values of z_0, while ADMSdef uses a constant value of 0.1 m.

6.2.1.3 Sensible Heat Flux

There is strong correlation between heat flux estimates from both the AERMET and ADMS pre-processor (Table 10). Similar differences between the datasets were observed for heat flux as were observed for boundary layer depth and friction velocity. The impact of inputting single or seasonal values of z_0, r, α or β has the smallest effect on AERMET's estimates of positive heat flux and ADMS's estimates of negative heat flux. AERMET displays a lower limit of –65 W/m^2 (apparent in Figure 5), while ADMS values reach –100 W/m^2. Although absolute differences over the dusk period did increase slightly (towards 40 W/m^2) during the summer months, this might be expected as fluxes are generally higher during these daylight periods. No daily or seasonal trends in relative differences between the datasets were identified.

6.2.1.4 Convective velocity scale (w_*)

In the instances where both models estimated a convective velocity, values were in fairly good agreement with AERMET predicting larger and much more frequent values than ADMS (see Figure 5). These results again point to AERMET estimating more frequent and extreme convective activity than ADMS.

6.2.1.5 Monin-Obukhov length

Correlation between datasets (Table 11) is similar to those of boundary layer heights and poorer than that of heat flux and friction velocity, reflecting the dependence of algorithms on previously calculated parameters. The high F2 factors (0.71 & 0.98) for agreement of AERMET estimates of L_{MO} when using single or seasonal values of z_0, r, α or β, and similarly high values for ADMS (0.96 & 0.82) suggest a small influence of these parameters on the met pre-processor algorithms for L_{MO}. However, the low F1.25 values for AERMET (0.06 & 0.11) demonstrate that the agreement is not perfect.

Estimates of $1/L_{MO}$ at the minimum limit value of -1.0 /m occur frequently in the AMETseas dataset (Figure 5), never reaching values above 0.7 /m. In contrast, ADMS frequently estimated $1/L_{MO}$ at the maximum limit value of 1.0 /m, with values reaching below -1.5 /m. AERMET generally predicts more strongly unstable conditions than ADMS, while ADMS predicts slightly stronger stability than AERMET (higher positive values of $1/L_{MO}$). The disparate occasions where ADMS predicts low negative values (slightly unstable conditions) and AERMET predicts high positive values (strongly stable conditions) occur where input wind speeds are 0.5 m/s, ie, hours which are not included in ADMS dispersion predictions. There are also occasions where ADMS predicts high strongly stable conditions and AERMET predicts negative values. These frequently corresponded to dusk and dawn hours throughout the year.

Overall agreement between the meteorological pre-processors is relatively encouraging, although conditions are identified where differences are at their greatest. This reflects the subtleties involved in the application of similar meteorological pre-processor methodologies. Similarly, Hall et al (2000) found that although h and L_{MO} values from ADMS and AERMOD calculated from identical input data showed large differences, values of the dimensionless h/L_{MO} showed broader agreement. The smallest differences were found between ADMS pre-processor output using single default values of z_0, r and α as input compared with using seasonal values of r and α. This suggests the influence of changing z_0, maybe the largest contributor to differences in processor output from meteorological related input. The impact of these differences on model predictions are investigated in the following sections.

6.2.2 Comparison of annual average model concentration predictions

Outputs of both the ADMS and AERMET pre-processors were used as input to both ADMS and AERMOD dispersion models. Predictions of the magnitude and location of the annual average concentration from each model run are given in Table 12. The location of the highest annual average concentration matched to within one grid point for ADMS and AERMOD predictions using default and seasonal values of r, α (or β) and z_0. Predicted peak concentrations from different meteorological inputs lay within 30% of each other, considered well within the uncertainty range that might typically be associated with a model prediction. Predictions from AERMOD using the AMETseas input (0.79 $\mu g/m^3$) and from

ADMS using ADMSdef input (0.97 μg/m^3) were within 23%. These are the predictions that most model users might compare.

ADMS predictions for the 40 m stack height tended to be slightly higher than those from AERMOD. Differences between model predictions for urban conditions did not appear to be significantly greater than those for rural characteristics for this chosen scenario. Differences between the models increased for the buoyant 40 m release scenario, with ADMS predicting an annual average 1.89 times higher than AERMOD. The inclusion or exclusion of wind speeds <0.75 m/s did not appear to significantly affect annual averages. Differences in model predictions from using different meteorological input are small compared to changing other input data, such as creating buoyant plumes.

6.2.3 Comparison of peak short term model concentration predictions

Predictions of the peak (100th percentile) concentration and location from each model run are given in Table 13. The location of the peak concentration is not expected to match between model configurations due to peak values being obtained from specific hours. AERMOD peak concentrations displayed greater variability than those of ADMS. ADMS predictions from its pre-processor inputs, using default or seasonal values of r and α, do not appear to vary greatly. However input of AERMET processed data with seasonal variation in r, β and z_0 significantly reduces predictions. This points to differences in values of z_0 influencing pre-processor outputs and subsequently model predictions more strongly than energy budget parameters.

Differences between the predictions from using the most standard datasets in both models is large, with ADMSdef peak value at 82.6 μg/m^3 and AMETseas peak at 207.2 μg/m^3. Similar trends are seen with the Urban scenario. With the exclusion of hours where wind speeds are less than 0.75 m/s (ie, u0.75), peak concentrations in AERMOD are significantly reduced to almost half the previous value (from 207.2 to 112.7 μg/m^3), highlighting the fact that peak concentrations are predicted to occur in lowest wind speed conditions, which are modelled in AMETseas but not in u0.75 configurations.

It is possible to draw out the six hours resulting in the highest concentrations from the AERMOD .apo output file for comparison with equivalent ADMS values (from the .max file). Table 14 displays the sixth highest hourly concentrations predicted by AERMOD and ADMS using ADMSdef, ADMSseas, AMETseas and AMET_u0.75 model configurations. Very minor changes in peak or sixth highest concentrations are seen with the ADMS results when using default or seasonal values of r and α. Much larger changes are seen between the peak and sixth values for both the AERMOD datasets. The AERMOD results also highlight the large difference in peak short term values when using different lower limits of wind speed. Both the peak and the sixth highest predictions from ADMS and AERMOD predictions match much more closely when lower wind speed limits are in agreement.

6.2.4 Comparison of model predictions from representative days

Figure 8 displays the generally good agreement between ADMS (ADMSdef) and AERMOD (AERMETseas) predictions of peak concentrations over 74 hours on 13 representative days where the large majority of predictions fall well within a factor of 2. The days chosen include:

- neutral conditions - overcast, windy
- stable conditions - clear skies, light winds
- unstable conditions - clear skies, light winds, and
- overcast conditions - light winds.

Figure 9 displays the agreement of downwind distance corresponding with these peak concentrations. Again, the majority of values are well within a factor of two, although ADMS displays more variable distances than AERMOD for the hours displayed.

Table 15 displays examples of individual hours from representative days where agreement between ADMS and AERMOD predicted concentrations were poor, particularly in light wind conditions. The most extreme differences occurred during the dusk and early evening periods of 18:00 March 30th and 16:00 October 21st. On both occasions ADMS predicts a boundary layer limit height of 50 m and slightly stable conditions while AERMOD predicts a higher boundary layer with low but positive sensible heat flux. Boundary layer heights estimated by the pre-processors for October 21st are displayed in Figure 10. This graph highlights the delayed collapse of the boundary layer in AERMET (17:00hrs) compared to that in ADMS (16:00hrs), leading to disparities in predictions for the hour of 18:00hrs. Poor agreement at 13:00hrs December 15th can be traced to ADMS estimating slightly unstable conditions while AERMOD predicts stable conditions.

Table 16 displays examples of individual hours where agreement between ADMS and AERMOD predicted concentrations was good. Moderate or high wind speeds were usually present during these hours, AERMOD often displayed moderate negative heat fluxes with relatively large boundary layer heights. Agreement between both the location and magnitude of the peak hourly concentrations identified remains strong despite large differences between ADMS and AERMOD estimated boundary layer parameters for those hours.

6.3 Summary

As discussed in earlier sections, ADMS and AERMOD follow broadly similar methodologies, however, differences between the systems soon become apparent when attempting to input non-standard met data and when comparing outputs from the two models. Output formats are unsurprisingly different due to the design of the models, with ADMS designed to meet UK regulatory requirements (eg, 99.7th percentiles of peak hourly concentrations) while

AERMOD was originally designed to meet US EPA designs. Hence, a detailed comparison of results entails laborious and costly data processing. However, results from such comparison can provide useful information as this section of the study has shown.

Differences are apparent in the estimated boundary layer parameters from ADMS and AERMOD. Some of these are due to the influence of inputs such as roughness length, while others may be more strongly associated with model parameterisation of the atmosphere and the growth of the PBL throughout the day. These differences are reduced when comparing values of h/L_{MO} which are considered to have a strong influence on dispersion parameters. Conditions of dusk and dawn do show larger disparities between the models, with AERMOD displaying an hour's delay in the influence of the setting sun compared to ADMS. Although peak boundary layer heights are much greater in AERMOD than ADMS, these periods do not appear to create obviously different predictions from the models (apart from dusk hours). Disparities at low wind speeds are also identified. If the model user has identified these conditions as of particular interest, it may be necessary to consider an alternative model with the ability to treat calms and low winds more realistically (ie, CALPUFF (Scire et al, 2000). The ADMLC has previously investigated dispersion at low wind speed (Lines and Deaves, 1999).

7 PROBABILISTIC MODELLING OF UNCERTAINTY DUE TO METEOROLOGICAL INPUT TO ADMS

This section of the report investigates the impact that uncertainties in meteorological data have on the predictability of both annual average air concentration and the various percentiles of the hourly concentration distributions. Model predictions have been made for SO_2 though it should be noted that no considerations of the deposition or atmospheric chemistry of SO_2 have been made, hence this represents a passive tracer for any chemical or radiological release.

7.1 Methods

The ADMS 3.1 atmospheric dispersion model was chosen for this section of the study as it is often used for predicting the air quality impact of stack emissions within the UK. From a simple consideration of the pre-processing of the meteorological data by ADMS 3.1 (Thomson, 2000) air concentrations would be expected to be relatively unaffected by the changes in relative humidity and air temperature that could occur due to instrument uncertainty or the uncertainty related to the stochastic nature of atmospheric turbulence. Furthermore, as plume depletion due to dry or wet deposition is frequently not considered when assessing compliance with air quality standards, precipitation will not be

considered here. Julian day and time can be accurately determined, however, the treatment of solar elevation by the model, which is a function of day and hour, is an approximation. However, Thomson (2000) suggested that the use of more detailed formulae would not significantly improve the predictability of the model.

From the above consideration it is clear that model predictions of air concentrations are likely to be strongly dependent on the wind speed, wind direction and cloud cover values supplied as input. Further considerations would have to include the roughness length, representing the aerodynamic effects of surface friction, and the assumptions related to the surface energy budget (Priestley-Taylor parameter, α and Albedo, r) as additional sources of uncertainty when processing meteorological data.

Monte Carlo (MC) methods allow the uncertainties in model output to be estimated by carrying out a suitably large number of model runs using random resampling of input data (Hanna et al, 2002). It is necessary, therefore, that appropriate (and realistic) distributions are assigned to the key input parameters. These distributions are themselves subject to a considerable degree of uncertainty, with expert elicitation exercises often being used to estimate the relevant distribution shapes and parameterisations (eg, Pasler-Sauer and Jones, 2000). In order to provide some confidence in the predictions of a Monte Carlo model, Hill et al (2002) compared Monte Carlo predictions with data on the dispersion of stack discharges of ^{41}Ar and ^{85}Kr emitted from BNFL Sellafield. Overall, the model was found to realistically, though not exactly, represent the range of field measurement values.

Monte Carlo methods were applied to ADMS 3.1 by creating 2000 meteorological data files from the original Ringway dataset. Each of these files contained a complete timeseries of hourly Monte Carlo sampled meteorological data for the entire 12 month period. Each meteorological file was assigned to a corresponding ADMS input file (APL file), enabling the modelling of 2000 different realisations of the same meteorological dataset. Meteorological and input (APL) data files were created, and results files were imported into Microsoft Excel™, using code written in Visual Basic Applications Edition (VBAE). All other stack characteristics and receptor details matched those of the 40 m non-buoyant testing scenario detailed earlier in this report. In addition to obtaining the annual average and hourly maximum values for each receptor, the 99.9, 99.8, 99.7, 99.6, 99.5, 99.4, 99.3, 99.2, 99.1, 99, 95, 90 percentiles were also acquired as output.

Three different scenarios were used to evaluate the uncertainty associated with the meteorological data. These were, uncertainties in:

(i) Basic meteorology (cloud cover, wind speed and wind direction);

(ii) Basic meteorology and surface energy budget (Priestley-Taylor parameter and Albedo)

(iii) Basic meteorology, surface energy budget and roughness length.

7.2 Determining appropriate probability distributions

7.2.1 Uncertainty in basic meteorology

The treatment of uncertainty in wind speed and wind direction followed the approach discussed in Hill et al (2002) which presented a simple Monte Carlo model coupled to the R91 atmospheric dispersion code. This model calculated the hourly uncertainty in model input and propagated these through to determine the uncertainty in model calculations of ^{41}Ar external gamma doses and ^{85}Kr air concentrations. The range of model predictions were then compared with a large number of ^{41}Ar and ^{85}Kr field measurements to determine the realism of the modelling approach.

Uncertainties in hourly wind speed, wind direction and σ_θ were determined by Hill et al (2002) by comparing simultaneous measurements of these scalars collected at two meteorological masts, one on each side of the BNFL Sellafield site. Coefficients of variation (standard deviation/mean) were determined for each pair of wind speed and σ_θ measurements and the differences in wind angle between the two meteorological sites were also determined. This analysis of meteorological uncertainty therefore captured both the instrument error and the natural stochastic variation in the meteorological measurements. In order to approximate the variation in meteorological uncertainty with the level of atmospheric turbulence, data were subdivided into nine wind speed bins, with the bounds of each bin being set to ensure that each contained approximately the same number of paired observations (approximately 350).

Uncertainties in the hourly wind speed and wind direction were assumed to follow a normal distribution with a mean given by the original value from the Ringway meteorological datafile. The standard deviation of the wind speed is given by the median coefficient of variation (CV) whilst the standard deviation of the wind direction was approximated by the median wind angle difference. The model used a feedback loop to allow the uncertainties in wind speed and wind direction to vary with the original wind speed, an important finding from the paired meteorological data collected at the BNFL Sellafield site. We have assumed that, in the absence of any other information, the parameterisations of these distributions, and their dependence on wind speed, are broadly applicable across a range of other sites.

The measurements of wind speed and wind direction uncertainty, from Hill et al (2002), are reproduced in Table 17. These results illustrate that uncertainty in wind speeds is inversely proportional to the mean wind speed for wind speeds less than 4.1 m/s, with the highest uncertainty (a CV of 0.19) being found to be associated with mean wind speeds less than 1.9 m/s. Wind speed uncertainty was found to be directly proportional to the mean wind speed for wind speeds higher than the aforementioned threshold, reaching an approximate plateau above 6.0 m/s with a CV of 0.15-0.16. The wind direction uncertainty was found to be inversely proportional to the wind speed, with a peak uncertainty (a median wind angle difference of 31.75°) for wind speeds less than 1.9 m/s. Wind direction uncertainty was found to reach a plateau region above approximately

4.1 m/s with a median wind angle difference of approximately 5.5° (close to the system measurement accuracy quoted in Table 1).

It should be noted that Hill et al (2002) also considered uncertainties in σ_θ. However, as σ_θ values were not given in the Ringway dataset it was not possible to include this source of uncertainty in the Monte Carlo model.

The uncertainty in the hourly cloud cover was also parameterised using a normal distribution, with the mean given by the original value from Ringway and applying a standard deviation of 1 okta (with no consideration of deteriorating accuracy overnight). The resulting values were rounded to the nearest integer and clipped to ensure that cloud cover could never be less than zero or greater than 8. This would imply a reduction in the uncertainty on cloud cover for periods with an original value of 0 or 8 oktas, though it would be difficult to justify applying a separate model to these data. Furthermore, as identified in an earlier section, the periods when cloud cover of 0 or 8 oktas occur are likely to be under-reported by manual observers using routine methods of cloud observation. It could therefore be argued that the observational data would actually be less uncertain during these periods.

7.2.2 Uncertainty in the surface energy budget

Default parameterisations of the surface energy budget are used by ADMS to calculate heat fluxes and Monin-Obukhov lengths from cloud cover and time of day. ADMS 3.1 uses a Priestley-Taylor parameter (α) of 1 (an estimate of the moisture availability of dry grassland) and a surface albedo value of 0.23. These default values were used for scenario (i). However, it is clear that these parameters are subject to a degree of uncertainty, hence scenarios (ii) and (iii) considered the range that these parameter might take.

In order to estimate the uncertainty on α we have assumed that the values of γ/s contribute a relatively small uncertainty in comparison to that due to assuming a Bowen ratio. The temperature dependence of γ/s was included in the Monte Carlo model as a deterministic value using the data from Holtslag and Van Ulden, (1983) as cited in CERC (2001) and interpolating a value from each hour's surface temperature reading from the Ringway datafile. The uncertainty in the hourly Bowen ratio was included by considering the range of values reported in EPA (1998) for wet and dry grasslands, reproduced in Table 18. A uniform distribution was applied by using the seasonal specific values for wet and dry conditions as the upper and lower limits to the distribution. No account could be made of any diurnal variations in Bowen ratio as ADMS uses Equation 8 to derive sensible heat fluxes with the eddy temperature (θ_*) calculated solely from cloud cover data. A fuller evaluation of the uncertainty in the Priestley-Taylor parameter was beyond the scope of this project.

The surface albedo was also allowed to vary. However, EPA (1998) illustrated that albedo only showed a relatively small variation with season or with land use type. Consequently, the additional complexity for scenarios (ii) and (iii) was limited to considering seasonal deterministic values for surface albedo as

presented in Table 18. These values match the cultivated grassland values given in the AERMET User Guide, which were also used for the ADMS and AERMOD inter-comparisons in the earlier section.

7.2.3 Uncertainty in the roughness length

In scenarios (i) and (ii) a fixed roughness length of 0.1 m was used. This was applied to both the meteorological site and to the source site. For scenario (iii) an estimate of the uncertainty in the roughness length was included in the model simulations.

Uncertainties arise in the roughness length, for most sites, due to the considerable spatial and temporal variability in land use and surface cover. For a dispersing plume the effective roughness length is likely to vary considerably along its trajectory (Hanna and Britter, 2001) whilst few meteorological sites are located in regions where each wind sector will have identical roughness lengths. Furthermore, the upwind "ootprint" that elevated measurements correspond with varies strongly with stability (Horst and Wiel, 1994). For example, wind speeds measured at 10 m in stable conditions will be relatively unaffected by nearby short roughness elements, though may be strongly dependent on tall roughness elements several hundred metres upwind.

Hill et al (2002) assumed that the uncertainty in roughness length could be approximated by a log-normal distribution, given that the distribution shape was likely to be strongly skewed by the impossibility of negative or zero values and by the large range that would typically be observed in the field. In this study we considered the roughness length for the meteorological site and for the source site separately, as it is often the case that meteorological sites may be located at a considerable distance from the actual source being considered. The log-normal distribution for the roughness length at the meteorological site was parameterised by assuming that the 5^{th} and 95^{th} percentiles of the distribution were 0.02 m (open grassland) and 0.3 m (agricultural areas) respectively, whilst higher values of 0.1 m (root crops) and 0.5 m (parkland/open suburbia) respectively were applied to the source site.

7.3 Results

Monte Carlo modelling, by its very nature, generates large quantities of data. The 2000 runs that were input per scenario generated more than 1.3 million output data points. In order to simplify this data it is convenient to determine appropriate statistics for describing the range of the results and the median value from the set of simulations. The range of data was evaluated as the ratio of the 97.5^{th} percentile to the 2.5^{th} percentile for the 2000 data points in each simulation for each receptor and output statistic (annual average, etc). This ratio can be interpreted as representing the maximum deviation between values that would be expected at a confidence limit of 95%. The median (the 50^{th} percentile) was determined directly from each data series.

Table 19 shows the ratios of the 97.5th percentile to 2.5th percentile for annual average concentrations of SO_2 at each of the receptor locations and for each of the input data scenarios. Similar ratios were found for scenarios (i) and (ii), varying between 1.06 and 1.33. For these two scenarios the percentile ratios did not vary strongly with distance, though generally higher ratios were found for receptor point locations to the south and west of the source. Results for scenario (iii) showed a substantial increase in percentile ratios over the results presented in the previous scenarios. Furthermore, the results for scenario (iii) showed a substantial reduction in the percentile ranges with distance from the source and their dependence on wind sector was markedly reduced.

The median values from the simulation of annual average SO_2 concentrations are shown in Table 20 alongside the deterministic results from the earlier model runs (as presented in Section 6). MC median values closely match deterministic predictions of annual average using one year's met data as input. All the scenarios returned similar median values at distances of 1000 m and greater, indicating the differences in energy budget and roughness length parameterisations would not significantly bias the model predictions. Furthermore, a good agreement was found between the median values and the deterministic results. Differences between the input scenarios, and between the median probabilistic value and the deterministic calculations were only noticeable at a downwind distance of 250 m from the source. The median concentration values at this distance were found to increase with the complexity of the uncertainty model, such that the highest concentration was predicted for scenario (iii).

The ADMS model was also setup to output various percentiles of the hourly concentration distribution. The uncertainty in these output were also evaluated by looking at the percentile ratios and median values of the Monte Carlo output using the same methods as were applied to the annual average air concentrations.

Table 21 shows the percentile ratios for the ADMS output of the 99.7th percentile of the hourly concentration distribution. The percentile ratios were found to be relatively consistent across scenarios (i), (ii) and (iii) in the Monte Carlo model, with the overall range of values being between 1.09 and 1.41. In general, slightly higher uncertainties were associated with receptor locations to the south and west of the source, though the increase in uncertainty associated with the use of scenario (iii) resulted in this effect being somewhat smoothed out. The percentile ranges reported in Table 21 did not show the strong dependence on downwind distance that was found for the annual average air concentrations.

The median values of the 99.7th percentiles of hourly concentrations predicted by the Monte Carlo model are shown in Table 22, alongside the deterministic values from ADMS. As found with the median values of the annual average air concentration, median 99.7th percentiles of hourly concentrations were relatively unaffected by the use of scenarios (i), (ii) or (iii) in the Monte Carlo model. This illustrates that the application of these scenarios in the Monte Carlo model has not resulted in any significant bias in the model output of the 99.7th percentile of

hourly concentrations. Again, a good agreement was found between the median probabilistic values and the deterministic results, with the largest differences occurring at sites which were shown, in Table 21, to have a wide probabilistic range.

7.4 Summary

The results for the basic meteorological data, scenario (i), provide an indication of the level of irreducible uncertainty in model predictions that would arise from meteorological uncertainties. Overall, the contribution of the uncertainty in basic meteorological data to predictions of both annual average air concentrations and the 99.7th percentile of hourly concentrations was relatively small, with ranges of 1.07–1.33 and 1.09 –1.38 respectively. The higher uncertainties tended to occur at receptors that received relatively infrequent winds from the site and there was a slight increase in uncertainty at the closest receptor location.

Overall, these results showed that the energy budget calculations in ADMS had relatively little impact on the overall uncertainty in annual averaged model outputs, whilst the roughness length contributes a relatively large influence on the model uncertainty that would occur due to the model user's influence on meteorological input data. Consequently, uncertainty can be expected to be relatively large at locations where there are large variations in surface roughness or when using meteorological data collected from a meteorological site located in a relatively heterogeneous landscape.

An interesting finding from this study is that uncertainties associated with the 99.7th percentile of hourly averaged air concentrations are similar (and potentially smaller) than those associated with the annual average concentration. Figure 11 shows the variation in uncertainty of various percentiles of the annual concentration distributions (as defined by the ratios of the 97.5th to 2.5th percentiles of the Monte Carlo output) for two receptor locations, to the north and south of the source at downwind distances of 250 m for scenario (iii). This figure clearly illustrates that the uncertainty in the various percentiles of the hourly concentration distribution tends to reduce before increasing to the 100th percentile (the highest hourly value). The differences between the plots of the receptor to the north and south of the site are likely to result from the large differences in the frequency of wind directions to these receptor sites. A low frequency of winds towards a receptor would result in long periods with a zero (or background) air concentration, with intermittent periods within the plume. Weather conditions and wind direction fluctuations within these periods could vary significantly hence uncertainties in percentile concentrations would increase significantly.

8 GUIDANCE FOR THE MODEL USER COMMUNITY

A significant source of uncertainty in the predictions of atmospheric dispersion models is due to the model formulations and model physics. This applies both to the formulae used to model atmospheric dispersion and the computations of the meteorological pre-processors. The inter-comparison of predictions of the meteorological pre-processors of ADMS and AERMOD, in section 6, has shown that the pre-processors, in general, show larger differences between the modelling systems than due to the uncertainties in parameterising the surface energy budget (ie, α or β, and r). Surface heat flux parameterisations also have an important effect but are not controllable by the user and effects are different between the models. Large differences are also observed between boundary layer parameter estimates from the ADMS pre-processor and from estimates made using the flux profile method to obtain stability data. This project was not designed to recommend the choice of a particular modelling system and broadly follows the recommendation of Carruthers et al (2001) that the differences between the models reflect true uncertainties in estimating turbulent dispersion in the atmospheric boundary layer. The following points summarise the relevant findings of the work completed within the report, however, it should be noted that only one mid-level stack height has been considered within modelling inter-comparisons and the effects of meteorological uncertainty on deposition have not been evaluated.

In order to assess the uncertainty due to model formulations and model physics, users are recommended to conduct an intercomparison of predictions from more than one model. It should be borne in mind that models such as ADMS and AERMOD are based on similar modelling methodologies and often produce broadly similar results. Hence, conducting an intercomparison of results will only be worthwhile when concentrations are close to a benchmark level or when considering a specific period when disparity conditions exist between the models. These disparity conditions, detailed in section 6, include the treatment of dawn and dusk, calm meteorology and the treatment of large and rapid variations in cloud cover. Where frequent calm conditions occur (greater than approximately 10% of the time) and when concentrations are close to a benchmark level, or when modelling a specific period with low wind speeds, model users are recommended to consider the application of a model with a capability to treat such conditions (for example CALPUFF (Scire et al, 2000)). It should be noted that peak air concentrations often are predicted during periods with low wind speed, hence it would be prudent, when reporting the percentiles of a concentration distribution, to reference the frequency of calm conditions, and record the minimum threshold wind speed used within the study.

The choice of meteorological data for input to atmospheric dispersion models also can be of significance. Model users are recommended to assess the representativity of the meteorological site that they use to the conditions at their source location. Previous ADMLC reports have discussed issues of data representativity including distance from observing sites, the use of NWP data and

ageing issues of historic data. Both of the two main UK suppliers of met data for dispersion models provide certificates of representativity upon request, unfortunately they do not routinely state the procedures used to determine the degree of representativity. Modellers intending to use output from one model's meteorological pre-processor as input to another model should consider the representativity of the re-constructed input, in particular the difference in model treatment of roughness length (and associated friction velocity) and surface heat flux.

The use of NWP meteorological data should be considered when the nearest surface observation station may be unrepresentative of the source location. It should be noted however that Met Office NWP data are currently only available with cloud cover output. Ideally, looking towards the future, we might expect higher spatial resolution data tailored to provide the most appropriate input to the dispersion models (ie, providing L_{MO}, u_* and $F_{\theta 0}$ and z_0 directly) to become available. As a further point, the mesoscale model, used to predict weather around the UK, and to provide NWP data for dispersion models, uses more advanced flow dynamics than can be implemented within the current regulatory dispersion models. It is suggested that future developments to the regulatory Gaussian dispersion models could consider how to incorporate the 3-dimensional NWP data.

Site specific wind fields could be modelled by using meteorological measurements recorded by the site operator. For most industries, these records will not extend to the full 5 year period that the Environment Agency requests in order to account for inter-annual variability. The US-EPA recognises this in their guidance and considers one year of site specific data to be acceptable. These on-site data can be relatively easily included when processing meteorological data for AERMOD and ADMS, however model users should be aware of the fetch requirements for obtaining representative meteorological measurements and should ensure that influences of local structures are minimised. The interpretation of locally measured temperature profiles, or sonic anemometer output, to estimate heat fluxes can also be useful, though again a detailed consideration of fetch requirements and instrument precision should be made. It also should be noted that these methods are particularly uncertain during periods of strong atmospheric stability. Measurements of solar radiation at locations close to a site can provide an alternative method of estimating daytime atmospheric stability in ADMS, though the ADMS to AERMOD converter supplied by Lakes Environmental requires cloud cover as input.

A further consideration when using a meteorological data set is to ensure that the met preprocessor has been supplied with accurate data specific to the site that the records were collected. Overall, the meteorological preprocessors were shown to be relatively insensitive to the parameterisation of the surface energy budget, through the choice of Priestley-Taylor parameter, suface albedo or Bowen ratio. Effects that are far more significant were likely to be observed due to uncertainties in the roughness length at the meteorological site. Model users should ensure that they are aware of the appropriate roughness length at the

meteorological site. It may be useful if the Met Office could provide details of the likely variability in roughness lengths at each of their surface observation sites to enable model users to account for this source of uncertainty in their assessments. Furthermore, detailed consideration of an appropriate roughness length for modelling dispersion downwind of a source should be made. For sites where the dispersing plume interacts with a range of scales of roughness elements this could include the consideration of an effective roughness length (eg, Hanna and Britter, 2001), perhaps specified on a sector basis, or the application of a roughness length map (CERC, 2001).

Emergency assessments are often conducted using screening level models that have the advantages of being relatively quick to setup and fast run-times. These models therefore require a lower number of "uncertain" meteorological parameters, though an increase in the uncertainty due to model formulations and model physics is unavoidable. Consideration should be given to the appropriateness of the modelling system used for emergency assessments. Model users should ensure that their system is suitable for the range of meteorological conditions they may encounter. For example, sites where a high annual frequency of calm conditions are observed should consider a modelling system, or methodology, that can operate in these conditions, whilst sites where emergency assessments may be required for tall stacks should ensure that their modelling system can account for vertical variations in turbulence and wind speed. Consideration should also be given, when setting up an emergency assessment system, to the choice of appropriate roughness lengths and the variability in roughness length. When conducting emergency assessments, model users are advised to consider the increased uncertainty, in plume trajectory, spread and the magnitude of peak concentrations during periods of low wind speed, convective conditions, during transition periods (dawn and dusk) and during periods when large and rapid changes in cloud cover occur. These considerations could include applying countermeasures to wider wind sectors or by applying an appropriate safety factor to concentration estimates.

9 RECOMMENDATIONS FOR FURTHER INVESTIGATION

The modelling assessments considered in this report were related to stack discharges, and focussed on a mid-range (40 m) stack height. Further studies could investigate a range of different source types including line and area sources, using similar Monte Carlo probabilistic methods to assess the factors contributing to model uncertainty. A more detailed consideration of the uncertainty in roughness length could also be made including an inter-comparison of the methods used by models to account for spatial variations in z_0.

The feasibility of making fuller use of the data supplied by the NWP model in dispersion modelling assessments should be considered. At a simple level this

could include the direct extraction of heat fluxes and friction velocities from the model, thus reducing the errors caused by the re-interpretation of data by model pre-processors. A detailed investigation into the impact of variations in cloud height on energy budget calculations could also be considered. The integration of the 3-dimensional wind field data, supplied by the NWP model, into Gaussian plume models could also be useful. This would be particularly relevant when predictions are required from elevated sources in a strongly stratified boundary layer, or when predictions are required over large downwind distances.

The validation and inter-comparison of meteorological pre-processors predictions with measured vertical gradients in wind speed, wind direction and temperature and with turbulence measurements from sonic anemometers could also help to address the uncertainty found between modelling systems. This may be particularly useful in ensuring that pre-processing algorithms developed overseas are applicable to the climate of the UK.

10 REFERENCES

Baldocchi DD, Hicks BB and Meyers TP (1988). Measuring biosphere-atmosphere exchange of biologically related gases with micrometeorological methods. *Ecology*, **69**, 1331-1340.

Barad ML (1958). Project Prairie Grass, A Field Program in Diffusion. *Geophysical Research Papers*, **59**, Vols I and II, AFCRC-TR-58-235, Air Force Cambridge Research Centre, 439 pp.

Bercowicz R and Prahm LP (1982). Sensible heat-flux estimated from routine meteorological data using the resistance method. *Journal of Applied Meteorology*, **21 (12),** 1845-1864.

Carruthers DJ, Holroyd RJ, Hunt JCR, Weng WS, Robins AG, Apsley DD, Thomson DJ and Smith FB (1994). A new approach to modelling dispersion on the earth's surface. *J Wind Eng Indus Aerodyn*, **52**, 139-153.

Carruthers DJ and Dyster SJ (2000). Boundary Layer Structure Specifications, ADMS Technical Specification P09/01P/00.

Carruthers DJ, McHuges CA, Dyster SJ, Robins AG and Thomson DJ (2001). Comments on Model Inter-Comparison Reports. CERC response to Hall et al (2000). http://www.cerc.co.uk/software/pubs/comparison_comments.pdf

Carruthers DJ, Weng WS, Hunt JCR, Holroyd RJ, McHugh CA and Dyster SJ (2000). Plume/Puff spread and mean concentration module specifications ADMS. Technical Specifications P10/01Q/00 P12/01Q/00.

CERC (2001). ADMS 3.1 Users Guide. Cambridge Environmental Research Consultants, Cambridge UK.

Cimorelli AJ, Perry SG, Venkatram A, Weil JC, Paine RJ, Wilson RB, Lee RF, Peters WD (1998). AERMOD, description of model formulation. US Environmental Protection Agency, Research Triangle Park, NC.

Cimorelli AJ, Perry SG, Venkatram A, Weil JC, Paine RJ, Wilson RB, Lee RF, Peters WD, Brode RW and Pauimer JO (2002). AERMOD: Description of Model Formulation Version 02222, EPA 454/R-02-002d. US Environmental Protection Agency, Research Triangle Park, NC.

Clarke RH (1979). *A model for short and medium range dispersion of radionuclides released into the atmosphere*. Chilton, NRPB-R91.

Dyer AJ and Hicks BD (1970). Flux-gradient relationships in the constant flux layer. *Quarterly Journal of the Royal Meteorological Society*, **96**, 715-721.

Dyer AJ (1981). Flow distortion by supporting structures. *Boundary Layer Meteorology*, **20**, 243-251.

EPA (1998). Revised draft users guide for the AERMOD meteorological pre-processor AERMET. US Environmental Protection Agency, North Carolina.Gifford F A, (1959). Statistical properties of a fluctuation plume dispersion model. *Advances in Geophysics*, **6**, 117-138.

Golder D (1972). Relations among stability parameters in the surface layer. *Boundary Layer Met*, **3**, 47-58.

Hall DJ, Spanton AM, Dunkerley F, Bennett M and Griffiths RF (2000). An inter-comparison of the AERMOD, ADMS and ISC dispersion models for regulatory applications. Technical Report P362, Environment Agency.

Hanna SR and Britter R (2001). The effect of roughness obstacles on flow and dispersion in urban and industrial areas. In: *Proceedings of the seventh international conference on harmonisation within atmospheric dispersion modelling for regulatory purposes*, pp 266-270. European Commission Joint Research Centre Ispra, Italy.

Hanna SR and Britter RE (2002). Wind Flow and Vapor Cloud Dispersion at Industrial and Urban Sites. Published by CCPS of the AIChE, New York 2002, ISBN 0 8169 0863 X.

Hanna SR, Wilkinson J, Russell A, Vukovich J, Frey HC (2002). Estimating uncertainties of air quality modelling systems using Monte Carlo approaches. Paper presented to the American Meteorological Society, May 2002.

Haugen DA, Kaimal JC, Bradley EF (1971). An experimental study of Reynolds stress and heat flux in the atmospheric surface layer. *Quarterly Journal of the Royal Meteorological Society*, **97**, 168-180.

Hill RA, Lowles I, Teasdale I, Chambers N, Puxley C and Parker T (2001). Comparison between field measurements of ^{85}Kr around the BNFL Sellafield reprocessing plant and the predictions of the NRPB-R91 and UK-ADMS atmospheric dispersion models. *Int J Environment and Pollution*, **16** (1-6), 315-327.

Hill R, Lowles I, Auld V and Parker T (2002). Probabilistic evaluation of models for the atmospheric dispersion of effluents released from a complex site. In: *Proceedings of the eight international conference on harmonisation within atmospheric dispersion modelling for regulatory purposes* (edited by Batchvarova E and Syrakov D), pp 48-52. Bulgarian Academy of Sciences.

Holtslag AAM and Van Ulden AP (1983). A simple scheme for daytime estimates of the surface fluxes from routine weather data. *J Climate Applied Meteorology*, **22**, 517-529.

Holtslag AAM and de Bruin HAR (1988). Applied modeling of the nighttime surface energy balance over land. *J Appl Met*, **27**, 689-704.

Horst TW and Weil JC (1994). How far is far enough? The fetch requirements for micrometeorological measurement of surface fluxes. *Journal of Atmospheric and Oceanic Technology*, **11**, 1018-1025.

Hunt JCR (1985). Turbulent diffusion from sources in complex flows. *Ann Rev Fluid Mech*, **17**, 447-458.

Hunt JCR, Holroyd RJ and Carruthers DJ (1988). Preparatory studies for a complex dispersion model. CERC Report HB9/88.

Hunt JCR, Kaimal JC and Gaynor JE (1988). Eddy structure in the convective boundary layer – new measurements and new concepts. *QJR Meteorol Soc*, **114**, 827-858.

Kidd J (2002). Comparison of NWP gridded weather data and site specific observed data for use in dispersion models. MSc Thesis for Applied Meteorology, University of Reading.

LAQM TG03 (2002). Part IV of the Environment Act, 1995. Local Air Quality Management. Technical Guidance TG-03.

Lines IG and Deaves DM (1999). Atmospheric dispersion at low wind speed. In Atmospheric Dispersion Modelling Liaison Committee Annual Report, 1996–97.

Lowles I (2002). Model comparison and uncertainty. AQMAU Model uncertainty workshop, June 2002.

Mirza AK, Nelson N, Weaver KN (2002). An Assessment of Alternative Sources of Met data for Use in Dispersion Modelling. Met Office report produced for ADMLC.

Moore DJ (1976). Calculation of ground level concentrations for different sampling periods and source locations. *Atmospheric Pollution,* **5160**, Amsterdam, Elsevier.

Nielsen LB, Prahm LP, Bercowicz R et al (1981). Net incoming radiation estimated from hourly global radiation and or cloud observations. *Journal of Climatology*, **1** (3), 255-272.

Oke TR (1978). Boundary Layer Climate. John Wiley and Sons, New York, New York, 372 pp.

Olesen HR, Brown N (1992). The OML meteorological preprocessor – a software package for the preparation of meteorological data for dispersion models. MST LUFT-A 122. National Environmental Research Institute, DK-4000 Roskilde, Denmark.

Panofsky HA and Dutton JA (1984). Atmospheric Turbulence: Models and Methods for Engineering Applications. John Wiley and Sons, NY, 417 pp.

Pasler-Sauer J and Jones JA (2000). Probabilistic accident consequence uncertainty analysis of the atmospheric dispersion and deposition module in the COSYMA package. *Radiation Protection Dosimetry*, **90** (3), 331-337.

Pasquill F and Smith FR (1983). Atmospheric Diffusion. John Wiley and Sons Inc, New York, 440 pp.

Paulson CA (1970). The mathematical representation of wind speed and temperature in the unstable atmospheric surface layer. *Journal of Applied Meteorology*, **9**, 857-861.

Scire JS, Strimaitis DG and Yamartino RJ (2000). A User's Guide for the CALPUFF Dispersion Model (version 5). Earth Tech, Inc, 196 Baker Avenue, Concord, MA 01742 (http://www.src.com/calpuff/calpuff1.htm)

Shi JP, Ng B (2002). Risk based pragmatic approach to address model uncertainty. Paper for the NSCA DMUG meeting, November 2002.

Smith J (2000). Options for the most appropriate Meteorological data for use in Short Range Dispersion modelling. ADMLC report prepared by the Met Office.

Sutton MA (1990). The surface-atmosphere exchange of ammonia. PhD thesis, University of Edinburgh.

Taylor GI (1921). Diffusion by continuous movements. *Proc London Math Soc,* **2** (20), 196-211.

Thé JL, Thé CL and Johnson MA (2000). User's Guide ISC-AERMOD View, Volume I, Lakes Environmental. ISBN 0-9681806-0-4.

Thé JL, Lee R and Brode RW (2001). Worldwide Data Quality Effects on PBL Short-Range Regulatory Air Dispersion Models. *Proceedings 7th Int Conf on Harmonisation within Atmospheric Dispersion Modelling for Regulatory Purposes*, Belgirate, Italy, pp 202-206.

Thom AS (1975). Momentum, mass, and heat exchange of plant communities. In: *Vegetation and the Atmosphere* (edited by Monteith J L), pp 57-109. Academic Press, London.

Thomson DJ (1992). An analytical solution of Tennekes' equations for the growth of boundary-layer depth. *Boundary Layer Meteorology,* **59**, 227-229.

Thomson DJ (2000). The met input module, ADMS 3 Technical Specification. Cambridge Environmental Research Consultants. Available from the website URL: http://www.cerc.co.uk/software/publications.htm.

Van Ulden AP and Holtslag AAM (1985). Estimates of atmospheric boundary layer parameters for diffusion applications. *J Climate Appl Meteor*, **24**, 1196-1207.

Venkatram A (1980). Estimating the Monin-Obukhov length in the stable boundary layer for dispersion calculations. *J Boundary Layer Meteorology*, **19**, 481-485.

Venkatram A (1992). Vertical dispersion of ground-level releases in the surface boundary layer. *Atmos Environ,* **26A,** 947-949.

Webb EK (1970). Profile relationships: The log-linear range and extension to strong stability. *Quarterly Journal of the Royal Meteorological Society*, **96**, 67-90.

Weil JC (1985). Updating applied diffusion models. *J Climate Appl Meteor,* **24** (11), 1111-1130.

Weil JC, Corio LA and Brower RP (1997). A PDF dispersion model for buoyant plumes in the convective boundary layer. *J Appl Meteor,* **36**, 982-1003.

WMO (1996*). Guide to meteorological instruments and methods of observation, Sixth Edition.* Publication of the World Meteorological Organisation Publication. ISBN : 92-63-16008-2.

Zeller K (1993). Eddy diffusivities for sensible heat, ozone and momentum from eddy correlation and gradient measurements. Research Paper RM-131. Fort Collins, US department of agriculture, forest services Rocky Mountain forest and range experiment station.

Zilitinkevich SS (1972). On the determination of the height of the ekman boundary layer. *J Boundary Layer Meteorology*, **3**, 141-145.

11 SYMBOLS AND NOTATION

C_p specific heat capacity of water

Cl cloud cover (in oktas)

d: zero plane displacement

$F_{\theta 0}$ sensible heat flux

g acceleration due to gravity

h boundary layer depth

h_{ic} convective boundary layer height

h_{im} mechanical mixed boundary layer height

k Von Karman's constant

L_{MO} Monin Obukhov length

PBL planetary boundary layer

PG	Pasquill Gifford - stability category
r	surface albedo
RH	relative humidity
Ri	Richardson number
S	rate of change of saturation specific humidity with temperature
T_0	absolute temperature
T_z	temperature at reference height z
T'	turbulent fluctuations in air temperature
T_*	eddy temperature constant
u_z	wind speed at reference height z
u_*	friction velocity
w	vertical wind velocity
w'	turbulent fluctuations in vertical velocity
w_*	convective velocity scale
z	vertical height (m)
z_0	roughness length (m)
α	modified Priestley Taylor parameter
β	Bowen ratio
θ_z	potential temperature at height z (°C)
θ_*	eddy potential temperature constant
λ	specific latent heat of vapourisation of water
Φ_z	wind direction at reference height z
ρ_a	density of air
σ_v	lateral turbulence parameter
σ_w	vertical turbulence parameter
σ_y	lateral dispersion parameter
σ_{ya}	ambient atmospheric turbulence component
σ_{yb}	source buoyancy induced turbulence component
σ_{yc}	building downwash induced component

σ_{yt} lateral turbulence induced component

σ_{yw} wind direction unsteadiness component

σ_z vertical dispersion parameter

σ_θ standard deviation of wind direction

Ψ_H empirically derived stability correction factors for heat

Ψ_M empirically derived stability correction factors for momentum

12 TABLES

Table 1: System resolution and accuracy for in-situ digital measurements recommended by the US-EPA

Variable	System Accuracy	Measurement resolution	Sensor specification
Wind speed	± (0.2 m/s + 5% of observed)	0.1 m/s	Threshold ≤ 0.5 m/s
Wind direction	± 5 degrees	1 degree	Threshold ≤ 0.5 m/s @10 deg
Ambient temperature	± 0.5 °C	0.1 °C	Time constant ≤ 1 min
Vertical temperature difference	± 0.1 °C	0.02 °C	
Precipitation	± 10% of observed or ± 5 mm	0.3 mm	
Solar radiation	± 5% of observed	10 W/m^2	2nd class standard resolution >± 10 W/m^2 Spectral response 285 nm to 2800 nm
Pressure	± 3 mb (0.3 kPa)	0.5 mb	
Vertical ΔT	± 0.1 °C	0.02 °C	Time constant ≤ 1 min
Dew point temperature	± 1.5 °C	0.1 °C	Time constant ≤ 30 min

Table 2: Analysis of the Ringway 2000 meteorological dataset to derive the frequency of occurrence of each of 7 stability classes, F(SC), and the average boundary layer properties for each class

The ADMS 3.1 meteorological pre-processor was used to derive boundary layer parameters from the original dataset and the relationship between Monin-Obukhov length and stability class from Golder (1972) was used for the banding of values, z_0=0.1

Stability Class	Frequency ofu SC	(m s^{-1})	u_* (m s^{-1})	$F_{\theta 0}$ (W m^{-2})	h (m)	θ_* (°C)	L_{MO} (m)
A	0.03	1.17	0.15	68.99	542	-0.389	-4
B	0.03	2.14	0.22	63.05	630	-0.23126	-15
C	0.08	3.43	0.33	56.18	687	-0.14256	-56
D	0.47	6.14	0.53	-7.1	625	0.011106	1820
E	0.19	3.38	0.25	-19.99	146	0.06475	68
F	0.06	2.29	0.13	-10.3	57	0.066589	19
G	0.13	1.31	0.03	-1.87	50	0.055283	1

Table 3: Error analysis on the effect of measurement error and sensor configuration on the predictions of the flux-profile method for estimating heat fluxes and friction velocities

CV: coefficient of variation (standard deviation/ mean)

Stability class	Number of heights	Coarse				Fine			
		95 %ile	50 % ile	5 %ile	CV	95 %ile	50 % ile	5 %ile	CV
		Friction velocity (m s^{-1})							
	4	0.14	0.15	0.16	0.05	0.15	0.15	0.15	0.02
A	2	0.13	0.15	0.17	0.08	0.14	0.15	0.16	0.03
	4	0.20	0.22	0.24	0.05	0.21	0.22	0.23	0.02
B	2	0.19	0.22	0.25	0.08	0.21	0.22	0.23	0.03
	4	0.30	0.33	0.36	0.06	0.32	0.33	0.34	0.02
C	2	0.29	0.33	0.37	0.08	0.31	0.33	0.35	0.03
	4	0.48	0.53	0.58	0.06	0.51	0.53	0.55	0.03
D	2	0.45	0.53	0.61	0.09	0.50	0.53	0.56	0.03
	4	0.22	0.25	0.28	0.07	0.24	0.25	0.26	0.03
E	2	0.22	0.27	0.32	0.11	0.25	0.27	0.29	0.04
	4	0.11	0.13	0.15	0.11	0.12	0.13	0.14	0.04
F	2	0.16	0.19	0.23	0.11	0.18	0.19	0.20	0.04
	4	0.02	0.04	0.06	0.30	0.03	0.04	0.05	0.11
G	2	0.27	0.30	0.35	0.08	0.29	0.30	0.32	0.03
		Heat flux (W m^{-2})							
	4	48.6	68.9	91.1	0.19	64.3	68.5	72.7	0.04
A	2	35.5	68.8	111.2	0.33	60.9	68.6	76.8	0.07
	4	46.2	62.8	81.9	0.17	59.0	62.7	66.3	0.04
B	2	35.4	62.6	96.3	0.29	56.7	62.7	69.2	0.06
	4	38.2	55.8	75.7	0.20	52.0	56.0	59.9	0.04
C	2	32.6	55.8	83.5	0.27	50.7	55.8	61.1	0.06
	4	-27.6	-7.2	14.1	-1.78	-11.3	-7.1	-2.8	-0.37
D	2	-24.6	-7.2	11.9	-1.62	-10.7	-7.1	-3.5	-0.31
	4	-28.2	-20.0	-11.1	-0.26	-22.0	-20.0	-18.2	-0.06
E	2	-29.6	-22.6	-16.5	-0.18	-25.3	-23.1	-20.9	-0.06
	4	-13.2	-10.2	-7.5	-0.17	-11.5	-10.5	-9.6	-0.05
F	2	-27.5	-22.0	-16.9	-0.15	-24.3	-22.1	-20.0	-0.06
	4	-7.8	-3.7	-1.3	-0.51	-5.0	-3.7	-2.5	-0.21
G	2	-234.3	-192.6	-155.7	-0.12	-208.7	-192.6	-177.4	-0.05

Table 4: Dispersion factors (s m^{-3}) at 6 downwind distances from a 40 m stack for the uncertainties in heat fluxes and friction velocities for the 4 point profile for coarse precision instrumentation

NA: divide by zero OR: over-range

Stability Class		100 m	400 m	700 m	1000 m	1500 m	2000 m
	95%ile	1.06E-04	1.61E-05	6.49E-06	3.90E-06	2.32E-06	1.67E-06
	50%ile	9.49E-05	1.34E-05	5.50E-06	3.33E-06	1.99E-06	1.43E-06
	5%ile	8.32E-05	1.15E-05	4.79E-06	2.92E-06	1.75E-06	1.25E-06
A	95:5	1.28	1.40	1.35	1.34	1.33	1.33
	95%ile	3.87E-05	1.78E-05	6.38E-06	3.37E-06	1.75E-06	1.14E-06
	50%ile	2.54E-05	1.55E-05	5.47E-06	2.91E-06	1.52E-06	9.95E-07
	5%ile	1.49E-05	1.36E-05	4.76E-06	2.55E-06	1.34E-06	8.80E-07
B	95:5	2.60	1.31	1.34	1.32	1.30	1.30
	95%ile	2.60E-06	1.68E-05	7.47E-06	3.93E-06	1.86E-06	1.10E-06
	50%ile	1.13E-06	1.52E-05	6.49E-06	3.31E-06	1.55E-06	9.21E-07
	5%ile	4.38E-07	1.40E-05	5.68E-06	2.85E-06	1.33E-06	7.93E-07
C	95:5	5.93	1.20	1.31	1.38	1.40	1.39
	95%ile	4.34E-09	9.12E-06	6.84E-06	4.60E-06	2.67E-06	1.77E-06
	50%ile	2.41E-10	7.98E-06	6.14E-06	4.11E-06	2.37E-06	1.57E-06
	5%ile	7.41E-11	7.14E-06	5.55E-06	3.59E-06	1.97E-06	1.24E-06
D	95:5	58.58	1.28	1.23	1.28	1.35	1.43
	95%ile	2.48E-12	1.10E-05	1.06E-05	7.83E-06	5.22E-06	3.87E-06
	50%ile	8.62E-17	4.36E-06	7.93E-06	6.95E-06	4.82E-06	3.56E-06
	5%ile	1.64E-23	8.93E-07	4.32E-06	5.27E-06	4.34E-06	3.04E-06
E	95:5	OR	12.35	2.45	1.49	1.20	1.28
	95%ile	0.00E+00	2.65E-07	2.94E-06	4.74E-06	5.03E-06	4.39E-06
	50%ile	0.00E+00	1.11E-10	7.99E-08	5.15E-07	1.45E-06	1.99E-06
	5%ile	0.00E+00	3.31E-15	5.24E-10	2.09E-08	2.12E-07	5.32E-07
F	95:5	NA	OR	5613.15	227.22	23.69	8.25
	95%ile	0.00E+00	0.00E+00	1.10E-20	1.65E-15	6.95E-12	3.13E-10
	50%ile	0.00E+00	0.00E+00	0.00E+00	0.00E+00	4.12E-19	1.47E-15
	5%ile	0.00E+00	0.00E+00	0.00E+00	0.00E+00	0.00E+00	0.00E+00
G	95:5	NA	NA	NA	NA	NA	NA

Table 5: Dispersion factors (s m^{-3}) at 6 downwind distances from a 40 m stack for the uncertainties in heat fluxes and friction velocities for the 4 point profile for fine precision instrumentation

NA: divide by zero OR: over-range

Stability Class		100 m	400 m	700 m	1000 m	1500 m	2000 m
	95%ile	1.00E-04	1.39E-05	5.68E-06	3.45E-06	2.07E-06	1.49E-06
	50%ile	9.58E-05	1.34E-05	5.50E-06	3.33E-06	1.99E-06	1.43E-06
	5%ile	9.12E-05	1.30E-05	5.34E-06	3.23E-06	1.92E-06	1.37E-06
A	95:5	1.10	1.07	1.06	1.07	1.08	1.09
	95%ile	2.99E-05	1.60E-05	5.64E-06	2.99E-06	1.57E-06	1.03E-06
	50%ile	2.55E-05	1.56E-05	5.47E-06	2.90E-06	1.52E-06	9.95E-07
	5%ile	2.16E-05	1.51E-05	5.31E-06	2.82E-06	1.47E-06	9.62E-07
B	95:5	1.39	1.06	1.06	1.06	1.06	1.07
	95%ile	1.49E-06	1.58E-05	6.69E-06	3.42E-06	1.60E-06	9.51E-07
	50%ile	1.14E-06	1.53E-05	6.49E-06	3.31E-06	1.55E-06	9.18E-07
	5%ile	8.74E-07	1.49E-05	6.32E-06	3.20E-06	1.50E-06	8.88E-07
C	95:5	1.71	1.06	1.06	1.07	1.07	1.07
	95%ile	4.00E-10	8.08E-06	6.42E-06	4.36E-06	2.53E-06	1.68E-06
	50%ile	2.42E-10	7.74E-06	6.16E-06	4.18E-06	2.44E-06	1.62E-06
	5%ile	1.83E-10	7.43E-06	5.90E-06	3.99E-06	2.30E-06	1.51E-06
D	95:5	2.18	1.09	1.09	1.09	1.10	1.11
	95%ile	1.18E-15	5.58E-06	8.62E-06	7.27E-06	5.07E-06	3.75E-06
	50%ile	8.52E-17	4.38E-06	7.96E-06	7.05E-06	4.94E-06	3.59E-06
	5%ile	3.02E-18	3.21E-06	7.18E-06	6.78E-06	4.80E-06	3.44E-06
E	95:5	391.55	1.74	1.20	1.07	1.06	1.09
	95%ile	0.00E+00	1.59E-09	2.80E-07	1.13E-06	2.28E-06	2.69E-06
	50%ile	0.00E+00	1.22E-10	8.40E-08	5.33E-07	1.48E-06	2.03E-06
	5%ile	0.00E+00	4.79E-12	1.83E-08	2.04E-07	8.47E-07	1.39E-06
F	95:5	NA	332.37	15.34	5.52	2.69	1.93
	95%ile	0.00E+00	0.00E+00	0.00E+00	1.60E-21	8.75E-16	4.26E-13
	50%ile	0.00E+00	0.00E+00	0.00E+00	0.00E+00	3.48E-19	1.30E-15
	5%ile	0.00E+00	0.00E+00	0.00E+00	0.00E+00	3.80E-25	4.82E-20
G	95:5	NA	NA	NA	NA	OR	OR

Table 6: Seasonal values of energy balance and surface roughness parameters for cultivated land

Source: Thé et al (2001) AERMET user guide

Relationship between Bowen ratio and Priestley Taylor parameter based on an average annual temperature of 15ºC

Season	Bowen ratio (ave moisture)	Priestley Taylor parameter	Albedo (ADMS)	Roughness length
Spring	0.3	1.23	0.14	0.03
Summer	0.5	1.07	0.2	0.20
Autumn	0.7	0.94	0.18	0.05
Winter	1.5	0.64	0.6	0.01
ADMS default	*0.6*	*1*	*0.23*	*0.1*

Table 7: Input parameters for the 40 m model test case scenario

Stack Parameters	Stack Characteristics
Emission height	40 m
Emission diameter	1m
Efflux velocity	5 m/s
Efflux temperature	15°C
Emission substance	SO_2
Emission rate	1 g/s
Gridding	-1000 to 1000 m, 64.5 m spacing
Receptor locations	250, 500, 1000, 1500 to N, S, E & W
Output concentrations	Annual and hourly average

Table 8: Statistical comparison of AERMET and ADMS boundary layer height

h	AMETseas-AMETdef	ADMSseas-ADMSdef	AMETseas-ADMSseas	AMETseas-ADMSdef
Mean bias (ratio of model/measured)	0.83	0.96	1.48	1.42
Average Difference	-122	-18	197	303
SD of difference	262	90	389	389
R2 Correlation	0.83	0.94	0.57	0.57
F1.25	0.35	0.91	0.32	0.33
F2	0.90	0.96	0.77	0.77

Table 9: Statistical comparison of AERMET and ADMS friction velocity

u_*	AMETseas-AMETdef	ADMSseas-ADMSdef	AMETseas-ADMSseas	AMETseas-ADMSdef
Mean bias (ratio of model/measured)	0.85	0.99	0.88	0.87
Average Difference	-0.052	-0.001	-0.043	-0.045
SD of difference	0.087	0.008	0.091	0.091
R2 Correlation	0.85	1.00	0.84	0.84
F1.25	0.48	0.97	0.48	0.45
F2	0.96	0.97	0.91	0.91

Table 10: Statistical comparison of AERMET and ADMS heat flux

$F_{\theta 0}$	AMETseas-AMETdef	ADMSseas-ADMSdef	AMETseas-ADMSseas	AMETseas-ADMSdef
Average Difference	-0.38	-3.07	8.68	6.94
SD of difference	10.05	9.12	13.84	34.93
R2 Correlation	0.96	0.95	0.87	0.86
$F_{\theta 0}$ positive F1.25	0.58	0.32	0.31	0.29
$F_{\theta 0}$ positive F2	0.95	0.80	0.70	0.73
$F_{\theta 0}$ negative F1.25	0.36	0.92	0.34	0.34
$F_{\theta 0}$ negative F2	0.95	0.97	0.84	0.85
Fraction Excluded	0.03	0.03	0.08	0.08

Table 11: Statistical comparison of AERMET and ADMS Monin-Obukhov length

$1/L_{MO}$	AMETseas-AMETdef	ADMSseas-ADMSdef	AMETseas-ADMSseas	AMETseas-ADMSdef
Average Difference	0.015	0.006	-0.083	-0.094
SD of difference	0.060	0.072	0.238	0.251
R2 Correlation	0.85	0.95	0.55	0.57
$F_{\theta 0}$ positive F1.25	0.06	0.91	0.03	0.03
$F_{\theta 0}$ positive F2	0.71	0.96	0.49	0.50
$F_{\theta 0}$ negative F1.25	0.11	0.39	0.18	0.21
$F_{\theta 0}$ negative F2	0.98	0.82	0.57	0.65
Fraction excluded	0.03	0.03	0.08	0.08

Table 12: Annual average concentrations

Model input			ADMS			AERMOD		
	Stack height	Buoy-ancy	X(m)	Y(m)	Conc (µg/m^3)	X(m)	Y(m)	Conc (µg/m^3)
ADMSdef	40	N	67	400	0.97	67	400	0.95
ADMSseas	40	N	67	400	0.94	67	467	0.90
AMETdef	40	N	67	400	0.99	67	400	1.03
AMETseas	40	N	67	400	1.00	67	400	0.79
URBAN	40	N	0	267	1.61	0	267	1.48
40m_b	40	Y	67	533	0.34	133	600	0.18
u0.75	40	N				67	400	0.78

Table 13: Maximum (100th%) hourly average concentrations

Model Input	ADMS					AERMOD				
	Date	Hour	X(m)	Y(m)	Conc (µg/m^3)	Date	Hour	X(m)	Y(m)	Conc (µg/m^3)
ADMSdef	19/06	06	-133	200	82.6	02/05	06	-400	0	67.6
ADMSseas	19/06	06	-133	200	89.7	06/04	07	-267	67	100.4
AMETdef	19/06	06	-133	200	88.9	13/01	11	133	67	195.3
AMETseas	30/09	13	-67	67	76.7	02/05	07	-133	67	207.2
URBAN	19/06	06	-67	67	62.2	21/07	06	-200	200	88.5
40m_b	30/05	09	0	133	12.2	23/08	10	-267	0	5.0
u0.75						20/02	10	-67	333	112.7

Table 14: Sixth highest hourly concentrations

	ADMS (ADMSdef)	ADMS (ADMSseas)	AERMOD (AMETseas)	AERMOD (AMET_u0.75)
	Conc (µg/m^3)	Conc (µg/m^3)	Conc (µg/m^3)	Conc (µg/m^3)
Highest hour	82.6	89.7	207.2	112.7
Sixth highest hour	51.4	52.9	141.2	34.8

Table 15: Sample hours of poor agreement between ADMS and AERMOD predictions

Date	Hour	Model	u	T	Cl	h	$F_{\theta 0}$	L_{MO}	Distance	Conc (µg/m^3)
Jan 08	06	**AERMOD**	4.1	4.8	1	**189**	**-21.3**	**239**	**1323**	**0.89**
		ADMS				*160*	*-34.4*	*76*	*602*	*5.8*
Mar 30	18	**AERMOD**	2.6	10.0	2	**1541**	**1**	**-549**	**537**	**14.8**
		ADMS				*50*	*-14.8*	*15*	*5148*	*0.93*
Mar 31	17	**AERMOD**	1.0	9.1	6	**631**	**18.1**	**-4**	**188**	**28.7**
		ADMS				*50*	*-0.56*	*1*	*Peak beyond 10 km*	
Jun 15	20	**AERMOD**	2.6	14.8	6	**303**	**-3.8**	**403**	**520**	**16.5**
		ADMS				*79*	*-13.6*	*33*	*1736*	*3.1*
Oct 21	16	**AERMOD**	2.1	11.3	4	**686**	**10.9**	**-44**	**333**	**22.2**
		ADMS				*50*	*-5.2*	*3*	*Peak beyond 10 km*	
Dec 15	13	**AERMOD**	2.1	4.2	5	**77**	**-2.3**	**43**	**1323**	**1.2**
		ADMS				*216*	*5.4*	*-115*	*427*	*14.8*

Table 16: Sample hours of good agreement between ADMS and AERMOD predictions

Date	Hour	Model	u	T	Cl	h	$F_{\theta 0}$	L_{MO}	Distance	Conc ($\mu g/m^3$)
Apr 03	16	**AERMOD**	9.3	2.9	8	**1948**	**9.8**	**-998**	**569**	**6.0**
		ADMS				*1463*	*-6.8*	*0.0001*	*422*	*4.6*
Jun 21	04	**AERMOD**	7.2	15.4	8	**1421**	**-39.6**	**860**	**507**	**6.4**
		ADMS				*572*	*-27.1*	*769*	*508*	*5.9*
Jun 21	20	**AERMOD**	6.7	15	6	**1315**	**-5.7**	**5009**	**426**	**8.2**
		ADMS				*524*	*-30.2*	*555*	*521*	*6.3*
Jun 21	21	**AERMOD**	7.2	13.5	5	**1399**	**-64**	**517**	**388**	**6.6**
		ADMS				*462*	*-54.4*	*370*	*538*	*5.9*
Jul 21	20	**AERMOD**	3.6	21.5	5	**492**	**-13.2**	**298**	**471**	**11.3**
		ADMS				*150*	*-24.5*	*77*	*745*	*7.4*
Jul 21	21	**AERMOD**	4.1	19.5	5	**552**	**-34.1**	**151**	**679**	**8.3**
		ADMS				*189*	*-28.9*	*106*	*745*	*7.4*
Oct 22	09	**AERMOD**	3.1	9.0	5	**285**	**15.4**	***-89***	**388**	**18.8**
		ADMS				*202*	*9.8*	*-196*	*389*	*14.8*
Oct 25	12	**AERMOD**	8.2	11.3	7	**1137**	**33.2**	***-658***	**400**	**7.6**
		ADMS				*1300*	*16.8*	*-2000*	*400*	*5.8*

Table 17: Analysis of the uncertainty in meteorological data determined from paired meteorological measurements

Data reproduced from Hill et al (2002)

Wind Speed bin ($m\ s^{-1}$)	Median coefficient of variation for Wind Speed (non dimensional)	Median Wind Angle Difference (degrees)
<1.9	0.19	31.75
>1.9 <2.5	0.17	22.15
>2.5 < 3.2	0.13	14.62
>3.2 <4.1	0.12	10.04
>4.1 <5.0	0.13	5.93
>5.0 <6.0	0.14	5.32
>6.0 <6.9	0.15	5.35
>6.9 <8.1	0.16	5.52
>8.1	0.15	5.27

Table 18: Variations in Bowen-ratios and surface albedo for grassland

Season	Bowen ratio		Albedo
	Dry surface	Wet surface	
Spring	1.0	0.3	0.18
Summer	2.0	0.4	0.18
Autumn	2.0	0.5	0.20
Winter	2.0	0.5	0.60

Table 19: Range of possible values (expressed at the 95% confidence level) for the annual average concentration of SO_2 determined from 2000 datapoints

	North	East	South	West
Distance = 250 m				
Scenario (i)	1.12	1.16	1.33	1.25
Scenario (ii)	1.10	1.12	1.27	1.20
Scenario (iii)	2.18	1.73	2.05	1.46
Distance = 500 m				
Scenario (i)	1.07	1.10	1.23	1.18
Scenario (ii)	1.06	1.09	1.20	1.16
Scenario (iii)	1.41	1.26	1.50	1.28
Distance = 1000 m				
Scenario (i)	1.07	1.11	1.25	1.17
Scenario (ii)	1.07	1.11	1.23	1.18
Scenario (iii)	1.21	1.15	1.33	1.23
Distance = 1500 m				
Scenario (i)	1.08	1.13	1.27	1.18
Scenario (ii)	1.08	1.13	1.26	1.19
Scenario (iii)	1.22	1.15	1.31	1.22

Table 20: Median annual average concentration of SO_2 determined from 2000 datapoints

	North	East	South	West
		Distance = 250 m		
Scenario (i)	0.69	0.60	0.16	0.27
Scenario (ii)	0.81	0.70	0.18	0.32
Scenario (iii)	1.11	0.86	0.23	0.36
Deterministic	0.71	0.64	0.13	0.29
		Distance = 500 m		
Scenario (i)	0.85	0.54	0.14	0.20
Scenario (ii)	0.86	0.52	0.13	0.19
Scenario (iii)	0.99	0.57	0.15	0.21
Deterministic	0.90	0.57	0.12	0.21
		Distance = 1000 m		
Scenario (i)	0.46	0.26	0.07	0.10
Scenario (ii)	0.45	0.24	0.06	0.09
Scenario (iii)	0.47	0.25	0.07	0.10
Deterministic	0.49	0.27	0.06	0.10
		Distance = 1500 m		
Scenario (i)	0.28	0.15	0.04	0.06
Scenario (ii)	0.27	0.14	0.04	0.06
Scenario (iii)	0.28	0.14	0.04	0.06
Deterministic	0.29	0.16	0.04	0.06

Table 21: Range of possible values (expressed at the 95% confidence level) for the 99.7th percentile of hourly concentrations of SO_2 determined from 2000 datapoints

	North	East	South	West
Distance = 250 m				
Scenario (i)	1.19	1.16	1.38	1.22
Scenario (ii)	1.16	1.15	1.24	1.21
Scenario (iii)	1.29	1.25	1.41	1.26
Distance = 500 m				
Scenario (i)	1.16	1.15	1.22	1.24
Scenario (ii)	1.15	1.13	1.20	1.23
Scenario (iii)	1.28	1.24	1.22	1.22
Distance = 1000 m				
Scenario (i)	1.11	1.11	1.19	1.16
Scenario (ii)	1.09	1.11	1.19	1.16
Scenario (iii)	1.13	1.14	1.24	1.19
Distance = 1500 m				
Scenario (i)	1.09	1.12	1.27	1.20
Scenario (ii)	1.09	1.12	1.27	1.21
Scenario (iii)	1.14	1.19	1.35	1.27

Table 22: Median values of the 99.7th percentile of hourly concentrations of SO_2 determined from 2000 datapoints

	North	East	South	West
		Distance = 250 m		
Scenario (i)	23.46	23.73	15.40	22.52
Scenario (ii)	22.40	21.59	15.16	20.71
Scenario (iii)	22.98	21.91	16.04	20.71
Deterministic	23.84	23.91	11.68	24.23
		Distance = 500 m		
Scenario (i)	12.79	12.38	8.57	11.13
Scenario (ii)	11.90	11.08	7.75	9.89
Scenario (iii)	11.61	10.88	8.01	9.69
Deterministic	13.04	12.13	8.23	10.51
		Distance = 1000 m		
Scenario (i)	6.01	5.86	4.43	5.36
Scenario (ii)	5.77	5.54	4.19	5.00
Scenario (iii)	5.83	5.57	4.20	4.97
Deterministic	5.98	5.91	4.28	5.22
		Distance = 1500 m		
Scenario (i)	4.13	3.97	2.88	3.56
Scenario (ii)	4.03	3.82	2.75	3.37
Scenario (iii)	4.04	3.82	2.76	3.32
Deterministic	4.16	3.96	2.62	3.67

13 FIGURES

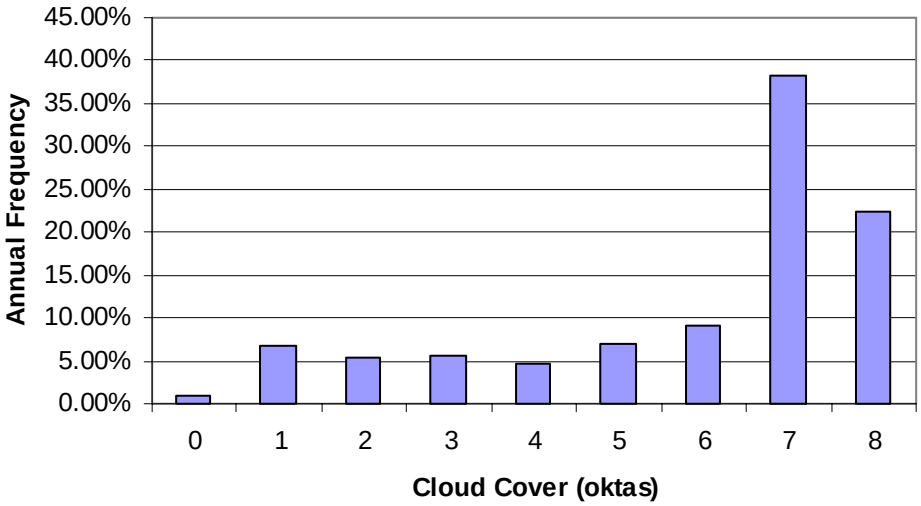

Figure 1: Frequency of cloud cover for Ringway 2000 dataset

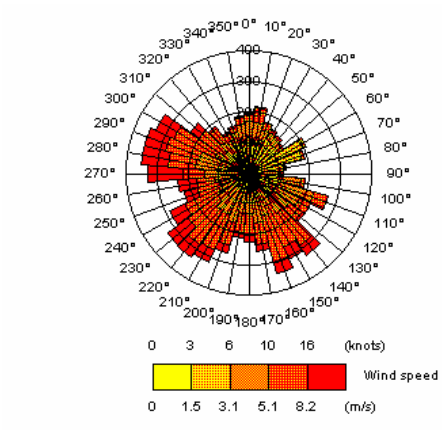

a) Sellafield site measurements

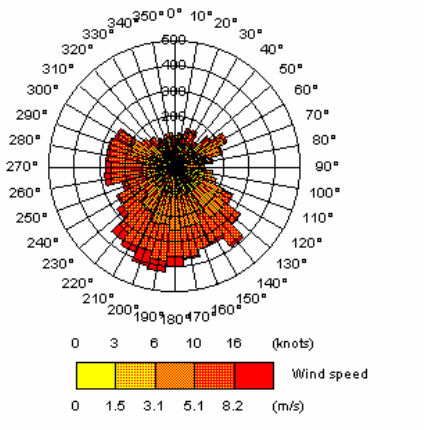

b) NWP from nearest grid to Sellafield

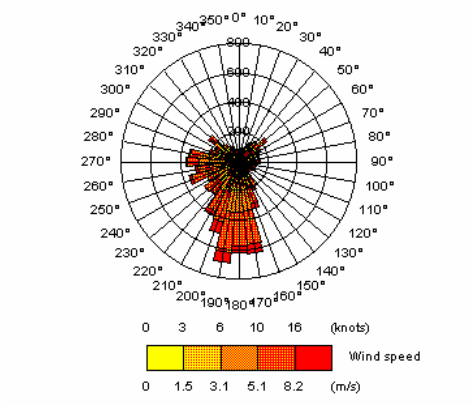

c) Ringway Met Office site measurements

Figure 2: Wind roses from a) measurements at Sellafield site, b) nearest NWP grid, and c) Ringway for 2000.[1]

[1]Wind roses created using ADMS windrose viewer

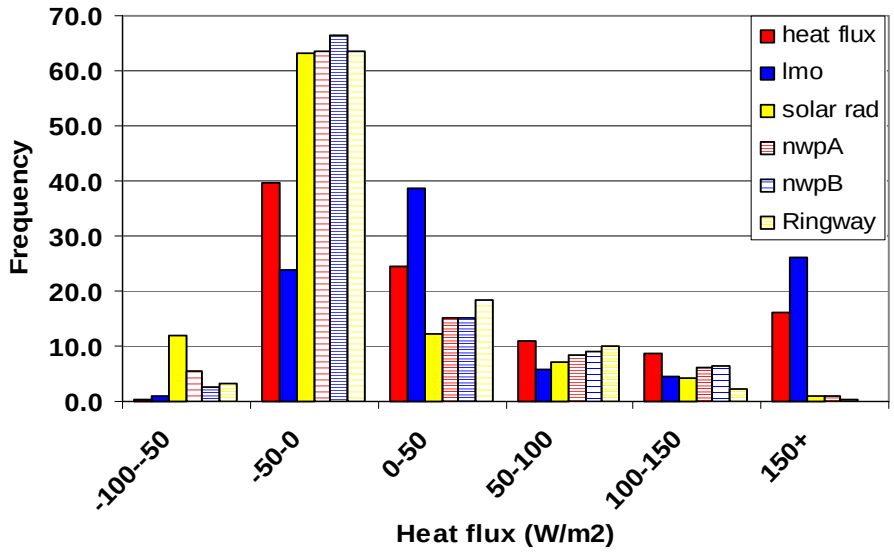

Figure 3: Binned frequency of heat flux estimates from 5 different met data inputs to ADMS

Heat flux: $F_{\theta 0}$ estimated from flux profile method
LMO: L_{MO} from the flux profile method used to estimate $F_{\theta 0}$ from ADMS pre-processor
Solar rad: Solar radiation Sellafield site measurements input to ADMS pre-processor
NWP A & B: NWP data (cloud cover) from two closest grid points to Sellafield site input to pre-processor
Ringway: Ringway, 2000 (cloud cover) input to ADMS pre-processor.

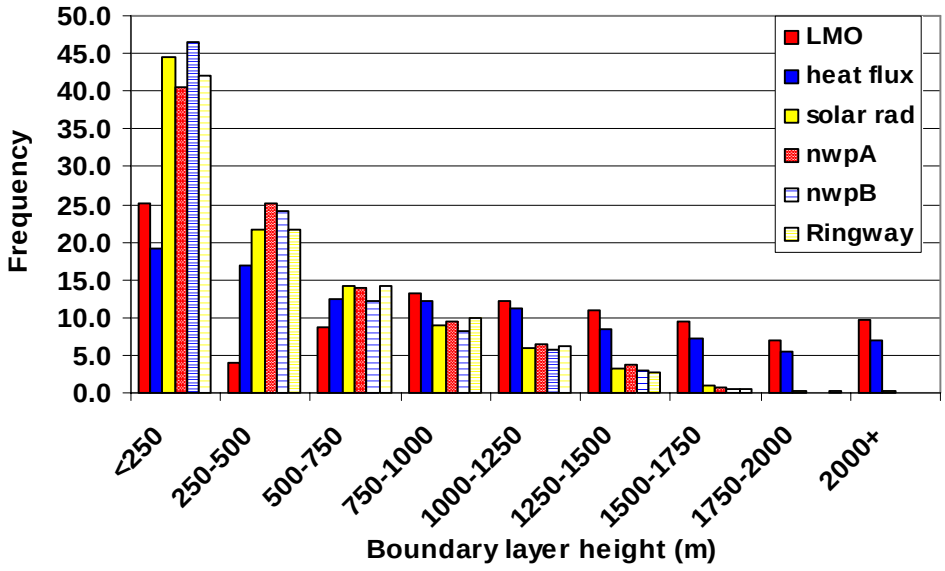

Figure 4: Binned frequency of boundary layer estimates from 5 different met data inputs to ADMS

Heat flux: $F_{\theta 0}$ from the flux profile method used to obtain *h* from the ADMS pre-processor
LMO: L_{MO} from the flux profile method used to obtain *h* from the ADMS pre-processor
Solar rad: Solar radiation Sellafield site measurements input to ADMS pre-processor
NWP A & B: NWP data (cloud cover) from two closest grid points to Sellafield site input to pre-processor
Ringway: Ringway, 2000 (cloud cover) input to ADMS pre-processor.

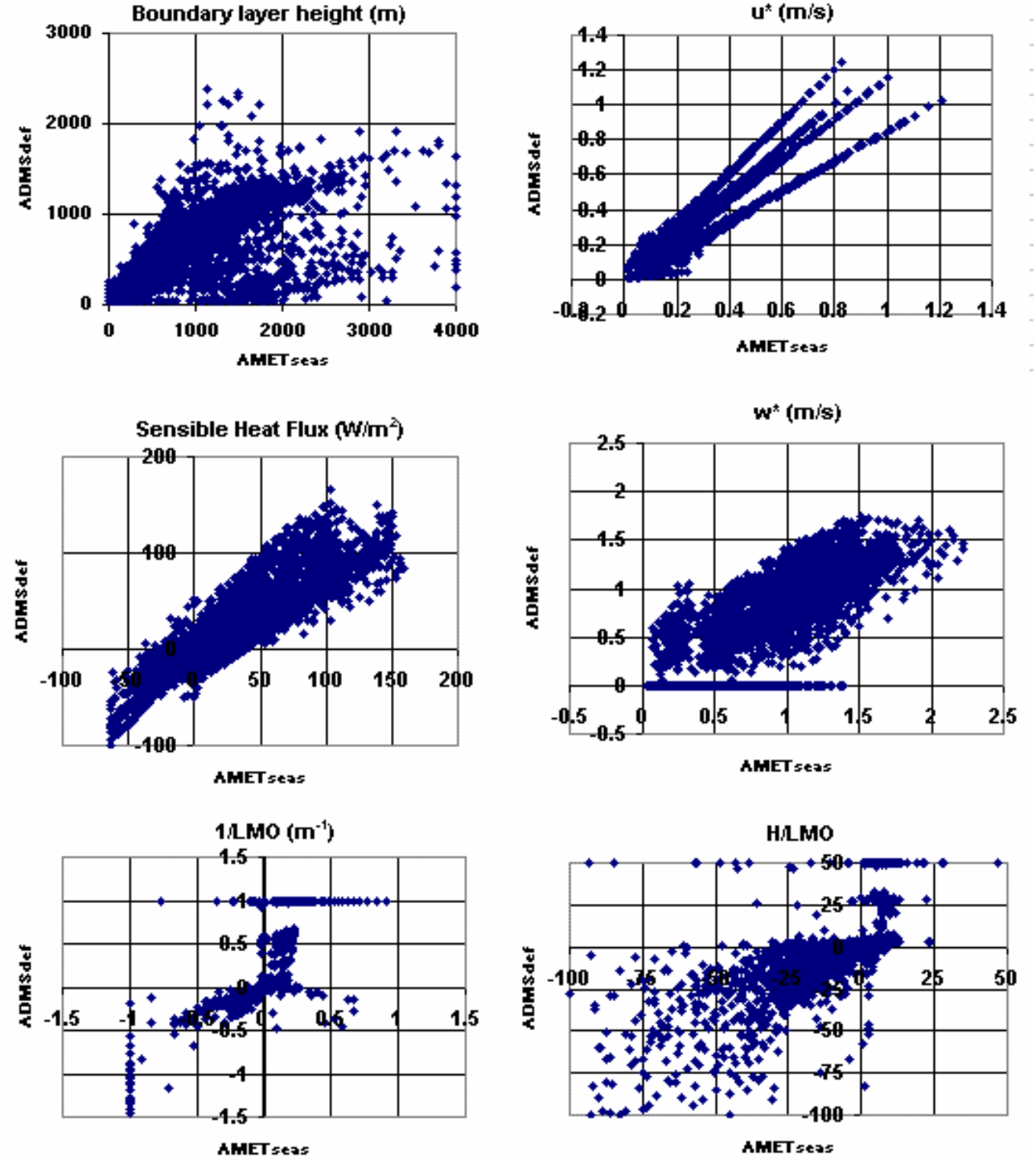

Figure 5: Correlation of boundary layer parameters between ADMS and AERMET pre-processors for Ringway, 2000

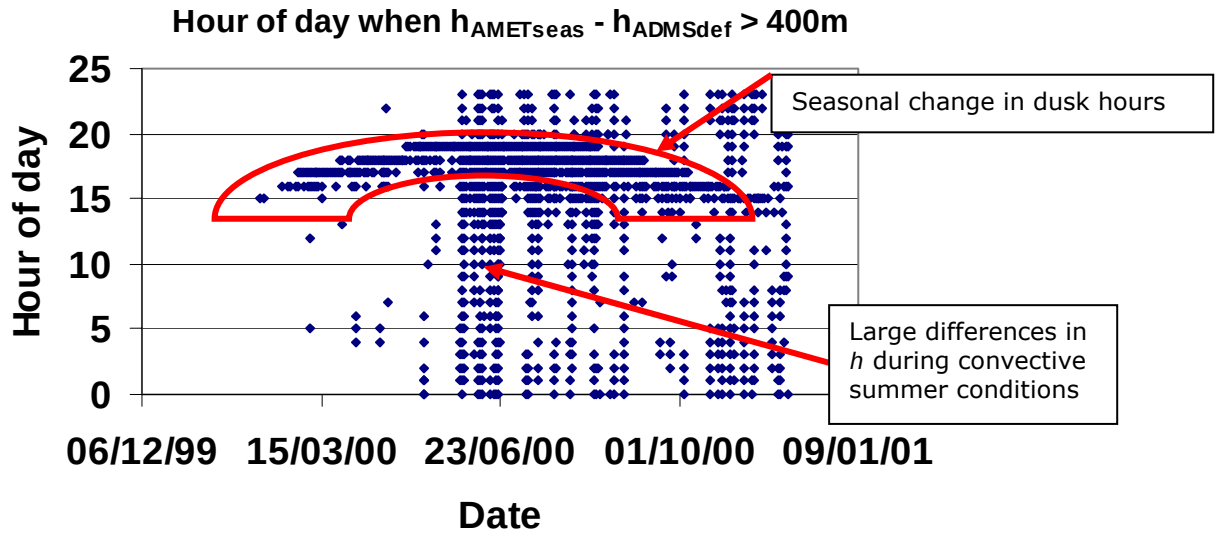

Figure 6: Hours during which disparity between ADMS and AERMET boundary layer heights are greatest

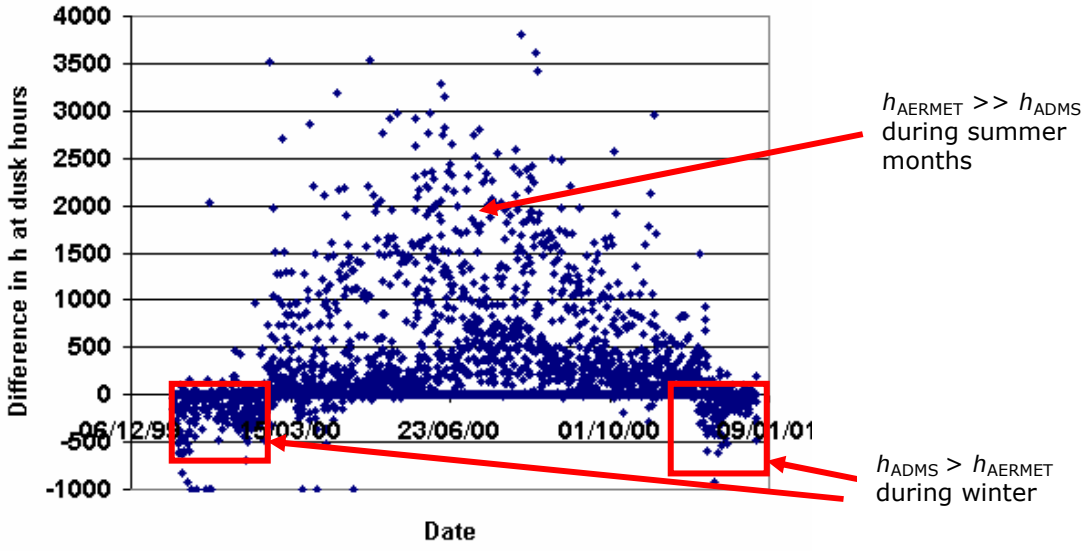

Figure 7: Seasonal dependence of boundary layer height differences between ADMS and AERMET

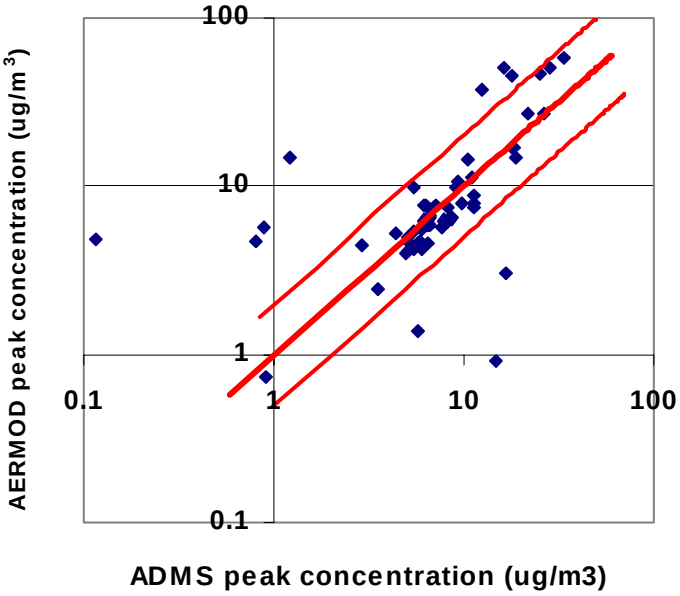

Figure 8: Correlation of peak concentrations from ADMS and AERMOD

Thick solid line indicates 1:1 agreement

Solid lines indicate within a 2:1 agreement

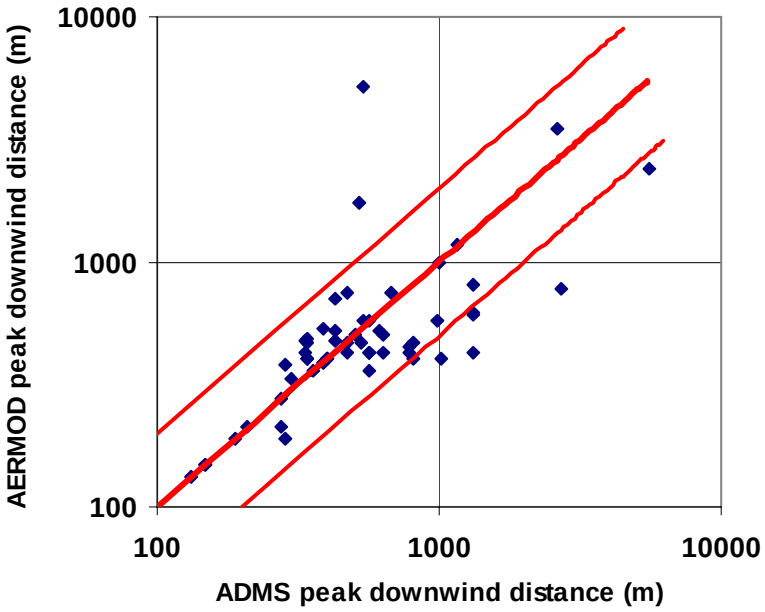

Figure 9: Correlation of downwind distance of peak concentration from ADMS and AERMOD

Thick solid line indicates 1:1 agreement

Solid lines indicate within a 2:1.agreement

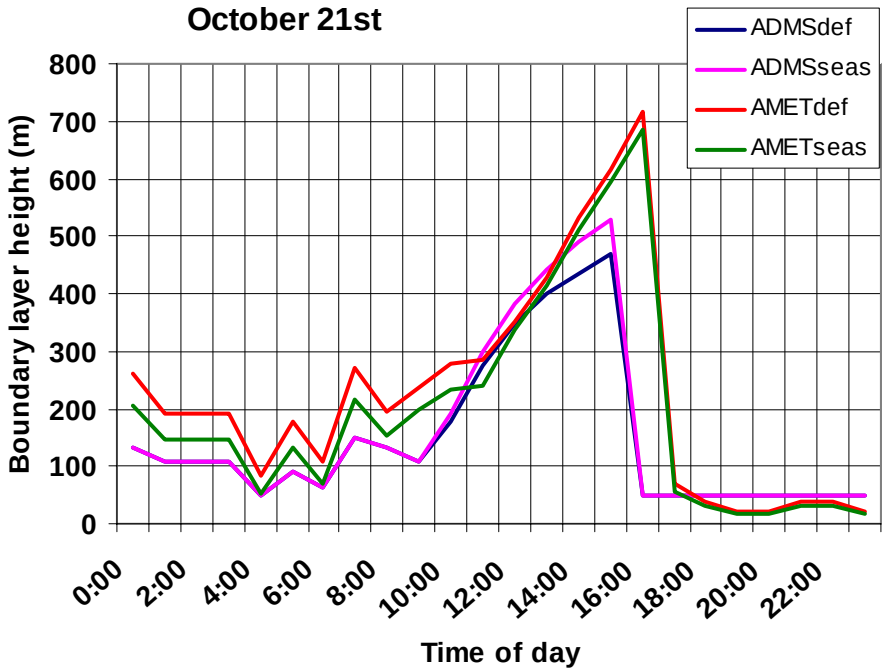

Figure 10: Boundary layer height estimates of ADMS and AERMET pre-processors for October 21st

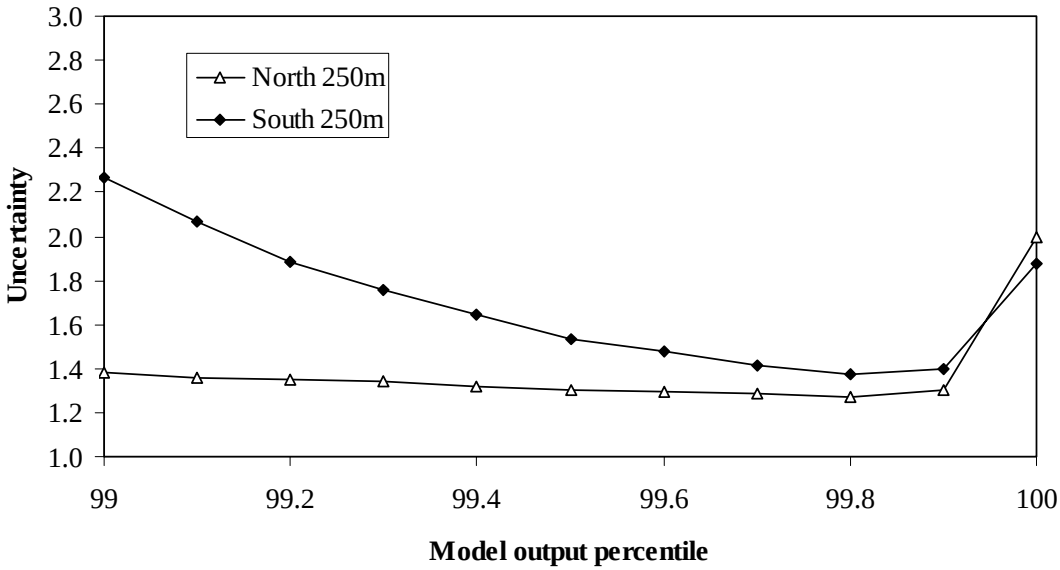

Figure 11: The relationship between uncertainty (as defined by the ratio of the 97.5th to 2.5th percentiles of the Monte Carlo simulations) and the various percentiles of the hourly concentration distribution output by ADMS

Data correspond to scenario (iii) of the Monte Carlo model and relate to a stack height of 40 m.

APPENDIX A RECONSTRUCTING TEMPERATURE AND WIND SPEED PROFILES

A1 Interpreting profiles to estimate boundary layer parameters

In Section 5.2 of this report a Monte Carlo method was presented for assessing the uncertainty in the predictions of the flux gradient micrometeorological method that arise from uncertainty in wind speed and potential temperatures. To recap, Equations A1 and A2 can be used to interpret vertical gradients in wind speed (u) and potential temperature (θ) to determine friction velocities (u_*) and eddy temperatures (θ_*). Where measurements are made at multiple heights gradients are determined from the measurement data using linear regression analysis.

$$u_* = k \frac{\partial u \{z-d\}}{\partial [\ln(z-d) + \Psi_M]} \qquad \textbf{Equation A1}$$

$$\theta_* = k \frac{\partial \theta \{z-d\}}{\partial [\ln(z-d) + \Psi_H]} \qquad \textbf{Equation A2}$$

Following the determination of u_* and θ_* it is relatively straightforward to calculate sensible heat flux and Monin Obukhov length for input into an atmospheric dispersion model using Equations A3 and A4.

$$F_{\theta 0} = -\rho_a \, C_p u_* \, \theta_* \qquad \textbf{Equation A3}$$

$$L_{MO} = -\frac{\rho_a \, C_p (\theta + 273) \, u_*^{\,3}}{k \, g \, F_{\theta 0}} \qquad \textbf{Equation A4}$$

It should however be noted that Ψ_H and Ψ_M in Equations A1 and A2 are semi-empirical stability correction terms (integrated with respect to height). We have used the derivations for a stable atmosphere of Thom (1975) (Equation A5).

$$\Psi_M = \Psi_H = \frac{5.2 \, (z-d)}{L_{MO}} \qquad \textbf{Equation A5}$$

Whilst for an unstable atmosphere we have used the derivation of Paulson (1970), Equations A6, A7 and A8.

$$\Psi_M = -2\ln\left(\frac{1+x}{2}\right) + \ln\left(\frac{1+x^2}{2}\right) - 2\,\mathrm{TAN}^{-1}(x) + \frac{\pi}{2} \qquad \textbf{Equation A6}$$

$$\Psi_H = -2\ln\left(\frac{1+x^2}{2}\right) \qquad \textbf{Equation A7}$$

Where TAN^{-1} is in radians and

$$x = \left[1 - \frac{16\,(z-d)}{L_{MO}}\right]^{0.25} \qquad \textbf{Equation A8}$$

It should be noted that Ψ_H and Ψ_M are both functions of the Monin-Obukhov length, which causes a degree of circularity in the use of this method for deriving heat fluxes and friction velocities. Consequently, these equations are often solved iteratively. An alternative to the iterative solution method was used herein. This method used the relationships between the Richardson's number (Ri) and the Monin-Obukhov length derived by Webb (1970) for stable conditions (Equation A9) and by Dyer and Hicks (1970) (Equation A10) for unstable conditions.

$$L_{MO} = \frac{[1-(5.2\mathrm{Ri})]\,(z-d)}{\mathrm{Ri}} \qquad \textbf{Equation A9}$$

$$L_{MO} = \frac{z-d}{\mathrm{Ri}} \qquad \textbf{Equation A10}$$

The Richardson's number (*Ri*) can be directly derived from the wind speed and temperature gradients using Equation A11 (Sutton, 1990).

$$\mathrm{Ri} = \frac{(z-d)\,g\,\delta\theta\,/\,\delta\ln(z-d)}{\theta\,[\delta u/\delta\ln(z-d)]^{\,2}} \qquad \textbf{Equation A11}$$

A2 Interpreting boundary layer parameters to estimate profiles

The previous section showed that it is relatively straightforward to determine boundary layer parameters from measurements of wind speed and temperature at a number of heights. We could therefore have used "real" field data within the Monte Carlo model detailed in Section 5.2, and applied error terms to those data and propagated the errors through Equations A1 – A11 in order to establish the uncertainty in the calculations of u_*, $F_{\theta 0}$ and L_{MO}. However an alternative method

was required, in order to relate the uncertainty in the application of the flux gradient method back to the meteorological conditions observed in the Ringway (2000) dataset.

Table 2 details the results of banding the Ringway (2000) dataset into seven discreet stability categories (A-G). This analysis provided a means of determining typical boundary layer parameters for each stability class. We then applied the flux gradient method in reverse to reconstruct the wind speed and temperature measurements that would be related to these profiles using Equations A12 and A13. The stability correction terms Ψ_H and Ψ_M were determined from the Monin Obukhov lengths using Equations A5 – A8.

$$u\{z-d\} = \frac{u_*}{k}\left[\ln(z-d) + \Psi_M\right] - \frac{u_*}{k}\ln(z_0) \qquad \textbf{Equation A12}$$

$$\theta\{z-d\} = \frac{\theta_*}{k}\left[\ln(z-d) + \Psi_H\right] - \frac{\theta_*}{k}\ln(z\{\theta = 0\}) \qquad \textbf{Equation A13}$$

It should be noted that z_0 in Equation A12 is the roughness height and $z\{\theta = 0\}$ in Equation A13 is the height at which potential temperature = 0. The value of $z\{\theta = 0\}$was determined by fitting the profile to a potential temperature, at a height of 2 m, of 15°C.

As a test of internal consistency in the above calculations, values of u_* and $F_{\theta 0}$ that were used to derive temperature and wind speed profiles (using Equations A12 and A13) were compared with those values output when the profiles were interpreted (using Equations A1-A11). For all stability classes, except G, the comparison showed the calculations were accurate to within approximately +/- 1%. A much larger calculation error was found when applying this method in category G. This was due to the very low values of both u_* and $F_{\theta 0}$, which increased the sensitivity of the method to the stability correction terms and to the assumption in Equation A11 that wind speed and temperature gradients were logarithmic.

Dispersion from Accidental Releases in Urban Areas

A report prepared for ADMLC by

J C R Hunt, D J Carruthers, R E Britter, N C Daish

Cambridge Environmental Consultants Ltd

This study was funded by the UK Atmospheric Dispersion Modelling Liaison Committee.

Publication date: March 2004
3 Kings Parade
Cambridge CB2 1SJ

EXECUTIVE SUMMARY

This report on dispersion from localised sources released suddenly, or over longer periods, in urban areas, together with the related air flow and meteorology, reviews the current understanding, experimental and numerical simulation data and the relative merits of different modelling approaches.

Our review follows others in analysing these phenomena and their modelling over the three spatial ranges relevant to urban areas, namely mesoscale, neighbourhood and building/street scales. At the local scale the nature of the airflow and dispersion patterns depends considerably on the type of layout of buildings and streets. We assess the current status and likely developments of 'fast approximate' modelling used in practice in emergency response mode and for scenario planning. It is noted that there are two types of models at building/street scale, both based on idealised calculations. One type considers how dispersion is affected by individual buildings and their wakes, while the other concentrates more on dispersion along and above street canyons. Such models have the capability of being combined and extended. Future work should include the special problems of dispersion in particular building complexes and the use of real time data to assess and predict releases whose occurrence is not detected until consequences have become apparent.

The development of the concepts and the calibration of these models require systematic use of 'fully computational models' with long runs on big computing systems, and laboratory and field experiments. It is noted that FCM's are being speeded up by innovative approximations, in particular by modelling the effect of buildings in terms of a force (or source) so that the representation of their shape is not exact and by ignoring Reynolds stresses in the dynamical equations which are solved inexactly by allowing numerical diffusion (caused by approximate discretisation of the equations) to simulate the physical process of turbulent diffusion. These should be focused particularly on the situations that characterise most European urban areas, namely oblique canyon flows and dispersion including the effects of gaps between buildings and side streets. Predictions from both types of models should be used to obtain ensemble statistics by calculating many realisations for differing input conditions and source locations.

A recommendation of the report is that there should be substantially more real-time monitoring of wind speeds and directions in urban areas, both ground-based and remotely, to enable these models to be used effectively. The concentrations of particles and gases within the buildings need to be predicted. These are related to their values outside the buildings which can be estimated using atmospheric dispersion modelling.

CONTENTS

1 INTRODUCTION

Previous studies have been performed and/or promoted by NRPB and ADMLC on developments in practical atmospheric dispersion modelling, notably dispersion over flat terrain parameterised by surface layer meteorology (Clarke 1979), complex processes of dispersion throughout the boundary layer (Hunt et al., 1988). Agencies in the USA have particularly focussed on complex terrain effects on dispersion (Britter and Hanna, 2003). The projects have significantly influenced the development of algorithms and software used in practice, e.g. for local releases near isolated buildings with complex atmospheric terrain processes (Carruthers et al., 1994) and for local releases near groups of buildings in near-neutral conditions (Hall et al., 1996).

This report, also commissioned by ADMLC, is a continuation of these previous studies. It focuses on the practical aspects of dispersion from accidental releases in urban areas. Building up from the scientific understanding, we base our review on our current experimental and numerical simulation data, scientific understanding and prediction capabilities (at a practical level) of dispersion from a variety of possible types of both steady and unsteady, and local and distributed sources of matter released in urban areas. Since the dispersion depends so closely on the air flow and other atmospheric processes, the review also covers these aspects of urban meteorology and modelling. The policy and research issues raised here are based on a literature survey, on our own studies and on useful conversations and meetings with other experts in this field (listed in the acknowledgements). Since this report is directed at users of models and decision makers, as well as to dispersion experts, summaries of the present conceptual framework and the types of modelling approaches currently available are presented in Tables 1-5.

We briefly outline here the main issues raised in each section of the report. In Section 2 we review the underlying concepts and prediction methods related to the airflow and meteorology of urban areas that are particularly relevant for understanding and modelling dispersion from local sources. We note how spatial and temporal patterns of flow and dispersion in urban areas greatly depend on the type of terrain where they are situated (e.g. hill, coast, desert), the prevailing meteorological conditions (e.g strong/weak geostrophic winds) and on the patterns and forms of urban building/street/open space (e.g. isolated building/canyons; high/low range of building heights, etc). Research in the related disciplines of mesoscale meteorology, geography and urban planning has led to useful concepts about all these features of urban areas. These studies have suggested that there are three characteristic ranges of length scale, each with their own general features and where different modelling approaches are necessary, depending on the requirements for accuracy and speed of computation. Research is developing rapidly within this field with important contributions coming from the CFD and wind engineering community because of their growing interest in predicting urban airflows, for example in the EC-supported QNET group (Hirsch, 2003) and in the ERCOFTAC network (Eames & Hunt, 2003). The EC COST initiative is also supporting the work on urban meteorology (Fisher, 2003). Many CFD studies in Japan of urban air flows, from

mesoscale to building scale, are now reported with innovative techniques and resulting in detailed predictions (see, for example, Journal of Wind Engineering, JAWE, No. 95, April 2003).

In Section 3 we review the objectives of dispersion predictions for accidental releases and thence the output and input constraints of modelling. The basic requirement is to know how material from a given type of source at a given location is displaced, spread out, diluted and transformed as it is carried by the natural wind and other air motion, such as those caused by traffic, building ventilation, explosions associated with the accident, or density currents associated with collapsing buildings (as occurred in New York on September 11, 2001). The spatial and temporal scales and accuracy of the required prediction depend on how the material released may be toxic, e.g. in very small quantities over short time scales (the most likely form of accidental release), and how it is transformed and deposited in the atmosphere, by chemical reactions and deposition. If such predictions are to be useful for emergency response following an accidental release it is essential that any computations should be fast (i.e. within minutes), and that input data should be available on this time scale. In some cases an 'accident' may not be known about until monitoring instruments pick up a rising concentration or until people/animals experience symptoms; then fast real-time computations are particularly urgent to locate the source using these data and also meteorological data. Then it may be possible to predict the future effects of the accident. However, it is also necessary to perform computations in order to understand and predict the possible consequences of accidental releases. These do not have to be in real time but, as with scenario studies of air pollution, it is necessary to perform a large number of such studies to cover all the possible types of accident, of meteorological scenarios and of accident consequences (e.g. for human health or arrangements for evacuation). Therefore even such off-line computations need to be fast (e.g. taking only a few minutes for each case).

Nevertheless, it is essential to validate simpler, fast methods by investigating thoroughly a few critical situations using the most accurate methods. These may take several hours to compute one case, for one location for a single meteorological situation. Depending on the spatial and temporal detail of the model and the output requirements, different data are required for the meteorology and for details of the accident. In some cases this is available, but in many cases will not be. Perhaps in future, as more monitoring instruments and closed-circuit TV are available in inner cities, where accidents might occur, it will be possible to access all their data in real time and incorporate it into prediction methods and emergency response systems. These are some of the considerations that determine the different levels of modelling and data input/output considered in this review.

In Section 4 we review the concepts and modelling methods for dispersion from typical accident releases in urban areas over the three characteristic scales, but starting from the local building/street scale, where the release occurs, to the neighbourhood and then the mesoscale covering the whole urban area. Following the rationale set out in Section 3, different approaches are described, from the most simple and rapid modelling to the most complex and computationally demanding. The key question is whether dispersion patterns from local sources

have some repeatable characteristic forms in urban areas as they do over level terrain, following Pasquill and Smith (1983). If so, this would enable robust and easily computable formulae to be used for the most common situations. In fact, this methodology has already been applied at the building/street scale in the models for dispersion from steady line sources (of vehicles) in urban street canyons (Berkowicz et al., 1997; McHugh and Stidworthy, 2000; Soulhac et al., 1998). This review concludes that this approach could be extended to local unsteady sources, especially as there is now more understanding and data about the flow and dispersion along and out of canyons.

In low density suburbs and some kinds of industrial estate where buildings are isolated, the main characteristic features of the air flow and dispersion that differ from those over level terrain are the interactions between the wakes of upwind buildings and the flows around downwind buildings. This is the basis of the UDM model (Hall et al., 2001) developed for accidental releases in urban areas at DSTL. The model has been extended to quite high density urban areas, with suitable empirical adjustment, and by extensive wind tunnel and field validation. The canyon and wake models have been extended to apply at the neighbourhood scale and even mesoscale. On the other hand, a separate modelling approach may be more appropriate for these scales much greater than the building/street scale. Here there is dispersion above and below the buildings, with the concentration varying in the horizontal direction on the neighbourhood scale. This is why detailed flow and dispersion modelling around individual buildings and streets may be superfluous and too time-consuming.

For dispersion on the urban area/mesoscale, matter from the accidental source is dispersed throughout the internal boundary layer or the mixed layer. It is usual to assume that the dispersion is similar to that over level ground with an appropriately enhanced level of roughness length z_0, e.g. as in Gaussian plume or 'box' models (Middleton, 1998). However as plumes or clouds of matter travel over extended urban scales the travel time is long enough that the air flow and the atmospheric stability can change, so that simple models can be seriously in error. For example flow reversal regularly occurs in urban areas in valleys so that urban area pollutants released during the day return to the urban area overnight – a relevant situation for many northern and western cities in the UK. This is an example where complex mesoscale airflow and dispersion modelling (e.g. using puff models such as RIMPUFF from Risø (Thykier-Nielsen et al., 1999) or more complex CFD models (Brown and Williams, 1998)) are absolutely necessary. The aim of the review here is to explain and describe these processes and models, with tables and diagrams, and suggest how the models should be used in practice.

Section 5 reviews the main field and laboratory experiments and numerical simulations on urban dispersion, especially those that can be made to test models and concepts. We make full use of recent reviews by Britter and Hanna (2003) and Hanna and Britter (2002).

Firstly field experiments on the urban scale and larger show broadly similar rates of dispersion for passive material released from localised sources as from those released over the whole urban area. This enables data from the latter to be used for the former problem over distances beyond the local building/street

scale. Thus elevated local sources over urban areas disperse as for sources over rural areas. These dispersion rates, as expected, are determined by the boundary layer stability, the ratios of Monin-Obukhov length scale to boundary layer height and changes in surface roughness/length and heat fluxes from rural to urban condition. These changes occur over the length scale of significant dispersion (~10km), therefore quasi-steady dispersion models have to be used with caution.

Secondly, experiments and simulations have shown special features of urban dispersion at the neighbourhood and street buildings scale, including how the mean transport direction differs from the mean flow above the buildings, the rapid vertical and horizontal spreading of plumes in wakes and canyons, the more complete mixing by the interacting wakes (with lower relative levels of fluctuation compared with rural terrain), the transition of dispersion below the buildings level to above them, and the variation in concentration downwind of source upwind and within the buildings. The lack of certain experiments is pointed out, notably these experiments are details of dispersion from local, short duration sources on the street building scales (such experiments have been performed for individual buildings).

An important conclusion about numerical simulation of flow around multiple buildings is that they are becoming more practical, especially since neither the boundary conditions in the buildings nor the details of the turbulence need to be modelled exactly. This suggests that random flight methods, RFM, could be adapted for fast computations of dispersion amongst buildings extending earlier work using this approach for single buildings. Note that the simple, fast algorithmic methods such as UDM or ADMS-Urban or RFM, which are based on experimental and numerical simulations, can be applied beyond these calibration experimental situations, but to apply these models with confidence to more complex configurations and problems requires further experiments and simulation.

In Section 6 we summarise the basic concepts and simple models that are appropriate for practical real-time or multi-scenario computations. Firstly some of the recent fast approximate models designed for practical use that have been here for the first time as well as those especially for the particular problems of dispersion of short release clouds in street canyons. Secondly more work is needed to interface models for the different scales. Thirdly new aspects have emerged in this review that need further study, including using real-time sensors and monitors to deal with accidents as they develop. Also the problem of dispersion of dust and aerosols generated within buildings is considered. It is necessary to consider the relation between the exterior and internal environment and perhaps the feasibility of technical means of suppressing the airborne particles.

2 METEOROLOGY AND AIRFLOW IN URBAN AREAS

2.1 Characteristic regions of flow

Over most urban areas, with overall scale L_O, as shown in Figure 1, there are considerable variations in the types, sizes and layout of buildings and streets. Over larger urban areas there are usually also significant variations in the natural topography. Both these urban scale features and meteorology including the airflow have general characteristics over different length scales. These need to be understood and related to each other when developing models for airflow and dispersion, see Table 1, Table 2. Over level terrain in light to moderate winds (3m/s) the direction and speed of the airflow only changes significantly over mesoscale distances (of order 30km) determined by the Coriolis effects, by the effect of the urban island on convergence/divergence and turning of the wind and by time variations in the flow forced by diurnal and synoptic effects. Where there are sharp variations in topography (or atmospheric conditions) the surface air flow changes locally (e.g. at the coast or edge of an urban area) on the scale of the boundary layer depth ($\lesssim$ 1km). However, the whole boundary layer flow does not adjust immediately to the change of surface conditions: this takes place over a mesoscale distance L_M which, in the atmosphere, is typically of order 30-50km. This distance is usually determined by the Rossby length scale $L_{Ro} = hN/f$ where N is the buoyancy frequency of the stable layer at or above the boundary layer of height h. Typically $N \sim 10^{-3}$ s^{-1}. For higher mountains of height H, e.g. Alps, Pyrenees, where the Froude number F = U/NH is small, then $L_R = HN/f \sim 10^2$km for buoyancy frequency (e.g. Hunt et al., 2001, 2003). In neutral conditions, L_M is determined dynamically by inertia and turbulence stresses, when $L_M \sim L_f = U/f$, usually a distance greater than 30km.

As shown in Figure 2, there is an internal layer with the depth l(x, y) above the ground, separating the air flow and pollutant above and below it. This layer depth tends to rise slowly over the area where the surface conditions change, e.g. due to temperature or surface roughness (see, for example, Garratt, 1993; Hunt & Simpson, 1982). Over mesoscale distances L_M the internal layer reaches the top of the boundary layer and so the whole boundary layer velocity and temperature profiles are changed.

Over shorter horizontal scales, the internal layer depth is much less than h, the depth of the boundary layer. Here the perturbed flow has separate characteristics over the intermediate neighbourhood scales L_N ($\lesssim$ 3km) and over the shorter building/street scales L_{BS} ($\lesssim$ 300m). The former scale L_N extends over groups of buildings/streets of similar size and type, and the internal layer depth l_N is greater than the height of the envelope or canopy of the buildings H_C. Note that there is significant mass, momentum and energy transfer between the flow in and above the canopy on this scale (which is not so important at the mesoscale). Even though on this scale many buildings and streets are included, their types of buildings and their patterns have significant effects on this exchange process and on the flow within the canopy. The physical features of the flow and the horizontal and vertical length scales for the three flow regions are related to each other in Table 1.

Turning to the main features of the flow and meteorology in the three characteristic flow regions of urban areas, we begin with those on the mesoscale. These are broadly categorised in Table 2 according to the relative effects of buoyancy to inertial forces produced by orographic or heat island effects on the one hand and the effects of Coriolis forces acting over the overall scale L_O of the urban area on the other. The former influences are essentially indicated by the value of the Froude number, defined as the ratio of the geostrophic wind U_G to the average velocity U_B produced by the buoyancy forces acting over the urban area, i.e. $F=U_G/U_B$. U_B is driven by the horizontal temperature (and density) changes $\Delta\theta$ (that may be natural or caused by the urban heat island) and is defined by $U_B = \sqrt{gl_0 |\Delta\theta| / \theta}$, where l_0 is the internal layer thickness (or H, the height of nearby mountains, if they dominate the local flow) and *g* is gravitational acceleration. Note that as a result of urban heat island effects $\Delta\theta/\theta$ increases with the scale of the urban area, but it also depends on the type of vegetation inside and outside the area. In European and North American cities, typical heating and albedo change cause $\Delta\theta$ to be positive, up to 10°C, except those in desert areas – for green cities in desert areas $\Delta\theta$ can be negative, typically -1°C (Oke, 1978; Mestayer and Anquetin, 1995). Since typically $|\Delta\theta| / \theta$ ~ 0.01, U_B~3m/s. Coriolis effects are significant if the mesoscale length scales, defined as L_f and L_{Ro}, are comparable with or less than L_O.

Referring to Table 2, we see that for case (i), typical small to medium scale urban areas, buoyancy and Coriolis effects are negligible and F > 1, and L_f, L_{Ro} > L_O. For Case (ii), as the urban area scale L_O increases, and if there are no thermal effects, Coriolis effects begin to be significant with turning of the wind. Case (iii) corresponds to where the urban heat island and thence the buoyancy velocity increases. This will change the stability and boundary layer depth over urban areas. But if, as in case (iv), the area is even larger, so that L_f, L_{Ro} < L_O, then the heat island and Coriolis effects are larger. This induces convergence and causes the flow moving towards the urban area to turn cyclonically (i.e. anticlockwise in the northern hemisphere), as has been measured, especially at night (Hunt & Simpson, 1982).

Strong buoyancy forces occur in the presence of mountains and sloping terrain, so that F<1, leading to marked diurnal variations in the wind speed and direction, over the urban area and outside it. Such areas are associated with sudden changes in the airflow, internal fronts and pooling of the air in valleys, all of which greatly influence dispersion of air pollution and products from accidental releases.

The static stability of the air stream usually changes as it moves into and out of the urban area, typically becoming less and more stable, respectively. However it should not be assumed that the boundary layer profiles over the urban area and downwind simply adjust towards the equilibrium states found in neutral, stable and unstable boundary layers over flat terrain. In fact there are characteristic features of the air flow on these scales, especially near hills, coasts and urban/rural boundaries, that can significantly affect dispersion, such as blocked flow, unsteady slope flows, gravity currents and boundary layer jets (e.g. Högström and Smedman, 1984; Owinoh et al., 2003).

The characteristic features of the air flow on the neighbourhood scale depend considerably on the grouping of the buildings/streets buildings (height H, breadth b, width *w*, distance between buildings d). In spacious suburban areas or tower block housing estates, the buildings are effectively isolated. However, in dense suburbs and inner city areas there may be a 'canyon' construction with long rows of buildings with narrow streets (e.g. Grimmond & Oke, 1999). The former are essentially porous to the oncoming boundary layer; the airflow slows down as it passes between the buildings, as a result both of their bulk displacement of the flow over and around the 'envelope' or canopy of the buildings and their drag. Downwind of a characteristic adjustment distance $\mathcal{L}_A$ (which is of the order of $H(d^2/wb)$ or H/β where β is the porosity, e.g. 10-30 building widths (Belcher et al., 2003)), the drag force dominates but is weakened by the sheltering effect of upwind buildings (see Figure 3). Also over this adjustment distance the air flow above the buildings first accelerates as a result of the vertical displacement by the buildings, and then the air flow begins to decelerate as slow moving fluid is expelled from below the level of the building envelope or canopy. Downwind of this adjustment distance, if the neighbourhood scale is large enough (i.e. $L_N > \mathcal{L}_A \sim 30H$) the air flow within the canopy, with wind speed U_C, is largely driven by turbulent shear stresses generated in the shear layer just above buildings (rather than by the impinging airflow). Above the buildings the wind speed U(z) rises from its average value U_H at the top of the buildings to a value close to U_G the geostrophic wind speed at a height just above the inner layer, where $z \sim l_N(x)$. Because of the variability H_c' in the heights of the buildings and the energetic gusts into and out of the urban canopy, there is an intermediate or roughness 'sub-layer' ($H_c < z < z_*$) whose thickness (z_*-H) is of the order of the height of the canopy, H_c. It lies between the canopy and the bottom of the upwardly-displaced surface layer which has most of the same characteristics as in the layer over a level surface. Thus for $l_N > z > z_*$,

$$U(z) \cong \frac{u_*}{\kappa} \ln\left(\frac{z - z_d}{z_0}\right) \qquad (2.1)$$

where z_d is the displacement height (which is of order H), z_0 is the roughness length, which depends on the resistance provided by the buildings in the canopy, and κ is von Karman's constant (Grimmond & Oke, 1999; Britter & Hanna, 2003; Belcher et al., 2003).

Downwind of the 'neighbourhood' or urban area where the buildings decrease in height, the mean air flow descends and accelerates. Typically in neutral conditions the mean velocity adjusts to within 10% of its ultimate (rural) value within about 30 lengths (e.g. Counihan et al., 1974). But when the rural surface layer is stably stratified the well mixed turbulence wake experiences low friction and continues further downwind, with a jet tending to form in the mean velocity profile (Owinoh et al., 2003).

By contrast, when the urban area is more densely packed with buildings and they are distributed in the 'canyon' form, on the neighbourhood scale the air does not flow between the buildings. Then it largely passes above the canopy envelope (with average height H_C) such as in the central area of Nantes

(Mestayer et al., 2002). The flow below the canopy height must depend on the particular street and building configuration at that scale. The flow above the canopy is essentially equivalent to airflow over a wide hill with length L_N and height H_C, but a significant roughness length z_0 that is of the order of the thickness of the shear layer over the buildings and the 'canyons' between them (Soulhac, 2000). The flow in the inner layer above the buildings and in the wake downwind of the neighbourhood region are similar to those for the first type of porous canopy.

On the building/street scale there are also characteristic features of the flow corresponding to different categories of building street shape and configuration. Various planning criteria and concepts have been proposed for defining these categories, for example rugosity (or mean canopy height H_C), relative rugosity (defined by height variability H'), sinuosity (of canyons), contiguity (e.g. Adolphe, 2001). These and related concepts have guided our suggested categorisation shown in Table 3 for building/street configurations and the consequences for air flow illustrated in Figure 3**.**

Fluid mechanical studies have shown how flows around individual buildings become significantly distorted in the presence of other buildings depending on the ratio b/d of the breadth b to separation distance *d* from the nearest building, on the ratio b/w of breadth b to the width w of the building and on the relative height to width ratio H/w. When there are many buildings, as in an urban areas, these flow interactions build up into characteristic flow patterns, which we now examine.

In category (vi) of Table 3, as Figure 3(a) shows, the separation distances d are large enough that $b/d \leq 1/3$, the flow around each building has approximately the same form as that of an isolated building, with recirculating flow regions, wakes and horseshoe vortex structures around its base. In slightly stable conditions the vortices can persist far downwind. In most urban cases where the flow is neutral and highly turbulent they are not significant. They are ignored for example in the UDM model of Hall et al. (1996). But the turbulent wakes from upwind buildings do impact on those downwind, enhancing the mixing. Also where the downwind buildings are almost aligned with the wind Figure 3a(ii) (i.e. $\cos \phi \leq w/d$), they distort the wake's vorticity so that the wakes tend to be aligned with the building (see examples in Eames & Hunt, 2003). This leads to the alignment of the mean flow along streets (with significant effects on dispersion, Davidson et al. (1995)).

When there are marked variations in the height of adjacent buildings, the wake vorticity shed from upwind buildings can produce sharp down-flows and increased trailing vorticity in the flow direction, (see Lawson, 1980). These effects contribute to mixing between the canopy and external flow, Figure 3b(ii). When tall buildings are closely packed (i.e. $H/w \geq 1$, $b/d \geq 1/2$), as the air flow passes around the buildings the wakes tend to disappear (because of cancellation of vorticity) and the streamlines are determined simply by the displacement or 'blocking effects' of the buildings (Davidson et al., 1995; Moulinec et al., 2003).

Categories (i), (ii), and (iii) correspond to different types of buildings and streets (and rivers in urban areas passing between high buildings) separated by relatively narrow canyons. Here the boundary layer flow mainly passes over the buildings and the canyon, but also drives both recirculating flow with a strong mean flow component along the canyon (Figure 3(c)). Theoretical analysis and preliminary computations (by Dr. S.E. Belcher at Reading University) confirm the wind tunnel results of Bottema (1993) that the wind speed tends to increase along the street, and that the effects of upwind side streets tend to amplify this acceleration (by inducing a down flow). This mechanism is analogous to that for the increasing wind speed downwind of buildings produced by strong longitudinal vortices (Kothari et al. 1986). Intense vortices tend to form in the streets on the downwind side of the canyon, and where major streets intersect. But locally formed vortices tend to break up at the end of the canyon or downwind of an isolated building, because of their self-destructive tendency in high turbulence (Miyazaki & Hunt, 2000; A.G. Robins, private communication). Isolated buildings, especially in slightly stable conditions can produce swirling wakes, far downwind (Kothari et al., 1986).

In categories (iii) and (v) when $b/d < 1/3$, corresponding to long buildings that are sufficiently separated from each other, the flow over an upwind building can descend into the space between them (Lawson, 1980). This flow is significantly sheltered and stagnation areas are larger than for isolated buildings. However some of the most sensitive buildings from the point of view of security are those where the separation distance is smaller, i.e. $b/d \geq 1$, the flow is further changed because there may be other complicating geometrical factors, such as the effect of a courtyard (which further slows up the flow) or open gateways, which can lead to sufficiently high local winds that they affect the overall flow pattern, Figure 3(d).

In conclusion it has been shown that most of the usual types of building/street shape and configuration found in urban areas can be categorised in geometrical terms that also correspond to the characteristic air flow patterns found in these situations for typical wind conditions. In particular there is a major distinction between flows determined by random interactions of wakes of well separated buildings and highly organised 'canyon' like flows that occur when the buildings form street canyons or, if they are separated, when they are positioned along streets. Flows in enclosed areas (e.g. courtyards) and very densely packed flows are other characteristic situations where wake analyses are least relevant.

2.2 Computational models for meteorology and air flow in urban areas

2.2.1 Different types of model

Here we review those computational models for both meteorology and air flow in urban areas that are used as input to models for calculating dispersion from local releases. The numerical and physical basis and operational attributes are summarised in **Table** 4 for the three ranges of length scale introduced in Section 2.1, and for the different types of model, ranging from off-line, fully computational models (FCM) to the fastest approximate models (FAM) that can

be run on PC's. The choice of the model depends on their practical purpose (in relation to dispersion modelling), the required level of spatial/temporal detail and scientific understanding involved, and on the detail and accuracy of meteorological and topographical input data. For research and for off-line validation studies, a variety of types of model tend to be used: some studies require great detail and accuracy about particular or commonly-occurring situations; others require simpler models for rapidly calculating a wide range of meteorological and topographic boundary conditions. When such models are analytically-based, their predictions can be easily understood and may be expressed in useful formulae.

The reason why it is necessary to have different types of model for the different distances is because every type of model can only represent a finite range of length scales, with ratio R of the largest to smallest, e.g. R_M for the meso scale. This ratio is limited by the capacity and speed of the computational systems and data input. Typically, in an FCM R_M may be as large as 100-300 (so that about 10^7 grid boxes might be included in a calculation). In the FAM used in practice, R_M may be of the same order ($\lesssim 100$), but the discretised methods are much faster than in the FCM (e.g. using 2-D Fourier methods, or models that aggregate individual elements such as streets).

Thus for example the smallest scale represented for each region is the ratio of the length of the region, e.g. L, to the ratio R, so that for the meso-, neighbourhood and building/street models these scales are L_M/R_M, L_N/R_N, and L_{BS}/R_{BS}. Usually there is some overlap, so that the smallest scales of one range are smaller than the largest scales of the next smaller range, i.e. $L_M/R_M > L_N$, $L_N/R_N > L_{BS}$.

2.2.2 Mesoscale models

On the mesoscale range the inputs to the models are the representation/ parameterisation of the topography and the natural features of the surface necessary for computations down to the smallest scale L_M/R_M (which typically is of order 1/3-1km) This is therefore the scale over which the surface conditions are averaged, including ground surface elevation $z_s(x, y)$ (averaged over this scale), roughness length $z_0(x, y)$, surface heat flux $F_\theta(x, y, t)$, surface temperature $\theta_s(x, y, t)$ (which is usually derived in operational mesoscale models by coupling the atmospheric model to a thermal model for ground temperature, allowing for radiation from/to the earth's surface). In fully computational models, FCM's, the boundary conditions at the edges of the domain (and, in some models, above the domain) have to be specified and are usually derived from larger scale regional or global numerical models. These are usually updated at regular intervals, e.g. every 3-12 hours, with observational data taken at all levels in the atmosphere. This process of 'data assimilation' is also beginning to be applied directly to mesoscale models, for example in urban areas with many measurement sites (this is quite usual in the USA, but not routine in Europe except in special campaigns such as for Olympic games, as occurred at Albertville in France and now in Athens).

A critical feature of any FCM, especially in the boundary layer and when the flow is influenced by mountains, buildings, surface heating, is the representation of

the effects on residual (or computed) scales greater than L_M/R_M of the turbulence at the smaller space and time scales. Some models, such as HOTMAC (Brown and Williams, 1998), contain quite complex sub-models of the turbulence statistics (with extra equation for the turbulent energy and dissipation rate (k-ε)), while others e.g. COAMPS (Hodur, 1997), MM5 (Anthes and Warner, 1978), MESONH (Cuxart et al., 2000), UK Met. Office unified models (Cullen, 1993), use eddy viscosity or even simpler parameterisations (e.g. assuming the form of the velocity profile). The experience from field studies in the USA is that for urban areas located on sloping terrain where buoyancy forms are significant (i.e. $F \lesssim 1$), the models with the more complex turbulence models are more accurate in these conditions. But the greatest improvements in accuracy, especially in predicting the mean wind speeds and wind direction in changing meteorological conditions, and in complex terrain - which includes London where winds are channelled between the hills (J. Zehnder, A.S.U.; P Clark, Met. Office, private communications) arise from using these models with finer resolution of the order of 1km or less. However even with finer resolution and complex modelling, such models still cannot predict some significant features of surface layer turbulence, such as evening transition of upslope flows and formation of gravity currents, or calculate relevant statistics of the turbulence for dispersion models, unless they are used as large eddy simulations, e.g. Carlotti (2002), which is only possible in research mode.

As explained in **Table** 4, these models take many hours to compute a single meteorological situation. Nevertheless, they are sufficiently reliable indicators to be used operationally in the USA to compute the future scenarios of air quality in large urban areas. For complex dispersion calculations (e.g. using the stochastic NAME model, Maryon and Buckland (1995)), their predictions have to be supplemented with more detailed input on the properties of the turbulence.

Fast approximate models, FAM's, for air flow and meteorology over mesoscale distances are being developed, based on recent research. These models are useful as qualitative guides to the complex flow that might occur on the mesoscale, and also for quantitative predictions as input to dispersion computations (Section 4).

As shown in **Table** 4, when local buoyancy effects are weak (i.e. $U_G/U_B \geq 1$), the air flow over an urban area is generally a perturbation of the oncoming flow. Then from semi-analytic models using perturbation methods faster computational schemes have been devised, e.g. for lee-wave prediction scheme 3DVOM over mountains (Vosper and Mobbs, 1996; see also web page http://www.uwern.ac.uk/uwern/orog_models.html), and are being developed in a general way to allow for orography, roughness change and some effects of surface heating (Owinoh et al., 2003; Hunt *et al*., 2003). Although these are perturbation methods, the changes in wind speed and direction predicted (and verified) by these models can be quite large (~50% or more). (Indeed this modelling approach is the basis for many of the parameterisations used in numerical weather prediction for global/regional models at resolutions of 30-50km.) The perturbation modelling approach being adopted in this range of meteorological flows is similar to that used for sub-mesoscale/neighbourhood scale orographic flows (e.g. in FLOWSTAR model (Carruthers et al., 1988), RIMPUFF (Thykier-Nilesen et al., 1999)), the main difference being that over the

larger scale the internal layer l reaches the top of the boundary layer h, so that the inversion height is affected as in hydraulic flows and Coriolis effects have to be included (which for example significantly influences flows along coasts and up and down large river valleys, e.g. Wippermann, 1984). Typically these models are run in the steady state. Once the time dependence over several hours is significant, a fully computational model is necessary.

When buoyancy forces are significant, $U_G/U_B<1$, no FAM is yet available to cover all the most significant type of air flow and meteorological condition that might be needed for dispersion calculations. However, models and physical estimates have been derived for some particular situations, especially when Coriolis forces play a small role. For example, upslope/down flows in confined Alpine-scale valleys, and, rather differently, in wide valleys with low slopes, large heat island effects, and sea/lake breezes (Blumen 1990; Hunt et al., 2003; Ohashi and Kida, 2002). Not only are the quasi-steady features of these flows now quite well described, but also their time/space dependence over the diurnal cycle. In the absence of strong geostrophic winds (or very stable local conditions) the local diurnally varying buoyancy forces control the flow and therefore they are quite predictable (e.g. a valley wind, or sea/lake breeze on a still day). Since the single most important aspect of the air flow needed for dispersion calculations is the direction of the wind, such physically-based models provide vital information for estimating the effect of accidental releases in complex terrain.

2.2.3 Neighbourhood scale models

On the neighbourhood scale, say 5km, fully computational models even with the latest computing systems cannot generally resolve the flow around every building. Typically for computations with 10^6-10^7 grid boxes the horizontal grid boxes are about 100m or greater in the horizontal direction. To resolve the velocity field round a building so as to calculate its drag effect on the overall flow, the grid boxes would have to be of the order of 1m or less. Therefore even FCM's can, at present, only calculate average features of the flow over these grid box scales, by estimating the average effects of buildings and streets onto the model.

As explained in Section 2.1 different modelling approximations are needed (even with an FCM) depending on whether the buildings in the neighbourhood in question form effectively porous or non-porous regions of resistance. If they are porous (Figure 3), i.e. lie in the category (i) of Table 3, the effect of the buildings is estimated by an average drag coefficient averaged over the whole volume occupied by the buildings and the space between them (typically this is of the order of the porosity β. The same approach has been used for FCM computations of flows through forests and agricultural crops (Finnigan, 2000).

The FCM input is the mesoscale flow field approaching the neighbourhood region (or the flow leaving the adjoining neighbourhood), e.g. suburbs adjoining city centre as in Figure 1. FCM output will be mean flow and basic turbulence statistics that depend on the particular closure model used, e.g. mixing length, turbulent energy-dissipation (k-ε) closure, or Reynolds stress closure (e.g. Pope, 2000; Hunt et al., 2001). All three of these models lead to estimates of turbulent energy, but only the latter also provide estimates of length scale, and the

space/time dependent evolution of turbulence structure, which is significant where the areas of building density or height change sharply. The third method allows for the anisotropy of turbulence, which changes in these transition zones. Such models predict the mean velocity field everywhere, (spatially averaged over the grid box), and the turbulence outside the canopy. Within the canopy, where large-scale inhomogeneous turbulence is generated by the shear layer over the top and by eddying motions around buildings, the spatially averaged models are deficient. This is why in the analogous mechanical engineering problem of flow between tubes in heat exchangers, the velocity field is computed in detail over a typical sample volume, e.g. surrounding 5 typical obstacles, in order to estimate average properties of the turbulence (see Eames & Hunt, 2003). A similar approach is now being considered in the numerical modelling of neighbourhood scale flows (Koutsourakis et al., 2003; JAWE No. 95, April 2003).

In the second type of urban area, which is effectively non-porous, the mean air flow passes over the building envelope as if over a hill with elevation $z_s(x, y)$. The roughness length z_0 also changes as a result of turbulence and recirculating flows in the courtyards, streets, etc. between the buildings. Estimating these parameters z_s, z_0 in terms of the building layout is only approximate, (e.g. $z_s \cong H_c$, $z_0 \sim H/30$). As with porous built-up areas, the parameterisations for calculating average flow properties can be estimated approximately by detailed computation of typical local areas. These calculations can also provide estimates of the local turbulence, needed for dispersion computations. (e.g. Soulhac, 2000). FCM's using turbulence closure models have been extensively applied to the kinds of recirculating flows that occur between buildings in non-porous urban areas; most validations have been for wind tunnel tests and engineering flows, where the kind of very large-scale eddies and downdrafts found in atmospheric flows are absent. Such motions can lead to more rapid exchange between the upper flow above and within the canopy layer (see review by Mestayer and Anquetin, 1995).

As shown in **Table** 4, and reviewed by Britter and Hanna (2003), most FAM's for the neighbourhood scale tend to focus on equilibrium flows within and just above the canopy. In a 'porous' canopy (Figure 2(a)), the mean velocity within the canopy $U_c(z)$ is driven by the turbulent shear stresses generated in the intense shear layer just above the canopy. Here the ratio of $U_c / U(z_*)$, where $U(z_*)$ is the velocity at the top of or above the roughness layer (Figure 2), depends on the porosity – a typical value being 0.3. In a non-porous canopy, typically in the inner city, where flows are determined by canyon and downdraft effects, this mean velocity ratio varies considerably over the range 0.3 to 1.0 (e.g. Soulhac, 2000).

Above $z = z_*$, but within the internal layer, the mean velocity profile is found in many experiments to have the form of Equation (2.1). Despite the unevenness and inhomogeneity of these boundary layer flows, the ratios of the r.m.s. values of the three components of turbulent velocity to the friction velocity u_* are quite comparable with their values over level terrain, i.e. $\sigma_u / u_* \cong 2.5$, $\sigma_v / u_* \cong 2.0$, $\sigma_w / u_* \cong 1.3$ (Rotach, 1995).

The approximate average velocity profile (2.1) is not applicable at the edges of 'neighbourhoods' where the density and heights of buildings vary, or in the

interiors of such regions, such as near parks, squares etc. At the edges of porous canopies, where the air flow in the canopy varies rapidly, an FAM approximate model has been developed based on the same approach as FCM by representing the canopy as a porous layer and (as for the FAM in the mesoscale range) solving perturbation equations semi-analytically to provide fast computation of the mean velocity and shear stress (Belcher et al., 2003; Coceal & Belcher, 2003). These have been verified against field and wind tunnel studies.

Over non-porous canopies (typically categories (i)-(v) in Table 3), the determining parameters (H_c, $z_0(x, y)$) are the same as for FCM over these elevation/roughness changes. The linearised FAM approaches give very similar results to those using FCM's (e.g. Belcher et al., 1990; review in Hunt et al., 1991b). An operational model for porous and non-porous canopies is available from CERC (http://www.cerc.co.uk) as part of the FLOWSTAR-ADMS system.

However, the use of this kind of FAM for neighbourhood scale urban canopies needs to be extensively tested, especially the average estimates of the recirculating flows and turbulence amongst the buildings. For this purpose it would be necessary to use detailed data (experimental or computational) about typical flow on the building/street scale, and then investigate whether these are characteristic for the neighbourhood scale. (This assumption is effectively the basis for the UDM and ADMS-Urban models.)

2.2.4 Modelling the building/street scale

The purpose of detailed flow modelling in and around individual buildings and the surrounding streets is, for the purpose of this study, firstly to understand how rapidly matter released 'accidentally' disperses locally. Secondly, detailed studies of these local scale flows are necessary, as explained in the previous section, to develop models over neighbourhood scales for flow and dispersion.

Fully computational methods, using a variety of turbulence modelling methods, have been extensively applied to computing flows around single buildings in turbulent boundary layers. Using turbulence closure methods many models have predicted mean velocities near the buildings within one or two widths; but such models (e.g. k-ε models) have tended to over-predict small-scale turbulence around the structure (Murakami, 1992) and under-predict the large scale atmospheric eddies. This leads to an over/under-prediction of the mean velocity defects in the wakes downwind of 3-D/2-D structures in the atmospheric boundary layer. Only the computationally intense method of Large Eddy Simulation, or LES (or unsteady modelling of the fluctuating flows using turbulence closure models), can represent accurately the distortion of the large scale eddy motion around the building and its effect on downwind wakes. (Rodi, 1997; Kim and Boysan, 1999).

Calculations using FCM with turbulence closure have also been performed on flow around small groups of buildings using resolutions down to about 0.1H. The predictions of the turbulence in these flows are more reliable than those of isolated structures because here most of the turbulence is generated locally between the buildings and is of smaller scale. (Similarly, wind tunnel models of dispersion around buildings are generally more reliable when the buildings are in

groups than when isolated because wind tunnels cannot simulate the low frequency fluctuation in wind direction.) This is because the primary interactions between the wake of one building and its impact on adjacent buildings are not sensitive to the structure of turbulence; however, the wakes of isolated or well-separated buildings are strongly affected by the form of the low frequency spectrum of turbulence. This is why in some institutions (e.g. Dr. J. Boris at US Naval Laboratory, Boris et al., 1992) work is being undertaken on dispersion in dense urban areas with fast FCM's in which approximate velocity fields are computed using classical grid box methods of finite size (say 1m) but neglecting completely any modelling of turbulent stress. This reduces the number and the order of the equations to be solved and speeds up the computation by a factor of 10 or more. The finite size of the grid effectively introduces numerical diffusion that simulates many of the same flow mean features developed using the more complex turbulence closures.

This approach of neglecting or greatly simplifying turbulence modelling has been used for many years in the Japanese construction industry for design studies on new large buildings (see Murakami, 1992) and in the aircraft industry for computing very complex flow around helicopters and in certain aero engine flows (Prof. W. Dawes, private communication). Another simplification to speed up the computation of the mean velocity field is to represent the effects of the individual buildings as a distributed force acting on the flow (or source/sink distribution) and thereby only approximately representing the shape of the building (Moulinec et al., 2003). (In most FCM calculations considerable computational resource and time is spent on exactly representing the building shape, while at the same time making considerable approximations in the flow. This is justifiable for aircraft design but not for most aspects of environmental modelling.) An approximation that is useful for computational modelling, especially circulation flow regions, is to simulate the vorticity in terms of the unsteady motion of many discrete vortices. This flow technique can be combined with Lagrangian unsteady dispersion modelling involving the tracking of particles (e.g. Turfus, 1988) This method may still provide useful techniques for investigating unsteady dispersion in two-dimensional recirculating flows such as street canyons.

There are at present no general FAM's that are capable of calculating the detailed flow around any isolated building or group of buildings, or even calculating those broad features of the flow needed for modelling dispersion close to the building. The main reason is that the unsteady separated shear layers that control the flow are much smaller scale than the building. This means that the recirculating flow region, which greatly affects the magnitude and time scale of concentration fluctuation, is not only highly unsteady but also very sensitive to the effects of nearby buildings. Nevertheless, the main features of the mean flow patterns and typical magnitudes of the mean and fluctuating velocity have been classified and partially quantified for many types of buildings and groupings. Therefore, although no practical FAM for the mean flow is available at present, these features of the flow field are now well enough known to derive useful quantitative FAM's for the dispersion as described in Section 4.

However for some dispersion problems quantitative FAM's have been developed that are found to be useful in practice for certain aspects of the flow/dispersion.

Firstly when buildings are far enough apart (i.e. λ_{bg} is small) that their near flow fields and their wakes are approximately independent, the wakes can be approximated as a perturbation to the approach flow, a theory (Counihan et al., 1974) that is used in the 'Buildings' module in ADMS (Robins and Apsley, 2000). The same model can be used approximately with linear superposition when buildings are separated by about 3H where H is their height. As the ratio of breadth, b, to height H, b/H, increases from 1.0 to 10 this minimum separation distance d_{min} increases linearly to about 10H (Figure 3a(i)).

When d is less than d_{min}, Figure 3a(ii), it is found that the recirculating regions of the wakes of the upwind buildings are elongated and extend to the nearest downwind building (e.g. Stoesser et al., 2003). For buildings designed in rows nearly parallel with the wind direction, the flow structure consists of turbulent recirculating regions in the spaces downwind of the buildings and relatively high-speed streams in the open streets between the buildings (Davidson et al. 1995). Describing the flow structure in this way provides the basis for FAM for dispersion calculations.

By contrast, when the buildings are placed in a staggered pattern relative to the wind direction, the wakes tend to disappear and the mean flow between the buildings consists largely of uni-directional bifurcating patterns of diverging and converging streamlines, with small regions of recirculating flow. Such flow can be computed by fast potential flow methods (Davidson et al., 1995), which are even faster if the buildings shape is approximated (Moulinec et al., 2003). This approach needs to be tested more thoroughly for cube-like buildings. Soulhac (2000) has shown that potential methods are also useful for street junctions.

For tall buildings in the atmospheric boundary layer (where H/b>1) the recirculating flow field in the wake is a region where streamlines enter and leave from the external flow (Lawson et al., 1988) Although in general there is no closed streamline 'bubble', because of the high turbulence there is strong mixing in the horizontal plane and, to a lesser extent, in the vertical direction. These streamline patterns are significantly affected by surrounding buildings (Figure 3b(ii)) whose wake interacting with the tall buildings tends to cause downwash (Britter and Hunt, 1979) and strong swirl around the sides of tall buildings. This enhances vertical mixing in the lower part of the downwind wakes and through lateral convergence reduces the downwind extent of the wake of the downwind building. Buildings placed sufficiently close downwind of tall buildings (where $d<d_{min}$) affect the vortex shedding and thence the whole wake structure. These wake-wake interactions are still not well understood qualitatively or quantitatively.

When the buildings are long enough and close enough, i.e. categories (i), (ii) and (iii) of Table 3, and the wind is at any angle, or if they are situated in rows and the wind is at a small glancing angle to the row, Figure 3a(ii), then characteristic canyon flows are formed in the streets between the buildings. The mean flow has a component along the street and a swirling motion in the perpendicular direction that tends to extend up to the top of the buildings. The peak mean and fluctuating velocities near the ground are comparable with those at the level of the top of the buildings. The key quantitative parameter for dispersion modelling is the ratio of the mean wind along the street V_s to the

mean wind U_H above the buildings at the height H (in the approach flow). Soulhac (2000) suggests (on the basis of computation and wind tunnels in a canyon without side streets) that V_s/U_H is about 0.3 when the angle of the approach flow lies between 0° and 60°. However, perturbation theory, the recent numerical simulation work of Dr. S.E Belcher (private communication) and informal observations in London suggest that this ratio lies in the range 0.5-1.0 for typical urban situations, at least with wide streets (i.e. for $b/d \lesssim 1$ and $75° \lesssim \phi$). When $\phi < 30°$, the along-street flow V_s takes a greater distance along the street to develop. This suggestion of larger values of V_s/U_H is in accord with the field observations of Soulhac (2000, p. 188), which, as he notes, differ in some important respects with his own idealised simulations. The analysis suggests that the value of V_s can be quite sensitive to the value of V_s at the upwind end of the canyon. Thus a major crossroads can have a large effect on the canyon flows downwind.

When the buildings either side of the street are of comparable height, a strong feature of the helical canyon flow is that it does not extend above the buildings. Therefore, as we show in Section 4 (following, in some respects, Soulhac (2000)), the appropriate FAM for these flows is to assume a canyon flow below the building level and a rough wall boundary layer flow above it. There are also mean velocities along the side streets, but these are only significantly smaller if $b/d \gtrsim 3$.

Finally we consider the air flow in typical courtyards and 'squares' connected to adjoining streets (Figure 3c). Here the interaction between the vorticity layer leading from the top of the buildings and impacting on surrounding buildings leads to even more complex recirculating flows than in street canyons. However, because of the finite extent of these flow regions, it can generally be assumed that (unlike elongated street canyons) there is only a small mean velocity component V_s below the building height, i.e. $V_s/U_H \lesssim 0.1$. However, the turbulence level is quite high in these re-circulating flows, with $\sigma_u \sim \sigma_v \sim (0.5\text{-}1.0) \cdot \sigma_u(z^*) \sim 1.2\text{-}2.5\ u_*$, so that $\sigma_u \sim V_s$ (Soulhac (2000), p. 222).

Simulations confirm that these are regions where fluid trajectories are well-mixed. This provides a basis for constructing FAM's for dispersion in these regions using semi-analytical diffusivity models.

In street canyons and in courtyard/squares, turbulent motions are also produced by the exhaust of local heating/ventilation systems and by traffic movement (Britter and Hanna, 2003). Those contributions, which are significant in low wind speed conditions, can simply be added to the turbulence generated by the air flow. The contribution of vehicle turbulence tends to be confined to the lowest 5-10m near the ground. Where the vehicle breadth is b_v and speed is U_v, the vehicles' average contribution to the turbulence velocity squared averaged over the width of the street is of order $\Delta\sigma_w^2 \sim \beta_v^2 \cdot U_v^2(b_v / d)$, where the semi-empirical factor β_v is of order 1/10, but depends on the density of the traffic. Typically $\Delta\sigma_w \sim 0.2$m/s for $U_v = 8$m/s, $b_v/d \cong 0.2$. This factor, which is included in ADMS-Urban, has been shown to the significant in reducing peak concentration of traffic induced air pollution in field experiments.

3 DISPERSION MODELLING METHODS, INPUTS AND OUTPUTS

3.1 Methods, objectives, constraints

There are different reasons for making quantitative predictions of dispersion from accidental releases, and therefore different objectives in developing any calculation procedures and systems. The practical situations in which these calculations are performed affect the methods that are used. Predictions are needed in real time, firstly in a 'direct mode' when an accidental release of a known strength and at a known location has occurred in order that the authorities can estimate how far, for how great a period, and how seriously there will be the adverse effect of the release on people, animals, etc. From these estimates decisions will be made about evacuation, medical responses, etc. In certain cases the accidental release continues over a period and may trigger other accidents, in which case the dispersion predictions can guide decisions about dealing with the source, e.g. in assessing the environmental benefits in relation to any risks involved, such as entering and dealing with the source zone. Secondly, in some situations, as occurred with the release of toxic gas in the Tokyo underground, predictions in the 'inverse mode' are needed because the exact location of the source are not known even though the effects on people of a toxic release of gas may already be apparent. Then prediction modelling methods need to be carried out using relevant meteorological observations (especially about the wind direction and strength) and medical data concerning the severity of symptoms in relation to concentration to infer the location of the source (information from mobile phone users would nowadays provide immediate information that could be of use). Thirdly, 'scenario' predictions are needed for evaluating the effects of different types of accidental releases in all the relevant meteorological conditions in order that responses to all likely eventualities can be planned in advance, and their relative risks can be assessed.

Whereas the dispersion predictions in the first case have to be performed, at least for initial estimates, in a matter of a few minutes, for the second case a few hours might be acceptable for computation of the dispersion for a particular scenario, taking all the meteorological conditions into account. With current methods and capabilities of computing it is not generally feasible to use Full Computational Methods (FCM's) for such a problem because of the large number of computations required, each of which may take more than one hour. However, as explained in Section 2.1, such methods are essential for testing and improving Fast Approximate Methods (FAM's). In some applications, e.g. for studying the security of a particular building and maintaining a local monitoring and prediction system, a devoted FCM could be justified, provided it was 'speeded' up and perhaps combined with an appropriate FAM.

The specific objectives for the first kind of direct prediction, i.e. where the source is known, are to calculate the statistics of the concentration denoted by $\langle C \rangle(\mathbf{x}, t; \Delta\mathbf{x}, \Delta t)$ at a point in space, $\mathbf{x}$, and time t averaged over certain spatial and temporal intervals $\Delta\mathbf{x}$, Δt. For small enough values of $\Delta\mathbf{x}$, Δt, the averaged value

of C (such as an instrument might measure or a person might experience) is equal to the local concentration at **x**, t i.e. $\langle C \rangle \approx C(\mathbf{x}, t)$. The input or source matter may be released over **x**, t at a rate $q_S(\mathbf{x}, t)$ units/ per unit volume/ per unit time.

In some cases the accidental release initiated at time t_S is concentrated effectively at a source point $\mathbf{x}_S$ and is released continuously with strength $Q_S(\mathbf{x}_S, t > t_S)$ so that

$$Q_S(\mathbf{x}_S, t) = \int_{\Delta V_S} q_S(\mathbf{x}, t) d\mathbf{x}$$

where ΔV_S is the small volume of the accidental release surrounding the effective release point $\underline{\mathbf{x}}_S$. If all the matter M_S is effectively released at one moment in time, t_S, then

$$M_S = \int_{t_S}^{t_S + T_S} Q_S dt \qquad (3.2)$$

where T_S is the short release time.

In many cases the accidentally released matter is transformed in the atmosphere into other chemical species with concentrations C_1, C_2, ... In some cases an accident may trigger other accidental releases, q_1, q_2, ...

More detailed concentration statistics are needed and can generally be estimated for the second kind of scenario calculation rather than the first kind of real time calculation. However, in both cases the statistics required are the mean concentration, $\overline{C}$, r.m.s. values of the fluctuations, C', and likely peak values $\hat{C}$. In principle these values are defined by repeated experiments. In practice they define values in relation to averages taken over particular intervals ($\Delta\mathbf{x}$) and periods (Δt) (Pasquill and Smith, 1983). Numerical field and wind tunnel studies have provided guidance about relating $C', \hat{C}$ to $\overline{C}$ for different types of release and flow field. The effects of closely-packed buildings tends to reduce $\hat{C}$ in relation to $C', \overline{C}$ as Mylne and Mason (1991) showed in the Porton-Cardington experiments reported by Davidson et al. (1995).

In order to make calculations of these concentrations it is necessary to have available the requisite general and particular data and to decide how they are to be used.

a the relations between the statistics of C(**x**,t) and the statistics of the mean and turbulent velocity fields **U**, **u** (e.g. defined over specific periods, say 1 hour). In certain circumstances the molecular diffusivity κ_S of the source gas is a relevant parameter. The statistical relations are known approximately and semi-empirically in ideal atmospheric conditions in air flow over level terrain with slowly changing meteorological conditions for localised sources. In these conditions the form of the mean concentration $\overline{C}$ and C′ are well-defined and repeatable (i.e. the plume profiles). They have been well validated: see, for example, Hunt et al., 2002 (NRPB review); Carruthers et al., 1994 (ADMS 3); Cimorelli et al., 1998 (AERMOD); Olesen et al., 1992 (OML); Thykier-Nielsen et al., 1999

(RIMPUFF); Scire et al., 1999 (CALPUFF). For complex flows such as those in urban areas, the semi-empirical approach can be usefully extended where it is observed or derived theoretically that well-defined repeatable plume/puff distributions also occur in these conditions. This is the approach that has been used for dispersion around hills, over roughness changes and around isolated buildings where plumes/puffs have forms that are simple modifications of the Gaussian profiles (e.g. a double plume structure in the wake of a building). This approach has also been extended to dispersion around groups of well-separated buildings in the UDM model (Hall et al., 1996). However, in close-packed buildings and in street canyons with arbitrary source distributions the mean spatial distributions are significantly non-Gaussian, at least on the building/street scale. Further downwind the distributions become Gaussian (see Section 5). The concentration fluctuations also have a different form. However, as in other complex flows (Hunt and Mulhearn, 1973; Riddle et al., 2003), good models of turbulent diffusion, based on the eddy diffusivity concept, provide useful approximate predictions for how the complex flows and geometrical shapes of the boundary affect the mean concentration field. As with the flow field calculations, more complex turbulent diffusion models can in principle provide more accurate predictions. However, in fact such models need to be at the more computationally intensive level of stochastic simulations or Large Eddy Simulations to provide significant improvement (e.g. Turfus, 1988; Rodi, 1997). These research tools may well help define better and quantify the characteristic dispersion patterns in urban areas that can then be incorporated into improved simple methods.

b All these models require input information and source distribution data about the mean flow field, turbulence and source distribution. Velocity field data in urban areas are (except in the USA) quite sparse. There may be only a few measurement points, and these are located on buildings or near ground level in parks or other open spaces. However approximate information about the wind direction can be gleaned from flags, steam from building heating systems, etc. Even these data could be useful for real-time predictions and a check on prediction. This sparsity of data means that the velocity and temperature statistics needed for dispersion calculations on the building/street and neighbourhood scales have to be in large part provided using mesoscale and neighbourhood scale air flow models (reviewed in Section 2). These are being tested in the current 'Dapple' experiment in London (R. Colville, private communication; see also the web site http://www.dapple.org.uk). The output winds of these models are representative of a neighbourhood area and are generally more suitable for urban dispersion models than local measurements which are highly influenced by the nearby buildings/street and are not so representative. The models also provide data for the mean velocity and turbulence above the buildings, unlike local measurements.

The meteorological input to these models is usually based on observations near the urban areas (e.g. at airports) or the predictions of regional/global meteorological models (which also provide 'analyses', i.e. estimates based on current data and past predictions of the current wind fields at the resolution of these models (~50km)). Note that in recirculating flows, such as occur in urban centres and

canyons, dispersion from local sources depends mostly on the time-averaged form of the mean flow field (e.g. zones of recirculating mean streamlines) and much less on the details of local gradients of velocity and turbulence (e.g. Puttock and Hunt, 1979).

There are other artificial components of the velocity field that also need to be included in these calculations, caused by traffic movement in the streets (which can be estimated in the main streets in urban areas using data from traffic monitoring), by air movement into and out of buildings, subways, etc. (with velocities in the range 0.1-1m/s), and by air movements associated with the accidental release (e.g. collapse of a building causing a gravity current as occurred in New York in 2001; an explosion causing an input and/or expulsion of air).

c The third main input to the dispersion modelling is information about the source or sources of matter associated with the accidental release. As already discussed, this information will generally be known from direct observation (which we assume for this discussion), but there are situations when, following an accidental release, this information is very limited, and dispersion modelling (together with other deductions and observations) is necessary to define the properties of the source. In this study, we consider possible source locations and types in relation to dispersion processes around buildings/streets and the flow fields in urban areas.
Assuming that the effective scale of the source size L_{Se} of the accidental release (see Figure 5) is smaller than the scale of the building, H, then the location of the source in relation to the building, greatly affects the nature of the dispersion from the source. It is only necessary to define this location within broad parameters (upwind, downwind, above, below, etc.) because research has shown this determines which characteristic patterns of dispersion result. This classification also guides the appropriate choice of FAM, as shown in Section 4.

In some cases the location of the source is inside the building, e.g. a subway system such as the London Underground, in which case there are two separate problems of dispersion, one within the building (e.g. Carrilho da Graca and Linden, 2002) and another in the atmosphere. Since there may be many outlets from the building, there could be several sources all around a building/along a street caused by such an accident (Figure 5).

The scale L_{Se} and time period T_S of the source are affected by the nature of the accident: an explosion or a building collapse can lead to L_{Se} and T_S being comparable to the building spatial scale H and flow time scale H/V_S where V_S is the wind speed along the street. On the other hand, a very small release of a toxic material could be on the scale of a few centimetres. Models for the 'mean' concentration averaged over several minutes are not very sensitive to the size, but peak fluctuations are quite sensitive to the source size and release time T_s, especially in approximately unidirectional or 'open' flow, such as above the buildings, or in a strong canyon flow (Thomson, 2000). In recirculating, highly turbulent flows, where there is strong mixing (i.e. fluid particles move apart very rapidly) the memory of the source characteristics rapidly disappears along the trajectory of the

source material, as numerous laboratory and field experiments have shown. This is why the mean and fluctuating concentration in these regions is less sensitive to the size, time scale and location of the source than in open flows (e.g. Hunt and Castro, 1981; Fackrell, 1984).

3.2 Accuracy and output of modelling calculations

The output that is required from dispersion calculations needs to be considered carefully before they are specified in any particular computational system. As explained in Section 3.1, in practical calculations the levels of accuracy and forms of output need to be 'fit for the purpose' for decision making. Although dispersion processes are determined by the flow field, because they are diffusive the accuracy in space and time and the reliability of the dispersion calculations may actually be greater than those of the flow field calculations described in the previous section, even when using lower spatial accuracy than the flow field.

The output specification needs to state the level of accuracy required in dispersion calculations over the locations (e.g. relative to sources) and over relevant length scales (e.g. street to urban scales). The accuracy usually needs to be greatest near the source, where the concentrations are highest and where the risks of damaging consequences are greater. Therefore where localised 'accidental' emissions are likely to occur more precision and better error estimates are needed for the calculations on the building/street scale than where the matter is dispersed over the neighbourhood and meso-scales, where concentrations are lower. Since the former calculations are sensitive to the precise location of the source and to the wind direction, in a given city centre area, or to building/street design, predictions of the local concentration near the source are sensitive to input and larger scale effects. They could be significantly in error. Therefore to assess all the possible consequences of an accident emission, the output should include calculations for slightly different wind conditions, source location and building/street geometry found in a given type of urban area. By following the approach that is now standard practice in numerically-based meteorological forecasting using NWP, such an 'ensemble' of computations, for each scenario defined by the source and meteorological conditions should lead to improved and more reliable estimates of the mean value and fluctuations of the concentration. (This approach, which has not yet been validated for dispersion modelling, is only feasible off-line, when models are being tested and extreme scenarios evaluated.)

The form of the output depends in part on how the dispersion of the calculation is to be used in practice or in research. Some calculations provide 'generic' or average estimates of the concentration distribution around a source of given height wherever it may be placed in an urban area of a given type (e.g. city centre, canyons, parks, or suburban streets defined by one of the categories in Table 3). Different estimates could be provided in categories of source height, which might be as broadly defined as sources above and below the average level of the 'canopy' H_c, For on-line prediction or in planning scenarios, these calculations need to be performed rapidly using FAM. However, as shown in Section 4, FCM's are useful for developing and calibrating FAM's, including the specification of the categories of scenario. For certain locations, e.g. near

particular high-security buildings or high-profile sites, it would be worthwhile to compute in detail the concentration distributions for a range of plausible accidental scenarios and meteorological conditions. These would have to use FCM (and/or wind tunnel/field studies for validation) in order to achieve acceptable levels of accuracy, e.g. for specifying response monitoring strategies.

Using an ensemble of computations does not greatly affect the shapes of these computational regions.

4 DISPERSION CONCEPTS AND MODELS

4.1 Dispersion near the source

The dispersion from an accidental release near the source at $\mathbf{x}_S$ depends on the nature of the source as well as on the local air flow. Suppose the source matter is released with energy E_S (which may vary in scale of seriousness from a few toxic particles being thrown in the air to the release associated with an explosion or the collapse of a building). Alternatively, the source accident may occur in a building or subway where the air flow defining the exterior dispersion is u_S over a scale L_S. Very near the source the dispersion is caused by the air motions associated with the release process, but they decrease rapidly away from the release point. Then once the solid or gaseous particles of the source material have spread out over a certain volume, say with dimension L_{Se}, atmospheric dispersion processes take over. This happens when the mean straining motions and turbulence on the scale of L_{Se} in the wind (which are of order $u_*(L_{Se}/L_x)^{1/3}$) are greater than the source induced motions (Hunt et al., 1985). Note that $E_S \sim L_S^3 u_S^2$. An estimate for the effective source size is given by

$$L_{Se} \sim (L_x^2 E_S^3 / u_*^6)^{1/11} \sim \left[L_x^2 L_S^9 (u_S/u_*)^6\right]^{1/11} \qquad (4.1)$$

and note that

$$u_*(L_{Se}/L_x)^{1/3} \sim u_S L_{Se} \sim E_S^{1/2} L_{Se}^{-3/2}$$

Equation (4.1) shows that the initial scale L_S is more significant for determining L_{Se} than the initial energy, since $L_{Se} \propto L_S$ to a first approximation, whereas $L_{Se} \propto (u_S/u_*)^{1/2}$. Thus in windy conditions in the atmosphere near the ground, where for the vertical component of velocity $L_x \sim 3$m and $u_* \sim 0.3$m/s, it follows that for a small explosion/accidental release where $L_S \sim 0.1$m and $u_S \sim 1$m/s, the initial scale of the cloud is $L_{Se} \sim 0.1$m. This would be much less than the building/street scale. For a large explosion where $L_S \sim 1$m, $u_S \sim 100$m/s, $L_{Se} \sim 10$m. Thus, depending on the energy of the accidental release process, the effective scale of the source cloud, L_{Se}, may be much less than or even comparable with the scale of the nearby street or buildings.

In some 'accidents' such as a bomb or in an intense fire the material is emitted at high temperature. Then the pollutant or toxic material rises as a buoyant plume, especially where the mean velocity is small. This determines the effective

height of the source location, z_{Se}, where atmospheric motions dominate the dispersion process. A clear example is when an accidental release occurs in the wake of a tall building, as was observed in New York in the twin towers disaster of 2001. There the smoke plumes reached the top of the buildings and before being advected downwind in a plume with diameter comparable to the width of the building. An alternative 'accident' might involve matter being released over a period T_S from a source moving with velocity U_S, e.g. a car at street level or a plane above the buildings. From such a source matter is also dispersed with energy E_S, which determines the effective size of the source L_{Se} for estimating atmospheric dispersion. Even without any chemical or other explosive energy, if the vehicle scale is L_S the energy E_S is at least of the order of $(1/100)U_S^2 L_S^2$ per unit distance as a result of the eddying motion in the wake of the vehicle (since the typical turbulent velocity is of order $U_S/10$). This would imply, by adapting the previous calculations,

$$L_{Se} \sim \left[L_S (U_S / u_*) L_x^{1/3}\right]^{3/4} \qquad (4.2)$$

so that for material released into the wake of a vehicle of scale 1m moving at 10m/s the effective source size L_{Se}~3m. In other words, the dispersion from eddying by a moving vehicle is mainly determined by the wake turbulence behind it until the cloud has reached 2 or 3 times the size of the vehicle – a mechanism that is already included in current urban dispersion models (Britter & Hanna, 2003; Carruthers et al., 2000). It also means that the effective source height z_{Se} is of order ½ L_{Se}, which will typically be greater than z_S.

The fact that source-related turbulence usually dominates the dispersion near the source means that in most 'accidents', the details of the atmospheric flow and dispersion near buildings on scales less than 1m are irrelevant.

4.2 Building/street scale

4.2.1 FCM and FAM methods

In Section 2 it was explained how the atmospheric flow in urban areas had different characteristic forms depending on the building/street configuration. These characteristic flows correspondingly produce characteristic patterns of dispersion both at the building/street scale and to a lesser extent on the neighbourhood scale. On the former scale the mean displacement and dispersion of a cloud of contaminant accidentally released from a small source volume $L_{SE} \leq$ b, H are strongly influenced by the local flows around buildings and in the streets, i.e. the cloud/plume dimensions are small enough that σ_x, σ_y, $\sigma_z \leq$ H, d. As with the air flow modelling, understanding and describing these patterns is the basis for fast approximate models (FAM). These are well developed for certain situations, but are in a formative stage for other situations as explained below.

Information about these (or any other airflow) patterns is not used as input in the fully computational models (FCM) because these models are determined by general equations and boundary conditions. However flow feature information

can be used to judge and interpret the correctness and sensitivity of their predictions.

In this section we begin by reviewing how FCM methods at varying levels of complexity that can be applied on this scale before considering the different methods of FAM and their application for the different types of building/street/source configuration. Table 5 summarise the main points.

The first stage in FCM calculations for complex flows is to compute the mean flow and the turbulence statistics and then to use these data in computations of the concentration distribution. As explained in Section 2.2, for well separated buildings, (b/d << 1), in the atmospheric boundary layer (e.g. in the suburban situation), the usual methods based on mean flow turbulence closure models do not completely represent the flow and dispersion process in highly unsteady eddying motions in the wake or the effects of large scale eddy motion in boundary layer turbulence. Typically these models make errors or order of 100% in the dimensions of separated flow regions or growth rate of wakes. They are significantly less accurate than the more computationally intensive large eddying simulation methods (e.g. Murakami 1992; Rodi, 1997) or stochastic simulation models (e.g. Turfus, 1988). However when the buildings are closer together, as in most of the cases of Table 3, the mean and turbulent flow fields and dispersion process are dominated by the interactions between the vorticity in the wakes shed off upwind buildings impinging on those downwind. The dispersion is more sensitive to the spacing and orientation of the buildings/streets than to the turbulence structure – as shown by various numerical and experimental studies.

These general principles explained by, as Riddle et al. (2003) showed, a commercial CFD code FLUENT was better for these situations than for isolated sources. Moulinec et al. (2003) quantified the 'topological' mechanism described in Davidson et al. (1995) in which the splitting of the streamlines as the flow passes between buildings effectively diffuses matter released from a local source. The longitudinal or steamwise dispersion is also enhanced as a cloud impacts on a building slowing up on the stagnation line and passing more rapidly around the sides. This process also slows down the cloud as it moves through the canopy (Eames *et al.* 2003). The wakes also amplify this process (Fackrell 1984). Hunt (1985) reviewed earlier studies showing that in these converging and diverging flows around obstacles the mean concentration fields are less sensitive to the turbulence structure (e.g. length scale) than in the unobstructed turbulent boundary layer.

One might conclude that these effects of dispersion being less sensitive to turbulence structure in complex urban flows CFD models results should be reasonably accurate provided they are applied with just sufficient detail to represent the mean flow features. This is why CFD methods are used with large computer resources by certain laboratories in the USA (e.g. Brown and Williams, 1998). On the other hand, it also means that FAMs are appropriate, using approximate models of the turbulence and mean flow for the different types of topology and pattern of the buildings and street. This is the rationale for the fast and easily-understood methods, now being used/developed in the UK and elsewhere, which we describe below.

4.2.2 FAM methods based on characteristic dispersion patterns

4.2.2.1 Dispersion very near the source

Assuming the location of the source $\mathbf{x_S}$ is known (Figure 5), calculations of the near field dispersion first depend on the effective source scale L_{Se} (which determines where the matter is dispersed by atmospheric motion) in relation to the separation distance between the buildings d. The 'accident' or the source is initiated at time t_S. If $L_{Se} \leq d$, then the matter disperses as if from a small isolated source. Given the time variation of the source strength $Q(\mathbf{x}_S, t)$ the average concentration at a point **x** and time t can be calculated as a time integral from the initiation of the source to the measurement time t:

$$C(\mathbf{x}, t) = \int_{t_s}^{t} Q(\mathbf{x}_S, t')\, C_C(\mathbf{x}, t - t'; \mathbf{x}_S)\, dt' \qquad (4.3)$$

Here, C_C is the concentration at **x** in an initially small cloud produced by unit source strength emitted at $\mathbf{x_S}$ at time t'_S. Many experiments have shown that provided the energy and/or scale of the turbulent velocity components do not vary greatly (say more than a factor of 2) over the volume occupied by the 'cloud' of contaminant released from the source in the presence of mean wind speed U , C_C can be approximated (near the source) by the basic Gaussian cloud profile $G_{C,o}$, i.e.

$$C_C = G_{C,o} = \exp\left(-[X^2 + Y^2 + Z^2]\right) / \left[(2\pi)^{3/2}\sigma_x\sigma_y\sigma_z\right] \qquad (4.4)$$

with $\sigma_x(\Delta t'), \sigma_y(\Delta t'), \sigma_z(\Delta t')$ being the dimensions of the cloud in the directions parallel and transverse to the local mean flow at time t after the release at time t'_s where $\Delta t' = t - t'$. Here $X^2 = [x - (x_S - U\Delta t')]^2 / 2\sigma_x^2$, $Y^2 = (y - y_S)^2 / 2\sigma_y^2$ and $Z^2 = (z - z_S)^2 / 2\sigma_z^2$. The reason for this form of profile is because of the essentially Gaussian nature of large scale turbulent eddying motions. The profile is not greatly affected by mean velocity gradients when the cloud travels over flat or undulating surfaces (e.g. Pasquill and Smith, 1983; Hunt et al., 2002).

The Gaussian cloud formula can be applied in terms of the distance $\tilde{x}$ along and distances $\tilde{y}, \tilde{z}$ perpendicular to w the mean streamline through the source, so that $X^2, Y^2, Z^2 = (\tilde{x} - \tilde{U}t)^2 / \sigma_x^2,\ \tilde{y}^2 / 2\sigma_y^2,\ \tilde{z}^2 / 2\sigma_z^2$, respectively. Note that $\tilde{x} = 0$ at x = x_S and $\tilde{y}$ can be calculated in terms of the coordinates of the mean streamline $y_c(x), z_c(x)$ (see Figure 3b(i)). The mean velocity along the mean streamline is $\tilde{U}(\tilde{x})$. The magnitudes of $\sigma_x, \sigma_y, \sigma_z$ depend on the variances of the turbulent velocity components and their integral length scales (assuming that the velocity components have similar statistical structure in the different directions).

Very near the source (say within 100m),

$$\sigma_x \cong \sigma_u \Delta t',\ \sigma_y \cong \sigma_v \Delta t',\ \sigma_z \cong \sigma_w \Delta t' \qquad (4.5a)$$

Because of the anisotropy of the turbulence these widths can differ by a factor of 2 or more.

Far from the source, where $(t - t') \gtrsim L_x / \sigma_w$ these cloud dimensions are approximately equal to integrals of the diffusivity components K_x, K_y, K_z $(\Delta t')$ taken along the trajectory, i.e.

$$\sigma_x^2(\Delta t') = 2\int_0^{\Delta t'} K_x(\Delta t'')\, d\Delta t'' \tag{4.5b}$$

A modified form of this expression can be used when the mean velocity varies along the plume (Hunt, 1985).

For sources on level ground, as the cloud's vertical dimension grows to greater than its source height z_S, it impacts on the ground. The resulting increase in the concentration is approximately modelled as a 'reflected' Gaussian profile by adding the image solution $G_{C,r}$, i.e. for $\sigma_z > z_S$,

$$C_C = G_{C,0}(X, Y, Z, \Delta t') + G_{C,r}(X, Y, Z, \Delta t'), \tag{4.6a}$$

where $G_{C,r} = G_{C,0}(X, Y, Z_R, \Delta t')$ and $Z_r^2 = (z + z_s)^2 / 2\sigma_z^2$, and also note $G_{C,r} = G_{C,0} \exp\left(-2z_S z / \sigma_z^2\right)$.

It is useful to note that if the source steadily emits q_A units per unit time in a wind with mean velocity U and there is a steady mean wind, the source leads to a steady plume downwind with concentration

$$C_P(\mathbf{x}) = q_S(\mathbf{x}_S)\, G_p(\mathbf{x} - \mathbf{x}_S) \tag{4.7a}$$

where

$$G_P = \int_{-\infty}^{t} C_C dt' \cong G_p(\mathbf{x} - \mathbf{x}_S) \tag{4.7b}$$

Here the Gaussian plume formula for uniform flow conditions above the ground

$$G_{P,0}(Y, Z, \tilde{x}) = \exp[-(Y^2 + Z^2)] / (2\pi U \sigma_y \sigma_z) \tag{4.8a}$$

After 'reflection' off the ground,

$$G_P = G_{P,0}(Y, Z, \tilde{x}) + G_{P,0}(Y, Z_r, \tilde{x}) \tag{4.8b}$$

4.2.2.2 Dispersion with large separation distances between buildings (b/d ≤ 1/3) – multiple cloud splitting models

In an urban area, with well-separated buildings after the cloud/plume has travelled a distance of order d it will impinge on to or pass over downwind buildings located at $\underline{x}_b^{(1)}, \underline{x}_b^{(2)}$ (see Figures 3 and 5). The diffusive and advective processes involved greatly affect the form of the profile of concentration at a given value of X, and the dimensions of the cloud/plume, depending on the cloud parameters in relation to the building scale H, b i.e. the mean height ratio $\hat{z}_c = z_c / H$, cloud dimensionless ratio $\hat{\sigma} = \max(\sigma_y, \sigma_z) / \min(H, b)$ and grazing distance ratio

$$\hat{n} = \min\left|\mathbf{x_c} - \mathbf{x_b}\right| / \max(\sigma_y, \sigma_z)$$

(Fackrell, 1984). Hunt and Castro (1981) extended the work of Vincent (1977) to dispersion of clouds in building wakes. The basic concepts for plumes were developed by Hunt and Mulhearn (1973), Puttock and Hunt (1979), Hunt et al. (1979) and Davidson et al. (1995). Robins and Apsley (2000) brought many of the results together for single buildings in the Buildings Module of the ADMS model. Hall et al. (1996, 2001) extended the results to cover dispersion around many buildings in their code UDM. We describe the characteristic processes below and outline the simple models that have been developed.

Impacting low level cloud

As the cloud approaches the building, if it is within a plume width of the centreline (i.e. $\hat{n} \leq 1$) it is swept round and over the building and is entrained into the recirculating wake.

If $\hat{\sigma} > 2$, the cloud is wider than the width of the building and so its width and peak concentration are not significantly changed by the impact. If σ_z > H, its depth is also not much changed. But for a tall building, if H/b > 2 and a narrow plume, defined by σ_z < b, then the cloud is diffused vertically in the wake, so that σ_z is increased by about b as the cloud passes around the building, but is not completely mixed up to the height of the building.

Also, for the 'puff' cloud the time taken for the cloud to detrain from the wake is of the order of min(6H, 3b)/U, so that the length of the plume σ_x is increased to about min(6H, 3b) if σ_x is less than this length (Fackrell, 1984). Thus if the cloud impacts centrally on the building, i.e. $\hat{n} \leq 1$, the change in the cloud dimensions downwind of the building are approximately given by

$$\Delta\sigma_x \sim \max\{\min(6H,3b) - \sigma_x, 0\} \tag{4.9a}$$

$$\Delta\sigma_y \sim \max\{b/2 - \sigma_y, 0\} \tag{4.9b}$$

$$\Delta\sigma_z \sim \max\{H - \sigma_z, 0\} \quad \text{if } H \lesssim 2b \tag{4.9c}$$

$$\Delta\sigma_z \sim \max\{b - \sigma_z, 0\} \quad \text{if } H \gtrsim 2b \tag{4.9d}$$

(Upwind of a tall building the 'downwash' can reduce σ_z and reduces entrainment into the wake and σ_z < H.)

Note that if the cloud 'grazes' the building, i.e. if $\hat{n} \sim 1$, then a proportion α of the cloud first is entrained and then detrained from the recirculating wake (see Figure 5). This leads to a changed concentration profile downwind of the wake with length P_W that approximates to a double plume structure as in the ADMS Building Module consisting of the depleted original $G_{C,0}$ and the Gaussian cloud/plume that detrains from the wake. Thus for $x > x_b + l_w$ and $\Delta t > \Delta t_b$

$$\begin{aligned} G_C &\cong (1-\alpha)G_{C0}(\tilde{X},\tilde{Y},\tilde{Z}) + \alpha G_{C,w}(\tilde{X}_w,\tilde{Y}_w,\tilde{Z}_w) \\ G_P &\cong (1-\alpha)G_{P,0}(\tilde{x},\tilde{Y},\tilde{Z}) + \alpha G_{P,w}(\tilde{x}_w,\tilde{Y}_w,\tilde{Z}_w) \end{aligned} \tag{4.10}$$

where

$\tilde{Y}^2 = \tilde{y}^2 / 2\sigma_y^2$, $\tilde{y} = y - y_c$ and $y_c \cong y_b + b/2 - y_c$, $\tilde{x}_w = x - x_b$ and $\tilde{X}_w^2 = (x - x_{cw})^2 / 2\sigma_{xw}^2$, $\tilde{Y}_w^2 = (y - y_b)^2 / 2\sigma_{yw}^2$, $\tilde{Z}_w^2 = z^2 / 2\sigma_{zw}^2$, $x_{cw} = x_b + U_w(\Delta t - \Delta t_b)$, $\Delta t_b = (x_b - x_S)/U$. The cloud/plume dimensions are functions of the wake turbulence and the distance downwind from the building ($x - x_b$) and travel time from detrainment i.e. $(\Delta t - \Delta t_b)$. Their effective values at $x = x_b + l_w$ is determined by the scale of the wake, for example $\sigma_{y,w}^2 \cong b^2/4 + \sigma_y^2(x - (x_b + l_w))$. Note that the wake cloud displacement $x_{c,w}$ depends on the slower wake velocity U_w.

The entrainment factor (α) decreases as the mean streamline moves further from the centreline of the building. If the accidental cloud plume is released in the near wake then α=1.

Note that within the recirculating wake, i.e. $x_b < x < x_b + l_w$, the mean concentration $\langle \overline{C}_{c,w} \rangle$ is approximately constant and determined by the value in the approach cloud/plume where it touches the wake, and

$$G_{C,w} \cong G_{c0}(\tilde{X}_{0,w}, \tilde{Y}_{0,w}, \tilde{Z}_{0,w}, \Delta t_w)$$
$$G_{P,w} \cong G_{p0}(\tilde{x}_{0,w}, \tilde{Y}_{0,w}, \tilde{Z}_{0,w}) \qquad (4.11)$$

where the displacement parameters are:

$\tilde{X}_{0,w}^2 = 0$

$\Delta t'_w = (x_b + l_{w/2} - x_S)/U$

$\tilde{x}_{0,w} = x_b + l_{w/2} - x_S$

$\tilde{Y}_{0,w}^2 \cong (y_S - y_b - b/2)^2 / 2\sigma_{yw}^2)$

$\tilde{Z}_{w0}^2 \cong (z_S - h/2)^2 / 2\sigma_{zw}^2 \quad (x \cong x_b + l_w/2)$

and $\sigma_{xw}, \sigma_{yw}, \sigma_{zw} = \sigma_x(\tilde{x}_{0,w})$ etc.

$$\alpha_c = \frac{\langle G_{c,w} \rangle}{G_{c,w}(y \approx b/2, z, \Delta' t_w)}$$

$$\alpha_p = \frac{\langle G_{p,w} \rangle}{G_{p,w}(y \approx b/2, z, \tilde{x} = b/2)}$$

Such expressions can be refined and calibrated for different types of buildings, and for different source positions relative to the building. One example has been written out here to show how even for one particular situation of a cloud impacting on a building there are complex aspects that have to be considered. But even though the structure changes quite markedly it does have characteristic features that recur for most types of building. In the UDM code (Hall et al., 1996), where many buildings are considered, these expressions are further simplified (and explained graphically) for example by ignoring the lateral displacement of the streamline through the source, ie assuming $y_c \approx y_S$.

This approach can be satisfactory even when wakes of buildings impact on each other by modelling appropriately the changed cloud dimensions. However, even with extensive empirical modification it is probably not an accurate or efficient model when buildings are close to each other and the wind is not perpendicular to the buildings. A downwind vortex causes the air flow to be significantly deflected some distance downwind of the building. The combined effect of many such building wake interaction leads to the characteristic dispersion pattern in 'canyon' flows considered in Section 4.2 (3).

Impacting elevated clouds

If the effective source of the cloud is at a height z_S above the ground, the cloud impacts on a downwind building if $\hat{n} \le 1$, or in more detail if $y_S - y_b - b/2 \lesssim \sigma_y$ and $z_S - H \lesssim \sigma_z$. If the vertical cloud depth is small compared to the height (i.e. $\sigma_z <$ *H*) then the cloud grazes the top of the building and is entrained into the wake. As with the laterally displaced low level cloud, this leads to a double cloud structure, as shown in Figure 3. So that for $x \ge x_b + w/2, \Delta t > \Delta t_b$

$$G_c \cong (1-\alpha) G_{c,0}\left(\tilde{X}, \tilde{Y}, \tilde{Z}, \Delta t\right) + \alpha G_{cw}(X_w, Y_w, Z_w, \Delta t) \qquad (4.12)$$

Here $\tilde{Z} = (z - z_c)^2 / 2\sigma_z^2$, $z_c \cong z_S + \zeta H$ ($\zeta \cong 1/2$ due to streamline convergence over the building). The functions G_{c0} and G_{cw}, α, and dimension parameters are constructed as in (4.10) by matching the wake concentration in the grazing plume to that in the wake.

This simple form shows how the concentration field varies markedly as the height of the source varies near a building. The results are consistent with wind tunnel concentration measurements of steady plumes in and near building wakes (Robins and Apsley, 2000).

4.2.2.3 Dispersion with moderate spacings between rows of buildings – canyon model H/d≳ 1/3)

As explained in Section 2, where buildings are located in rows with separation gaps d that are comparable with their height H, (i.e. streets), the recirculating flow in the wake of the upwind row tends to extend across the street, and there is usually a significant mean velocity V_s along the street (see Figure 3a(ii) and Figure 6). Note that for convenience separate streamline coordinate systems are used within and above the canyon, with $\tilde{\mathbf{x}}_c$ denoting the coordinate relative to the canyon flow. First consider a cloud/plume released below the top of the building.

a For a cloud released below the top of the building, the initial phase of dispersion, described in Section 4.2.2(i) (for $\Delta t < \Delta t_1$) ends when the cloud width (defined relative to the local mean wind spread along the street) $\tilde{\sigma}_y$ is comparable with the street width (i.e. $\tilde{\sigma}_y \sim 5$).

b For $\Delta t > \Delta t_1$ before the vertical growth of the cloud reaches the tops of the buildings, i.e. $\sigma_z + z_S < H$ the cloud grows in the flow direction as it is advected along the street. In this phase the cloud profile has an

approximately Gaussian 'street' form in the vertical and longitudinal directions i.e

$$C \sim Q_s\left[G_{C,0}\left(\tilde{X},\tilde{Z},\Delta t\right)+G_{C,r}\left(\tilde{X}_C,\tilde{Z}_r,\Delta t\right)\right] \tag{4.13a}$$

where

$$G_{C,0} \sim \frac{\exp\left[-\left(\tilde{X}^2+\tilde{Z}^2\right)\right]}{(2\pi)\cdot d\cdot\sigma_x\sigma_z} \tag{4.13b}$$

and the second term is caused by ground reflection as defined in (4.6b). The values of σ_x, σ_z are greater (by typically a factor of 2 or more) than their values in open country for the same value of u_* (because of longitudinal dispersion in the streamwise direction and recirculating flows with vertical components).

If the source is effectively steady the resulting plume profile in the canyon (from 4.7) is

$$G_P \sim \exp\left(-\tilde{z}^2\right)\Big/2\pi V_s.d\cdot\sigma_z+\exp\left(-\tilde{z}_r^2\right)\Big/2\pi V_s.d\cdot\sigma_z\,, \tag{4.14a}$$

c In the third phase, where $\sigma_z\left(\tilde{x}\right)>H-z_s$, $\tilde{x}\geq\ell_H$ and $\Delta t > t_2$, the cloud reaches the top of the buildings and then is dispersed by the wind moving at speed U_H at an angle θ to the street. The cloud concentration decreases rapidly (in fact exponentially) along the street. If the source is near the ground (and $\sigma_z \gtrsim H$) the cloud is well mixed and dispersing upwards. But if the source is elevated (i.e. $z_S \sim H$) there continues to be downward vertical dispersion in this phase. The following approximate analysis is derived from the basic solution of Turfus (1986) for dispersion from a steady localised course where the mean velocity reverses near the ground (see Appendix). The profile for a cloud $z_S < H$ for $\tilde{x}_c \gtrsim l_H \sim (U/u_*)(H-z_S)$ and $z < H$ below the top of the buildings

$$G_{C,c} \cong \exp\left(-\frac{\tilde{x}}{10H}\right)\gamma_z(z/H)\gamma_C\left(\tilde{X};\tilde{x}_c\right) \tag{4.15a}$$

where $\tilde{x}_c = y - y_S$

$$\gamma_z(z/H) = \cos(\mu/H) \tag{4.15b}$$

where μ varies slightly with the angle θ of the approach wind (see A.9a)

$$\gamma_c = \frac{10\exp\left(-\tilde{X}^2\right)}{Hd\cdot\tilde{\sigma}_x} \tag{4.15c}$$

where $\tilde{X} = \left[\tilde{x}_c - V_s\Delta t\right]^2 / 2\tilde{\sigma}_x^2$, and $\tilde{\sigma}_x$, as usual, is a function of $\tilde{x}_c$, the distance from the source along the canyon.

For a steady source, the formula for a plume is similar where

$$G_{C,p} \approx \gamma_p G_{Cc} \tag{4.15d}$$

where $\gamma_p \approx \frac{1}{\gamma_c} \cdot \frac{2.5}{V_c H d}$

Above the level of the buildings over the canyon, where z = H and $-d/2 > \tilde{y}_c > d/2$,

$G_{C,c} \approx G_{C,c}(x_c, z \cong H)$

where $\gamma_z(1) = \left(0.4 / \sqrt{10 \cos\theta}\right)$ (4.16)

(Note $\tilde{y}_c = x$ is here the horizontal coordinate perpendicular to the street axis.)

Just downwind of the canyon, the concentration is given by (A.16a) (A.14B) for cloud/plume sources (i.e. x>d/2).

d Further downwind in the fourth phase $\Delta t > \Delta t_3$ the cloud moves and disperses over the buildings as if it had been released from a virtual source position at (x_{sH}, γ_{sH}, H)) upwind of the street (see Figure 6) at time t_{sH}. Estimates of this position/release time are $x_{sH} \cong x_S - 25H$, $t_{sH} \cong t_S$, i.e.

$$G_{c,H} \cong \frac{2}{(2\pi)^{3/2}\sigma_{xH}\sigma_{yH}\sigma_{zH}} \exp\left(-\left(\tilde{X}_H^2 + \tilde{Y}_H^2 + \tilde{Z}_H^2\right)\right) \quad (4.17a)$$

for a continuous source.

$$G_{p,H} \approx \frac{G_{c,H}}{U_H}\sqrt{2\pi}\sigma_{x,H} \quad (4.17b)$$

(Note that the dimensions of G_c, G_p are different.) Here the coordinates for the cloud/plume through the source are given by:

$$X_H = \frac{\left(\tilde{x} - U_H(t - t_S)\right)}{2\tilde{\sigma}_{x_H}^2}, \quad (4.17c)$$

(where $\tilde{x} \cong (x - x_{sH})\cos\theta + (y - y_{sH})\sin\theta$ and $\sigma_{x,H}^2 \cong \sigma_x^2(\tilde{x})$);

$\tilde{Y}_H \cong \frac{\tilde{y}^2}{2\sigma_{y,H}^2}$ where $\tilde{y} \cong (y - y_{s,H})\cos\theta - (x - x_{s,H})\sin\theta$), and

$\tilde{Z}_H = \frac{(z - H)^2}{2\sigma_z^2}$

Note that the cloud/plume dimensions at x = 0, $y = \tilde{x}_c \sim \ell_H$ where phase 3 becomes phase 4 match each other so that

$$\tilde{\sigma}_{x,H}\left(\tilde{x} = -x_{s,H}\sin\theta\right) \sim \left[\tilde{\sigma}_x^2(\tilde{x} \sim l_H)\sin^2\theta + d^2\cos^2\theta\right]^{1/2}$$
$$\tilde{\sigma}_{y,H}\left(\tilde{x} = -x_{s,H}\cos\theta\right) \sim \left[\tilde{\sigma}_x^2(\tilde{x} \sim l_H)\cos^2\theta + d^2\sin^2\theta\right]^{1/2} \quad (4.17d)$$

From these formulae for the concentrations in the cloud in the canyon and above buildings, estimates can be derived for the concentration in side

streets downwind. Where the side streets are quite short and extend over a distance of order 5-10H, matter from the source is advected along the side street and concentration is approximately equal to that in the main street where the accident occurs (in the direction of the wind). But for $x \gtrsim 10H$, matter from the source mainly reaches side streets by being diffused downwards, so that the concentration is approximately equal to the value at the level z = H (given by (4.17a,b)).

The main features of the model given here are found in the detailed computation of Soulhac (2000) of a source released in rectangular grids of streets. (He used a diffusivity model for diffusion.)

In particular he showed how in a street with an angled wind the effect of a ground level source leads to the concentration at the top level of the buildings ($z = H$) increasing slowly and then decreasing quite rapidly, when it is advected away parallel to the wind in a wide plume (with width σ_y much greater than the width of the street). This was consistent with field data in Lyon (Soulhac, 2000).

In some cases the clouds may be released above the buildings ($z_s > H$). Then, as shown in Figure 7, the cloud is carried parallel by the wind above the buildings. But as it diffuses downwards, it may enter one or more large streets (when $g \gtrsim H$, there will be a significant canyon wind along the streets). Then by a similar mechanism as for low level sources in canyons the matter will be transported along each of these streets a distance of order 10H before being detrained again into the wind above the buildings. This leads to a split plume structure above the buildings.

This situation approximately corresponds to the field experiment conducted at Dugway, Utah (Griffiths et al., 2000) with a source placed above one of the elongated cuboids which were aligned in 'streets' The wind direction was not quite perpendicular to the buildings ($\theta \sim 150°$); it was observed that the plume did not follow the wind direction but was systematically displaced parallel to the streets by a few building lengths (see also Section 5).

This situation needs to be analysed in more detail in future research. Note that the typical peak concentration, denoted by $\hat{G}$, in the canyon is of the order of the concentration at $z = H$ of the unentrained plume, i.e.

$$\hat{G}_C(x, t) \cong G_{C,0}(x, y = y_S, z = H, \Delta t) \qquad (4.18a)$$

$$\hat{G}_{P,v}(\tilde{x}) \sim G_{P,0}(x, y = y_S, z = H) \qquad (4.18b)$$

where G_{C0}, $G_{P,0}$ are given by (4.4), (4.8). Note that because the flux downwards into the canyon over short distances (distances where $\tilde{\sigma}_y <$ $10H$ or, ($\tilde{x} \lesssim$ 1km), the buildings do not block the downward diffusion of the plume, and therefore there is no 'reflection' term in (4.18a,b). But over a flat surface or over a long distance ($\tilde{x}$ > 1km) from an elevated source over streets (when $\sigma g > 10H$), the matter in the street diffuses

up into the plume and then the reflection effect has to be included. (This leads to an approximate doubling of the formula in (4.18).)

4.2.2.4 Close packed buildings with no canyon effect b/d ≳ 1/2 - topological splitting and lengthening mechanisms

In some city centres and some kinds of industrial plant (such as refineries), the spacing between buildings are within about two or three widths (i.e $b/d \gtrsim 1/3$), and the gaps between the building do not form continuous 'canyons'. Then the streamlines move irregularly between the buildings, converging and diverging as they do so, as sketched in Figure 3b. The wake lengths l_w are reduced by converging flows if buildings are staggered or their displacing effects are reduced if the buildings are in lines. Theoretical calculations (e.g. Hunt, Puttock & Snyder, 1979), supported by numerical simulations (Davidson et al., 1995; Moulinec et al., 2003) show how as the streamlines diverge and 'split' near stagnation points, clouds of contaminant that move along or near the stagnation streamlines are advected either side of the building. This process of lateral spreading within the canyon can be so great that the plume width is determined by the geometry of the building and that spacing, i.e.

$$\sigma_{y_c} \sim \frac{1}{2}(b/(d+w))x\,, \tag{4.19a}$$

where this is larger than the width determined by turbulent diffusion, i.e.

$$\sigma_{yc} \sim (\sigma_v/\langle U_c \rangle)\ x. \tag{4.19b}$$

The streamwise longitudinal dispersion is amplified (Eames et al. 2003).

This shows that if $\sigma_v/U_c \cong 1/10$, then $b/d \gtrsim 1/4$ for the topological spreading to be greater than the turbulent diffusion. When $b/d \lesssim 1/3$ the spreading effect by the wakes (as described in Section 4.2.2 (2) above) is an additive effect. But when $b/d \gtrsim 1/3$, the converging flow between the buildings tends to reduce the sizes of the wakes by acceleration of the cross-diffusion and cancellation of vorticity from one side of the wake to the other (Hunt & Eames, 2002; Moulinec et al., 2003) – see Figure 3. This is a further reason why the topological dispersion is the dominant process for closely-packed buildings. The marked difference, by a factor of 2-3, between lateral dispersion of matter released among cuboid buildings placed in staggered, unaligned arrays compared to that of an isolated source over a flat surface was observed in the laboratory and field experiments repeated by Davidson et al. (1995). The photographic evidence showed quite clearly the splitting of the plume near the front stagnation point.

These experiments showed that for closely-packed buildings whose width is comparable to their height (i.e. $b \sim H$) when the source height z_S is less then the height of the buildings ($z_s < H$) the concentration is well-mixed in the vertical direction as a result of mean streamline displacements, and recirculating flows in the wakes and enhanced turbulence on the upwind faces of buildings (see Figures 3b(ii), 5(a)(iii)). In general (unlike the canyon case) the average wind speed in the 'canopy' below building height, $\langle U_c \rangle$, is in the same direction as the wind over the buildings, so that an approximate formula for the concentration

source in these cases (when averaged over all positions of the source). The cloud is detrained into the upper floor above the buildings.

For z_s < H and $\ell_H \geq \tilde{x} > d$. Hence the concentration of a cloud has a 'buildings' and a detrained component.

$$G_{C,c} \cong G_{C,B} + G_{C,d} \tag{4.20a}$$

(Figure 7), where

$$G_{C,B} \cong \alpha_C(t)\frac{\exp\left[-\left(\tilde{X}_c^2 + \tilde{Y}^2\right)\right]}{2\pi H\sigma_{xc}\sigma_{yc}} \tag{4.20b}$$

Here

$$\tilde{X}_c = \left(x - x_s - \langle U_{CH}\rangle t\right)$$

where the advected speed of the cloud is the weighted average of that in the canopy and in the flow above, i.e. $U_{CH} \cong \left\{\langle U_C\rangle + (\sigma_z / H)U_H\right\}/2$.

The smaller detrained component in the faster moving upper cloud is given for

$$G_{C,d} \cong G_{C,B}(z = H)\cdot\frac{1}{\sqrt{2\pi}\sigma_{z,H}}\exp\left\{-\frac{(z-H)^2}{2\sigma_{z,H}^2}\right\}$$

where

$$\sigma_{z_H} \sim \sigma_w\left(\tilde{x} - \frac{\ell_H}{3}\right)\Big/U_H .$$

(Hence the detrained component is only significant when $\tilde{x} \sim \ell_H$.)

For a plume,

$$G_{pc} \cong \alpha_c\frac{\exp\left(-\tilde{Y}^2\right)}{\sqrt{2\pi}H\sigma_y\langle U_c\rangle} \tag{4.21}$$

Above the canopy (formula not given) the front of the upper lower concentration cloud is carried by the faster wind U_H, while the back of the cloud moves at the slower speed of the canopy cloud. Hence the downwind length of the upper cloud σ_{xH} is of order $\left(U_H - \langle U_C\rangle\right)t$ (Figure 8). Its concentration can be calculated explicitly in terms of the flux from the canopy cloud. The typical value in the upper cloud is

$$\hat{G}_{C,H} \sim \frac{\hat{G}_{C,c}}{\sigma_{x,H}\sigma_{z,c}} \tag{4.22}$$

This is significantly less than in the canopy $\hat{G}_{C,c}$ because σ_{xH} is much greater than σ_{xc} when $\sigma_z \lesssim H$).

The formula for a steady plume is simpler, namely

$$G_{pH} = \alpha_H \frac{\exp\left(-\left(\tilde{Y}_H^2 + \tilde{Z}_H^2\right)\right)}{\pi\sigma_{y,H}\sigma_{z,H}U_H} \tag{4.23a}$$

where $\tilde{Y}_H^2 = (y - y_S)^2 / 2\sigma_{yH}^2$, $\tilde{Z}_H^2 = (z - H)^2 / 2\sigma_{zH}^2$, and the plume dimensions are calculated in terms of the turbulence above the buildings. Note that here the wind speed U_H is greater than U_c, and therefore to calculate the normalising coefficients α_c, α_H, the plume flux is unity, i.e.

$$\int_{-\infty}^{\infty}\int_{0}^{H}\langle U_C\rangle G_{P,c}\,dydz + \int_{-\infty}^{\infty}\int_{H}^{\infty}\langle U_H\rangle G_{P,H}\,dydz = 1 \tag{4.23b}$$

It follows that $\alpha_c + \alpha_H = 1$. Since the concentration profile is continuous at $z = H$,

$$\frac{\alpha_c}{H\langle U_C\rangle} = \frac{2\alpha_H}{\sqrt{2\pi}\sigma_{zH}U_H} \tag{4.23c}$$

Hence

$$\alpha_c = 1 \Big/ \left\{1 + \frac{\sqrt{2\pi}}{2}\left(\frac{\sigma_{z,H}}{H}\right)\left(\frac{U_H}{\langle U_c\rangle}\right)\right\} \tag{4.23d}$$

Further downwind on the neighbourhood scale, as discussed in Section 4.2.3, the cloud has diffused vertically a significant distance so that its horizontal diffusion so that $\sigma_{zH} > H$. Its horizontal diffusion caused by the shear is such that the cloud streamwise dimensions σ_z above and below the canopy become approximately equal. Then the expressions (4.9) – (4.23) are no longer valid for the canopy cloud or plume.

Now consider when some of the close parked buildings in an urban area are tall (i.e. $H \gtrsim 2b$) and $b/d > 1/3$. Then, even though there is an amplified rate of vertical dispersion as a result of vertical swirling and turbulent motion around the buildings (Figure 8), neither the average vertical concentration profiles nor the detrainment from their wakes are uniform over the depth of the average canopy layer *H*.

Given an approximate estimate for the rate of growth of σ_z in terms of the vertical turbulence σ_w ($\cong \langle U\rangle/10$) and the spatial average of the variation of the mean vertical velocity ~ $\frac{1}{3}\langle U\rangle b^2/d^2$ leads to (by considering detrainment from their wakes)

$$\sigma_z \sim x\left\{\frac{1}{10} + \frac{1}{3}(b/d)\right\} \tag{4.24}$$

This shows that if $b/d \sim 1/3$, the cloud/plume grows at about twice the rate as over a flat surface, so that with buildings of height H~100m, the distance downwind of the source for the cloud to reach the tops of the buildings would be in the range 0.5–1km.

4.2.2.5 Dispersion in enclosed spaces

A high level environmental hazard might occur if an accident occurs in am enclosed space such as a courtyard surrounded by moderate to tall buildings in an urban area, where typically $H/d \geq 1/3$ (see Table 3, Figure 3d).

The competing dispersion mechanisms that chiefly have to be considered are

a mixed by the recirculating flow in the courtyard with typical velocity $\langle U_c \rangle \sim 1/3 U_H$, and

b detrainment from the courtyard into the flow above the buildings with a typical detrainment velocity $u_* \sim U_H/10$. (This detrainment rate would be even smaller if the courtyard were partially covered, e.g. at a railway station or under a road flyover.)

These estimates imply that any material released will be well-mixed in the courtyard before it is significantly dispersed over a time $T_{DC} \sim 10d/U_H$. Thus if the total quantity M_S of matter in the source is rapidly released (on a timescale $H/\langle U_c \rangle$ – say 10 seconds) the typical concentration in the enclosed space $\hat{C}_{C_E}$ from the release of a cloud, is inversely proportionate to the volume of the courtyard i.e.

$$\hat{C}_{C_E} \sim M_S/(d^2 H) \qquad (4.25a)$$

If the source material is continuously released at a rate Q_S on a time scale that is long compared with the typical dispersal time T_{DC}, then the concentration depends on the detrainment rate, so that

$$\hat{C}_{C_E} \sim Q_S/(u_* d^2) \sim Q_S/U_H d^2/10 \qquad (4.25b)$$

These estimates of concentration levels may be significantly greater (by a factor of 3 or more) than would occur in a street canyon with a steady source (after the matter has spread across the street) where

$$\hat{C}_{C_C} \sim \frac{Q_S}{V_S d^2} \sim \frac{3Q_S}{U_H d^2} \qquad (4.25c)$$

Clearly more detailed calculations and experiments are needed to test these predictions because of their serious implications. If, as sometimes occurs, the courtyard has a sizeable opening (of width b) the high velocity winds V_0 passing through it contribute to the ventilation of the courtyard space (e.g. Lawson, 1980). But this will still be less than the detrainment at the level of the buildings (because $V_0 b^2 \sim U_H b^2 \leq u_* d^2$ since $b^2/d^2 \leq 1/10$). See Hall et al., 1999.

4.3 Neighbourhood Scale dispersion models

4.3.1 Length scales and processes

Once a cloud or continuous plume has been advected from the source in an urban area and passed over and around several buildings and streets, its dispersion is then determined by the average properties of the mean velocity field and turbulence within and above the 'canopy' of buildings. On the neighbourhood scale the buildings and streets are assumed to have similar

forms, and both the larger effects of the mesoscale meteorological and even chemical processes can be neglected: see Table 1. Hence the distances and plume dimensions lie within the following ranges defined by the length scales L_N of the neighbourhood region and depth h of the atmospheric boundary layer.

$$L_N \gtrsim x - x_S \gtrsim 3d$$

$$L_N \gtrsim \sigma_x \gtrsim 3d \quad (4.26)$$

$$h > \sigma_z > H$$

Typically these regions might include 10^3 individual streets and/or buildings.

The key physical mechanisms of dispersion on this scale are the differences in mean wind speed and velocity $\langle U_c \rangle, U_H$ within and above the canopy. In 'porous' canopies, such as suburban areas and spaciously designed urban centres, the ratio of speeds $\langle U_c \rangle / U_H$ is significantly greater than the turbulence intensity σ_w/U_H ~ 1/10 so that the cloud/plume is advected by the main wind within as well as above the canopy. In addition the topological and wake dispersion processes (described in Section 4.2) are as significant as turbulent eddying for dispersing matter both horizontally and vertically within the canopy.

However, the scales of the largest horizontal eddying motions of the turbulence within the canopy are of much smaller scale (~d) than those in undisturbed boundary layers (which recent research show range up to 2km, Högström et al. (2002)).

This is why, although the turbulent velocities may be higher than in the undisturbed boundary layer, over the large distances of the neighbourhood scale the lateral dispersion σ_y above the buildings is likely to be comparable with the lateral dispersion in the canopy (see Davidson et al., 1995). Note that in the region downwind of an area with high buildingds and a deep canopy, where the building heights decrease, matter dispersed in the canopy is advected as a wake cloud/plume, just as behind a single building. Its depth where it leaves the deep canopy is comparable with the main building height there.

In city centres with closely-packed buildings and narrow streets, the ratio $\langle U_c \rangle / U_H$ is much less than σ_w/U_H and therefore the urban area is effectively non-porous, the mean streamlines and the cloud/plume pass above the buildings and matter reaches the street and spaces downwind of the source by entrainment and downward diffusion into the street. Because there are mean flows along the street at an angle to the plume, there will be some extra lateral diffusion as a result of this process (see Figure 10b).

4.3.2 Review of FCM and FAM Models

The neighbourhood scale is an intermediate range in term of flow modelling, in that some methods are based on detailed or 'discrete' modelling to predict average properties of dispersion, while others are based on 'continuum' modelling approaches using average/statistical descriptions of the aggregated properties of the canopy and the flow (see Table 5).

Fully Computational Models

In methods based on the discrete modelling approach, flow fields are calculated for thousands of buildings and streets and thence dispersion from any accidental sources. Basic (mixing length) models for turbulent shear stresses and eddy diffusion fluxes with coarse resolution meshes are likely to provide reasonable estimates for the dispersion within and above the canopy from sources within the canopy (Hall and Cowan, 1998; Kim and Boysan, 1999) because the dispersion process above the canopy is largely vertical – which is adequately predicted by such models. Such a modelling approach may take hundreds of hours on workstations. Faster computational modelling approaches for dispersion are now being explored. Since, as explained in Section 4.2, the dispersion is dominated by wakes and the topology of the streamlines passing around the buildings, it follows that it is the broad size and overall dimensions of a building that determine divergence/convergence and splitting of streamlines. Also the detailed structure of turbulent eddying has a relatively small influence (if the buildings are closely packed). Therefore computational models can be used with approximate equations, approximate boundary conditions (for the buildings) and quite coarse mesh sizes (e.g. 1/10 the size of the building). Of course some constraints are absolutely necessary such as the finite energy of the flow, mass continuity, zero flux through buildings, etc. One way to reduce these constraints for the dispersed matter is to track Lagrangian particles through the flow, allowing for a turbulent component (Turfus, 1988). This approach enables small computers to obtain results in a few hours or less.

If such an approach becomes widespread it will be even more necessary to calibrate and understand its merits and drawbacks by using detailed and accurate computational modelling techniques that have been thoroughly validated, such as Large Eddy Simulation methods (Rodi 1997), stochastic simulation methods (Hort et al., 2002; Turfus, 1988), and time-dependent Reynolds-averaged models.

The more usual approach to speeding up FCM methods for ‘multi-body’ flow/dispersion calculations such as this is to use the continuum approach. This requires some estimates of turbulence parameters such as mixing lengths or eddy diffusivities for the canopy (on the neighbourhood scale), but these characteristics cannot be deduced from turbulence closure models, although they may be estimated from detailed calculations of flow/dispersion around a few ‘typical’ buildings/streets – not a straightforward or accurate process (see Moulinec et al., 2003).

Since the way that the main street canyons deviate the wind direction leads to the dominant process for dispersion in closely-packed city centres, in that case, as Soulhac (2000) demonstrated, FCM can be used for dispersion from sources in urban areas by computing the dispersion along the major streets and in the open flow above the buildings. This would be similar to the widely-adopted method of modelling traffic-generated pollution in urban areas by calculating the concentrations in a few key street canyons with the rest of the urban area being regarded as a rough surface. (e.g. Carruthers et al., 2000).

In order to have even faster models to estimate dispersion for many possible source scenarios, source positions and meteorological conditions, it is necessary

to have even faster models even if they are more approximate. These are considered in Section 4.3.3.

Note that provided the models are incorporated into computational systems, whether they are 'fully computational' or 'fast approximate', either may be suitable for the inverse calculation problem of estimating (by successive iterations) the location and nature of the source from measurements (or inferred measurements) of the concentration distribution. However this requires special programming methods to optimise the search algorithm.

Fast Approximate Models

4.3.2.1 Discrete Models

For dispersion from sources in suburban areas with detatched buildings and where street canyon effects can be neglected, the multiple cloud splitting models described in Section 4.2.2 (2) have been developed to apply to large numbers of buildings. In order to simplify and speed up the computation time, groups of overlapping split plumes are merged and formed into new, larger plumes. This is a standard computational procedure of 'rediscretisation' that has been used in puff models of diffusion (e.g. in RIMPUFF). This technique enables the UDM model to be applied on the neighbourhood scale (Hall et al., 1996).

Despite the fact that the model's assumptions formally preclude its application to closely-packed buildings in city centres, a comparison can be made with plumes even in these parts of urban areas because, as explained in Section 4.3.1, the cloud/plume on the neighbourhood scale is broadly Gaussian and similar to that over level ground. But there are significant differences between actual and Gaussian plumes, e.g. in how the plume penetrates into street canyons and is transported along them over a finite distance (as Soulhac's simulations showed). These differences could only be introduced into the multiple cloud splitting model by considerably distorting the basic models. Nevertheless, as comparisons with field data have shown (Brook et al., 2002) that the UDM model describes many of the observed plume features. Perhaps following the analysis made here about the canyon processes and other aspects of dispersion in canyons and in the presence of close-packed buildings, it will be possible to look at this comparison again in more detail to generalise their model further.

4.3.2.2 Continuum Models

The alternative approach to computing the concentration distribution over the neighbourhood scale is to consider that the canopy is a porous space with a lower wind speed $\langle U_c \rangle$ and different turbulence structure to that in the boundary layer flow above the buildings. We differentiate between the situation where $\langle U_c \rangle / U_H$ is large enough for the canopy to be considered porous. Then over the neighbourhood scale for a short-period accidental release the resulting cloud diffuses above the canopy and travels over it at a speed U_H. In most cases where the canopy is non-porous, the cloud/plume dispersion over the building/street scale takes place in a canyon or an enclosed space/courtyard.

The dimension $\tilde{\sigma}_x$ in the direction of the mean wind on the N scale can be expressed in terms of the length σ_{xB} it develops over the B/S scale when $\Delta t \sim t_H \sim l_H/U_H$ and its subsequent growth in the upper boundary layer (e.g. Chatwin, 1968).

When $\Delta t > \Delta t_{Bs} \sim 10H/U_H$ or $\Delta t_N = \Delta t - \Delta t_B > 0$

$\tilde{\sigma}_x^2 \sim (\sigma_u^2 \Delta t^2 + \sigma_{xB}^2)$

Porous canopy

Within a porous canopy (e.g. as described in Section 4.2.2 (2) and (4)) the cloud travels at a lower speed $\langle U_c \rangle$. Through vertical diffusion, this distorts the front and rear of the cloud (see Figure 8b) by a finite length $\Delta\sigma_x \sim H^2 (U_H - \langle U_c \rangle)/K_z \sim 10H$. This is of the same order as σ_{xB}. Within an urban canopy the wind travels along typical street canyons (even if the buildings are detached – see Section 2.2.4. This also widens the cloud/plume's horizontal dimension σ_y by a fixed distance (~10H) along the streets. As the simulations of Soulhac (2000) demonstrate, over most of the neighbourhood region the plume width $\tilde{\sigma}_y (\sim 0.1\tilde{x}$ >0.1-1.0km) is of the same order as this extra sideways displacement (if H ~ 30m) – see Figure 10b(ii).

For a steady source, the structure of the resulting plume in the N region is primarily determined by its form in the boundary layer above the buildings as given by (4.22), where $\alpha_H \cong 1$. On the N scale the value of $\langle U_c \rangle$ is only significant in determining the virtual origin and $\Delta\sigma_x$. The lateral plume dimensions $\tilde{\sigma}_y$ in and above the canopy are approximately the same as that for a cloud above a rough surface, as discussed above.

We conclude that over the neighbourhood scale the determining parameters are the wind speed U_H and turbulence σ_u, σ_v, σ_w above the canopy and the initial parameters of the cloud/plume when it reaches the top of the canopy or, equivalently, the virtual source at the level of the canopy. Using suitable fast approximate models for the flow field over urban areas (e.g. RIMPUFF, FLOWSTAR), the variation of the mean velocity and turbulence above the canopy can be calculated. The FLOWSTAR code (Carruthers et al., 1988) also predicts how $\langle U_c \rangle$ varies within the canopy.

Non-porous canopy

When the neighbourhood area is 'non-porous' and consists of closely packed buildings, so that the average canopy velocity is small compared to the turbulent velocity (i.e. $\langle U_c \rangle / U_H < \sigma_w/U_H \sim 1/10$), the mean air flow and transport of the source material on the neighbourhood scale is primarily above the buildings (Figure 10a). If the source is below the building height, it first of all disperses upwards (on the building/street scale) over a distance l_H to the tops of the buildings. Then the concentration of a cloud or plume is calculated as if it were moving over a rough solid surface of height H.

Downwind of the built up area the cloud/plume structure resembles that in the wake of a wide building of height H. Note that the concentration below the canopy is equal to the concentration at the top of the buildings.

The flow field and dispersion over such a 'non-porous' region is similar to that over a low hill with roughness change (since the effective surface roughness length z_0 over the central urban area is greater than that upwind). FAM methods are available for point, line and area sources (e.g. ADMS, AERMOD).

4.4 Dispersion modelling over the meso-scale

Over a distance of order L_o~10km and travel time L_o/U from the source the turbulent eddies diffuse the source material vertically through the boundary layer up to a height h. However, on this distance and over this time scale the wind speed and temperature profile may change significantly as a result of changes in surface elevation, temperature and roughness and diurnal change. For some kinds of accidental release (e.g. soluble or reactive gases or small particles) there can be substantial changes in the flux of the original material in the cloud/plume, and new material may be created.

The FCM approach is now widely used for regulatory predictions of airborne pollutants over large urban areas. Meteorological models provide data for the mean wind field and turbulence that are then used to calculate dispersion. Using at least 10^7 grid boxes (which takes several hours of computation) satisfactory predictions have been made of the broad features of dispersion from localised sources of pollution over mesoscale distances and time scales in urban areas with complex terrain (e.g. Phoenix, El Paso, Salt Lake City in the US). For example, these have shown how pollutants are advected up and down slopes, out of and into urban areas, as the heating of the slopes caused over the diurnal period (Pardyjak et al., 2003). Some mesoscale codes used simple turbulence models (e.g. mixing length) or even standard boundary layer profiles (as in the UK Met. Office mesoscale code (Cullen, 1993)), while others such as the HOTMAC code used at Los Alamos (Mellor & Yamada, 1974; Brown and Williams, 1998) use multi-equation turbulence and eddy diffusion models. Generally it is found that having a small enough grid size in the computation is more essential than the complexity of the turbulence model in determining the accuracy of the code. Only when Δx is of order 1km (by comparison with standard codes with 12km) are flow fields in complex terrain reliable enough to compute dispersion on the meso-scale of 10km. But currently this method is only available at the research level (e.g. Capon, 2002).

For dispersion in flows with significant variation in direction and speed at different heights and different times, the only reliable modelling method is to track individual fluid particles or track many clouds of particles from the source. The former method is now used for regional and synoptic scale dispersion prediction from localised sources, such as nuclear accidents and volcanoes, e.g. Maryon & Buckland (1995). Assumptions have to be made about how atmospheric turbulence on scales less than ~$3\Delta x$ diffuses particles as they are advected by the 'resolved' flow field on scale Δx. This method requires large

computer resources and then can be computed in minutes. For studying critical events in UK urban areas this method should be considered.

In the alternative and faster and less accurate FCM approach, the movement and distorting of larger clouds are computed in the meso-scale flow field, however that may be calculated. Many field experiments have validated this approach, especially over rather flat terrain in Scandanavia (which includes their urban areas) using the RIMPUFF model. This model includes an algorithm for 're-discretising' the clouds after they have been greatly distorted, mainly through wind shear. They have not been so well-tested in very complex terrain with strong stratification. Thus, in principle, it is well-adapted to mesh with the UDM model for building/street and neighbourhood scales. This kind of Lagrangian puff model is fast enough for most purposes.

In terms of FAM, the most basic method for estimating dispersion on the mesoscale (where σ_z becomes equal to or greater than h) is to assume that the concentration profile is approximately constant below the top of the boundary layer, so that for a continuous source Q_s, and for steady meteorological conditions,

$$C(x,y) = \frac{Q_S}{U_H h \sigma_y \sqrt{2\pi}} \exp(-\tilde{Y}^2) \qquad (4.26)$$

This 'box-model' approach has been used for comparison with urban dispersion experiments by Middleton (1998). This has proved satisfactory on neighbourhood scale ($\gtrsim$ 1km from source).

To model the transition of the plume between the neighbourhood and mesoscale regions, it is usual (as with other Gaussian plume models, e.g. Pasquill and Smith, 1983; Hunt et al., 1988) to estimate approximately the plume profile by one (or more) reflection terms when $\sigma_z \gtrsim h/2$, i.e.

$$G_{p,H} = G_{p,H0} + G_{p,H,R}$$

where G_{pH0} is given by (4.22) with α_H = 1, and

$$G_{p,H,R} = G_{p,H,0} \exp\{[(x-h)^2 - (z-(2h-H))^2] / 2\sigma_z^2\}$$

With such a model it is also necessary to estimate the effects on cloud/plume dimensions of undulating terrain and significant changes in stratification over the urban terrain. When, as is usual, the depth of the mixed layer, h, and U_H change over the diurnal period these expressions can be extended by using a FAM for the flow field and turbulence (as discussed in Section 2) and thence correcting the values of σ_x, σ_y, $\sigma_z(\tilde{x})$. Also, the time dependence should be considered especially when considering clouds of contaminant being released. If the wind reverses (i.e. changes direction by 180°) the concentration can increase with time, over several days (as occurs with sea/land breezes in Los Angeles). On the other hand, the effects of mountains can also lead to dispersion through complex upslope/downslope winds (Pardyjak et al., 2003), so the long-term effect (over several days) of an accidental release can be quite sensitive to the regularity of

the cycle of diurnal meteorological conditions, or to the existence of stagnant conditions when $U_H << \sigma_u$ (e.g. Hunt, 1996).

In conclusion, in order to use a FAM that calculates C(**x**, t) over the three sub-regions of a large urban area, it is necessary to decide what level of output is required in terms of accuracy and computational time and then

a in which type of urban area the source is located (it is lies within the canopy) by reference to Table 3

c which type of flow field model is appropriate for the three sub-regions (also considering the relevant physical factors to include, using Table 2 and Section 2)

d appropriate dispersion model(s) for the sub-regions considering the factors in Table 5 and the review in Section 4. Some of these models are already available as standard software systems, especially for the neighbourhood and meso-urban scale. (These can also be used as 'screening' models to provide quick estimates, Hanna et al. (2002).) But others, such as those for dispersion in inner city 'canyons', are still in the form of formulae that need to be integrated into dispersion software systems and tested against experiments and detailed simulations.

This review has mainly focused on models for mean concentrations. However, fluctuations need to be estimated in order to assess all the risks associated with accidental releases. There is some evidence from the experiments, Davidson et al. (1995), that the intensity of fluctuations is lower in clouds/plumes released among buildings, and are also qualitatively different. There is much less chance of a large scale of wind gust reducing the concentration to zero, so that the probability density function is closer to a log-normal distribution than to a cut-off Gaussian (Mylne, 1992).

5 URBAN DISPERSION EXPERIMENTS

5.1 Introduction

In this section we present and discuss experiments relevant to the dispersion of a pollutant near/within/above the urban environment. Only those experiments relevant to a compact source are considered and we deliberately omit experiments designed for directly addressing continuous emissions from many vehicles. Such experiments typically involve traffic estimation and roadside monitoring of pollutants arising from traffic emissions. It is possible to make some deductions from such experiments that can be used for compact source problems though this is not straightforward.

The chapter also does not address meteorological experiments in the urban environment.

There are several categories of relevant dispersion experiments:

- Field experiment in real cities

- Field experiment with artificial structures
- Laboratory experiments with modelled realistic cities
- Laboratory experiments with modelled artificial structures
- Laboratory or field experiments with dispersion near a small number (one or two or three) of buildings

These categories will be treated in turn.

5.2 Field experiments in real cities

5.2.1 St Louis: McElroy and Pooler (1968)

Dispersion experiments from low-level sources in real cities are rare. The St. Louis experiments of McElroy and Pooler (1968) led to the 'urban category' curves for σ_y and σ_z of Briggs (1973) for use in conventional Gaussian plume models (see Hanna, et al., 1982). These are shown in Table 6.

5.2.2 Birmingham (1999): Britter et al. (2002)

To test out an experimental technique in an urban area and to provide field data, three experiments were designed within the UK Urban Regeneration and the Environment (URGENT) programme, sponsored by the Natural Environment Research Council (NERC) as a result of a collaborative effort between the University of Bristol, the University of Cambridge and Cambridge Environmental Research Consultants Ltd. (CERC).

The experiments were performed in the City of Birmingham using a finite duration release of perfluoromethylcyclohexane (PMCH) and perfluoro-methylcyclopentane (PMCP). Both PMCH and PMCP have a very low background concentration (~ 10^{-5} $\mu g/m^3$) in the atmosphere. They are also inert, non-toxic and non- depositing.

The three experiments took place in Birmingham (UK) in July 1999, February 2000 and August 2000 respectively. They were performed during the PUMA (Pollution of the Urban Midlands Atmosphere) campaigns, which were also part of the URGENT programme and provided the necessary meteorological data. The PUMA campaigns collected extensive data from various meteorological sites within the Birmingham urban area. Standard meteorological data such as wind speed, wind direction, temperature and relative humidity were available as 15-minute averages for the three tracer experiments.

Each tracer experiment was set up with a 'top hat' temporal evolution of the tracer release rate. The spatial and temporal experimental design was determined using simple steady-state models and an advanced operational dispersion model ADMS 3 (CERC, 2000).

Most receptors were placed in an arc within the city centre, while some other receptors were placed well outside the city centre. The source-receptor distance for the inner arc was initially chosen to be 3-4 km for the July 1999 experiment and later reduced to 1 km for both the February and August 2000 experiments (Figure 11).

Due to a limited number of available air bag samplers (constrained by the financial resources and personnel available), the receptors were distributed within an arc of about 60°, suitable for south-westerly wind conditions; these being, for the city of Birmingham, the most frequent winds.

The July 1999 and August 2000 experiments were successful, while the plume was partially missed by the receptors for the February 2000 experiment and, due to a technical failure, the most important receptor failed. The partial missing of the plume was the result of an unexpected change in the forecast wind direction.

The August 2000 experiment clearly showed that the receptors that see the maximum concentrations (and are presumably close to the centre line of the plume) experience a short time delay (roughly equal to the source-receptor distance divided by the wind speed). The concentration then rapidly rises to maximum values that are maintained for a time comparable to the release time. This is followed by a slow decrease towards the background level. A similar, though less clear-cut, interpretation can be made for the July 1999 experiment.

All the results show considerable variability; a variability consistent with dispersion experiments in the field but probably made worse by the urban complexity, the quite short sampling times being used and the fact that the results are from one realisation of an unsteady problem.

Figures 12 and 13 show selected experimental concentration histories for both the July 1999 and the August 2000 experiments with the origin moved to the release time. The rapid rise, elevated plateau, and slow decrease in concentration towards the background level can be discerned. The slow decrease is most probably due to material being retained in the wakes of the buildings and slowly released. The concentration data can be fitted with an exponential decay curve with a well-defined time constant. This time constant for the concentration decrease of the July experiment was estimated to be about 7 minutes, and about 4 minutes for the August experiments. These estimates are based on data from 50-100 minutes for the July 1999 experiment and 20-50 minutes for the August 2000 experiments. However in both experiments the concentration tends to remain above the background levels for very long periods. There is, apparently, a very slow decay that occurs over a long period, probably some hours beyond the total duration of the experiments. This long-lived plateau might be due to material being taken inside the complex configuration of buildings through natural and forced ventilation and then released with a time constant comparable to building air-exchange rates. The measurements from the July 1999 experiment showed that the maximum concentration occurred for receptor S1.3, which is consistent with a wind direction of about 230º. This is about 30º less than the actual wind direction. The reason for this could be an initial offset of the plume produced by the buildings situated in front of the release point (Theurer, 1995) but further investigation is still required (see also discussion in Section 4.2.2).

The maximum concentration for the August 2000 experiment was recorded at Site 3.4, which is consistent with a wind direction of 219º. This wind direction is about 20º less than that measured at the PUMA meteorological stations.

The advection velocity is smaller in the experiment than in the model suggesting that at the 1 km scale a more refined 'neighbourhood scale' may be required for modelling transient problems. The analysis of measurements from the July 1999 experiment performed at a scale of 3.5 km and the August 2000 experiment at a scale of 1 km showed that the concentration time history is asymmetrical, the rise occurring much more rapidly than the decrease. The decrease occurred with a time constant of about 7 minutes for the July 1999 experiment and about 4 minutes for the August 2000 experiment.

The good agreement between the measurements and the predictions of a dispersion model (ADMS 3) for the July 1999 experiment suggested that models based on gross flow characteristics such as the roughness length are likely to be valid for the 3.5 km scale and larger (i.e. the neighbourhood scale as defined in Section 2). This is probably due to the fact that the concentration plume at the scale of the July 1999 experiment is very deep compared with the building heights. In this case, a very detailed description of the flow and dispersion through and above the buildings may not be necessary; the concentration plume is not likely to be affected when it is very deep compared with the height of the buildings.

The second and third experiments were performed with a source to receptor distance of about 1 km. The results from the second experiment were not conclusive. The third experiment also showed a strongly asymmetrical concentration time history. Comparison of measurements with ADMS 3 model results showed a good qualitative agreement. However, the observed advection speed was less than predicted. It would appear that at a source-receptor distance of 1 km or less a more refined 'neighbourhood scale' model may be required for modelling transient problems.

An archived data set is available (Cooke et al., 2000) for these field experiments.

5.2.3 Salt Lake City (2000): Allwine et al. (2002)

The first paper on this experiment contains the following abstract.

A unique atmospheric tracer and meteorological study shows the complicated patterns of contaminant transport around buildings, through an urban area, and into the surrounding region.

This major field project was funded by the US Department of Energy's Chemical and Biological National Security Program and has the short title of URBAN 2000. The URBAN 2000 study was embedded within DOE's Vertical Transport and Mixing (VTMX) study conducted simultaneously in the greater Salt Lake Valley. The comprehensive meteorological and tracer field campaign was conducted during October 2000 with seven nightlong intensive operation periods (IOP's). Instrumentation was deployed over three experimental domains: urban, downtown and building.

The tracer releases consisted of:

- Eighteen 1-hour sulphur hexafluoride (SF_6) releases from one downtown SLC location
- Twelve 6-hour perfluorocarbon (PFT) releases from two downtown SLC locations
- Twelve 8-hour PFT releases from two locations around the greater SLC area.

Only data from the SF_6 releases are available at the time of writing so only these are discussed here. IOP's 1,3 and 6 did not involve tracer releases. IOP's 2,4,5 and 7 were releases from a line source 30m long at a rate of 1g/s. The releases were over hourly periods from 0000 to 0100, 0200 to 0300 and 0400 to 0500. IOP 10 was similar but the release was from a point source. IOP 9 was a point source with a release rate of 2g/s over periods 2100-2200, 2300-0000 and 0100-0200 in order to coincide with the expected higher winds in downtown SLC.

The integration times of tracer samples varied from 5 minutes for SF_6 samplers near the release to 4 hours for PFT samplers in the very far field.

Preliminary tracer results presented in Allwine et al. (2002) were based on 30-minute averaged data for IOP. These are shown in Figure 14 from Franzese (personal communication). The essential features to note are:

- The very large plume width at the source (from this point source experiment). The source position is at 4512.7km Northing and 425.2km Easting. Allwine et al. state that

  throughout the 1-hour release period the tracer took different pathways along roadways in the first two to three blocks from the release location.

  The large lateral spread may be 'geometric' in character rather than 'diffusion like' (consistent with the analysis in Section 4.2.2).
- The occurrence of upwind plume movement (which suggests high turbulence levels and low wind speeds)
- The very long residence time of the pollutant after the source has been switched off, in excess of 30 minutes.

The six tracer release experiments fell into two general meteorological categories, namely light winds (9 and 10) and very light winds (2, 4, 5, 7). These experiments have been analysed by Hanna et al. (2003), who found:

- The point source (IOP 9) was not much different to the 30m line source (IOP 10).
- All the very light wind experiments gave very complicated concentration patterns (see IOP 7 in Figure14(c)).
- σ_y values were calculated at various arc positions in IOP 10. These emphasise the large value of the lateral plume extent close to the source and the tendency towards a '+1' slope in the far field. The plume widths are significantly larger than those provided by Briggs' (1973) urban curves.

One further useful observation for IOP 10 made in Allwine et al. (2002) from ground level and building top measurements was that the plume was well-mixed over a 60m height around 600m downwind from the source.

5.2.4 Los Angeles (2001): Rappolt (2001)

These experiments were sponsored by the US Marine Corps and took place in August and September 2001. Eleven trials produced satisfactory experiments. Short-term (5-minute) SF_6 releases were made from point sources near street level in the downtown area. Fifty monitors were placed within 1km. of the release and 2.5-minute averages were provided over a 30-minute period during each trial. Release rates were in the range 0.75-5.0 g/s.

A summary of the data produced from these trials is available in Hanna et al. (2003). It is unclear what other analysis or interpretation of this data has been made.

5.2.5 Barrio Logan : Venkatram et al. (2002)

The barrio Logan area of San Diego is mainly single storey residences located downwind of an industrial belt. Tracer experiments were carried out during August 21-31, 2001. SF_6 was released from a single source 5m above the ground at a rate of 4.44 g/s. 50 sampling sites were located along arcs at 100, 500, 1000 and 2000m from the source. Little specific information on the experimental details appears to be available. The analysis sought to relate the lateral plume growth to the on-site measured turbulence and to compare the maximum measured concentrations with a simple model.

5.2.6 London: DAPPLE programme (2003)

This study, Dispersion of Air Pollutants and Penetration into the Local Environment (DAPPLE), is funded by the UK Engineering and Physical Sciences Research Council (EPSRC) at £1.5M over 3 years. It is being undertaken by a consortium of six UK universities. The project has two elements: urban air quality arising from traffic; and a series of tracer releases in an urban environment over a scales of 1000m or less. Field studies, wind tunnels studies, computational fluid dynamics and simpler modelling procedures are included in the study.

The first campaign was in June 2003 and took place near Marylebone Road and Gloucester Place in Central London. Only one tracer release experiment was undertaken in this first campaign. SF_6 and perfluorocarbons were released over a 15-minute period and ten sampling stations measured ten 3-minute averaged concentrations. By staggering the tracers by 1.5 minutes it was possible to artificially reduce the sampling time. Experimental design was aided by simple analysis and extensive wind tunnel work at the University of Surrey.

Preliminary analysis of the field experiment indicated results that were anticipated. Of particular interest was evidence of large variations in the 3-minute averaged data over a 30-minute period. This appeared to be due to large changes in the concentration pattern as a result of changes in wind direction and speed. In other words, the near-field pattern may be quite sensitive to small changes in the wind velocity.

5.2.7 Oklahoma City: (2003)

This Joint Urban 2003 (JUT) meteorological and tracer release study in Oklahoma City is to take place from June 28 to July 31, 2003. It is funded by the US Department of Defense: Defense Threat Reduction Agency and the US Department of Homeland Security. It is a multi-million dollar study with most of the major US research groups involved. Ten intensive operational periods (IOP's) are planned for the 34-day period. The general approach is not dissimilar to that for the Salt Lake City experiment though more convectively unstable conditions are expected. Indoor air infiltration studies are included within the project. Experimental design was aided by simple analysis, computational fluid dynamics and extensive wind tunnel work at the University of Hamburg, Germany. There is a web site that is openly accessible.

5.3 Field experiments with artificial structures

In the following, the parameters β_p and β_f refer to the plan and frontal area density, respectively.

5.3.1 Kit Fox experiments, Nevada

The Kit Fox field experiments (Hanna and Chang, 2001) showed clear evidence of substantial reductions in ground-level concentrations from a ground-level source for conditions in which the plume centroid was comparable to or smaller than the obstacle heights. The reductions were a factor of approximately 3 as z_0 changed from 0.002m to 0.02m and were a further factor of approximately 3 as z_0 changed from 0.02m to 0.2m. These experiments used a dense gas, carbon dioxide, as the pollutant; however, the preceding statement is based only on experiments at the highest wind velocities when the dense gas effects would be minimal.

5.3.2 Cardington UK (1993)

These experiments (Davidson et al., 1995) were based on an array of approximately cubical structures 2.2m by 2.45m by 2.3m. 39 obstacles were placed in two configurations, namely a staggered configuration and an aligned configuration. The spacing between the obstacles was twice the relevant building dimension. These correspond to β_p and β_f of 0.11. In the staggered configuration the flow is deflected onto neighbouring obstacles whereas in the aligned configuration channels were created through which the flow can pass.

With the small number of obstacles the experiment must be seen as an isolated region of obstacles rather than a section of a larger uniform area. Thus the obstacle array leads to flow deflection over, and possibly around, the obstacle array. This deflection, though interesting in itself, leads to considerable difficulty in interpreting and extrapolating the results. The experiments all had sources at half the obstacle height and upstream of the array. Thus the growth of the plume both laterally and vertically is a result of a kinematic distortion as well as turbulent diffusion.

The significant difference between the aligned and staggered arrays is very evident. For the staggered array case the obstacles also clearly produce a wider plume than in their absence when only the background atmospheric turbulence is present.

The paper does not provide a clear database of the measurements and it is uncertain where the raw data now reside.

The results of this experimental programme are often quoted to support the argument that the ground level concentrations are unaffected by the obstacles, that is, the ground level concentration is the same with and without the obstacles. This is quite possible if the increased plume dimensions are balanced by a reduction in the advection velocity. However the unusual nature of this experiment, particularly the upwind source, suggests caution when applying this observation to other scenarios.

5.3.3 UMIST Environmental Technology Centre Dispersion Test Site (Alcar): Macdonald (1997)

These field experiments used cubes of nominal side 1.125m. Approximately 100 cubes were used with area packing such that β_p and β_f were 0.16. The main parameter varied was the ratio of width w to height H. Ratios of w/H=1, 2, 4 and 8 were used with arrays of between 7 and 8 rows.

All experiments appear to be with the source a distance H upstream of the obstacle array and either in front of an obstacle or in front of an opening. For reasons discussed earlier this situation, though of interest, does confuse the kinematic distortion of the plume with actual turbulent mixing and dilution. As stated by Macdonald et al. (1998a)

The effective lifting of the centre of mass of the plume…is caused by a combination of the deflection of the mean streamlines over the array and the intense vertical mixing in the wakes within the obstacle canopy.

Additionally the dispersion is much influenced by the impact region, defined by the authors as the first two rows. The dispersion from releases within the urban canopy may have quite different behaviour.

The report is concerned with comparing the field experiments with the wind tunnel simulations described in Section 5.5.2. It is concluded that the field experiments were consistent with the findings of the wind tunnel experiments and that:

a Area density and array layout (in line or staggered) had relatively weak influence on plume spread.
b Variability in obstacle heights did not have much influence other than a slight increase in vertical plume spread.
c Wind direction did not have much effect on dispersion in arrays of individual cubes, but the effect was quite pronounced on arrays of obstacles (w/H>1), where there was usually a large lateral shift of the plume centreline.

d Joining the cubes into wider obstacles (w/H>1) greatly enhanced the lateral spread.

e Arrays with the same effective z_0 but consisting of taller, thinner elements resulted in enhanced vertical plume spread.

f Velocity profiles were strongly influenced by obstacle area density and as a result strong variations in concentration could occur even with the same plume spread parameters, due to the inverse relationship between concentration and mean advection velocity.

The difference between the field and model experiments appeared to be the result of the amplification of the effect of wind meander due to lateral deflection of the plumes by the arrays.

5.3.4 Dugway Experiment (2001): Venkatram et al. (2002)

These experiments, performed at Dugway Proving Ground, Utah, from 12 July to 26 July 2001, used an urban canopy simulation with a 9 by 5 array of barrels with height 0.91m and diameter 0.57m and a β_f of 0.16. Tracer was released continuously both upstream and within the array. Mean and turbulent velocities were determined with sonic anemometers at 3 locations.

The lateral plume dimension was nearly doubled by the presence of the obstacles while the concentrations near ground level were reduced typically by a factor of four. However not enough basic data are provided in this reference to allow effective use to be made of the experiment. The reference is more concerned with a comparison of data with a specific model.

5.4 Laboratory experiments with modelled realistic cities

5.4.1 Nantes: Kastner-Klein et al. (2000)

This was a wind tunnel study of central Nantes, France. It is particularly important as use was made of advanced laser-doppler techniques in order to provide mean flow and turbulence characteristics within the urban canopy and street canyons. Rather surprisingly it was observed that the turbulence levels were relatively uniform throughout the urban canopy and scaled roughly on the friction velocity. The city had relatively large (0.5-0.7) values of the β parameters.

5.5 Laboratory experiments with modelled artificial structures

5.5.1 Davidson et al. (1996)

Experiments were undertaken in wind tunnels at the Department of Applied Mathematics and Theoretical Physics, University of Cambridge, and at the US Environmental Protection Agency, Research Triangle Park, NC. In the former the wind tunnel was not able to simulate an atmospheric boundary layer and thus the results are less useful and will not be considered further. The US EPA tunnel

has a large simulated atmospheric boundary layer. It is difficult to extract dispersion results that might be generally applicable from this study as the results were with a source upstream of the obstacle array. However the deceleration of the flow as it enters the array is well evidenced.

5.5.2 Simulated Urban Array Study: Macdonald et al. (1998a, 1998b)

This study was a wind tunnel model of a field experiment undertaken at Porton Down by CBDS of DERA. The model was at a 1:10 scale. The results were presented at a conference and the accompanying description is limited. The full-scale experiment was based around 1.12m cubes. These were arranged singly, in pairs, in groups of 4, in groups of 8 and also as a series of two-dimensional obstacles. The obstacles (groups of cubes) were arranged as in-line and staggered arrays. Up to 100 cubes were laid out in any one experiment. For the individual cube experiments the ratio β_p and β_f ranged through 0.049, 0.11, 0.16, 0.20, 0.33, 0.44, 0.69, 0.91. Macdonald et al. (1998a) is mainly concerned with a comparison between wind tunnel and field, whereas Macdonald et al. (1998b) provides more data, albeit incomplete, of the wind tunnel model.

Additional experiments were undertaken with square-based obstacles with varying height as an attempt to mimic more realistic flow situations.

The source was located on the ground on the centreline of the array, either upwind of the array or inside the array (usually in the wake of an obstacle).

It appears that the data plotted in the paper are all for an upwind source though this is not made explicit.

The results were presented in a slightly unusual way in that ‘baseline curves’ were determined by averaging all the experiments undertaken using basic square and staggered arrays of cubes. Other results were presented in terms of deviation away from this baseline curve.

There was surprisingly little effect of the obstacle area density on the ground level concentrations. Area densities of 0.0 and 0.069, 0.091 gave larger (about 50%) concentrations than the baseline curves while all the intermediate area densities gave ground level concentrations smaller (about 30%) than the baseline curves.

If the source was placed within an along-wind street canyon most of the concentration data showed no variation from the baseline curves. Two (out of 15) data points show concentration amplifications by factors of 3 and 5.

The effects of wind direction, obstacle width and obstacle height variability are also described.

Although not relevant for the dispersion experiments, all the related velocity measurements suffered from a significant error in the determination of the friction velocity, a result of the limited fetch of the roughness array.

5.5.3 Macdonald et al. (2001)

These were dispersion experiments using simple arrays of cubes in a water flume. Obstacle packing densities β_p and β_f of 0.0625, 0.16 and 0.44 were used. Additional experiments with two-dimensional billboards were also undertaken. These will have the same β_f but a β_p of zero. The concentrations in the obstacle arrays (compared with those in the absence of obstacles) were lower at short distances from the source. This was believed to be the result of the very rapid dilution of the plume after initial interaction with the obstacle wakes within the array. However at distances downstream greater than 10H, the concentration in some of the arrays was slightly higher than in the unobstructed plume. Generally the results are difficult to interpret.

6 CONCLUSIONS AND RECOMMENDATIONS

Using previous research on dispersion in complex flows and studies of urban planning in relation to dispersion, this review has identified how dispersion from localised 'accidental' sources in urban areas has different characteristics over varying distances from the source, which correspond to the three sub-regions of the flow fields – building/street (B/S) scale, neighbourhood (N) scale and meso-urban (M) scale – and in different types of building/street dimensions and layout described in Tables 1-5. These characteristics are useful for developing and testing/critiquing models and for providing broad estimates of the dispersion parameters and flow field.

In considering fully computational models based on grid box calculations (using statistical moments or stochastic simulations) we conclude that they can predict basic statistical features of the flow and dispersion of an appropriately decreasing spatial resolution away from the source. This requires use of a 'nesting' approach with fine detail computations (Δx ~ 1m) near the source on the building/street scale, out to 1km from the source, and then coarser resolution (Δx ~ 10m, Δz ~ 1m (increasing vertically)) on the neighbourhood and meso scales. Different representations for the physical processes in the numerical models are required over these different scales.

Such models are useful for research, for very specific studies (e.g. of critical situations) and for validation of fast approximate models. Even with the largest computers they are not (yet?) practical for operational or even multi-scenario studies, since they take several hours to run. However, these can be speeded up by approximating the equations and the representation of the buildings and using coarser resolution for discretising the equations. Initial attempts look promising. Reasons have been given here as to why such methods might be justifiable because of the physical processes involved in dispersion around buildings.

We recommend that this unconventional approach to computational fluid dynamics is explored further.

For the next few years most practical calculations for real time decisions and scenario/planning studies will be conducted using fast approximate models.

Different models are needed for the three sub-regions and for all the relevant types of building/street layout. In some cases the models, such as the Porton's UDM (Hall et al., 1996), can be applied over the B/S and N scales, but they do not satisfactorily account for the inner city canyon flow and dispersion to account for the effective displacement of plumes/clouds along canyons. Some FAM methods are already available and widely used for industrial and traffic emissions in urban areas, but these are not suitable for accidental emissions on all three sub-regions needed for practical predictions. In particular, the models for dispersion of traffic emissions along streets in urban areas (as in ADMS-Urban (Carruthers et al., 2000); Berkowicz et al., 1997; SIRANE (Soulhac et al., 2001)) need to be extended to allow for localised, short-time releases and for elevated releases within or above the canyons. Experimental data, reviewed in Section 5, is available for testing these required modifications. Suggestions have been made here about how such modifications might be introduced and how they might be matched to dispersion formulae over the larger N and M scale sub-regions.

Although the UDM code is not in principle valid for these canyon flows, in practice it is being applied there by suitable ad hoc modifications, for example Griffiths et al. (2002). These modifications should be compared with other models specially designed for canyon flow and dispersion.

In reviewing FAM for the flow and dispersion over the N scale we have noted that there are different approaches depending on whether a 'discrete' approach is used, accounting at some level of approximation for up to thousands of buildings, or a 'continuum' approach based on representing the average effects of buildings in terms of their resistance and on the special lateral, streamwise and vertical dispersion effects of 'topological' streamwise splitting, blocking and wake mixing. The magnitude of the mechanism, which depends on the building/street layout, has been estimated in this report as the basis of limited research and experimental testing. But the methodology proposed of considering average plume/cloud dispersion in separate layers – within and above the canopy – including the transport processes at the interface between these layers is quite general although it has still not been well tested. (Recent research may be applicable that demonstrates general relations between the average velocity and streamwise ('blocking') dispersion of particles moving through a group of obstacles or buildings…the overall shape of the group (elongated, circular, etc.) and the 'layout' of the obstacles within the group (Eames et al., 2003).) This may help with interpreting experimental data on the movement of clouds through urban areas (see Section 5.2).

Note that FCM methods have been developed (e.g. using CFD methods with statistical turbulence modelling) for the 'continuum' as well as the 'discrete' approach (with wind tunnel validation studies, e.g. Coceal and Belcher, 2003). In general it is much faster to use the former approach (even if the 'discrete' computations are speeded up, as described earlier).

Applications of dispersion models over the N scale depends on the building/street layout. For suburban areas where the building height H is very small (~1/100) compared to the boundary layer depth, as the plume height σ_z rises to the top of the boundary layer most of the dispersion in the N sub-region occurs where σ_z is

large compared with H and therefore the processes within the canopy are of most importance. This is why (as Section 5 demonstrates) FAM based on simple Gaussian plume profiles are satisfactory in these types of N sub-regions provided he initial (generally asymmetric) spreading by street canyon effects is allowed for on the B/S scale. The dilution of the cloud/plume over the whole region L_N is a factor of $(100)^2$. This also means that the concentration in the M region is very weak indeed.

By contrast in large urban city centres where H ~ h/5 (for neutral conditions), over the horizontal scale L_{BS} of the building/street scale (~10H), as defined by dispersion out of a canyon, the vertical transport of the contaminant above the canyon has already reached one third of the depth of the boundary layer (i.e. where σ_z ~ (h/3 + H). This is why for the N region in city centres the dispersion processes within the canyon are much more important than for the suburban areas, as the US and French field experiments reported in Section 5 and by Soulhac (2000) confirmed.

On the M scale some limitations of operational meso-scale meteorological models needed for the FCM approach have been noted. These models are only worth using where they can reliably predict the critical meso-scale phenomena that are likely to occur on this scale. At present they appear to be satisfactory when there are large-scale pressure gradients 'driving' the wind (provided that the resolution is as small as 1-2km). But for thermally-driven flows on slopes in or near urban areas these operational models are not sufficiently accurate to predict (even within a few hours) the timing and strength of these up/down-slope winds. If there is a network of measuring stations these winds can be determined experimentally for use in real time or scenario studies. Note that very detailed meso-scale research models (e.g. RAMS of Pielke, 1984) have still not been shown to predict these complex thermally-driven flows. FAM methods have been developed for particular aspects of these meso-scale flows, e.g. synoptically-driven stratified winds over varying roughness (as in FLOWSTAR or the 3DVOM (developed at Leeds – see http://www.uwern.ac.uk/uwern/orog_models.html), or, in neutral winds, in RIMPUFF, WASP). But further R&D is needed, extending this approach to allow for thermally-driven flows and more complex boundary layer structure over urban areas with significant thermal fluxes. Coriolis effects are also significant. On the M scale, as on shorter scales, some FAM methods simply predict dispersion without first calculating the flow field (e.g. AERMOD). Others (as in ADMS combined with FLOWSTAR) first calculate the flow field and then compute the dispersion. As the flow field modelling improves. The latter approach is more likely to lead to improved dispersion models than the former approach, which would have to introduce more ad hoc corrections to dispersion to allow for more complex flow field effects.

In this review we have mainly focused on near-neutral conditions (except at the M scale) because mostly in city centres the air flow is neutral or slightly unstable with strong turbulence. However, in the outer suburbs and on the M scale processes at the top of the boundary layer and surrounding the urban area stratifications effects are significant. The studies of Rotach (1995) have shown that turbulence structure above the canyon varies with stability broadly as it does over level ground when expressed in terms of scalings based on the Monin-

Obukhov length L_{MO} and near-surface fluxes. Although, as Zilitinkevich et al. (1998) have pointed out, there are limitations to this approach when the building height H is of the order of L_{MO}, it provides a more systematic basis for including stratification effects than using the less general Pasquill-Gifford categories. This is particularly necessary for elevated sources when the P-G approach underestimates the effects of convective and stable conditions (Hunt et al., 1991a). Since simple models and meso-scale models are now being developed for the surface heat flux and surface temperature in urban areas, tested against data (S.E. Belcher, unpublished; Owinoh et al., 2003), the M-O approach becomes even more relevant for modelling and interpreting dispersion.

Our last set of conclusions/recommendations concerns the applications of these models to help improve the security and response systems to minimise risks associated with 'accidental' releases of contaminant in urban areas.

a More data on wind direction in urban locations is needed both for real-time and scenario predictions. Flows along street canyons are quite sensitive to the wind direction and the street geometry. Data can be used to test the flow field models and as input to flow/field dispersion predictions. Many heating/ventilation systems on buildings have anemometers; perhaps these can be used. At the very least, the data might come from video surveillance cameras following an accident when dust and smoke are released. This is particularly necessary in cities located in very complex terrain (e.g., in the UK, Bath, Bristol, Sheffield, Edinburgh) where wind directions can vary greatly across the urban areas, especially in stable conditions.

b Systematic methods need to be introduced using data and models to estimate the location and strength of the source of an accident in the event that its only effect is to cause casualties over an area. Sources may be located in subways or in underground systems or in/on buildings. Using concentration data (in some approximate form) to infer the location of a source requires the 'inverse' use of these models. This is a standard mathematical approach but needs to be developed for this application.

c FAM can be used in real time using real-time data to predict how a cloud or plume will disperse over minutes and hours following an 'accidental' release. We conclude that such models probably need to be programmed for the particular types of urban area and complex terrain involved, as shown in Tables 1-5. We are not convinced that there is any current method that is sufficiently comprehensive for all relevant situations. FCM methods should be used to validate and improve FAM in particular cases, e.g. those of greatest sensitivity or security risk. Desk-based/physical trials are needed for relevant urban areas to test the application of these systems. Wind tunnel studies are also useful for testing these methods (Soulhac, 2000).

7 ACKNOWLEDGEMENTS

We are grateful to Dr. Roger Kingdon and colleagues at DSTL who, together with colleagues elsewhere, provided helpful input during the compilation of this review. We are also grateful to the reviewers and in particular Dr David Hall of Envirobods for providing many useful comments on a draft of this report.

8 REFERENCES

Adolphe, L. (2001) A simplified model of urban morphology: application to an analysis of the environmental performance of cities. Environment and Planning B: Planning and Design **28**, 183-200.

Allwine, K.J., Shinn, J.H., Streit, G.E., Clawson, K.L. and Brown, M. (2002) Overview of Urban 2000: a multiscale field study of dispersion through an urban environment. Bull. Am. Meteorol. Soc. **83**, 521-536.

Anthes, R.A. and Warner, T.T. (1978) Development of hydrodynamic models suitable for air pollution and other mesometeorological studies. Mon. Wea. Rev. **106**, 1045-1078.

Astrup, P.N., Jensen, N.O. and Mikkelsen, T. (1999) Surface roughness model for LINCOM. Risø National Laboratory, Denmark.

Bartzis, J.G., Venetsanos, A., Varvayani, M., Catsaros, N. and Megaritou, A. (1991) ADREA-I: a three-dimensional transient transport code for complex terrain and other applications. Nuclear Technology **94**, 135-148.

Belcher, S.E., Jerram, N. and Hunt, J.C.R. (2003) Adjustment of a turbulent boundary layer to a canopy of roughness elements. J. Fluid Mech. **488**, 369-398.

Belcher, S.E., Xu, D.P. and Hunt, J.C.R. (1990) The response of a turbulent boundary layer to arbitrarily distributed roughness change. Q. J. R. Met. Soc. **116**, 611-635.

Berkowicz, R., Hertel, O., Sørensen, N.N. and Michelsen, J.A. (1997) Modelling Air Pollution from Traffic in Urban Areas. In Proceedings from IMA meeting on Flow and Dispersion Through Obstacles, Cambridge, England, 28-30 March, 1994, eds. R.J. Perkins and S.E. Belcher, pp. 121-142.

Blumen, W. (Ed.) (1990) Atmospheric processes in complex terrain. American Met. Soc.

Boris, J.P., Grinstein, F.F., Oran, E.S. and Kolbe, R.L. (1992) New insights into large eddy simulation. Fluid Dynamics Research **10**, 199-228.

Bottema, M. (1993) Wind climate and urban geometry. Ph.D. thesis, Eindhoven University of Technology, The Netherlands.

Briggs, G.A. (1973) Diffusion estimation for small emissions. Paper No. 79 Atmospheric Turbulence and Diffusion Laboratory, NOAA, Oak Ridge, TN.

Britter, R.E. and Hanna, S.R. (2003) Flow and dispersion in urban areas. Ann. Rev. Fluid Mechanics **35**, 469-496.

Britter, R.E. and Hunt, J.C.R. (1979) Velocity measurements and order-of-magnitude estimates of the flow between two buildings in a simulated atmospheric boundary layer. J. Ind. Aero. **4**, 165-182.

Britter, R.E., Caton, F., Di Sabatino, S., Cooke, K.M., Simmonds, P.G. and Nickless, G. (2000) Dispersion of a passive tracer within and above an urban canopy. In Proceedings of the Third Symposium on the Urban Environment, American Meteorological Society, pp. 30-31.

Brook, D.R., Beck, N.V., Clem, C.M., Strickland, D.C., Griffiths, I.H., Hall, D.J., Kingdon, R.D. and Hargrave, J.M. (2002) Validation of the Urban Dispersion Model (UDM). In Proceedings of 8th International Conference on Harmonisation within Atmospheric Dispersion Modelling for Regulatory Purposes, Sofia, Bulgaria, 14-17 October 2002, pp. 8-12.

Brown, M.J. and Williams, M.D. (1998) An Urban Canopy Parameterization for Mesoscale Meteorological Models. Los Alamos National Laboratory, Report LA-UR-98-3831.

Capon, R. (2002) Modelling low level winds with the Met Office New Dynamics model. Internal Report No. 133, NWP Scientific Paper No. 66, Met. Office, JCMM, Reading University, Reading, UK. To appear in Meteorological Applications, 2003.

Carlotti, P. (2002) Two point properties of atmospheric turbulence very close to the ground: comparison of a high resolution LES with theoretical models. Boundary Layer Meteor. **104**, 381-410.

Carlotti, P. and Hunt, J.C.R. (2000) Spectra of turbulence in boundary layers near the ground. In Proceedings of 8th European Turbulence Conference, Barcelona, pp. 307-310. Kluwer. Submitted to Journal of Flow Turbulence and Combustion.

Carrilho da Graca, G. and Linden, P.F. (2002) Simplified modeling of cross-ventilation airflow. ASHRAE Trans. **109**, 1-14.

Carruthers, D.J., Hunt, J.C.R. and Weng, W.-S. (1988) A computational model of stratified turbulent airflow over hills – FLOWSTAR I. In Computer Techniques in Environmental Studies (ed. P. Zanetti), pp. 481-492. Springer-Verlag.

Carruthers, D.J., Holroyd, R.J., Hunt, J.C.R., Weng, W.-S., Robins, A.G., Apsley, D.D., Thomson, D.J. and Smith, F.B. (1994) UK-ADMS: A new approach to modelling dispersion in the Earth's atmospheric boundary layer. Journal of Wind Engineering and Industrial Aerodynamics **52**, 139-153.

Carruthers, D.J., Edmunds, H.A., Lester, A.E., McHugh, C.A. and Singles, R.J. (2000) Use and Validation of ADMS-Urban in Contrasting Urban and Industrial Locations. Int. J. Environment and Pollution **14**, 1-6.

CERC (2000) ADMS 3 User Guide. Cambridge Environmental Research Consultants Ltd.

Chatwin, P.C. (1968) The dispersion of a puff of passive contaminant in the constant stress region. Q. J. R. Meteorol. Soc. 94, 350-360.

Cimorelli, A.J., Perry, S.G., Venkatram, A., Weil, J.C., Paine, R.J. Wilson, R.B., Lee, R.F. and Peters, W.D. (1998) AERMOD: Description of Model Formulation. (12/15/98 Draft Document) Prepared for Environmental Protection Agency, Research Triangle Park, NC. (Docket No. A-99-05; II-A-1). 113pp.

Clarke, R.H. (1979) A model for short and medium range dispersion of radionuclides released to the atmosphere. National Radiological Protection Board report NRPB-R91.

Coceal, O. and Belcher, S.E. (2003) A canopy model of mean winds through urban areas. Submitted to Quarterly Journal of the Royal Meteorological Society.

Cooke, K. M., Di Sabatino, S., Simmonds, P., Nickless, G., Britter, R.E. and Caton, F. (2000) Tracer and Dispersion of Gaseous Pollutants in an Urban Area. Birmingham Tracer Experiments. Technical Paper CUED/A-AERO/TR.27. Department of Engineering, Cambridge University.

Counihan, J., Hunt, J.C.R. and Jackson, P.S. (1974) Wakes behind two-dimensional surface obstacles in turbulent boundary layers. J. Fluid Mech. **64**, 529-563.

Cullen, M.J.P. (1993) The unified forecast/climate model. The Meteorological Magazine **122**, 81-94.

Cuxart, J., Bougeault, P. and Redelsberger, J.L. (2000) A multi-scale turbulence scheme for LES and mesoscale modelling. Q. J. R. Meteorol. Soc. **126**, 1-30.

Davidson, M.J., Mylne, K.R., Jones, C.D., Phillips, J.C., Perkins, R.J., Fung, J.C.H. and Hunt, J.C.R. (1995) Plume dispersion through large groups of obstacles – a field investigation. Atmospheric Environment **29**, 3245-3256.

Davidson, M.J., Snyder, W.H., Lawson, R.E., Hunt, J.C.R. (1996) Plume dispersion from point sources upwind of groups of obstacles – wind tunnel simulations. Atmospheric Environment **30**, 3715-3725.

Eames, I. and Hunt, J.C.R. (2003) Complex flow problems. ERCOFTAC Bulletin No. 56 (Editors).

Eames, I., Hunt, J.C.R. and Belcher, S.E. (2003) Lagrangian and Eulerian properties of steady flows through groups of obstacles. Submitted to Journal of Fluid Mechanics. [Summary version in ERCOFTAC Bulletin No. 56.]

Fackrell, J.E. (1984) Parameters characterising dispersion in the near-wakes of buildings. J. Wind Eng. and Industrial Aero. **16**, 97-118.

Finnigan, J. (2000) Turbulence in plant canopies. Ann. Rev. Fluid Mech. **32**, 519-571.

Fisher, B.E.A. (2003) Meteorology factors influencing urban air pollution. Presented at 4th International Conference on Urban Air Quality: Measurement, Modelling and Management, Charles University, Prague, Czech Republic, 25-27 March 2003.

Garratt, J.R. (1993) The Atmospheric Boundary Layer. Cambridge University Press. 334pp.

Griffiths, I.H., Brook, D.R., Hall, D.J., Berry, A., Kingdon, R.D., Clawson, K.L., Biltoft, C., Hargrave, J.M., Clem, C.M., Strickland, D.C.H. and Spanton, A.M. (2002) Urban Dispersion Model (UDM) validation. In Proceedings of the American Meteorological Society Fourth Symposium on the Urban Environment, Davis, California, May 2002.

Grimmond, C.S.B. and Oke, T.R. (1999) Aerodynamic properties of urban areas derived from analysis of surface form. J. Appl. Meteor. **38**, 1262-1292.

Hall, D.J. and Cowan, I.R. (1998) Modelling of atmospheric dispersion near buildings. NAFEMS International Journal of CFD Case Studies, April 1998, pp. 7-18.

Hall, D.J., Macdonald, R., Walker, S. and Spanton, A.M. (1996) Measurements of dispersion within simulated urban arrays – a small scale wind tunnel study. Building Research Establishment, BRE Client Report CR 178/96, November 1996.

Hall, D.J., Walker, S. and Spanton, A.M. (1999) Dispersion from courtyards and other enclosed spaces. Atmospheric Environment **33**, 1187-1203.

Hall, D.J., Spanton, A.M., Griffiths, I.H., Hargrave, M., Walker, S. and John, C. (2001) The UDM: a puff model for estimating dispersion in urban areas. In Proceedings of 7th International Conference on Harmonisation within Atmospheric Dispersion Modelling for Regulatory Purposes, Belgirate, Italy, pp. 256-260.

Hanna, S.R. and Britter, R.E. (2002) Wind flow and vapor cloud dispersion at industrial and urban sites. Center for Chemical Process Safety, AIChE, 3 Park Ave., New York, NY 10016-5901. 208 pp. plus CD-ROM.

Hanna, S.R. and Chang, J.C. (2001) Use of the Kit Fox field data to analyze dense gas dispersion modeling issues, Atmospheric Environment **35**, 2231-2242.

Hanna, S.R., Briggs, G.A. and Hosker, R.P. (1982) Handbook on atmospheric diffusion. DOE/TIC-11223 (DE82-002045). NTIS/USDOC, Springfield, VA. 102 pp.

Hanna, S., Britter, R. and Franzese, P. (2002) Simple screening models for urban dispersion. In Proceedings of 8th International Conference on Harmonisation within Atmospheric Dispersion Modelling for Regulatory Purposes, Sofia, Bulgaria, 14-17 October 2002, pp. 269-273.

Hanna, S.R., Britter, R.E. and Franzese, P. (2003) A baseline urban dispersion model evaluated with Salt Lake City and Los Angeles data. Submitted to Atmospheric Environment.

Hirsch, C. (2003) The QNET-CFD Network Newsletter, Volume 2, No. 1, April 2003 (Ed.).

Hodur, R. (1997) The Naval Research Laboratory's Coupled Ocean/Atmosphere Mesoscale Prediction System (COAMPS). Mo. Wea. Rev. **125**, 1414-1430.

Högström, U. and Smedman, A. (1984) The wind regime in coastal areas with special reference to results obtained from the Swedish Wind Energy Program. Boundary-Layer Meteorol. **33**, 351-373.

Högström, U., Hunt, J.C.R. and Smedman, A.-S. (2002) Theory and measurements for turbulence spectra and variances in the near neutral surface layer. Boundary-Layer Meteorol. **103**, 101-124.

Hort, M., Devenish, B. and Thomson, D. (2002) Building affected dispersion: development and initial performance of a new Lagrangian particle model. In Proceedings of 15th AMS Symposium on Boundary Layers and Turbulence.

Hosstan et al. (2002)

Hunt, A. and Castro, I.P. (1981) Scalar dispersion in model-building wakes. J. Wind Engineering and Industrial Aerodynamics **17**, 89-115.

Hunt, J.C.R. (1985) Turbulent diffusion from sources in complex flows. Ann. Rev. Fluid Mech. **17**, 447-485.

Hunt, J.C.R. (1996) Atmospheric diffusion from a steady source in a turbulent airflow at low mean wind speeds. Note to UK Atmospheric Dispersion Modelling Working Group (National Radiological Protection Board), Report R292, pp. 19-22.

Hunt, J.C.R. (1999) Environmental forecasting and modelling turbulence: their 'deterministic' and 'statistical' foundations and future prospects. In Determinism and Turbulence (ed. M. Lesieur). Also to appear in Physica D **133**, 270-295 (Proceedings of Los Alamos Conference on Predictability).

Hunt, J.C.R. and Eames, I. (2002) The disappearance of laminar and turbulent wakes in complex flows. J. Fluid Mech. **457**, 111-132.

Hunt, J.C.R. and Mulhearn, P.J. (1973) Turbulent dispersion from sources near two-dimensional obstacles. J. Fluid Mech., **61**, 245-274.

Hunt, J.C.R. and Simpson, J.E. (1982) Atmospheric boundary layers over non-homogeneous terrain. Chapter 7 of Engineering Meteorology (ed. E. Plate), pp. 269-318.

Hunt, J.C.R., Carruthers, D.J. and Kilbane-Dawe, I. (2002) Developments in regulatory air pollution modelling. NRPB report.

Hunt, J.C.R., Fernando, H.J.S. and Princevac, M. (2003) Unsteady thermally-driven flows on gentle slopes. To appear in Journal of the Atmospheric Sciences.

Hunt, J.C.R., Holroyd, R.J. and Carruthers, D.J. (1988) Preparatory studies for a complex dispersion model. CERC Report HB9/88. This report will also appear on the ADMLC web site, http://ww.admlc.org.uk.

Hunt, J.C.R., Holroyd, R.J., Carruthers, D.J., Robins, A.G., Apsley, D.D., Smith, F.B. and Thomson, D.J. (1991a) Developments in modelling air pollution for regulatory uses. In Proceedings of 18th NATO-CCMS Int. Tech. Mtg. on Air Pollution Modelling and its Applications, Vancouver, Canada. Ed. H. van Dop, Plenum, New York.

Hunt, J.C.R., Olafsson, H. and Bougeault, P. (2001) Coriolis effects on orographic and mesoscale flows. Q. J. R. Met. Soc. **127**, 601-633.

Hunt, J.C.R., Puttock, J.S. and Snyder, W.H. (1979) Turbulent diffusion from a point source in stratified and neutral flows around a three-dimensional hill. Part I. Diffusion equation analysis. Atmospheric Environment **13**, 1227-1239.

Hunt, J.C.R., Rottman, J.W. and Britter, R.E. (1985) Some physical processes involved in the dispersion of dense gases. In Proceedings of IUTAM Symposium on Atmospheric dispersion of heavy gases and small particles (eds. G. Ooms and H. Tennekes), Springer, pp. 361-395.

Hunt, J.C.R., Orr, A., Rottman, J.W. and Capon, R. (2003) Coriolis effects in mesoscale flows with sharp changes in surface conditions. Conference on shallow layer flows, Delft. Submitted to Quarterly Journal of the Royal Meteorological Society.

Hunt, J.C.R., Tampieri, F., Weng, W.-S. and Carruthers, D.J. (1991b) Air flow and turbulence over complex terrain: a colloquium and a computational workshop. J. Fluid Mech. **227**, 667-688.

Kastner-Klein, P., Rotach, M. and Fedorovich, E. (2000) Experimental study on mean flow and turbulence characteristics in an urban roughness sublayer. In Proceedings of

14th AMS Symposium on Boundary Layers and Turbulence, Aspen, CO, August 7-11, 2000.

Kim, S.-E. and Boysan, F. (1999) Application of CFD to environmental flows. Journal of Wind Engineering and Industrial Aerodynamics **81**, 145-158.

Kothari, K.M., Peterka, J.A. and Meroney, R.N. (1986) Perturbation analysis and measurements of building wakes in a stably-stratified turbulent boundary layer. Journal of Wind Engineering and Industrial Aerodynamics **25**, 49-74.

Koutsourakis, N., Vlachogiannis, D., Sfetsos, A. and Bartzis, J.G. (2003) CFD in atmospheric dispersion problems – state of the art. QNET-CFD Network Newsletter **2(1)**, 10-13.

Lawson, T.V. (1980) Wind Effects on Buildings. Volume 1: Design Applications. Applied Science Publishers Ltd.

Lawson, R.E., Jr., Snyder, W.H. and Hunt, J.C.R. (1988) Flow structure of recirculating wake flows downwind of surface-mounted obstacles. Preprint Volume 8th Symposium on Turbulence and Diffusion, April 1988, San Diego. Am. Met. Soc., Boston.

Macdonald, R.W. (1997) Measurements of Dispersion within Simulated Urban Arrays - A 1:10 Scale Field Experiment. Report to DSTL on Agreement 2044/014/CBDE. Environmental Technology Centre, UMIST, UK.

Macdonald, R., Griffiths, R.F. and Hall, D.J. (1998a) A comparison of results from scaled field and wind tunnel modelling of dispersion in arrays of obstacles. Atmospheric Environment **32**, 3845-3862.

Macdonald, R.W., Hall, D.J., Griffiths, R.F. (1998b) Scale model study of building effects on dispersion in the urban canopy at intermediate source distances. In Proceedings of 5th International Conference on Harmonisation within Atmospheric Dispersion Modelling for Regulatory Purposes, Rhodes, Greece, 18-21 March 1998.

Macdonald, R.W., Carter-Schofield, S.L. and Slawson, P.R. (2001) Measurements of mean plume dispersion in simple obstacle arrays at 1:200 scale. Presented at the 5th Annual GMU/DTRA Transport and Dispersion Modelling Workshop, 18-19 July 2001, George Mason University, Fairfax, VA.

Maryon, R.H. and Buckland, A.T. (1995) Tropospheric dispersion: the first ten days after a puff release. Q. J. R. Met. Soc. **121**, 1799-1833.

McElroy, J.L. and Pooler, F. (1968) The St. Louis dispersion study – Volume II – analysis. National Air Pollution Control Admin. Pub. No. AP-53, US DHEW Arlington, VA. 50 pp.

Meinders, E.R. and Hanjalic, K. (1999) Vortex structure and heat transfer in turbulent flow over a wall-mounted matrix of cubes. Int. J. Heat Fluid Flow **20**, 255-267.

Mellor, G.L. and Yamada, T. (1974) A hierarchy of turbulence closure models for planetary boundary layers. J. Atmos. Sci. **31**, 1791-1806.

Mestayer, P.G. and Anquetin, S. (1995) Climatology of cities. In Diffusion and transport of pollutants in atmospheric mesoscale flow fields (eds. A. Gyr and F.-S. Rys), Kluwer Academic Pubs., pp. 165-189.

Mestayer, P.G., Vachon, G. and Rosant, J.-M. (2002) The Nantes '99 data base for model validation of air quality in streets. In Proceedings of 8th International Conference on Harmonisation within Atmospheric Dispersion Modelling for Regulatory Purposes, Sofia, Bulgaria, 14-17 October 2002, pp. 297-300.

Middleton D.R. (1998) A new box model to forecast urban air quality: BOXURB. Environmental Monitoring and Assessment **52**, 315-335

Miyazaki, T. and Hunt, J.C.R. (2000) Turbulence structure around a columnar vortex: rapid distortion theory and vortex wave excitation. In Proceedings of the European Turbulence Conference (ETC-7) (ed. U. Frisch), Kluwer. Also J. Fluid Mech. **402**, 349-378.

Moulinec, C., Hunt, J.C.R. and Nieuwstadt, F. (2003) Disappearing wakes and scalar diffusion in tube bundles. Submitted to Journal of Flow Turbulence and Combustion. (See also ERCOFTAC Bulletin No. 56, pp. 5-9.)

Murakami, S. (1992) Computational Wind Engineering One: Proceedings of the 1st International Symposium on Computational Wind Engineering (Cwe92), Tokyo, Japan, August 21-23, 1992. Elsevier Science. 924pp.

Mylne, K.R. (1992) Concentration fluctuation measurements in a plume dispersing in a stable surface layer. Boundary-Layer Meteorol. **60**, 15-48.

Mylne, K.R. and Mason, P.J. (1991) Concentration measurements in a dispersing plume at a range of up to 1000m. Q. J. R. Met. Soc. **117**, 117-206.

Ohashi, Y. and Kida, H. (2002) Effects of mountains and urban areas on daytime local-circulations in the Osaka and Kyoto regions. Journal of the Meteorological Society of Japan **80**, 539-560.

Oke, T.R. (1978) Boundary layer climates. Methuen, London. 372pp.

Olesen, H.R., Løfstrøm, P., Berkowicz, R. and Jensen, A.B. (1992) An improved dispersion model for regulatory use: the OML model. In *Air Pollution Modelling and its Applications IX,* Plenum Press, New York (eds. H. van Dop and G. Kallos).

Owinoh, A., Orr, A., Hunt, J.C.R. and Clark, P. (2003) Numerical modelling of boundary layer flow over a low hill with abrupt surface heat flux change. To be submitted.

Pardyjak, E.R., Fernando, H.J.S., Hunt, J.C.R., Grachev, A.A. and Anderson, J. (2003) Evolution of nocturnal circulation in complex terrain: Phoenix Air Flow Experiment (PAFEX-1). Submitted to Boundary Layer Meteorology. (See also 'Structure of atmospheric boundary layer over the complex terrain of the Phoenix Valley' in Proceedings of 13th Conference on Boundary Layers and Turbulence, Am. Met. Soc.)

Pasquill, F. and Smith, F.R. (1983) Atmospheric Diffusion. 3rd edition. Ellis Horwood Ltd., Chichester.

Pielke, R.A. (1984) Mesoscale meteorological modelling. Academic Press.

Pope, S.B. (2000) Turbulent flows. Cambridge University Press. 806pp.

Puttock, J.S. and Hunt, J.C.R. (1979) Turbulent diffusion from sources near obstacles with separated wakes. Part I. An eddy diffusivity model. Atmospheric Environment **13**, 1-13.

Rappolt, T. (2001) Field test report: measurements of atmospheric dispersion in the Los Angeles urban environment in summer 2001. Report number 1322, prepared for STI, Bel Air, MD, by Tracer Environ. Sci. and Tech., San Marcos, CA 92071. 33 pp. plus data CD.

Riddle, A., Carruthers, D., Sharpe, A., McHugh, C. and Stocker, J. (2003) Comparisons between FLUENT and ADMS for atmospheric dispersion modelling. To appear in Atmospheric Environment.

Robins, A.G. and Apsley, D.D. (2000) Modelling of building effects in ADMS. ADMS Technical Specification, Paper P16/01N/00. See http://www.cerc.co.uk/software/pubs/ADMS3-1TechSpec/P16_01.pdf.

Rodi, W. (1997) Comparison of LES and RANS calculations of the flow around bluff bodies. J. Wind Eng. and Industrial Aero. **69-71**, 55-75.

Rotach, M.W. (1995) Profiles of turbulence statistics in and above an urban street canyon. Atmospheric Environment **29**, 1473-1486.

Roth, M. (2000) Review of atmospheric turbulence over cities. Q. J. R. Meteorol. Soc. **126**, 941-990.

Scire, J.S. Strimaitis, D.S.and Yamartino, R.J. (1999) A user's guide for CALPUFF dispersion model (Version 5). Earth Tech Inc., Concord, MA. See also http://www.src.com/calpuff/calpuff1.htm.

Soulhac, L. (2000) Modélisation de la dispersion atmosphérique à l'intérieur de la canopée urbaine. Ph.D. thesis, École Centrale de Lyon.

Soulhac, L., Weber, B. and Perkins, R.J. (1998) A practical model for dispersion in a network of streets. In Proceedings of International Conference on Air Pollution Modelling and Simulation (APMS '98), Champ-sur-Marne, France, 1998, pp. 253-262.

Soulhac, L., Mejean, P. and Perkins, R.J. (2001) Modelling vehicle-generated atmospheric pollution in a quartier of Lyon using the model SIRANE. In Proceedings of 7th International Conference on Harmonisation within Atmospheric Dispersion Modelling for Regulatory Purposes, Belgirate, Italy.

Stoesser, T., Mathey, F., Froelich, J. and Rodi, W. (2003) LES of flow over multiple tubes. ERCOFTAC Bulletin No. 56.

Theurer, W. (1995) Point sources in urban areas: modelling of neutral gas clouds with semi-empirical models. In Wind Climates in Cities, pp. 485-501. Eds. J.E. Cermak, A.G. Davenport, E.J. Plate and D.X. Viegas. Kluwer Academic Publisher, Dordrecht.

Thomson, D.J. (2000) Concentration fluctuations in ADMS 3, including fluctuations from anisotropic and multiple sources. . ADMS Technical Specification, Paper P13/07D/00. See http://www.cerc.co.uk/software/pubs/ADMS3-1TechSpec/P13_07.pdf.

Thykier-Nielsen, S., Deme, S. and Mikkelsen, T. (1999) Description of the Atmospheric Dispersion Module RIMPUFF. Report RODOS(WG2)-TN(98)-02. Risø National Laboratory. See also http://www.rodos.fzk.de/RodosHomePage/RodosHomePage/Documents/Public/Handbook/Volume3/4_2_6_RIMPUFF.pdf

Turfus, C. (1986) Diffusion from a continuous source near a surface in steady reversing shear flow. J. Fluid Mech. **172**, 183-209.

Turfus, C. (1988) Calculating mean concentrations for steady sources in recirculating wakes by a particle trajectory method. Atmospheric Environment **22**, 1271-1290.

Venkatram, A., Upadhyay, J., Heumann, J. and Klewicki, J. (2002) The development and evaluation of a dispersion model for urban areas. 4th AMS Symposium on the Urban Environment, Norfolk, VA, May 2002.

Vincent, J.H. (1977) Model experiments on the nature of air pollution transport near buildings. Atmospheric Environment **11**, 765-774.

Vosper, S.B. and Mobbs, S.D. (1996) Lee waves over the English Lake District. Q. J. R. Met. Soc. **122**, 1283-1305.

Wippermann, F. Air flow over and in broad valleys: channeling and counter-current. Beitr. Phys. Atmos. **57**, 92-105.

Zilitinkevich, S., Grachev, A. and Hunt, J.C.R. (1998) Surface frictional processes and non-local heat/mass transfer in the shear-free convective boundary layer. In Buoyant Convection in Geophysical Flows (eds. E.J. Plate and E. Fedorovich). Kluwer, Dordrecht.

9 NOTATION AND ABBREVIATIONS

b	Building breadth
b_v	Size of vehicles
C	Mean (ensemble average) concentration at a point
$\langle C \rangle$	C averaged over a given volume and time scale
$\overline{C_{Dx}}$	Average drag coefficient of buildings in canopy
d	Gap or separation distance between buildings
E_S	Energy with which source material is emitted
f	Coriolis frequency
f_B	Buoyancy frequency
F_θ	Surface heat flux
g	Gravitational acceleration
G	Gaussian concentration profiles – subscripts denote particular (e.g. multiple Gaussian) forms to allow for reflection, wakes, within and above canopy, etc.)
h	Boundary layer height
H	Building height
H_c	Canopy height
H_c'	Standard deviation of canopy height, H_c
k-ε	Kinetic energy and energy dissipation model of turbulence
K_x, K_y	Eddy diffusivity components used for dispersion calculations
l_O, l_N	Length scales of internal layers over the urban area, neighbourhood scale
$\mathcal{L}_A$	Adjustment length for mean flow to adjust as it enters the porous canopy
L_c	Distance from the source over which the concentration is to be calculated
L_M, L_N, L_{BS}	Length scales of the (sub-)regions M, N, BS
L_S	Length scale over which source material is emitted
L_{Se}	Effective source size of accidental release
l_w	Length of the wake of a building
L_x	Length scale of atmospheric turbulence near the source
L_ϕ	Distance over which a street canyon changes its direction (Table 3)
M_S	Source strength at a point
$\hat{n}$	Normalised grazing distance between centrelines of plumes/clouds and nearby buildings
$\overline{q_H}$	Flux per unit area/time at top of canyon
q_S	Source strength per unit volume
Q_S	Source strength at a point / per unit time
R_M, R_N, R_{BS}	Ratio of the length of the sub-region, L_M, L_N or L_{BS}, to the smallest scales resolved in that region
t	Time
T_S	Period of release of source cloud
u_*	Friction velocity of the turbulent velocity profile of the atmosphere
U	Mean velocity, with subscripts denoting location/physical process
U_S	Velocity with which source material is emitted
U_v	Vehicle speed in a street
U_c	Mean wind along the street canyon
V_S	Volume

w	Building length
$\mathbf{x} = (x, y, z)$	Coordinates of a point
X, Y, Z	Normalised displacements relative to the source (or mean streamline through the source)
$z_0(x, y)$	Roughness length for wind profile
z_d	Displacement height for logarithmic wind profile
$z_S(x, y)$	Surface elevation of the ground
α	Factor for weighting different components in double plume/cloud structure (e.g. centreline plume and wake)
β	'Porosity' of an urban canopy [$\beta \sim bw/d^2$]
β_v	Factor for σ_w dependent on traffic
$\gamma_l, \gamma_c, \gamma_z, \gamma_p$	Functions for modifying Gaussian profiles, G
$\Delta\sigma_x, \Delta\sigma_y$	Increase in cloud/plume dimensions near a building
Δt	Time difference
θ	Mean temperature
$\sigma_u, \sigma_v, \sigma_w$	R.m.s velocity components (of the order of u_*)
$\sigma_x, \sigma_y, \sigma_z$	Dimensions of the cloud/plume
ϕ	Angle between wind direction and normal direction to a street (Figures 3, 6), i.e. $\phi = 90°$ if wind is along the street.

Subscripts

b	Building location/time
B	Buoyancy
BS	Building/Street scale
c	Canyon
C	Cloud concentration for unit source strength
f	Coriolis
G	Geostrophic
H	At top of buildings/canyon
I	Image of undistorted cloud/plume
M	Mesoscale
N	Neighourhood scale
o	Undistorted cloud/plume in uniform flow
o,w	Undistorted cloud/plume at location of wake
O	Overall urban area
P	Plume concentration for unit source strength
R	Reflected plume
Ro	Rossby
S	Source
Se	Effective source
v	Vehicle
W	Cloud/plume in wake
*	Turbulence-related level for log profile, or turbulent source

Superscripts

*	Along-wind distance from upwind edge of canyon (in Appendix)

Diacritics

~	Coordinates and plume dimensions relative to the mean streamline through the source (or through virtual sources), e.g. $\tilde{X}$
^	Average value over the central region of a plume or cloud (i.e. 'central' value), e.g. $\hat{C}$

Abbreviations

BS	Building/street sub-region
FAM	Fast approximate model
FCM	Fully computational model
M	Mesoscale region
N	Neighbourhood sub-region

Table 1 – Scale ranges of urban air flow and dispersion.

	Range	Determining factor(s)	Relation to urban and meteorological scales
1.	**Mesoscale** L_M (~30km)	Flow over buildings Significant orographic / Coriolis effects Surface influences and pollutants mixed through boundary layer	$L_M \sim L_O$ for large urban areas l_O ($x \sim L_M$) ~ h
2.	**Neighbourhood scale** L_N (1-10km)	Flow and dispersion above and between buildings Average geometrical features dominate mean flow/dispersion Growing internal layer above buildings	$L_N < L_O \lesssim L_M$ Typically $L_N \sim L_I$, inner city scale l($x \sim L_N$) $\lesssim$ h
3.	**Building / street scale** L_{BS} (~3-1000m)	Flow and dispersion determined by features below building level (except for elevated releases) Mean geometrical and flow features on scale L_{BS} (not smaller) mainly determine dispersion Internal mixing layers below/above buildings are of order of building/ street dimensions	10H $\gtrsim L_{BS} \gtrsim$ w, b , d l $\lesssim$ H (this defines upper scale of L_{BS})

Table 2 – Main types and features of urban mesoscale.

Increasing effects of orography/heat island →

←Increasing scale	$F = U_G/U_B$ $L_O L_{RO}$	>1 (typically windy environment over flat plain)	~1 (typically moderate wind over flat surface)	<1 (hilly terrain; near coast)
	$\lesssim 1$	(i) Roughness slow down; boundary layer depth varies.	(iii) Weak flow convergence, change in stability over urban area	(v) Slope flows in open valleys; sea breezes; slope flows and pooling in bounded valleys
	$\gtrsim 1$	(ii) Also anticyclonic turning of wind; weak convergence /divergence on left/right.	(iv) Strong central convergence and cyclonic turning.	(vi) Interactions between orographic and urban heat island flows. Significant variations in orographic heat island flow across the urban area.

Note: U_G is the geostrophic wind speed,

$U_B = (gh|\Delta\theta|/\theta)^{1/2}$ is the buoyancy-induced local wind speed

L_f is the Coriolis advection length (= U/f)

L_{Ro} is the Rossby length scale defined by stratification and Coriolis effects (= hf_B/f)

Table 3 – Typical street / building configurations in urban areas.

Increasing width w ↓ \ b/s	Increasing separation, d →	
	b/s ≳ 2	b/s ≲ 1
b/w ≳ 10	(i) Canyon (H/w > 2) Residential street ($H/w \lesssim 1$)	(iv) City squares*, parksides
1-5	(ii) Long blocks (e.g. industrial estates)	(v) Enclosed spaces (e.g. courtyards)
b/w ≲ 2	(iii) Closely-packed industrial sites; ancient settlements**	(vi) Square blocks (e.g. houses), $H/w \lesssim 1$ Office blocks, $H/w \geq 1$

In the above *s* is the distance to the nearest building.

Note:

(a) Mixed cases occur, such as office blocks as part of streets (so H/w varies).

(b) Long and square blocks are usually aligned in streets (i.e. angle between two nearest cases $\Delta\theta_{12}$ is 180°).

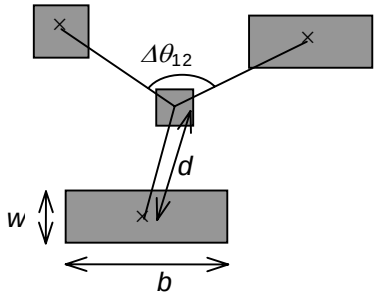

(c) Note that L_ϕ is the distance over which the orientation of the street changes by $\Delta\phi$. This is aerodynamically significant when $\cos\phi \lesssim 0.2$, $\Delta\phi \lesssim 0.2$ and $L_\phi \lesssim 10d$.

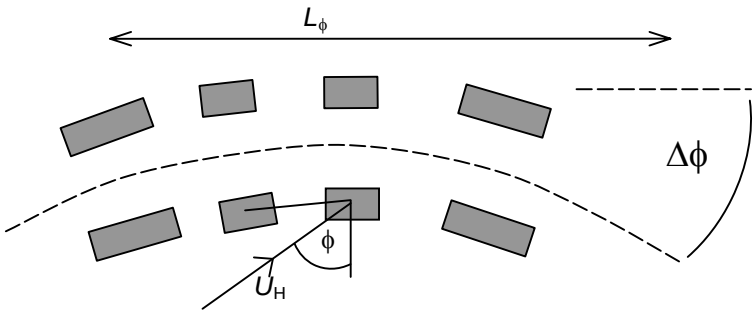

* Long buildings with large space (Le Corbusier Habitation!) are rare except for city squares/courtyards.

** Wide buildings close together are rare except on certain industrial estates.

Table 4 – Types of computational model for urban meteorology and air flow.

1. Mesoscale

i. Full computational models (FCM)

Based on grid box numerical methods; full physics (fluid dynamics and thermodynamics).

Input: from synoptic (or regional) numerical weather prediction models and local surface conditions, e.g. surface fluxes for heat, F_θ, water vapour, F_v, roughness length, $z_0(x, y)$ and surface elevation $z_s(x, y)$, and special effects e.g. emissions, dust, snow, and coastal surface data.

Output: mean flow, turbulence statistics from above building envelope up to tropopause as a function of space and time over the urban area.

Typical number of grid boxes for 1/3-1km resolution on 30-100km grid is 10^6-10^7. Takes about 3 hours per 1 hour run, faster for lower resolution model.

ii. Fast approximate models (FAM)

a Flow perturbation models (suitable where $U_G/U_B \gtrsim 1$) using fast/approximate numerical and analytical methods, simple physics (for turbulence, stratification profiles), input from observational data (reduced) or NWP models and from local surface conditions.

b Local flow/thermal models (especially where $U_G/U_B \lesssim 1$) using formula/fast approximate models for special conditions/physics, e.g. slope winds, sea breeze, thermal convection; often adjusted for local conditions.

c Mass consistent models to compute flow fields given data at several points in the flow domain and surface elevation z_s. (Only suitable if such data exist for all relevant cases.)

d Typical resolutions can be on a horizontal scale of 100m or less.

e These models can be run over a few minutes on PC's for each case. Current simplified models do not account for unsteady conditions over large urban areas (where L_O/L_f, $L_O/L_{Ro} \gtrsim 1$).

2. Neighbourhood scale

iii. FCM using CFD methods

Grid point numerical models with approximate representation of buildings and open spaces (as porous medium; or distributed forces; as approximate shapes); approximate turbulence and heat transfer models; input from mesoscale models or assumed data.

Output: mean and turbulence profiles within the building envelope and up to the boundary layer/inversion layer height.

Typical horizontal resolution is greater than the spacing between buildings. For a 'neighbourhood' of 5km (e.g. city centre) with 10^6-10^7 points, the resolution would be 100m for an 'accurate' computation.

iv. FAM

a Flow perturbation models (applicable where ln z_0 or F_θ vary significantly) using fast/approximate numerical and analytical methods with buildings/open spaces described by average properties and their relative fluctuations (e.g. average building height H, spacing d, and also typical rms fluctuations in H and d); simple turbulence and heat transfer models for canopy flows; input from mesoscale models or local data, and estimates of distributed effects of buildings.

Output: mean flow within and above the canopy and turbulence above the canopy.

b Local flow/thermal models (where ln z_0 or F_θ are approximately uniform). Formulae based on local dynamical and thermodynamic balance and estimates of distributed effects of buildings; input based on average wind, thermal flux and estimates of distributed effects.

3. Building/street scale

i. FCM using CFD methods

Grid box numerical models with accurate representation of buildings, approximate turbulence and heat transfer models; input from neighbourhood models or assumed data. (Very fast versions using idealised (e.g. inviscid) equations with finite numerical diffusion and approximate boundary conditions for buildings.)

Output; mean flow and turbulence profiles around buildings of different shape and grouping within an urban area.

Typical computational domain is greater than building/length spacing L, or d (100m) and grid size of 1m or less.

Note sensitivity to inflow conditions from other buildings and atmospheric turbulence. Models better for clusters of buildings than isolated buildings (where large scale atmospheric turbulence has less influence). Simpler methods are accurate/fast enough for practical use in off-line diffusion calculations.

ii. FAM

Local flow models (used for diffusion models).

a Turbulent wakes of individual buildings based on perturbation methods and typical flows near buildings.

b Closed packed buildings modelled by ideal (potential) flow

c Idealised models for interactions when wakes of upwind building impinge on downwind structures.

d Canyon models (semi-empirical formulae – not yet well established).

e Canyon/street intersection models (e.g. ideal potential flow).

Table 5 – Types of computational model for dispersion prediction.

1. Building/Street Scale

i. Full Computational Models (FCM)

a Steady/unsteady C.F.D models.

b Unsteady, Large Eddy Simulations – mainly for research use.

Note: these types of models are also applied on Neighbourhood scale, given enough computer resources or acceptance of approximation.

ii. Fast approximate models (FAM) for practical application

a Eddy diffusion computations using approximate or idealised flow and building geometry (scenario studies/research).

b Stochastic modelling. Computational methods, allowing for eddying motions in the wakes of buildings and concentration fluctuation (scenario studies) (using approximate flow/topology models).

c Approximate modelling of ensemble average concentration based on ideal/simplified flow/dispersion models for relevant types of situations (as in Table 3) and meteorological conditions. Usually based on interpolations between different types of idealised distorted puff/plume structure. These are fastest methods appropriate for operational conditions.

Note – all models either require input for source strength, location(s), size; or else concentration distribution (in order to deduce source information).

2. Neighbourhood Scale (assuming insufficient computational resources/time to calculate on building/street scale)

* Both FCM and FAM approaches involve approximate modelling of average diffusion process to account for the turbulence and flow between the large numbers of buildings on this scale.

eg. porous medium to represent average effects of buildings (as for flow)

plus effective diffusivity to represent dispersion processes around individual buildings,

or aggregation of dispersion process around individual buildings/street to produce average process on neighbourhood scale (UDM).

In FCM concentration fields are computed. In FAM idealised plume/puff/box model structure is assumed.

* All methods require input concentration field from building/street scale, e.g. virtual source location/scale/distribution (often asymmetric).

3. Mesoscale

i. FCM

Eulerian grid box or Lagrangian particle tracking methods using turbulence models (not suitable for real time emergency response computation), above canopy.

Input: from building/street or neighbourhood scale models or data.

Output: mean and fluctuating concentrations.

ii. FAM

a Advection and eddy diffusion or Lagrangian stochastic models over urban areas with simplified (but time-dependent) flow fields and turbulence profiles (scenario studies/ research).

b Approximate, fast models suitable for real time emergency response based on idealised models of flow field turbulence profile (above the canopy) allowing for time dependent flows, and where necessary terrain, e.g. valleys.

* 'box' model (well within boundary layer)

* puff/plume models (with segmentation into smaller puffs/grid boxes as time progresses)

* combining simplified Eulerian grid box and puff/plume models

Note: fluctuations (rms and pdf) in concentration can be estimated.

Table 6 – Formulae for lateral and vertical dispersion coefficients, $\sigma_y(X)$ and $\sigma_z(X)$, as functions of downwind distance X (metres) for rural and urban conditions (Briggs' (1973) curves as reported in Hanna et al. (1982)).

Pasquill Stability Class	σ_y (m)	σ_z (m)
	Rural	
A	$0.22x\ (1 + 0.0001x)^{-1/2}$	$0.20x$
B	$0.16x\ (1 + 0.0001x)^{-1/2}$	$0.12x$
C	$0.11x\ (1 + 0.0001x)^{-1/2}$	$0.08x\ (1 + 0.0002x)^{-1/2}$
D	$0.08x\ (1 + 0.0001x)^{-1/2}$	$0.06x\ (1 + 0.0015x)^{-1/2}$
E	$0.06x\ (1 + 0.0001x)^{-1/2}$	$0.03x\ (1 + 0.0003x)^{-1}$
F	$0.04x\ (1 + 0.0001x)^{-1/2}$	$0.016x\ (1 + 0.0003x)^{-1}$
	Urban	
A-B	$0.32x\ (1 + 0.0004x)^{-1/2}$	$0.24x\ (1 + 0.001x)^{1/2}$
C	$0.22x\ (1 + 0.0004x)^{-1/2}$	$0.20x$
D	$0.16x\ (1 + 0.0004x)^{-1/2}$	$0.14x\ (1 + 0.0003x)^{-1/2}$
E-F	$0.11x\ (1 + 0.0004x)^{-1/2}$	$0.08x\ (1 + 0.0015x)^{-1/2}$

Figure 1 – Characteristic features of the terrain, buildings and meteorology on the meso- (regional) scale of significance for urban dispersion. L_o and L_I are the overall and inner city length scales, respectively. Note that U_G is the geostrophic wind, U_B is the typical wind speed associated with local buoyancy effects, e.g. downslope winds from nearby mountains. H_c is the canopy height and H_c' is the standard deviation of building height.

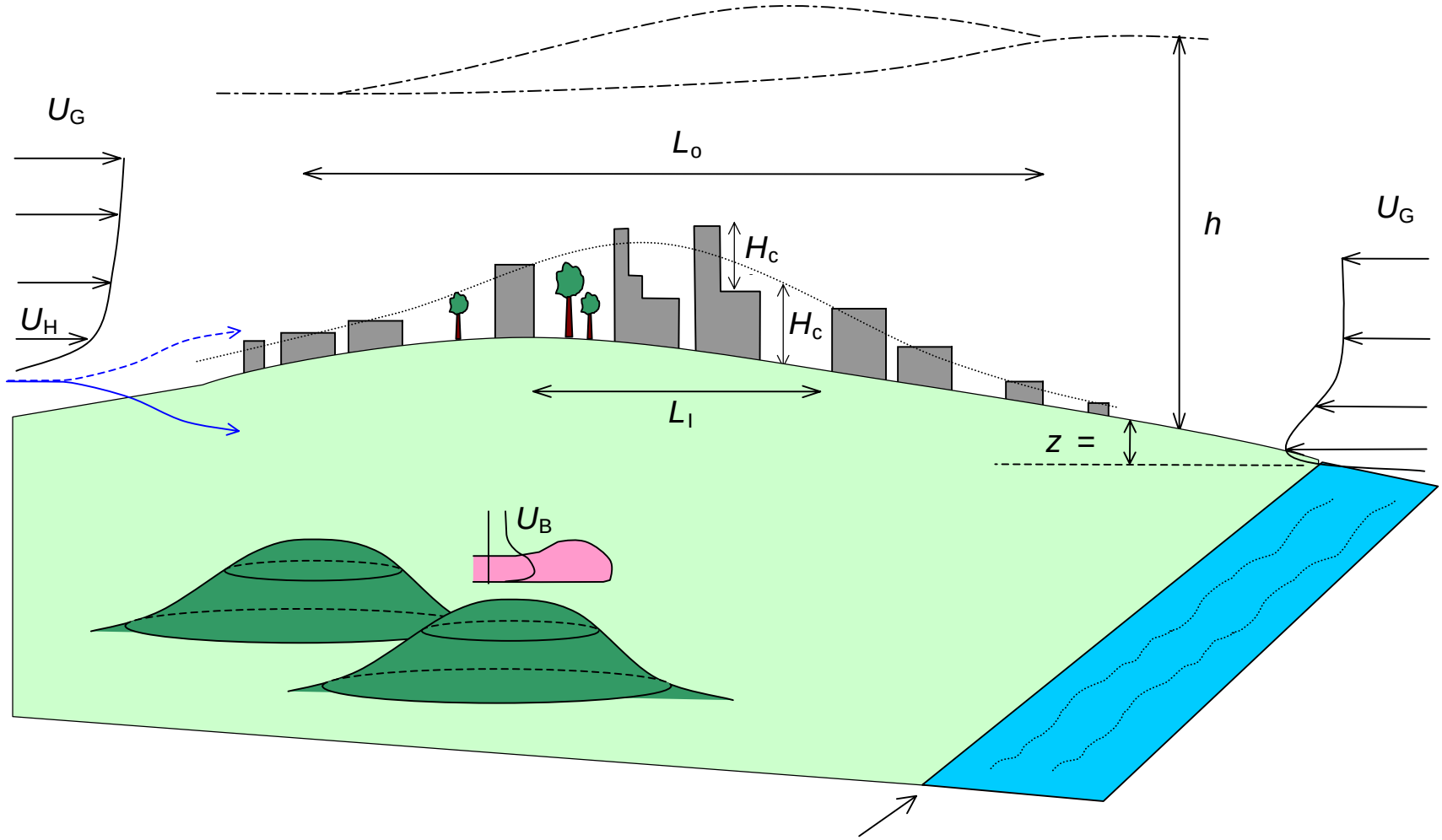

Figure 2 – Characteristic features of building envelope and zones of air flow in neighbourhod scale. (Note that the definition of this scale depends partly on the level of detail of the computation.)

(a) 'Porous' canopy – with isolated buildings. l_O and l_N are the heights of the perturbed layers above the buildings; z_* is the height. $\mathcal{L}_A$ is the adjustment distance.

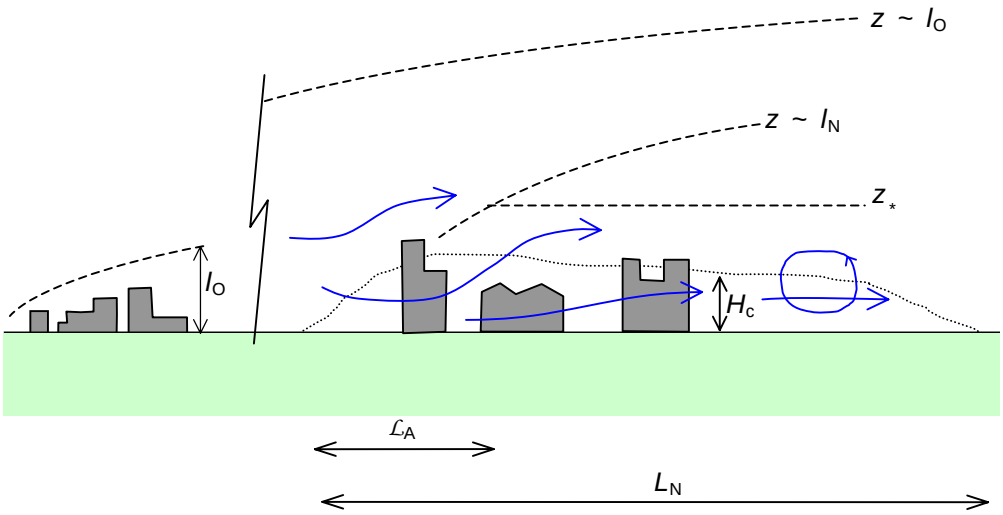

(b) Non-porous canopy, where the mean flow passes over the canopy.

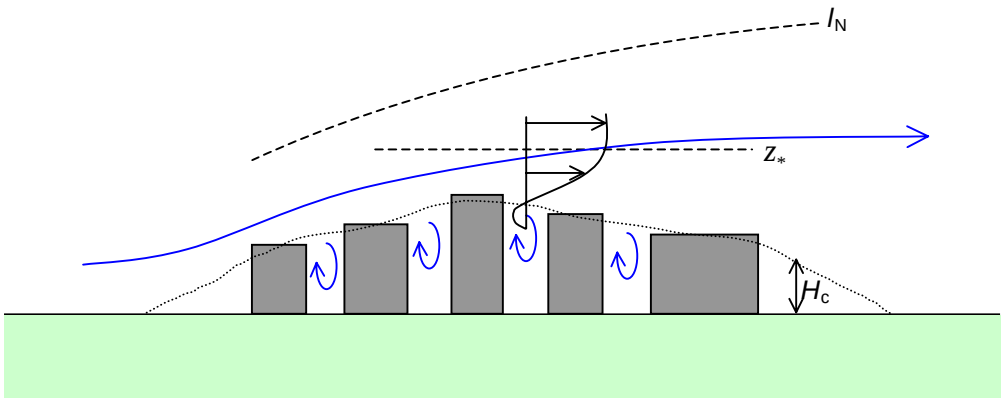

Figure 3a – Typical building/street configuration.

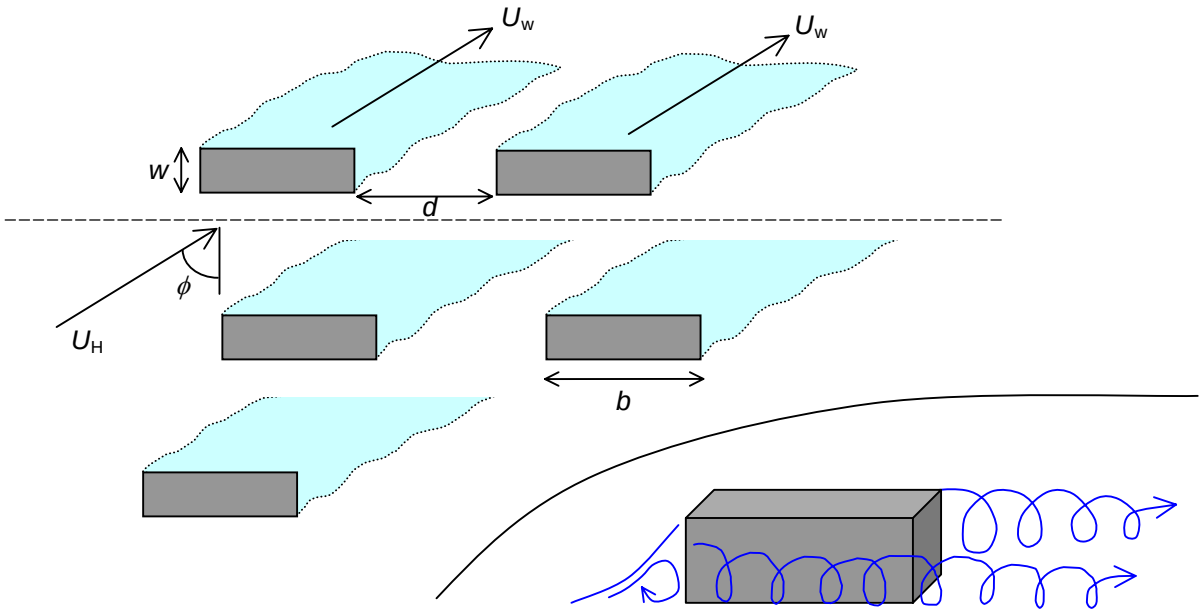

(i) Normal approach angle ϕ small enough (i.e. $\cos\phi > 2w/d$) for independent wakes to be formed (approximately parallel to the approach wind). Note the complex forms of building wakes, in which swirl may persist.

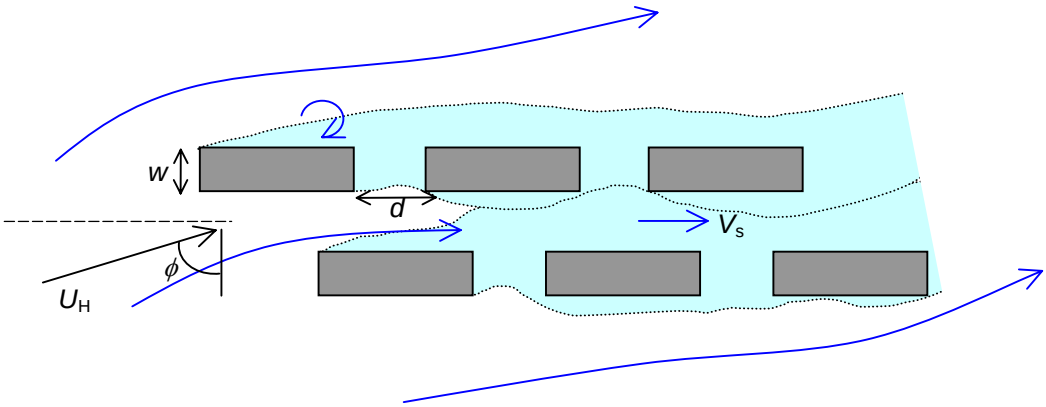

(ii) Normal approach angle ϕ large enough (i.e. $\cos\phi \lesssim 2w/d$) for wakes to merge and 'canyon' flow to develop in streets between the buildings.

Figure 3b – Tall buildings.

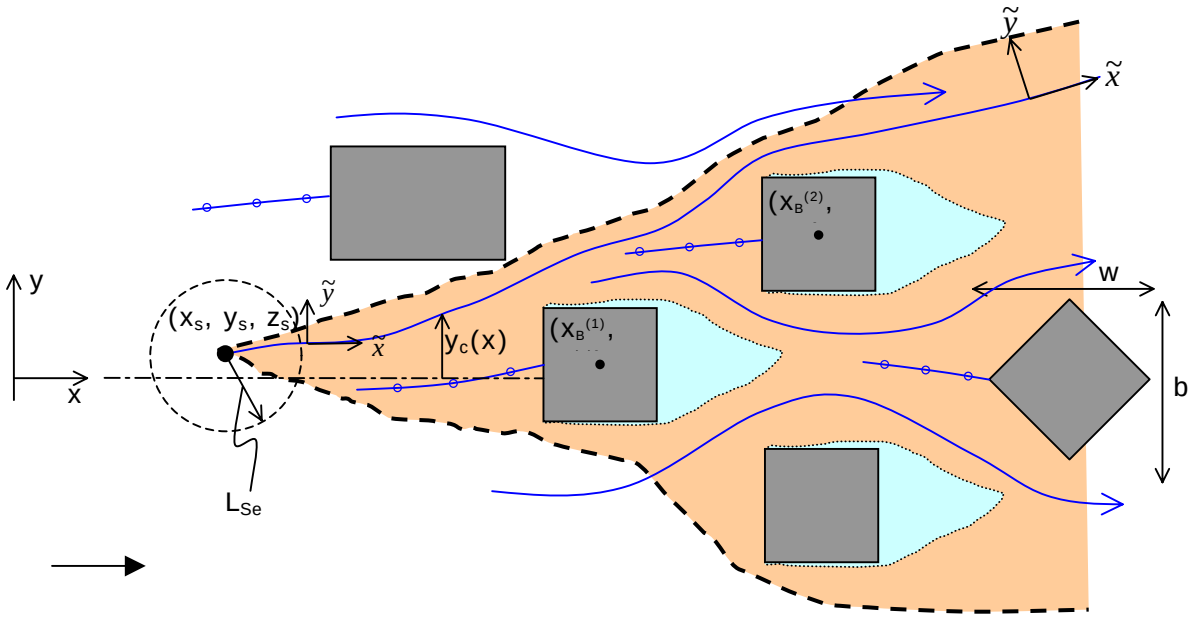

(i) Staggered buildings (comparable height), located at $\{x_B^{(i)}, y_B^{(i)}\}$, close to each other. Note how wakes can 'disappear' through converging streamlines, while lateral diffusion is enhanced by diverging streamlines ('topological' diffusion). Streamlines are indicated by solid arrowed lines. The streamline through the source at (x_s, y_s, z_s) is $y_c(x)$; $\tilde{x}, \tilde{y}$ are coordinates parallel and perpendicular to this streamline. Streamlines marked with small circles are mean streamlines ψ_{stag} passing through stagnation points where plumes split. The cloud/plume resulting from the source is the shaded area enclosed by heavy dashed line. L_{Se} is the effective size of the source outside which atmospheric turbulence determines the dispersion.

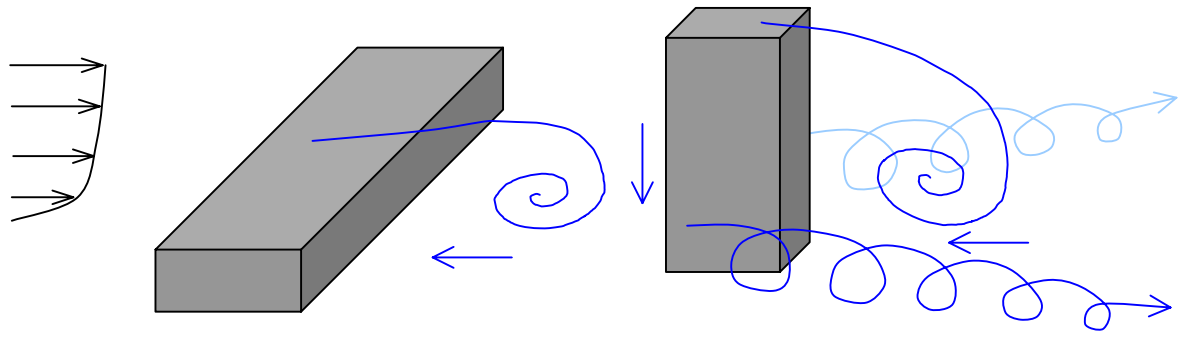

(ii) Effects of uneven building heights. Note strong reverse and downdraft winds (e.g. Lawson, 1980; Britter & Hunt, 1979).

Figure 3c – Street (or urban river) with angled cross wind and side streets.

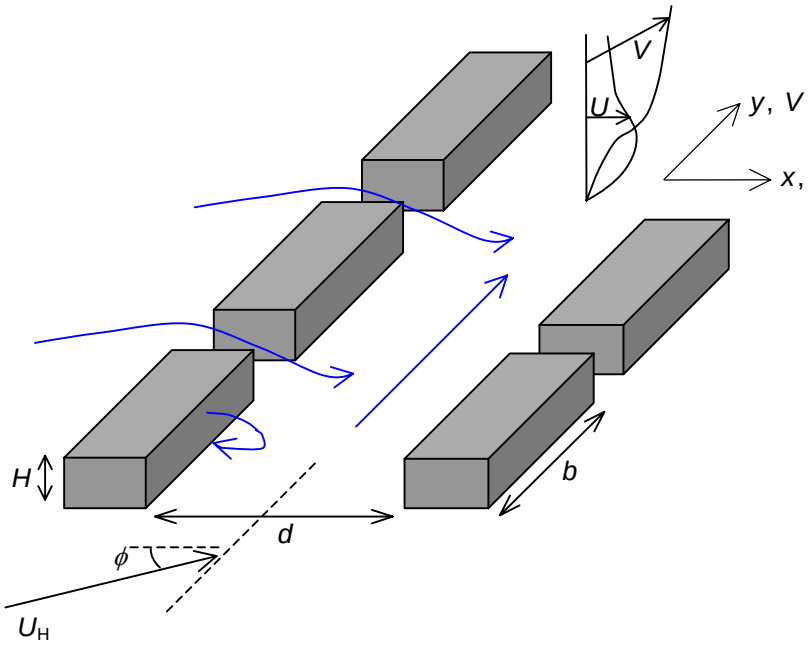

Note that if *H*/*d* ≤ 10 a street canyon vortex forms, the wind is deflected along the street and typically increases with *x* (complicated by effects of side streets).

Figure 3d – Enclosed spaces, e.g. courtyards.

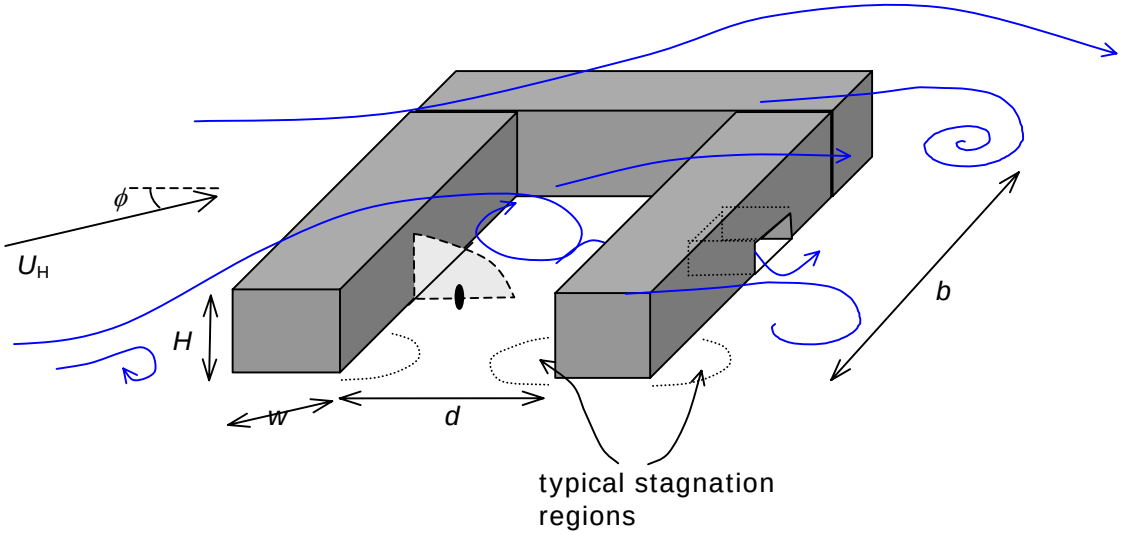

Typical instantaneous streamlines of the large scale flow in a courtyard, where b/d ~ 1, b/w ~ 3, H/d ~ 1/3, H/w ~ 1. The shaded area indicates the region of highest concentration of matter released in the courtyard.

Figure 4 – Typical mean velocity / turbulence distribution.

(i) 'Average profiles of the magnitude of wind speed, scaled by its value at z = h [canyon height]: (a) averaged over all available data; (b) approaching flow normal to the canyon (from SW (full line and stars) and parallel to the canyon (dashed line and circles); (c) approaching flow normal to the canyon from NE (full line and stars) and the same but only runs with wind speed larger than 3m/s at position 21R [canyon roof] (dashed line and circles).' From Rotach (1995).

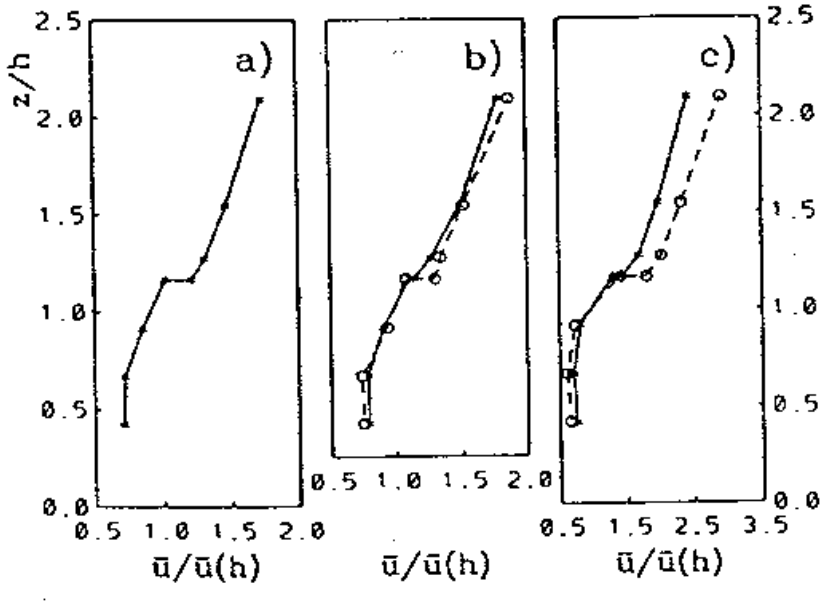

(ii) 'Variation of u_* /U for neutral conditions with non-dimensional heights (a) z_s'/z_0 and (b) z_s/z_H. [z_s is sensor height above ground; $z_s' = z_s - z_d$, where z_d is zero-plane displacement height.] The line in (a) is based on the log-profile…and the line in (b) is an empirical fit…'. From Roth (2000).

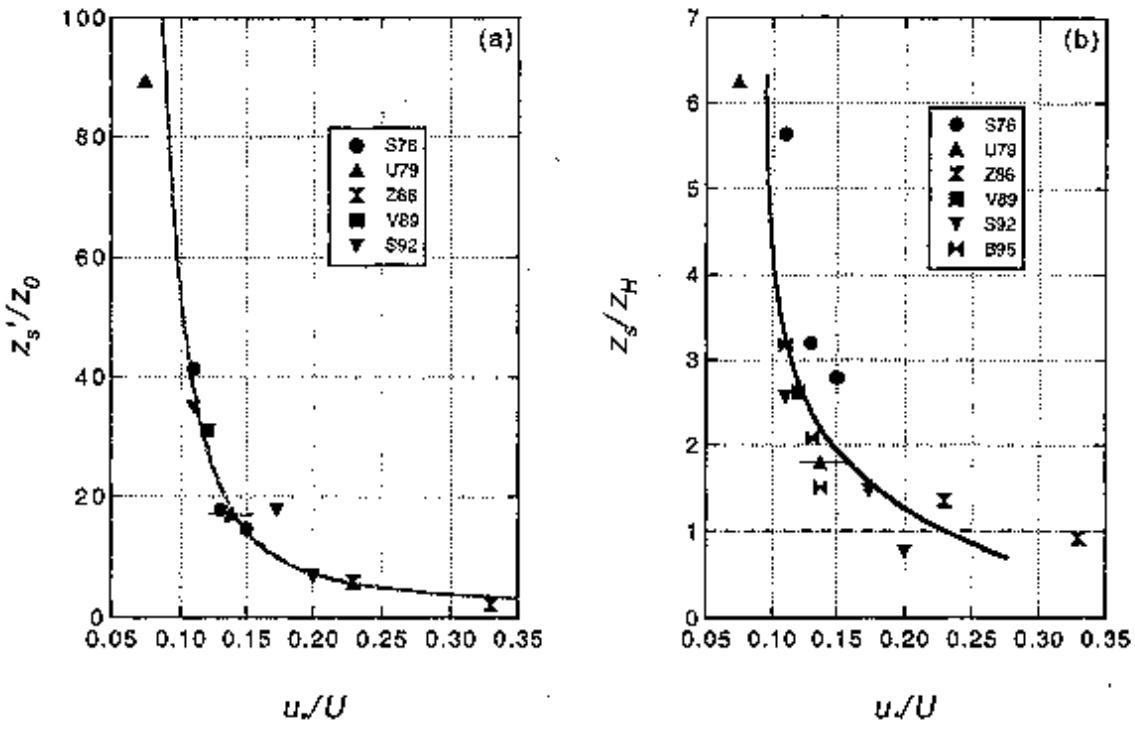
(a)
S76
U79
Z86
V89
S92
z_s'/z_0
u_*/U
(b)
S76
U79
Z86
V89
S92
B95
z_s/z_H
u_*/U

Figure 5 – Characteristic urban diffusion mechanisms. (a) Single building

(i) Source outside wake/canyon, showing impaction of the plume from Source (1), wake entrainment (E) and detrainment (D) from Sources 1 and 2. Note how the plume profile G(z) has a split structure in the wake with unentrained component G_{p0} and detrained component G_{pw}. G_c denotes the typical outline of a cloud emitted upwind, showing the additional longitudinal dispersion associated with the blocking and wake effects. Here the reference cloud outline in the absence of buildings is shown as a dashed line with small circles, with streamwise dimension σ_{x0}.

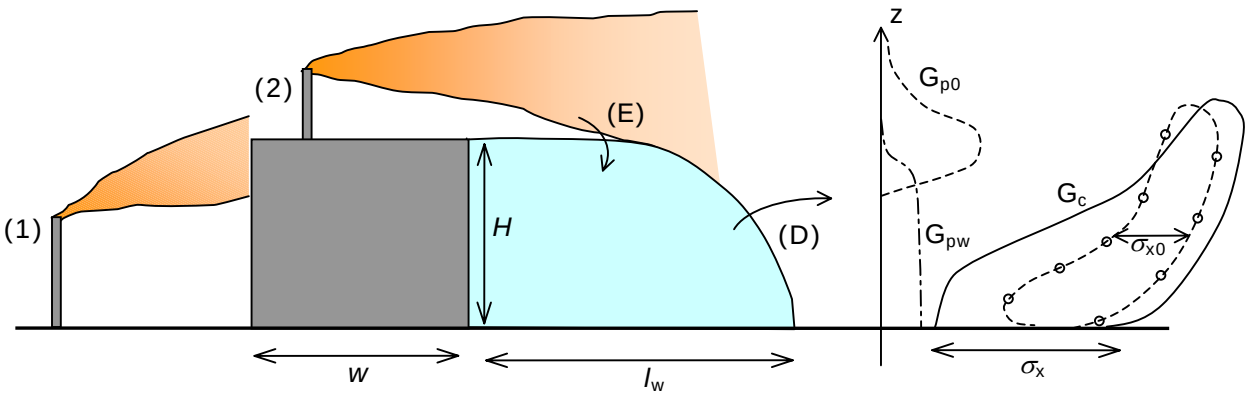

(ii) Source inside wake/courtyard, canyon/building with a single wake component in the plume profile downwind of the recirculating regions for cube-like and tall cuboidal building. In the latter case, the concentration may not be well-mixed over the whole height.

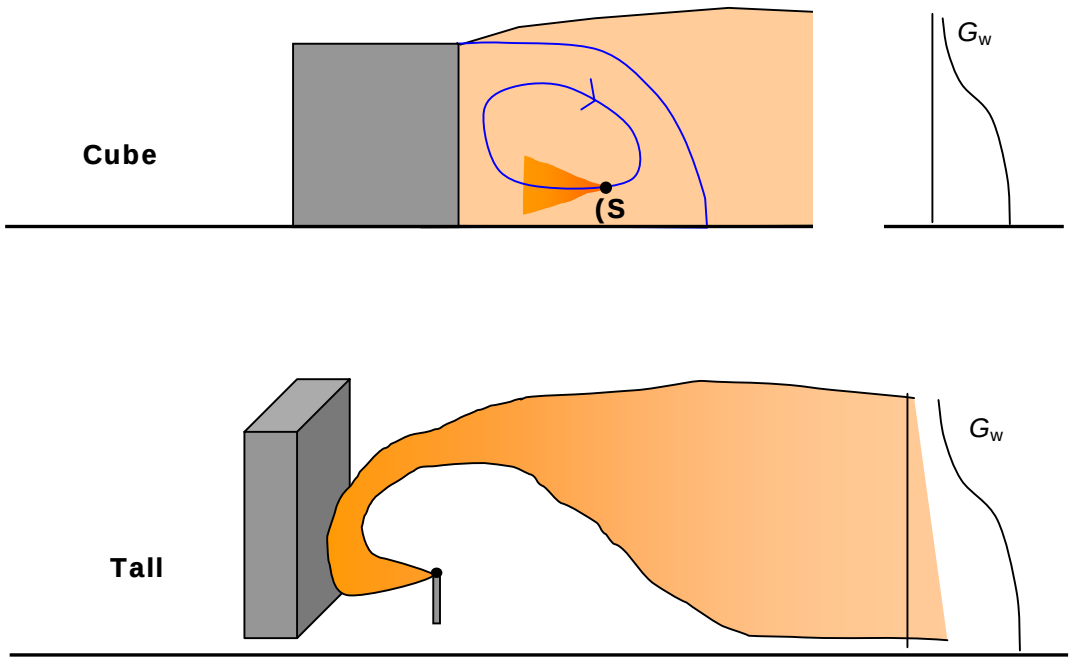

Figure 5 – Characteristic urban diffusion mechanisms: (b) multiple buildings (see also Figure 3).

(i) In building/street region (for well-separated buildings, b/d $\lesssim$ 1): plume dimensions less than building width

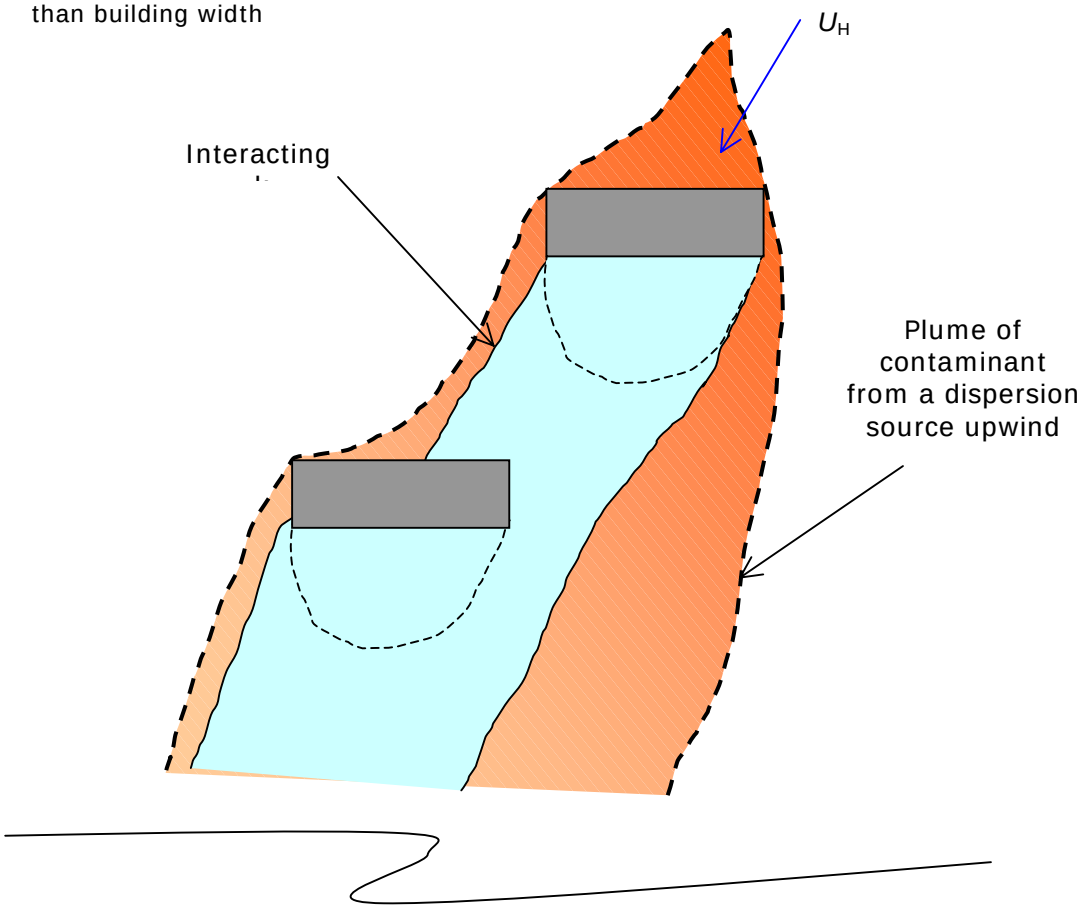

(ii) Far from the source, on neighbourhood scale: plume is much wider than the building width

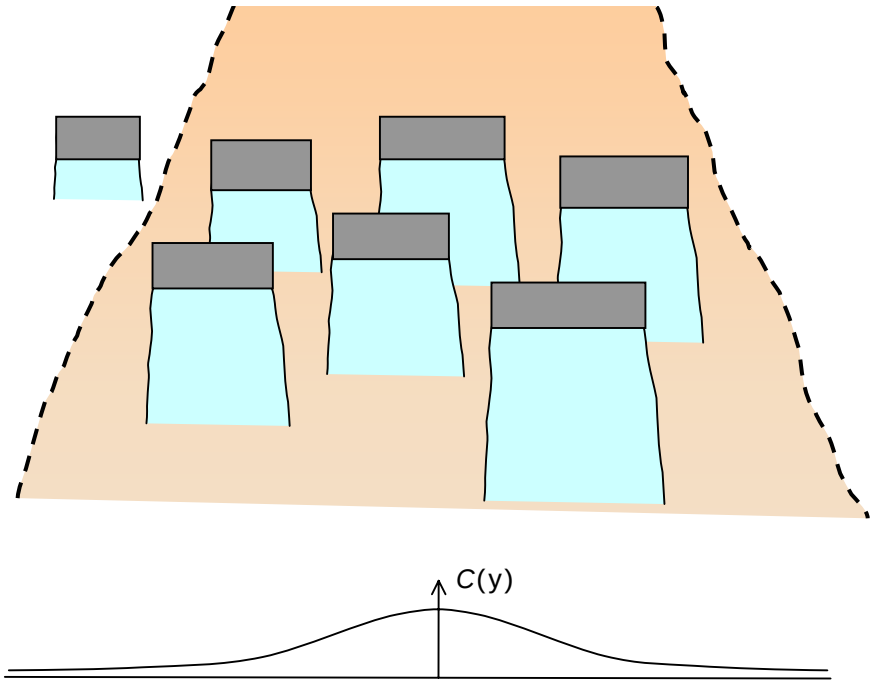

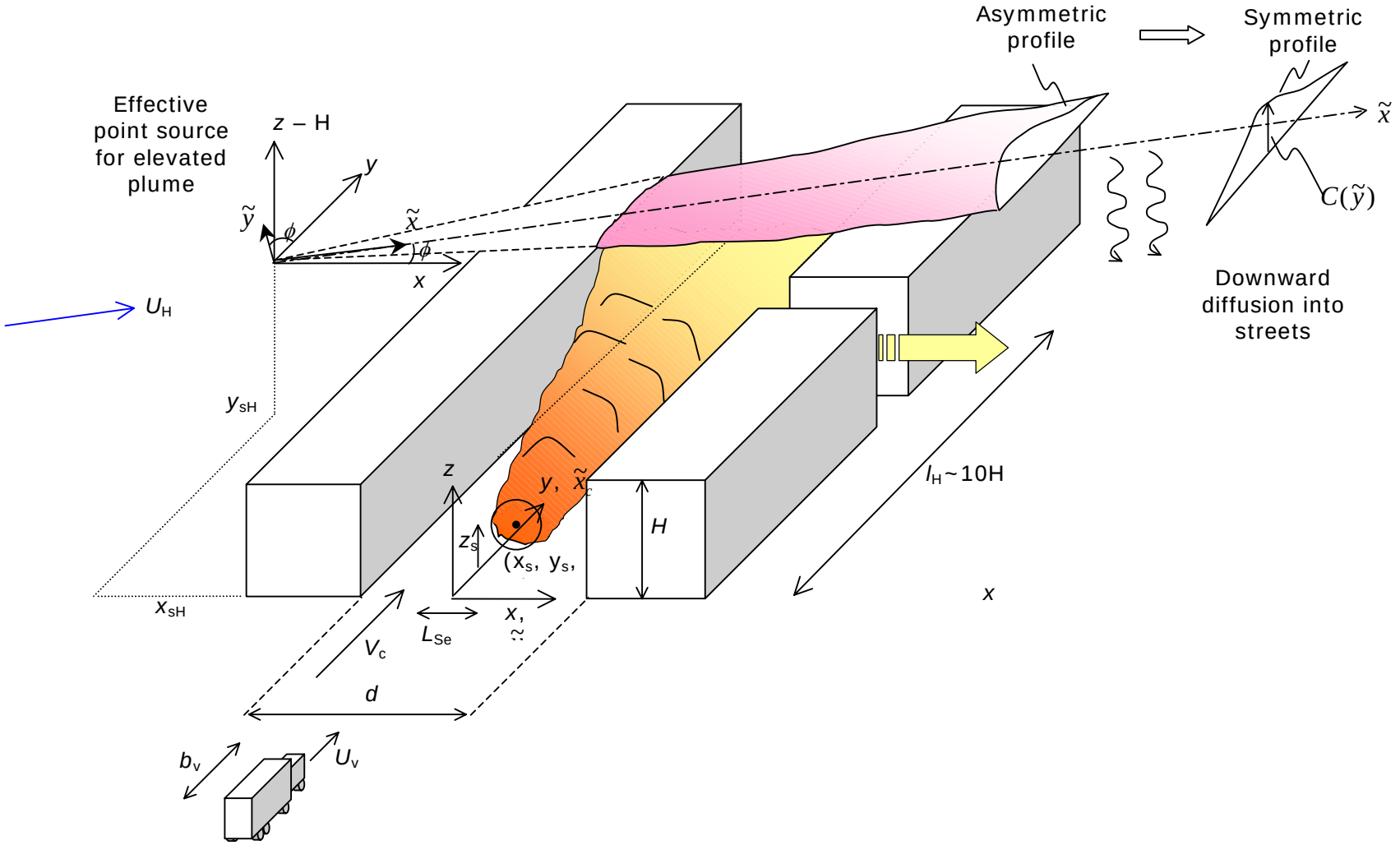

Figure 6– **Accidental release at (x_s, y_s, z_s) of initial scale L_{Se} in a canyon of width d and height H with crosswind, showing how on the Building/Street scale the plume is advected along canyon a distance y_{sH} and then carried downwind in a cloud/plume that initially is skewed (along the street), but far downwind on neighbourhood scale returns to standard Gaussian form. (x_{sH}, y_{sH}) is the location of the virtual source for dispersion over the Neighbourhood scale. Note that vehicles with scale b_v and speed U_v also affect the turbulence.**

Figure 7 – Distorted plume caused by 'canyon' winds and diffusion from an elevated source.

(a) Plume boundaries (fixed proportion of centerline concentration at given value of x) in horizontal plane, showing components: unentrained (dash-dot line), detrained (dashed line) and plume in canyon below building height (shading).

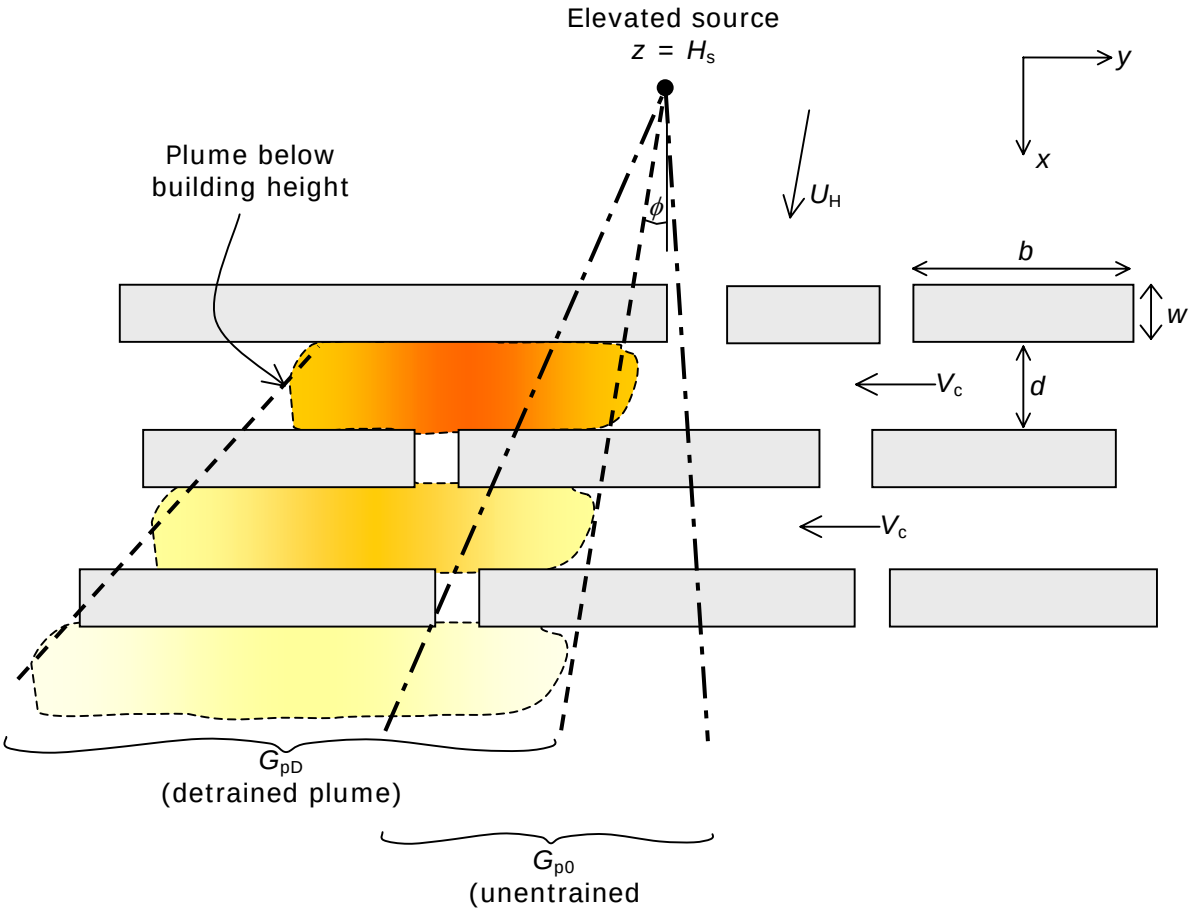

(b) Plume boundary (for some level of concentration) in a vertical plane above the buildings

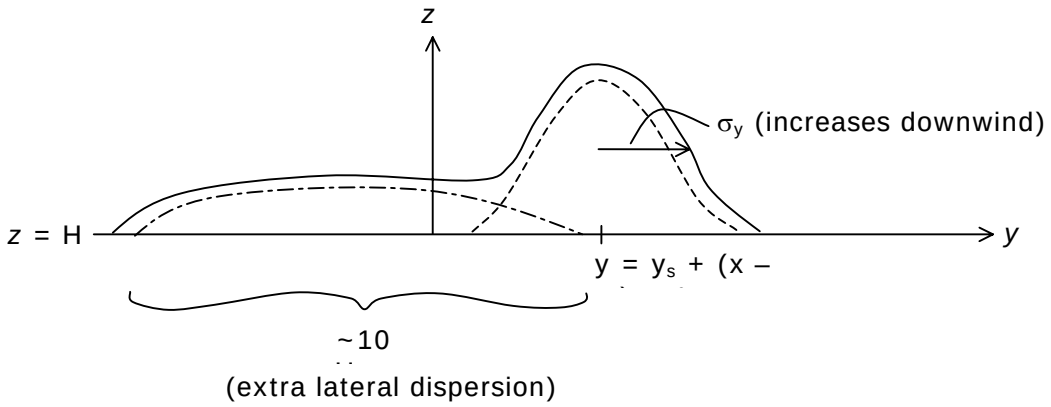

Figure 8

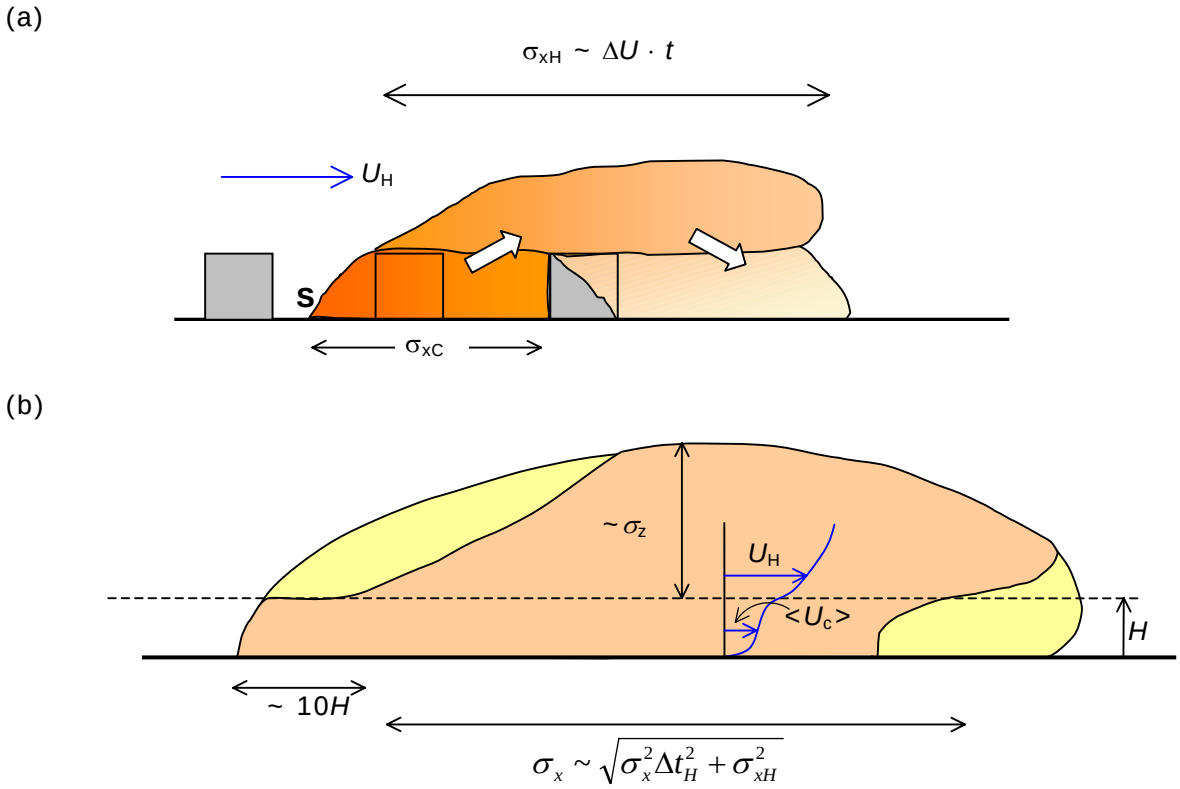

Outlines of cloud released in a 'porous' canopy with closely-packed cube-like buildings (H/w ~ 1): (a) on Building/Street scale where $\sigma_z \lesssim H$, $\sigma_x \lesssim 10H$, with a high concentration cloud in the canopy and a low concentration cloud above it; (b) on the Neighbourhood scale, where $H \lesssim \sigma_z < h$, $H \lesssim \sigma_x < L_N$, where the dispersion above the canopy determines the concentration within it.

Figure 9

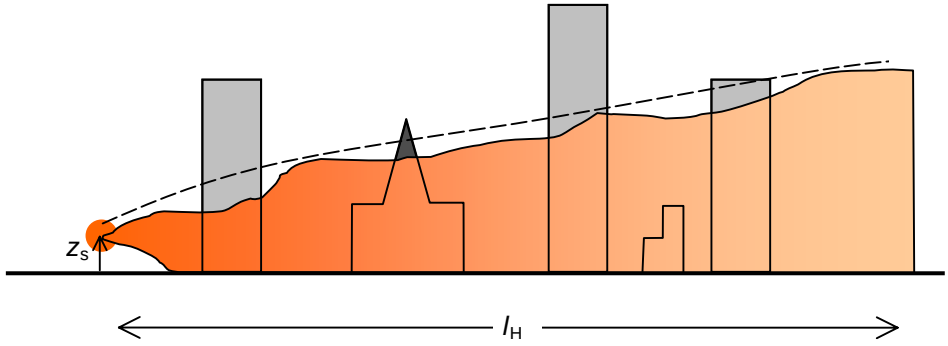

Vertical growth of a cloud/plume with outline (solid line) and average over the whole area (- - -dashed line). The source is in an urban area with high closely-packed buildings ((H/w $\gtrsim$ 2, b/d > 1/3) showing how the wakes disperse the plume up to height *H* over a horizontal distance l_H (as seen in field trials – see Section 5).

Figure 10

(a) Porous canopy

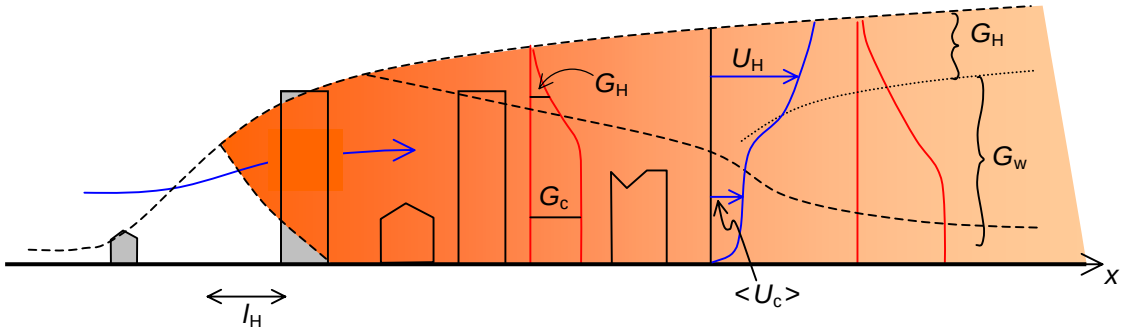

Net air flow through the buildings with average velocity $<U_c>$ (~0.3-0.5U_H). Plume has double structure within and above canopy structure, and also downwind.

(b) Non-porous canopy ($<U_c>/U_H < \sigma_w/U_H$)
Plume disperses from a source within the canopy into the airflow over the canopy and then is dispersed downwards. Note some dispersion upwind of source S. (Here the source material is released in the form of a cloud and the cloud has travelled a few building heights.)

(i) vertical cross-section

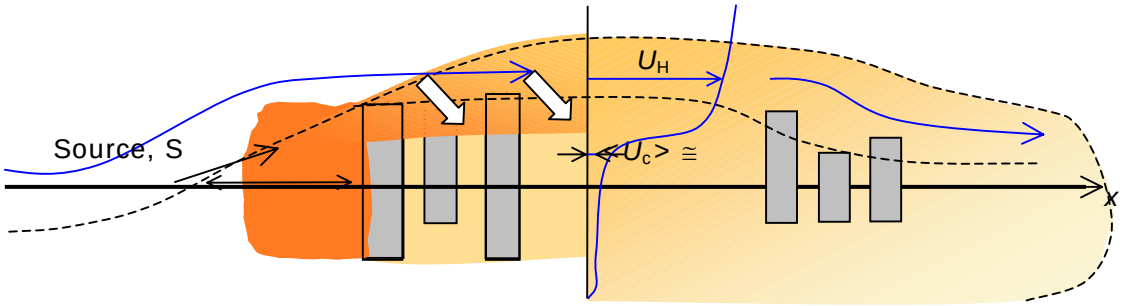

(ii) plan view showing matter being carried along streets in the downwind directions, outside the edge of the upper plume ($z > H_c$).

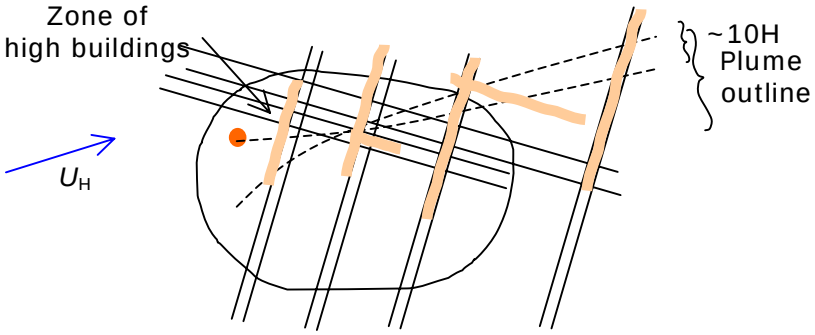

Figure 11 –Third experiment: tracer release (R3) and sampling sites (S3.n) in the main arc. Birmingham, UK, 2nd August 2000. The distance between the release and the sampling sites is about 1 km.

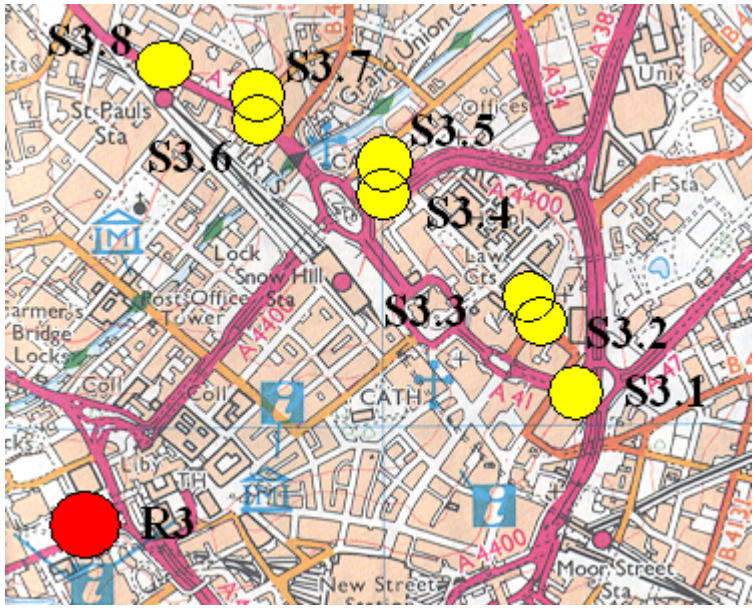

Figure 12 –Comparison between measured concentration and ADMS3 model predictions for the July 1999 experiment.

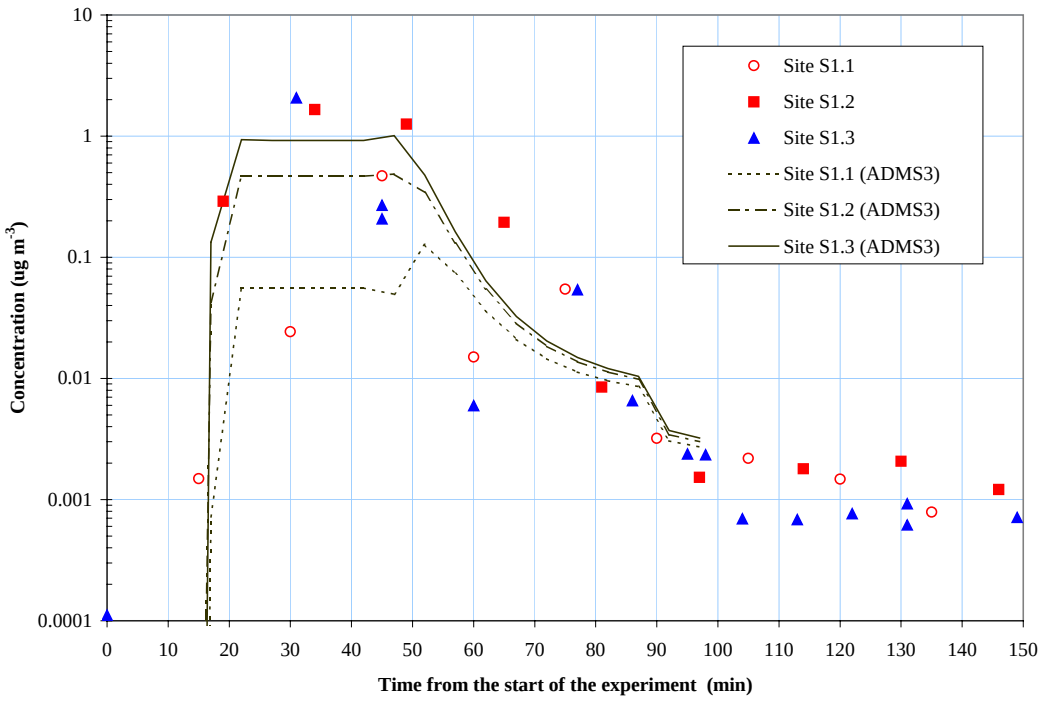

Figure 13 –Comparison between measured concentration and ADMS3 model predictions for the August 2000 experiment for Site S3.5.

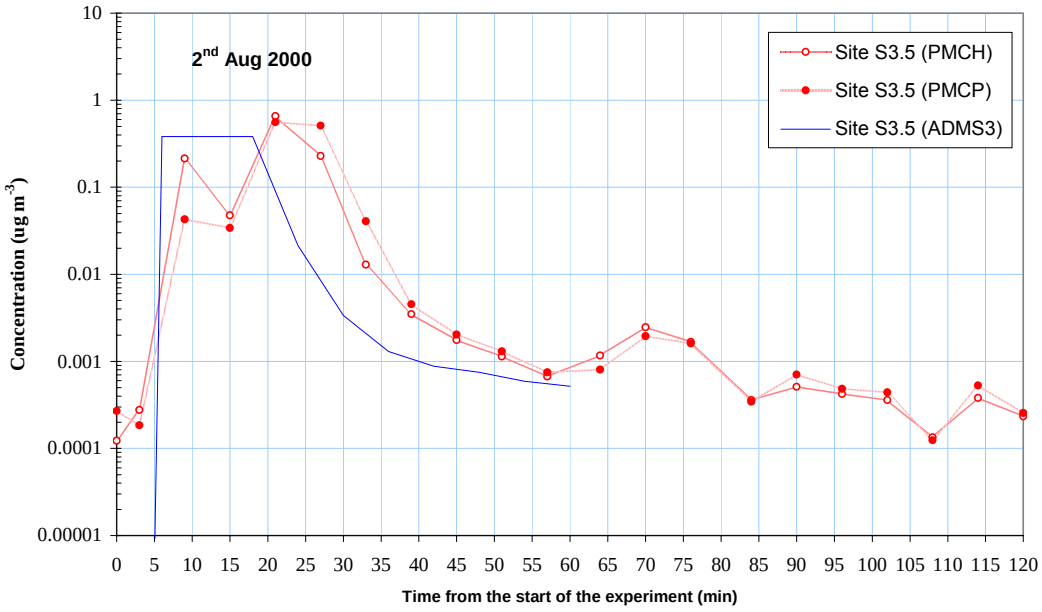
2nd Aug 2000
Site S3.5 (PMCH)
Site S3.5 (PMCP)
Site S3.5 (ADMS3)
Concentration (ug m-3)
10
1
0.1
0.01
0.001
0.0001
0.00001
0 5 10 15 20 25 30 35 40 45 50 55 60 65 70 75 80 85 90 95 100 105 110 115 120
Time from the start of the experiment (min)

Figure 14 – Salt Lake City test, October 26, 2000: (a) half-hour averaged ground-level concentration; (b) near-source half-hour averaged ground-level concentration.

(a)

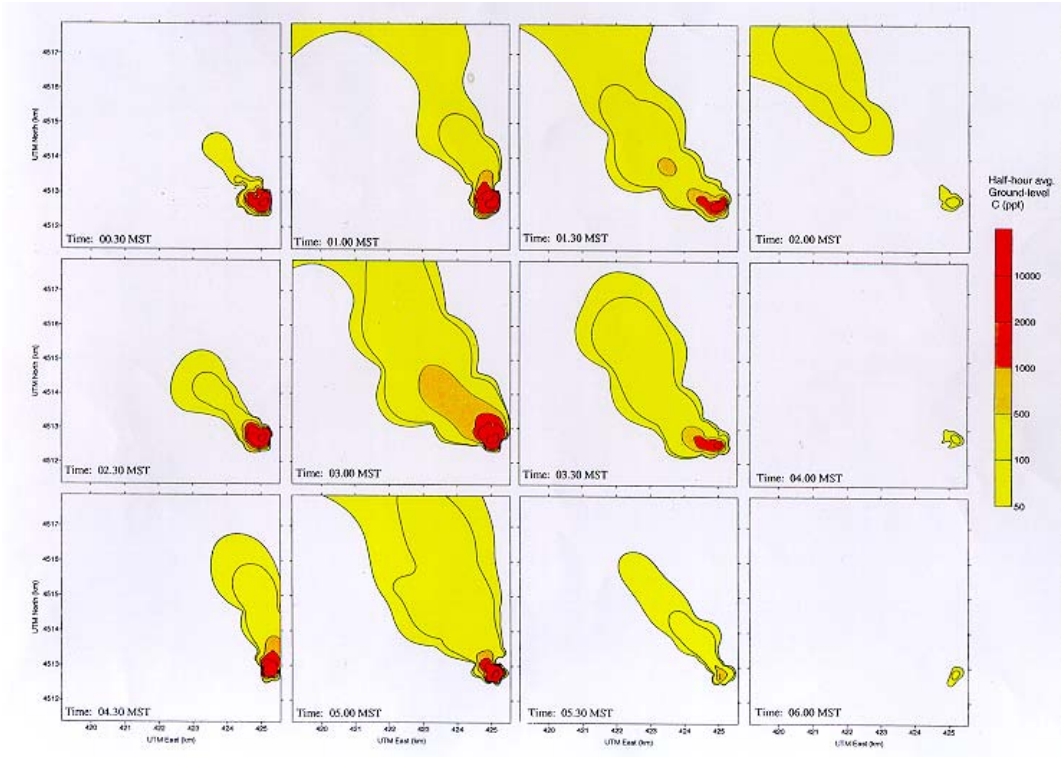

(b)

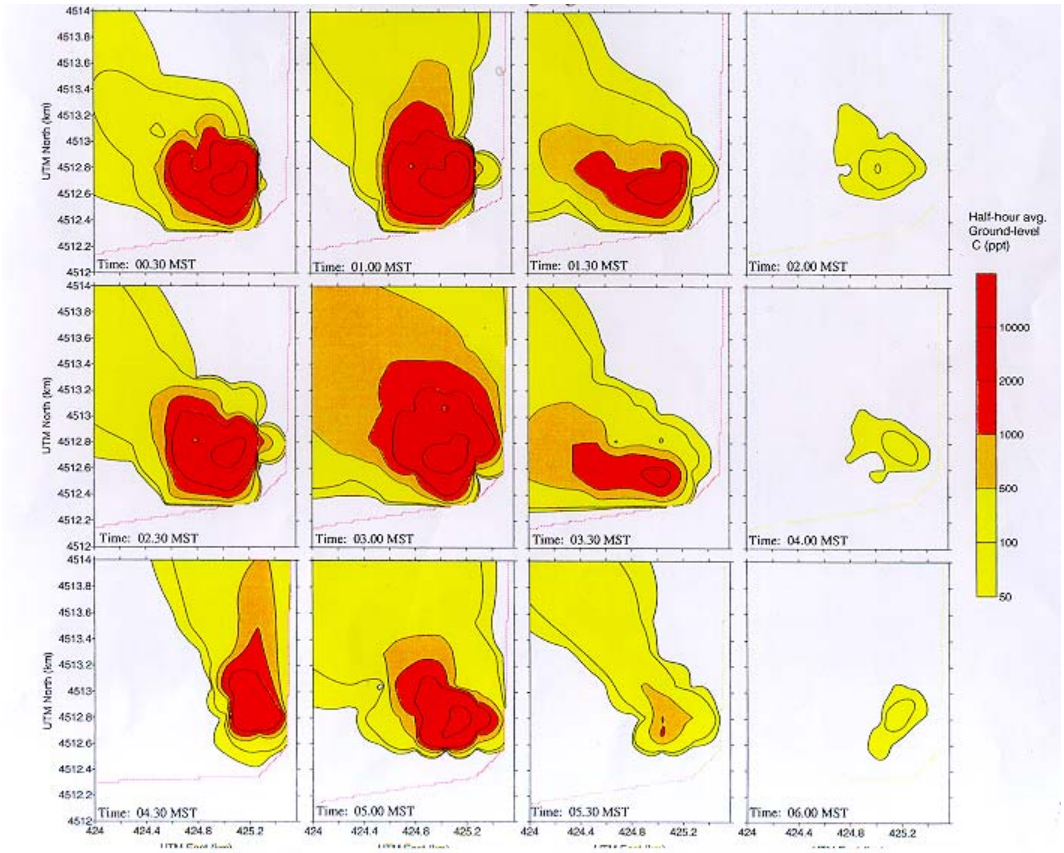

Figure 14, ctd. (c) Salt Lake City test, IOP7 (low wind conditions).

(c)

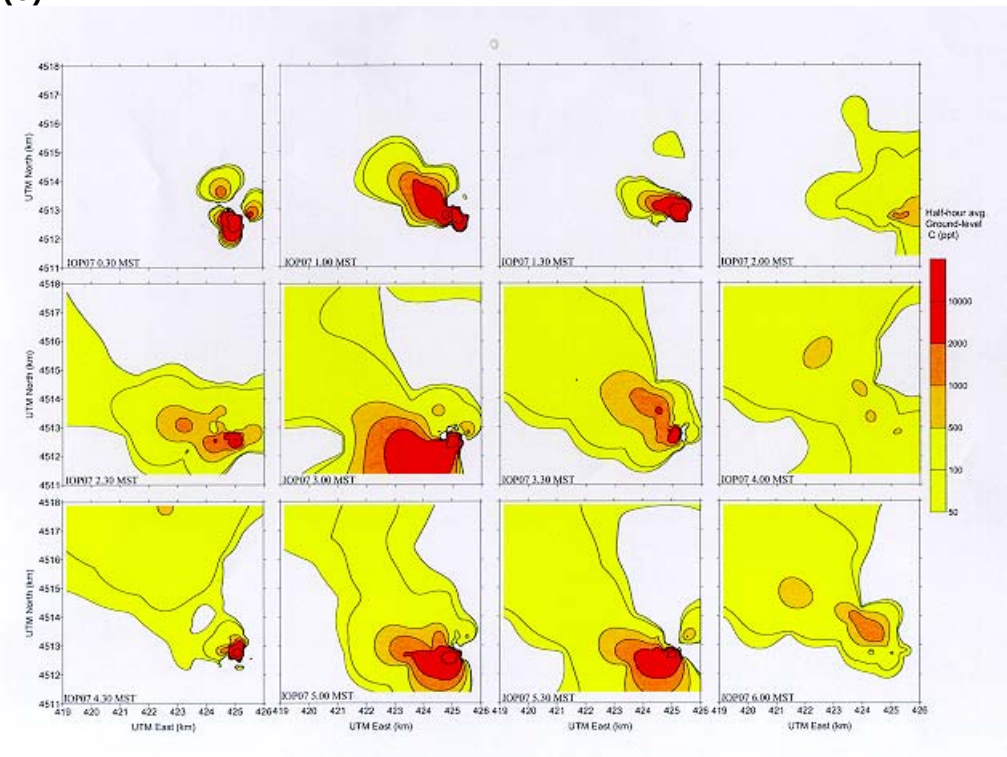

APPENDIX A

DISPERSION FROM A STEADY SOURCE IN A STREET CANYON WITH CROSS WIND

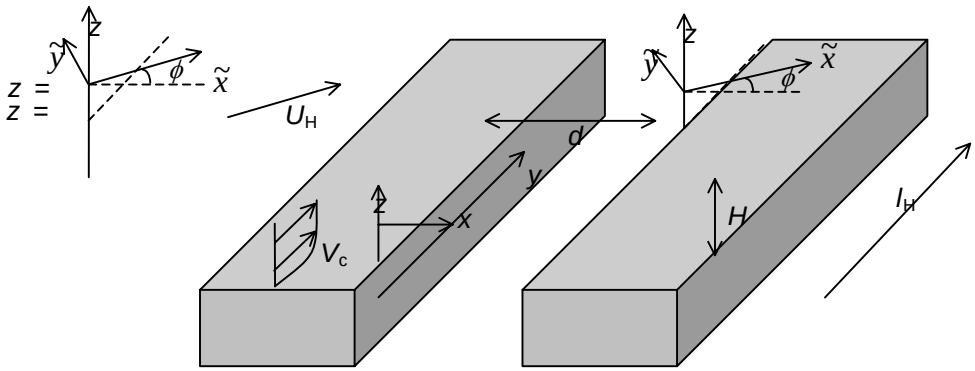

Figure A-1 – Coordinate system for the analysis of dispersion from a source in a canyon at x = y = z = 0.

The background to this analysis is given in Section 4. It focuses on the third stage (iii) when the plume from a source at $y_s = 0$, $z_s < H$ moving down the canyon with velocity V_c is well-mixed across the canyon and diffuses up into the cross flow with velocity U_H at an angle ϕ to the x-axis. As shown below this occurs when $y \sim l_H \sim V_c H^2/K_c$. The canyon is assumed to be limited by impervious buildings on each side.

For this steady problem, use eddy diffusion model with constant diffusivities K_c, K_H in the canyon and the upper flow, respectively. The equations are:

In the canyon:
$$V_c \frac{\partial C}{\partial y} = K_c\left(\frac{\partial^2 C}{\partial z^2} + \frac{\partial^2 C}{\partial x^2}\right) \cong K_c \frac{\partial^2 C}{\partial z^2} \quad (z < H) \qquad \text{(A1)}$$

Above the canyon:
$$U_H \cos\phi \frac{\partial C}{\partial x} + U_H \sin\phi \frac{\partial C}{\partial y} \cong K_H \nabla^2 C \quad (z > H) \qquad \text{(A2a)}$$

In terms of coordinates parallel and perpendicular to the upper wind, $(\tilde{x}, \tilde{y}, z)$,

$$U_H \frac{\partial C}{\partial \tilde{x}} \cong K_H\left(\frac{\partial^2 C}{\partial \tilde{y}^2} + \frac{\partial^2 C}{\partial z^2}\right) \quad (z > H) \qquad \text{(A2b)}$$

Let $q_H(y)$ be the average flux of contaminant from the canyon into the upper flow. Total source strength is Q_S in the canyon. Following Turfus (1986), the solution when $\sqrt{K_c y / V_c} \gtrsim H$ is

$$C = \hat{C}e^{-\lambda y/H}\cos(\mu z/H). \qquad \text{(A3)}$$

Downwind of the source this is the leading order term in an expansion of the form $C = \sum \hat{C}_n e^{-\lambda_n y/H}\cos(\mu_n z/H)$ that matches with the solution in Stage (ii) when the plume depth σ_z is much less than the canyon height H so that $K_c \partial C/\partial z = 0$ at z = 0. Substituting (A3) into (A1) implies

$$-V_c\lambda/H = -K_c\mu^2/H^2$$

so that

$$\mu = \sqrt{\frac{V_c \lambda H}{K_c}} \qquad \text{(A4)}$$

Thence the vertical flux at the top of the canyon (per unit area per unit time) is

$$\overline{q}_H(y) = K_c\hat{C}e^{-\lambda y/H}(\sin\mu)/H \qquad \text{(A5)}$$

Note $d \cdot \int_0^\infty \overline{q}_H(y)dy = Q_S$. Hence

$$\hat{C} = \frac{\lambda Q_S}{d \cdot K_c \sin\mu} \qquad \text{(A6)}$$

Now match with the solution in z > H to calculate λ.

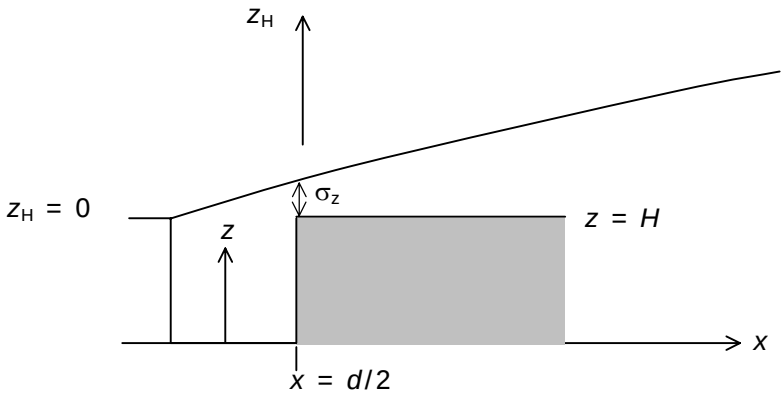

Figure A-2

Consider the local solution above the canyon: then

Canyon flux into the upper flow = downwind flux at x = d/2 (A7)

i.e.

$$d \cdot \overline{q}_H \cong C(z = H) \times U_H \times \sigma_z\ (x = d/2)$$

where $\sigma_z(d) \sim \sqrt{\frac{d \cdot K_H}{U_H \cos\phi}}$

Thence from (A5), (A6) and (A7),

$$\sin\mu \cdot d \cdot K_c / H = \cos\phi \cos\mu \cdot U_H \sqrt{d \cdot K_H / U_H \cos\phi}$$

Therefore μ is determined by the eigenvalue problem

$$\tan\mu = \left[\frac{d \cdot U_H \cos\phi}{K_c}\right]^{1/2} \cdot \sqrt{\frac{K_H}{K_c}} \cdot \left(\frac{H}{d}\right) \qquad \text{(A8)}$$

For typical values

$$K_c(x) \sim 0.4\sigma_w H \sim 0.4K_c H/10 \sim 0.4U_H H/20$$

$$K_H(d) \sim \frac{U_H d}{10}$$

and so

$$\tan\mu \sim (10\cos\phi)^{1/2} / 0.4 \qquad \text{(A.9a)}$$

Note that μ is approximately independent of the narrowness of the street, i.e. H/d: from (A.9a), when $\phi = 0$, $\mu \cong 1.5$ and when $\phi = \pi/4$, $\mu \cong 1.4$. Hence l is not at all sensitive to ϕ, and μ is only weakly sensitive when $\phi \gtrsim \pi/3$. Hence

$$\lambda \cong \frac{K_c}{V_c H} \sim \frac{2 \times 0.4}{10} \sim 0.1 \qquad \text{(A9b)}$$

Hence in the canyon,

$$C \sim \frac{Q_S}{d \cdot K_c} e^{-y/(10H)} \cos(\mu z / H) \qquad \text{(A10a)}$$

showing that the concentration decays exponentially along the canyon over a scale $l_H \sim 10H$. This is consistent with the computation and experiments of Soulhac (2000).

Note that the vertical flux

$$\overline{q}_H(y) \cong \frac{Q_S}{d \cdot H} e^{-y/(10H)} \qquad \text{(A10b)}$$

when $y > l_H$ since sin $\mu \cong 1$. Also,

$$C(y = H) \cong \frac{Q_S}{d \cdot K_c} e^{-y/(10H)} (0.4 / \sqrt{10\cos\phi}) \qquad \text{(A10c)}$$

when tan $\mu >> 1$.

The approximate solution for the mean concentration in the upper flow (z > H), in the upper coordinate system, is

$$C(\tilde{x}_H, \tilde{y}_H, z_H) = \int_{-\infty}^{\infty} \frac{d \cdot q_H(\tilde{y}'_H)^*}{2\pi U_H (K_H / U_H)\, \tilde{x}^*(\tilde{y}'_H)} \exp\left\{-\left[\frac{z_H^2}{4(K_H / U_H)\, \tilde{x}^*(\tilde{y}'_H)} + \frac{(\tilde{y}_H - \tilde{y}'_H)^2}{4(K_H / U_H)\, \tilde{x}^*(\tilde{y}'_H)}\right]\right\} d\tilde{y}'_H \quad \text{(A11)}$$

where $\tilde{x}^*$ is the distance from the upwind side of the canyon, at a displacement $\tilde{y}$, $\tilde{x}^* = \tilde{x}_H - \tilde{y}_H \tan\phi$, U_H is the speed of the upper flow and $\tilde{x}_H$ is the distance parallel to the upper flow from the point (-d/2, l_H). Note that because the buildings either side are impervious, all the plume material lies above z = H.

Note that in (A11), in order to simplify the integral,

$$\overline{q}^*_H(\tilde{y}) \cong \frac{Q_S}{d \cdot l_H \cos\phi} \exp\{-\tilde{y} / (l_H \cos\phi)\} \quad \text{for } \tilde{y} > 0 \gtrsim \frac{H^2 V_c}{K_c} \quad \text{(A12a)}$$

However, for $\tilde{y} < 0$ the plume has not significantly diffused vertically into the upper flow. Hence approximately

$$\overline{q}^*_H(\tilde{y}) \cong 0 \quad \text{for } \tilde{y} < 0 \quad \text{(A12b)}$$

The solution (A11) shows how the concentration in the upper flow (z > H) is effectively dispersing from a source Q_S at $\left(-x^*_{Hs}, y^*_{Hs}\right)$ – see Figure A-3. This location is estimated by assuming in the upper flow the plume width $\tilde{\sigma}_y \sim \tilde{x}/10$. Since the plume width at the top of the canyon (normal to the mean wind) is $l_H/\cos\phi$, it follows that the distance from the virtual source $S_{(v)}$ to the top of the canyon ($\tilde{x}_H = 0, \tilde{y}_H = 0$) is $\tilde{x} = \tilde{x}_{Hc} \sim l_H / \cos\phi$. Since $\tilde{\sigma}_y \sim l_H \cos\phi \sim 10H\cos\phi$ at this point,

$$\tilde{x}_{Hc} \sim 10\tilde{\sigma}_y \sim 100H\cos\phi \quad \text{(A13a)}$$

Therefore

$$x_{sH} = -\tilde{x}_{Hc} \cos\phi \cong 100H\cos^2\phi \quad \text{(A13b)}$$

$$y_{sH} = l_H - \tilde{x}_{Hc} \sin\phi \cong 10H(1 - 5\sin 2\phi) \quad \text{(A13c)}$$

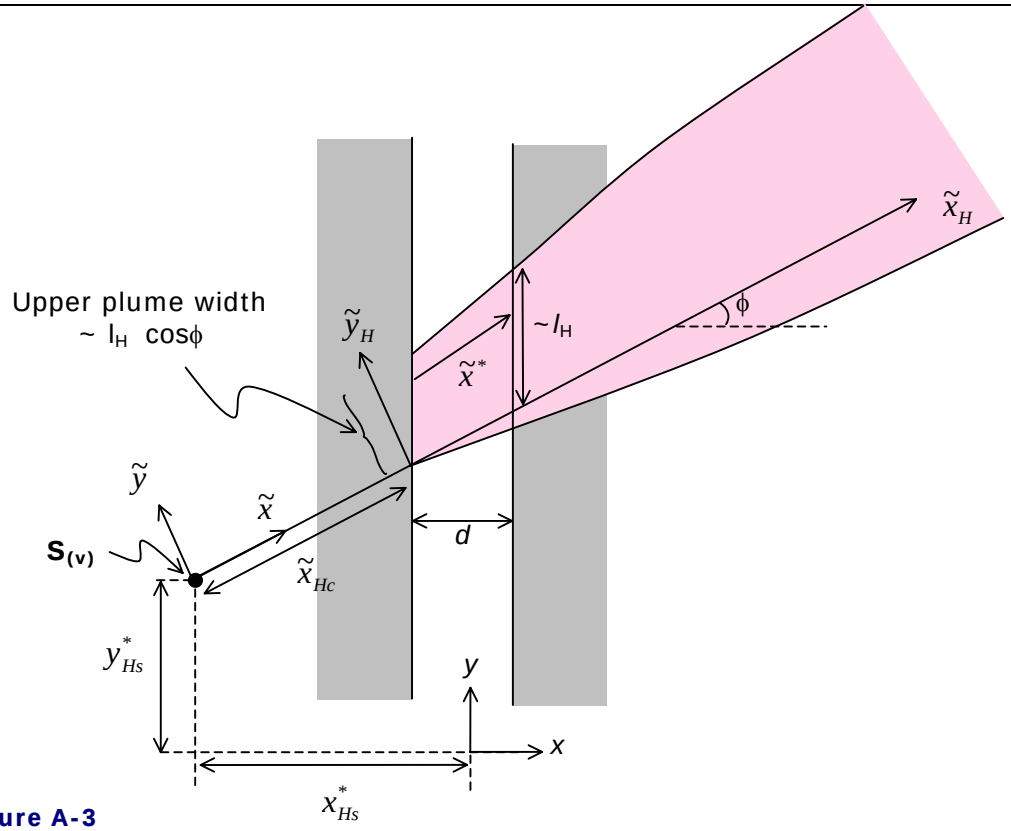

Figure A-3

Therefore, from (A11), the concentration in the upper flow just downwind of the canyon has the form of a line plume (with variable strength along the line x = -d/2),

$$C \cong \frac{\overline{q}^*(\tilde{y})}{U_H\sqrt{\pi(K_H/U_H)\tilde{x}^*}} \exp\left\{-z_H^2/[H(K_H/U_H)\tilde{x}^*]\right\} \qquad \text{(A14a)}$$

for $\tilde{x}^* > d/\cos\phi$, $\tilde{y} > 0$, $z > H$. This profile has an asymmetric form relative to the centreline.

Far downwind (Stage (iv) of the plume's development), the profile is determined by dispersion from the virtual source, i.e. for $\tilde{x}^* >> l_H \sim 10H$, $z > 0$

$$C \sim \frac{Q_S}{U_H\pi\tilde{\sigma}_y\sigma_z} \exp\left\{-\left(\frac{\tilde{y}^2}{2\tilde{\sigma}_y^2}\right)+\left(\frac{z_H^2}{2\sigma_z^2}\right)\right\} \qquad \text{(A14b)}$$

where $\tilde{\sigma}_y, \sigma_z$ are functions of $\tilde{x}$ (the distance from the virtual source). (For uniform diffusivity, $\sigma_y^2 = 2(K_H/U_H)x$.) If the buildings and side streets are porous, this solution is valid below the top of the buildings.

An unsteady source with volume M_s released at time t_s in the canyon leads to the formation of a cloud with length $\tilde{\sigma}_x = \sigma_y \cong \sqrt{2\tilde{K}_{xc}\Delta t} \cong \sqrt{2(\tilde{K}_{xc}/U_H)y}$, where $\Delta t = t - t_S$, travelling with speed V_S. (Here $\tilde{K}_{xc}$ is the longitudinal diffusivity in the canyon which is typically 2 or 3 times greater than K_c as a result of shear dispersion, e.g. Pasquill and Smith, 1983.) Consequently, the length of the cloud as it reaches the top of the canyon ($\tilde{\sigma}_x(\tilde{x} \sim l_H)$) is very much greater than the width (d) of the canyon, i.e.

$$\tilde{\sigma}_x(\tilde{x} \sim l_H) \sim l_H \sim 10H >> d$$

Therefore the profile within the cloud, $C_{c,c}$ within and above the canyon is similar to that within the plume, $C_{p,c}$, given by (A10a), i.e. for z > H,

$$C_{c,c} = C_{p,c} = \frac{1}{\sqrt{2\pi}\sigma_x} \exp\left\{-\frac{(y - V_S\Delta t)^2}{2\tilde{\sigma}_x^2}\right\} \cdot \left(\frac{V_c M_S}{Q_S}\right) \qquad \text{(A15a)}$$

Now the flux $q_{H,c}$ into the upper flow per unit area per unit time varies with y and time:

$$q_{H,c}(y, t) = \frac{M_S U_H}{Q_S} q_H(y) \cdot \frac{1}{\sqrt{2\pi}\sigma_x} \exp\left\{-\frac{(y - V_S\Delta t)^2}{2\tilde{\sigma}_x^2}\right\} \qquad \text{(A15b)}$$

The effective virtual source is at the same location as for the plume. The cloud concentration in relation to the plume concentration (A14a) is

$$C_{c,H} = C_{p,c} \times q_{Hc}(y, t) / q_H(y) \qquad \text{(A16a)}$$

Far downwind,

$$C(\tilde{x}, \tilde{y}, z') \sim \frac{2M}{(2\pi)^{3/2}\tilde{\sigma}_x\tilde{\sigma}_y\sigma_z} \exp\left\{-\left[\frac{(\tilde{x} - U_H\Delta t)^2}{2\tilde{\sigma}_x^2} + \frac{\tilde{y}^2}{2\tilde{\sigma}_y^2} + \frac{z^2}{2\sigma_z^2}\right]\right\} \qquad \text{(A16b)}$$

Effect on atmospheric dispersion of changing land use around Heathrow

A report prepared for ADMLC by

D J Harvey

ADM Ltd

This study was funded by the UK Atmospheric Dispersion Modelling Liaison Committee

Publication date: January 2003
The Lodge, The Long Road
Farnham
Surrey GU10 4DL

CONTENTS

1 INTRODUCTION

Atmospheric dispersion models require a number of parameters (eg, wind speed, wind direction, temperature and cloud cover) describing the state of the atmosphere into which pollutants are dispersed. Traditionally these parameters have come from manual surface observations of weather conditions made each hour. Because of the uncertain nature of the atmosphere and normal year to year variation in weather, it is usual to use a number of years of hourly observations of meteorological data when making predictions of dispersion in the atmosphere. Often dispersion modellers are faced with a difficult choice on the selection of the most representative observing station from which to obtain meteorological data. Sometimes there is a difficult choice to be made between a close observing station for which only old data are available and a more distant station where recent data are available.

Concerns about climate change and changing land use often raise concerns that meteorological data from any one observing station will have a fixed 'lifetime'. This is to say that data before a certain time should not be used or the increased uncertainties in model predictions need to be acknowledged if it is used. This study investigates whether meteorological data can have a lifetime.

Using meteorological data from London Heathrow Airport measured over the past 50 years; this study investigates whether the increased development and urbanisation of the area is reflected in the meteorological data and whether this in turn affects the results of dispersion modelling.

This study has been undertaken by Atmospheric Dispersion Modelling (ADM) Ltd of behalf of the Atmospheric Dispersion Modelling Liaison Committee (ADMLC).

This study follows earlier work undertaken by the Meteorological Office for ADMLC which concluded that meteorological data sets can have a 'lifetime', especially sites such as Heathrow where there has been significant change in land use over the years (NRPB, 2002). Concern has been raised however that the stack height and grid size used in the modelling study have reduced the confidence in the findings and conclusion of the study. This study repeats some of the previous work, uses two additional sources and a grid size that ensures the maximum concentrations are captured. In addition, predictions have been made to see if the effects on dispersion of the urbanisation of the region surrounding Heathrow can be replicated in the modelling.

The remainder of the report is structured as follows:

- Section 2 - Description of the methodology
- Section 3 - Prediction and discussion of time series meteorological data
- Section 4 - Prediction and discussion of spot and hourly average meteorological data
- Section 5 - Provides a summary and conclusions.

2 METHODOLOGY

2.1 Introduction

This section describes the methodology and assumptions of this study and the emissions data used.

2.2 Model input data

A hypothetical source was used in the study reported in NRPB-W3 (2002), this source and two additional hypothetical ones have been used in this investigation, as shown in Table 2.1. 'The data shown in the table for the study reported in NRPB-W3 source are, where possible, taken from the NRPB report, but have been supplemented by ADM Ltd's best estimates for quantities whose values are not presented in the report (eg, roughness length). Of the two grid sizes given, the 50km grid was used in the study reported in NRPB-W3.

TABLE 2.1 Model input data

Parameters	Study reported in NRPB-W3	Additional source one	Additional source two
Grid Reference (m)	0,0	0,0	0,0
Stack Height (m)	10	40	150
Exit Diameter (m)	1.0	1.0	4.0
Exit Velocity (m s^{-1})	15	5	25
Flue gas emission temp (deg C)	150	15	130
Pollutant Mass Emission Rate (g s^{-1})	1000	1000	1000
Grid Size (km)	Grid A: 50 x 50 Grid B: 0.5 x 0.5	2 x 2	7.5 x 7.5
Grid Spacing (m)	Grid A:1,667 Grid B: 16.7	67	250
Common Values			
Number of Grid Points	31 by 31		
Surface Roughness (m)	0.2		
Latitude (deg)	52		
ADMS Options (buildings/terrain etc)	none used		
Met Options	Hourly Met data with 10 deg Sectors		

The source used in the study reported in NRPB-W3 (2002) was selected to ensure that the predictions presented in the previous study can be reproduced. The two additional sources were selected from the sources used in the Environment Agency's October 2000 inter-comparison study (R&D Tech Rep P353). This will facilitate cross referencing of the predicted concentrations with other work and the finding of this study will be representative of a wider range of sources.

2.3 Factors affecting dispersion

There are a number of factors that will affect how emissions disperse once released to atmosphere. The five factors having the greatest effect on dispersion are:

- physical characteristics of the emissions;
- weather;
- nature of the surface;
- terrain; and
- building downwash.

For the purpose of this study the effects of terrain and building downwash have been excluded.

2.3.1 Physical characteristics of the emissions

Provided that exhaust gases have sufficient velocity at stack exit to overcome the effects of stack tip downwash, which is almost certainly the case for stack exit velocities of 15 m s^{-1} or more, the physical characteristics of the flue gases will determine the amount of plume rise and hence the effect on ground level pollutant concentrations. The degree of plume rise usually depends on the greater of the thermal buoyancy or momentum effects.

The physical exit parameters of the three sources modelled are as described below.

- **Study Reported in NRPB-W3;** 10 m high source with exit velocity of 15 m s^{-1} and temperature of 150 deg C. For almost all wind speeds the emissions from this source will rise clear of the stack and the final plume rise will be determined by the buoyancy of the plume. Dispersion from this source will be influenced by near surface effects due to its low, 10 m release height.
- **Additional Source 1;** This 40 m high low buoyancy and low momentum source will not have much plume rise. For wind speeds greater than about 8 m s^{-1}, emissions from this source will be drawn down into the lea of the stack, effectively reducing the stack height. This effect is known as stack tip downwash. It should however be noted that this effect is only included in the ADMS dispersion model when the building model is being run. This source is referred to in this report as having no buoyancy; in practice for ambient temperature of less than 15 deg C there will be some minor buoyancy effects.
- Additional Source 2; The 150 m high, 130 deg C emission is representative of a large incinerator or power generating plant where plume rise is determined by the buoyancy of the emissions. Given the 25 m s^{-1} exit velocity, there will be no stack tip downwash.

2.3.2 Weather

The most important meteorological parameters governing the atmospheric dispersion of pollutants are wind speed, wind direction and atmospheric stability.

- Wind direction determines the broad transport of the plume and the sector of the compass into which the plume is dispersed.

- Wind speed can affect plume dispersion by increasing the initial dilution of pollutants and inhibiting plume rise.
- Atmospheric stability is a measure of the turbulence of the air, particularly of the vertical motions present. For dispersion modelling purposes, one method of classifying stability is by the use of Pasquill Stability categories, A to F. Another is by reference to the surface heat flux present at the ground.

New generation dispersion models, such as ADMS and AERMOD, do not allocate the degree of atmospheric turbulence into discrete categories as was the case with models such as ISC and R91. These models use a parameter known as the Monin-Obukhov length which, together with the wind speed, describes the degree of turbulence in the atmosphere. The Monin-Obukhov length is derived from a number of parameters which include temperature, cloud cover, wind speed, time of the day and day of the year.

2.3.3 Nature of the surface

Roughness Length (Zo)

The nature of the surface can have a significant influence on dispersion by affecting the velocity profile with height and the amount of atmospheric turbulence. Estimating surface roughness is difficult and prone to error and can only be directly estimated if the wind velocity profile (with height) is known. The surface roughness length is influenced by the characteristics of the surface over which the wind has blown over a distance of some kilometres. Changes in the size of surface elements will result in changes to the velocity profile, which may only become fully established some kilometres down wind of the point of change. For any site it is likely that the actual velocity profile will not be matched by any one roughness length, and the velocity profile will vary depending on the wind direction and time of year. The profile is also likely to change over the years if the land use around the site changes.

For large airports in urban areas such as Heathrow, the actual roughness length will be affected by both the surrounding urban environment and the open flat nature of the airport. The terms rural and urban are often used as shorthand when discussing roughness. Urban implies relatively rough surfaces (buildings, etc) and rural implies relatively smooth surface (sea, grassland, etc). In reality urban and rural may be very rough or very smooth and all things in between. In this study urban is taken to mean rough and rural as smooth.

In the centre of Heathrow, for instance, the low part of the boundary layer may be 'rural' in nature (say Zo of 0.1 m to 0.3 m) and the upper part of the boundary layer may be 'urban' in nature (say Zo of 0.3 m to 1.0 m). The UK Meteorological Office estimate the surface roughness length at Heathrow to be 0.2 m; it is not known how or when this estimate was made (personal comm).

The US Environmental Protection Agency modelling guidance (Appendix W) (US EPA) suggests two methods for determining whether 'urban' or 'rural' dispersion parameters should be used in ISC. Both methods are based on a 3 km radius of the site, suggesting that this is the distance of the upwind fetch needed to establish a

boundary layer profile that is not changing distance down wind. The methods are based on either land use or population density, although caution is advised when using the population density approach. The land use method suggests the use of ‘urban’ coefficients if more than 50% of the area within 3 km of the site has buildings.

Figure 2.1 shows the land use in the region of Heathrow as it was in 1950 and again in 2000. The figure shows that there has been a significant change in land use. An approximate estimate of the land area covered by buildings within 3 km of the centre of Heathrow in 1950 is 6%; this increased to about 37% by 2000. The estimate of land use suggests that the dispersion parameters in the region of Heathrow has moved from 'rural' to nearly 'urban' over the 50 year study period. It is therefore suggested that the roughness length in the region of Heathrow has changed from being rural in nature to urban in nature over the 50 years that meteorological data have been recorded at Heathrow. In any case, it is certain that the roughness length will have increased over this period.

Albedo and Bowen Ratio

The albedo is the fraction of total incident solar radiation reflected. Typical values range from 0.1 for dense forests to 0.9 for fresh snow.

The daytime Bowen ratio is an indicator of surface dryness. While the diurnal variation of the Bowen ratio may be significant, the Bowen ratio usually attains a fairly constant value during the day. Midday values of the Bowen ratio range from 0.1 over water to 10.0 over desert.

Both the Albedo and Bowen ratio will have changed as the land around Heathrow has been developed. The effects that changes in these parameters have on dispersion have not been investigated in this study. It is possible that these parameters may have similar or greater effect on dispersion than roughness length.

2.4 Meteorological data

Table 2.2 shows a summary of the meteorological data used in this assessment.

TABLE 2.2 Heathrow meteorological data

Year	Spot measurements*	Hourly average measurements
1950	✓	
1955	✓	
1960	✓	✓
1965	✓	✓
1970		✓
1975		✓
1980		✓
1985	✓	✓
1993		✓
1996		✓
1999		✓

* Spot observations are 10 minute average values.

Historically, measurements were either taken manually or were read manually from charts; for this reason 10 minute averages were estimated running up to the hour to which they were assigned. These data are termed spot measurements. As automatic data collection became more widespread, true averages of the data over the whole hour were reported. It should be noted that for light wind speeds the one hour average wind direction may not have much meaning.

Predictions have been made with all the meteorological data sets listed in the table above.

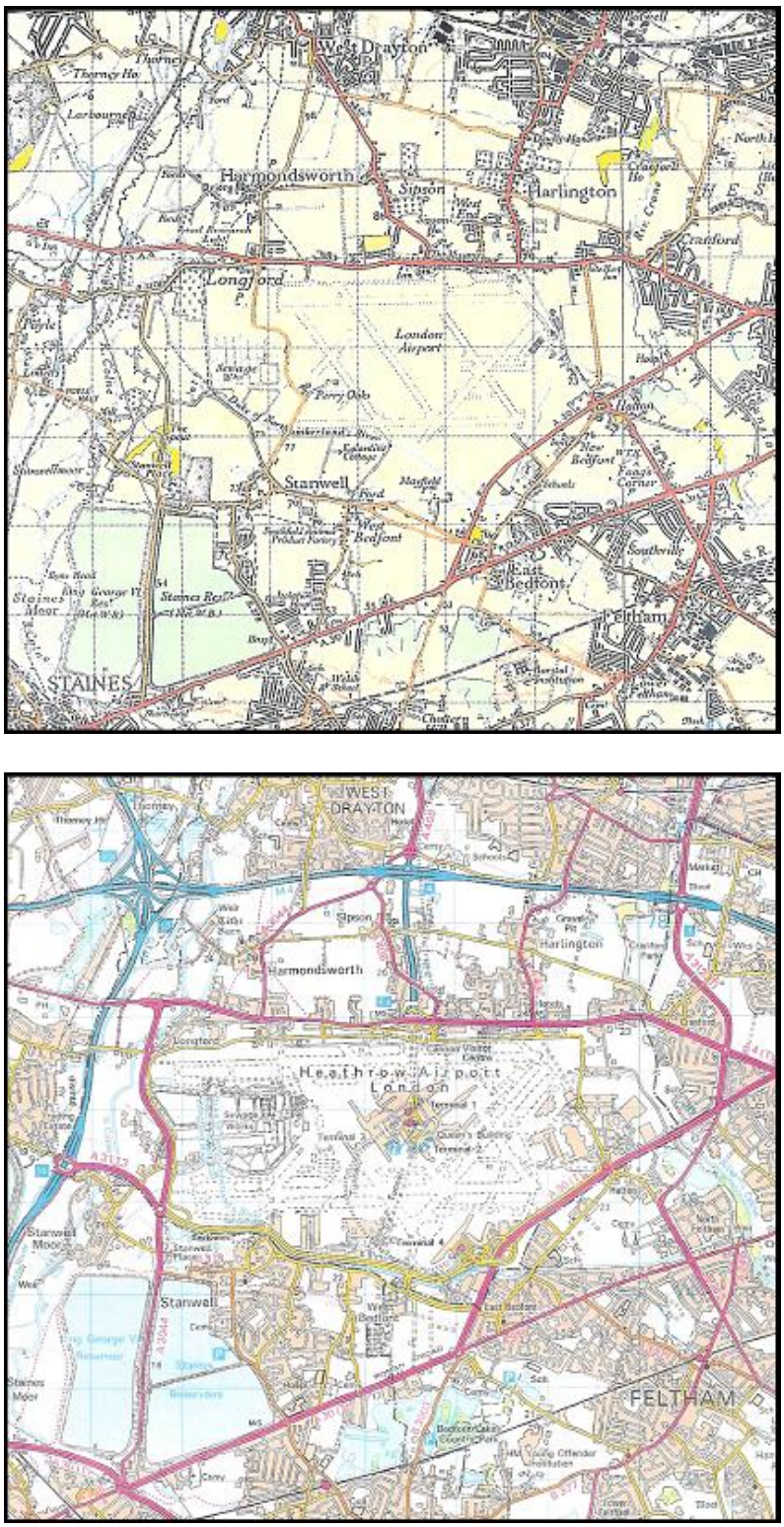

FIGURE 2.1 Land use around Heathrow (1950 and 2000)

Reproduced under the terms of the OS Pan-Government Licence Agreement

2.5 Receptor grid spacing

If the receptors grid spacing is too large, the possibility exists that the maximum ground level concentration may be missed. If the maximum is missed one may find that apparent changes in maximum concentrations are due to small changes in the location of an unchanging maximum. The receptor spacing should be such that adding more receptors on a finer grid would not significantly increase the reported maximum concentration. In practice the selection of receptor spacing is a compromise between model limitations, computer processing time and a desire to understand the extent of the impacts on air quality. Environment Agency guidance suggests the use of a grid resolution equal to 1.5 times the stack height (LAQM, 2002). Table 2.3 shows the receptor spacing used in the study reported in NRPB W3 and that used in this further work.

TABLE 2.3 Receptor spacing

Source/study	Stack height (m)	Receptor Spacing (m)	Receptor spacing/ stack height
Study reported in NRPB-W3	10	1,667	167
ADM Ltd Study with NRPB-W3 Source	10	16.7	1.7
ADM Ltd Study Additional Source One	40	67	1.7
ADM Ltd Study Additional Source Two	150	250	1.7

3 PREDICTED CONCENTRATIONS AND DISCUSSION – TIME SERIES OF METEOROLOGICAL DATA

3.1 Introduction

This section describes the predicted concentrations and presents a discussion of the findings resulting from modelling the sources, with the different years of meteorological data; all other parameters were kept constant.

3.2 Predicted concentrations using the time series of meteorological data

Predictions have been made of the ground level concentrations for the statistics and scenarios shown in Table 3.1. In each case predictions have been made with each of the 14 sets of meteorological data assuming a surface roughness length at both the observing station and modelled emission source of 0.2 m.

TABLE 3.1 Description of model runs

Scenario		
Source	Grid size	Receptor spacing
10 m Stack with Buoyancy	50 km by 50 km	1667 m
10 m Stack with Buoyancy	500 m by 500 m	16.7 m
40 m Stack no Buoyancy	2 km by 2 km	66.7 m
150 m Stack with Buoyancy	7.5 km by 7.5 km	250 m
Percentiles Predicted		
15 Minute Average	Hourly Average	
100, 99.9	100, 99.9, 99.8, 99.7, 99.6, 99.5, 99, 98, 95, 90, 80	

Table 3.2 shows complete details of the 86 separate ADMS 3.1 model runs and the maximum predicted ground level concentrations for each model run. The presented predictions are the concentrations at the receptor where the maximum concentration for a given statistic is predicted. For example the 99.8th percentile of hourly averages is the maximum 18th highest hourly concentration at any of the receptor grid locations.

3.3 10 m stack with buoyancy

Predictions have been made with the source data used in the study reported in NRPB-W3 (2002) to ensure that the previous findings are reproducible by ADM Ltd and that factors such as model version and input data not specified in the previous report do not significantly influence the predicted concentrations.

Table 3.3a shows the predicted concentrations for the 10 m high source for both the original 50 km by 50 km receptor grid (spacing of 1667 m) and the 500 m by 500 m grid (spacing 16.7 m). Where predictions are available for both the spot and hourly average weather data, the hourly average weather data predictions have been presented. A sensitivity analysis of model predictions to the use of spot or hourly average weather data is examined in Section 5 of this report.

Table 3.2 Maximum predicted ground level concentrations for each model run

Run name				Description	Met data/Ro(m)	Spot/ mean	Ro (m)	Grid size	Source height (m)	Diameter (m)	Temp (deg C)	Velocity (m/s)	Emission rate (g/s)
1	10	50s	L	10 m with Buoyancy	1950 / 0.2	spot	0.2	50 km by 50 km	10	1.0	150	15	1000
2	10	55s	L		1955 / 0.2	spot	0.2			1.0	150	15	1000
3	10	60s	L		1960 / 0.2	spot	0.2			1.0	150	15	1000
4	10	65s	L		1965 / 0.2	spot	0.2			1.0	150	15	1000
5	10	85s	L		1985 / 0.2	spot	0.2			1.0	150	15	1000
6	10	60	L		1960 / 0.2	mean	0.2			1.0	150	15	1000
7	10	65	L		1965 / 0.2	mean	0.2			1.0	150	15	1000
8	10	70	L		1970 / 0.2	mean	0.2			1.0	150	15	1000
9	10	75	L		1975 / 0.2	mean	0.2			1.0	150	15	1000
10	10	80	L		1980 / 0.2	mean	0.2			1.0	150	15	1000
11	10	85	L		1985 / 0.2	mean	0.2			1.0	150	15	1000
12	10	93	L		1993 / 0.2	mean	0.2			1.0	150	15	1000
13	10	96	L		1996 / 0.2	mean	0.2			1.0	150	15	1000
14	10	99	L		1999 / 0.2	mean	0.2			1.0	150	15	1000
15	10	50s	S	10 m with Buoyancy	1950 / 0.2	spot	0.2	500 m by 500 m	10	1.0	150	15	1000
16	10	55s	S		1955 / 0.2	spot	0.2			1.0	150	15	1000
17	10	60s	S		1960 / 0.2	spot	0.2			1.0	150	15	1000
18	10	65s	S		1965 / 0.2	spot	0.2			1.0	150	15	1000
19	10	85s	S		1985 / 0.2	spot	0.2			1.0	150	15	1000
20	10	60	S		1960 / 0.2	mean	0.2			1.0	150	15	1000
21	10	65	S		1965 / 0.2	mean	0.2			1.0	150	15	1000
22	10	70	S		1970 / 0.2	mean	0.2			1.0	150	15	1000
23	10	75	S		1975 / 0.2	mean	0.2			1.0	150	15	1000
24	10	80	S		1980 / 0.2	mean	0.2			1.0	150	15	1000
25	10	85	S		1985 / 0.2	mean	0.2			1.0	150	15	1000
26	10	93	S		1993 / 0.2	mean	0.2			1.0	150	15	1000
27	10	96	S		1996 / 0.2	mean	0.2			1.0	150	15	1000
28	10	99	S		1999 / 0.2	mean	0.2			1.0	150	15	1000

Table 3.2 (contd)

Run	name			Predictions with one hour averaging time (µg m^{-3})														15 minute averaging time (µg m^{-3})		
				Annual average	100	99.9	99.8	99.7	99.6	99.5	99	98	95	90	80	60	50	Annual average	100	99.9
1	10	50s	L	217	4,755	4,482	4,099	3,936	3722	3392	2752	2130	1472	887	110	0	0	226	7870	6775
2	10	55s	L	206	4,813	4,645	4,568	4,288	4110	4082	3636	2741	1420	706	18	0	0	218	7942	7295
3	10	60s	L	137	5,065	4,464	4,110	3,887	3736	3491	2849	1885	1021	333	13	0	0	142	8227	6927
4	10	65s	L	150	4,882	4,224	4,093	3,925	3781	3529	2724	1934	1104	389	25	0	0	156	8028	6500
5	10	85s	L	130	4,743	4,224	4,099	3,829	3545	3360	2691	1861	1044	443	32	0	0	129	7867	6058
6	10	60	L	131	4,767	4,187	3,883	3,793	3507	3331	2669	1841	1034	407	15	0	0	133	7845	5852
7	10	65	L	147	4,680	4,273	4,055	3,788	3695	3391	2756	2018	1082	358	26	0	0	151	7773	6806
8	10	70	L	174	4,717	4,197	4,104	4,006	3774	3430	2703	1997	1229	619	33	0	0	179	7834	6499
9	10	75	L	132	4,725	4,102	3,963	3,610	3380	3223	2805	1978	984	326	7	0	0	128	7844	5508
10	10	80	L	140	4,732	4,201	4,089	3,921	3731	3471	2835	2013	1047	305	22	0	0	141	7853	6032
11	10	85	L	123	4,787	4,262	4,091	3,888	3744	3451	2615	1872	986	426	31	0	0	125	7807	6482
12	10	93	L	118	4,867	4,209	3,899	3,594	3255	3007	2604	1567	863	333	24	0	0	119	7964	5744
13	10	96	L	113	4,757	4,186	3,784	3,561	3316	3188	2608	1765	846	200	3	0	0	117	7757	6232
14	10	99	L	160	4,680	4,471	4,107	4,063	3977	3837	2849	2162	1209	461	49	0	0	164	7731	7153
15	10	50s	S	5,266	53,203	47,876	47,180	46,888	46675	46367	45328	43242	36091	24909	7184	6	0	5308	56907	49,418
16	10	55s	S	3,275	48,958	47,580	46,737	45,920	45536	45132	42571	38705	28013	13233	390	0	0	3312	55525	48,994
17	10	60s	S	4,105	48,818	47,669	46,734	46,576	46188	45816	43950	41208	32348	19408	1782	0	0	4145	50509	49,234
18	10	65s	S	4,276	48,875	47,727	46,955	46,558	46354	46083	44455	41525	32452	19988	3080	0	0	4311	50526	49,238
19	10	85s	S	4,158	48,877	47,181	46,754	46,078	45783	45585	43408	39970	31440	18605	2796	0	0	4201	50492	48,797
20	10	60	S	4,261	48,782	47,614	46,829	46,584	46314	46072	44569	41893	33718	19976	1929	0	0	4313	51648	49,169
21	10	65	S	4,116	48,846	47,678	46,942	46,382	46094	45778	43949	41193	31902	18737	3028	0	0	4142	50443	49,303
22	10	70	S	4,230	49,136	47,900	47,156	46,705	46269	45952	44431	41905	33569	19261	3278	0	0	4261	50738	49,592
23	10	75	S	3,207	48,541	46,864	46,303	45,838	44979	44362	41989	37727	25940	13534	1295	0	0	3227	50322	48,449
24	10	80	S	3,788	48,942	47,239	46,157	45,372	44858	44277	42244	38907	30048	17536	2004	0	0	3844	51629	48,703
25	10	85	S	3,676	48,501	46,847	46,234	45,628	44999	44615	42243	38640	29206	15738	1791	0	0	3721	50257	48,333
26	10	93	S	2,917	48,828	46,015	45,603	44,828	43968	43360	40002	35222	24292	11613	742	0	0	2954	50655	47,601
27	10	96	S	2,886	48,690	46,933	46,009	45,271	44454	43761	41267	37059	25000	10229	167	0	0	2910	50381	48,427
28	10	99	S	4,221	48,345	46,923	46,225	45,417	45182	44687	42187	39026	31118	19334	3690	1	0	4280	50033	48,583

Table 3.2 (contd)

Run name	Description	Met data/Ro(m)	Spot/ mean	Ro (m)	Grid size	Source height (m)	Diameter (m)	Temp (deg C)	Velocity (m/s)	Emission rate (g/s)
29 _40 50s	40 m Stack no Buoyancy	1950 / 0.2	spot	0.2	2,000 m by 2,000 m	40	1.0	15	5	1000
30 _40 55s		1955 / 0.2	spot	0.2			1.0	15	5	1000
31 _40 60s		1960 / 0.2	spot	0.2			1.0	15	5	1000
32 _40 65s		1965 / 0.2	spot	0.2			1.0	15	5	1000
33 _40 85s		1985 / 0.2	spot	0.2			1.0	15	5	1000
34 _40 60		1960 / 0.2	mean	0.2			1.0	15	5	1000
35 _40 65		1965 / 0.2	mean	0.2			1.0	15	5	1000
36 _40 70		1970 / 0.2	mean	0.2			1.0	15	5	1000
37 _40 75		1975 / 0.2	mean	0.2			1.0	15	5	1000
38 _40 80		1980 / 0.2	mean	0.2			1.0	15	5	1000
39 _40 85		1985 / 0.2	mean	0.2			1.0	15	5	1000
40 _40 93		1993 / 0.2	mean	0.2			1.0	15	5	1000
41 _40 96		1996 / 0.2	mean	0.2			1.0	15	5	1000
42 _40 99		1999 / 0.2	mean	0.2			1.0	15	5	1000
43 150 50s	150 m Stack with Buoyancy	1950 / 0.2	spot	0.2	7,500 m by 7,500 m	150	4	130	25	1000
44 150 55s		1955 / 0.2	spot	0.2			4	130	25	1000
45 150 60s		1960 / 0.2	spot	0.2			4	130	25	1000
46 150 65s		1965 / 0.2	spot	0.2			4	130	25	1000
47 150 85s		1985 / 0.2	spot	0.2			4	130	25	1000
48 150 60		1960 / 0.2	mean	0.2			4	130	25	1000
49 150 65		1965 / 0.2	mean	0.2			4	130	25	1000
50 150 70		1970 / 0.2	mean	0.2			4	130	25	1000
51 150 75		1975 / 0.2	mean	0.2			4	130	25	1000
52 150 80		1980 / 0.2	mean	0.2			4	130	25	1000
53 150 85		1985 / 0.2	mean	0.2			4	130	25	1000
54 150 93		1993 / 0.2	mean	0.2			4	130	25	1000
55 150 96		1996 / 0.2	mean	0.2			4	130	25	1000
56 150 99		1999 / 0.2	mean	0.2			4	130	25	1000

Table 3.2 (contd)

Run	name		Predictions with one hour averaging time (µg m^{-3})														15 minute averaging time (µg m^{-3})		
			Annual average	100	99.9	99.8	99.7	99.6	99.5	99	98	95	90	80	60	50	Annual average	100	99.9
29	_40	50s	868	63,774	27,970	19,605	17,121	15064	13986	10371	7951	6139	3857	608	0	0	887	67186	29,166
30	_40	55s	825	101,657	55,458	46,102	38,460	34034	28723	18485	12156	6559	2654	22	0	0	855	113354	56,978
31	_40	60s	714	89,003	50,312	44,224	36,494	31079	26812	14393	9285	5395	2963	117	0	0	720	102062	51,778
32	_40	65s	772	78,841	61,650	54,806	39,803	33516	28164	15006	8524	5571	3140	214	0	0	779	88932	63,819
33	_40	85s	899	78,201	48,770	40,911	33,916	29559	24714	16934	11366	6303	3844	381	0	0	905	85855	51,979
34	_40	60	747	71,535	49,984	37,133	31,450	24472	20921	14542	10190	5685	3159	144	0	0	758	74397	50,825
35	_40	65	748	63,434	38,787	31,007	27,600	24771	20961	13808	8352	5517	2959	205	0	0	755	65249	41,070
36	_40	70	821	91,214	38,886	32,257	26,537	24292	23009	15303	9905	5782	3141	269	0	0	830	98740	40,645
37	_40	75	789	69,431	37,073	31,786	24,362	22346	21530	14802	9472	6270	2923	105	0	0	797	75401	39,460
38	_40	80	874	87,437	43,415	38,255	32,343	28967	24593	15917	9967	6368	3713	163	0	0	894	92003	45,400
39	_40	85	941	81,495	48,156	44,235	40,545	36451	31848	20678	12784	6616	3840	223	0	0	955	101062	51,268
40	_40	93	929	94,355	73,268	58,051	54,850	51278	48538	34417	17312	7142	3004	65	0	0	937	106124	75,924
41	_40	96	716	93,288	51,706	44,582	38,558	33046	27701	18930	12188	5603	2099	10	0	0	721	115082	55,177
42	_40	99	1103	128,996	62,435	54,848	49,229	45752	42336	25840	15406	7269	4458	627	0	0	1117	146556	65,364
43	150	50s	8.0	373	260	237	229	220	213	191	150	61	10	0	0	0	8	424	288
44	150	55s	5.4	436	283	252	235	219	208	167	114	29	0	0	0	0	6	459	304
45	150	60s	6.4	416	298	254	225	208	199	166	132	45	3	0	0	0	7	465	327
46	150	65s	6.8	473	275	237	222	215	210	181	131	49	4	0	0	0	7	510	290
47	150	85s	6.1	446	283	250	233	221	209	171	127	37	3	0	0	0	6	481	310
48	150	60	7.1	415	291	271	241	225	208	179	143	49	4	0	0	0	7	466	316
49	150	65	6.4	386	261	231	223	213	204	168	124	44	3	0	0	0	7	444	293
50	150	70	7.3	437	268	246	234	225	219	193	151	46	4	0	0	0	7	487	295
51	150	75	5.0	437	273	255	240	228	220	181	110	16	0	0	0	0	5	486	296
52	150	80	5.0	424	260	236	219	204	198	163	107	31	2	0	0	0	5	478	288
53	150	85	5.4	443	288	255	237	221	214	176	111	31	1	0	0	0	6	480	311
54	150	93	5.1	463	299	267	241	216	205	167	109	20	0	0	0	0	5	493	318
55	150	96	4.2	392	276	243	223	207	193	150	90	16	0	0	0	0	4	484	303
56	150	99	6.0	492	294	243	228	216	206	174	115	44	4	0	0	0	6	529	322

Table 3.2 (contd)

Run name				Description	Met data/Ro(m)	Spot/ mean	Ro (m)	Grid size	Source height (m)	Diameter (m)	Temp (deg C)	Velocity (m/s)	Emission rate (g/s)
57	40	99	r	Roughness Length and 40 m Stack	1999 / 0.01	mean	0.01	2000 m by 2000 m	40	1	15	5	1000
58	40	99	r		1999 / 0.1	mean	0.1			1	15	5	1000
59	40	99	r		1999 / 0.2	mean	0.2			1	15	5	1000
60	40	99	r		1999 / 0.3	mean	0.3			1	15	5	1000
61	40	99	r		1999 / 0.4	mean	0.4			1	15	5	1000
62	40	99	r		1999 / 0.5	mean	0.5			1	15	5	1000
63	40	99	r		1999 / 1.0	mean	1.0			1	15	5	1000
64	150	99	r	Roughness Length and 150 m Stack	1999 / 0.01	mean	0.01	7500 by 7500	150	4	130	25	1000
65	150	99	r		1999 / 0.1	mean	0.1			4	130	25	1000
66	150	99	r		1999 / 0.2	mean	0.2			4	130	25	1000
67	150	99	r		1999 / 0.3	mean	0.3			4	130	25	1000
68	150	99	r		1999 / 0.4	mean	0.4			4	130	25	1000
69	150	99	r		1999 / 0.5	mean	0.5			4	130	25	1000
70	150	99	r		1999 / 1.0	mean	1.0			4	130	25	1000
71	10	99	r	Roughness Length and 10 m Stack	1999 / 0.01	mean	0.01	500 by 500	10	1	150	15	1000
72	10	99	r		1999 / 0.1	mean	0.1			1	150	15	1000
73	10	99	r		1999 / 0.2	mean	0.2			1	150	15	1000
74	10	99	r		1999 / 0.3	mean	0.3			1	150	15	1000
75	10	99	r		1999 / 0.4	mean	0.4			1	150	15	1000
76	10	99	r		1999 / 0.5	mean	0.5			1	150	15	1000
77	10	99	r		1999 / 1.0	mean	1.0			1	150	15	1000
78	10	50		Met data site roughness length	1950 / 0.1	mean	0.3	500	10	1	150	15	1000
79	10	80			1980 / 0.2	mean	0.3			1	150	15	1000
80	10	96			1999 / 0.3	mean	0.3			1	150	15	1000
81	40	50			1950 / 0.1	mean	0.3	500	10	1	150	15	1000
82	40	80			1980 / 0.2	mean	0.3			1	150	15	1000
83	40	96			1999 / 0.3	mean	0.3			1	150	15	1000
84	150	50			1950 / 0.1	mean	0.3	500	10	1	150	15	1000
85	150	80			1980 / 0.2	mean	0.3			1	150	15	1000
86	150	96			1999 / 0.3	mean	0.3			1	150	15	1000
87	10	96			1996	Spot	0.2	500	10	1	150	15	1000
88	10	97			1997	Spot	0.2			1	150	15	1000
89	10	98			1998	Spot	0.2			1	150	15	1000
90	10	99			1999	Spot	0.2			1	150	15	1000
91	10	_00			2000	Spot	0.2			1	150	15	1000

Table 3.2 (contd)

Run	name			Predictions with one hour averaging time (µg m^{-3})														15 minute averaging time (µg m^{-3})		
			Annual average	100	99.9	99.8	99.7	99.6	99.5	99	98	95	90	80	60	50	Annual average	100	99.9
57	40	99	r 828	187,459	76,197	64,226	57,718	52,609	48,600	31,350	16,068	5,344	1,501	6	0	0	847	217261	79,535
58	40	99	r 979	145,299	66,457	57,480	51,861	48,086	44,518	27,685	15,466	6,629	3,842	287	0	0	1003	166217	70,973
59	40	99	r 1,103	128,996	62,435	54,848	49,229	45,752	42,336	25,840	15,406	7,269	4,458	627	0	0	1117	146556	65,364
60	40	99	r 1,195	117,687	59,794	51,962	47,318	43,894	40,871	24,928	14,994	7,558	4,931	950	0	0	1209	133083	62,703
61	40	99	r 1,265	108,874	58,412	50,280	45,487	42,781	40,355	25,035	14,867	7,887	5,227	1,289	0	0	1284	122659	61,005
62	40	99	r 1,320	101,900	56,278	48,801	44,233	41,830	39,217	24,305	14,922	8,028	5,478	1,566	0	0	1349	117529	59,506
63	40	99	r 1,545	79,762	50,768	44,160	40,156	37,584	35,039	21,848	14,117	8,643	5,911	2,449	1	0	1571	113561	53,544
64	150	99	r 3.5	451	270	232	209	196	182	133	68	6	0	0	0	0	4	491	302
65	150	99	r 4.7	409	283	235	215	202	194	159	95	29	2	0	0	0	5	445	309
66	150	99	r 6.0	492	294	243	228	216	206	174	115	44	4	0	0	0	6	529	322
67	150	99	r 7.2	509	292	253	233	222	213	182	127	56	7	0	0	0	7	550	318
68	150	99	r 8.2	475	288	260	238	226	221	187	141	68	11	0	0	0	8	516	307
69	150	99	r 9.1	444	278	259	240	229	223	193	153	76	14	0	0	0	9	511	305
70	150	99	r 13.0	432	286	262	255	249	243	214	177	118	34	1	0	0	13	558	313
71	10	99	r 1,649	47,571	42,629	36,419	33,369	31,771	31,038	26,468	22,864	14,632	4,858	52	0	0	1,678	48,671	43,593
72	10	99	r 3,257	46,050	42,154	41,319	40,658	40,292	39,686	36,730	33,600	25,666	14,143	1,624	0	0	3,306	47,046	44,057
73	10	99	r 4,221	48,345	46,923	46,225	45,417	45,182	44,687	42,187	39,026	31,118	19,334	3,690	1	0	4,280	50,033	48,583
74	10	99	r 4,980	51,865	50,114	48,953	48,488	48,261	47,880	45,990	43,170	34,738	22,638	5,629	2	0	5,044	53,289	51,599
75	10	99	r 5,619	54,399	52,410	51,837	51,421	51,036	50,633	49,053	46,293	38,368	25,970	7,605	2	0	5,691	55,906	53,892
76	10	99	r 6,265	56,202	54,456	53,774	53,524	53,174	52,684	51,551	48,887	40,598	28,128	9,877	8	0	6,341	57,836	55,742
77	10	99	r 8,774	64,948	62,088	61,649	61,115	60,921	60,795	59,710	57,738	51,026	38,755	18,603	171	0	8,849	69,234	63,145
78	10	50	5,559	51,949	50,358	49,770	49,207	49,020	48,849	47,383	45,177	37,444	26,107	8,224	14	0	5,596	55,647	51,941
79	10	80	4,217	51,740	49,886	48,824	48,191	47,792	46,993	45,129	42,372	32,887	19,823	2,943	0	0	4,272	53,940	51,448
80	10	96	3,405	51,661	49,857	49,343	48,421	47,844	47,303	44,982	40,833	28,599	13,719	440	0	0	3,431	53,178	51,386
81	40	50	995	71,798	36,119	23,716	21,384	18,911	16,753	12,487	9,217	6,811	4,539	871	0	0	1,015	73,047	37,482
82	40	80	958	89,174	43,843	39,279	36,003	30,233	26,524	17,740	10,998	6,968	4,313	283	0	0	979	93,862	47,131
83	40	96	769	88,653	52,875	44,618	36,918	30,031	27,565	18,267	11,705	5,947	2,606	26	0	0	777	99,337	55,744
84	150	50	8.2	389	268	253	238	232	226	194	158	62	9	0	0	0	8.4	475	297
85	150	80	5.5	419	272	243	232	219	209	173	113	37	3	0	0	0	5.7	490	297
86	150	96	5.0	380	275	243	227	215	202	164	104	23	0	0	0	0	5.0	493	300
87	10	96	2,774	48,751	46,575	45,831	44,810	44,230	43,814	40,951	36,323	23,923	9,679	199	0	0	2,804	50,135	48,164
88	10	97	3,741	48,758	46,928	46,084	45,695	45,167	44,785	42,868	39,816	30,067	16,289	1,198	0	0	3,794	50,409	48,639
89	10	98	3,877	48,969	47,363	46,894	46,179	45,990	45,612	43,509	39,982	29,467	17,324	2,169	0	0	3,910	51,182	48,986
90	10	99	4,349	48,432	47,127	46,584	45,922	45,613	45,301	43,722	40,863	31,680	20,225	3,568	1	0	4,402	50,181	48,863
91	10	00	4,761	48,600	47,101	46,097	45,723	45,516	45,136	43,073	40,235	32,258	22,168	5,538	2	0	4,830	50,128	48,792

TABLE 3.3a Maximum predicted ground level concentrations for 10 m stack (µg m^{-3})

	Percentile (averaging time)					
	1 Hour				15 Minute	Annual
Grid size/year	100	99.9	99.8	99.7	99.9	average
50 km by 50 km (1,667 m spacing)						
1950	4,755	4,482	4,099	3,936	6,775	217
1955	4,813	4,645	4,568	4,288	7,295	206
1960	4,767	4,187	3,883	3,793	5,852	131
1965	4,680	4,273	4,055	3,788	6,806	147
1970	4,717	4,197	4,104	4,006	6,499	174
1975	4,725	4,102	3,963	3,610	5,508	132
1980	4,732	4,201	4,089	3,921	6,032	140
1985	4,787	4,262	4,091	3,888	6,482	123
1993	4,867	4,209	3,899	3,594	5,744	118
1996	4,757	4,186	3,784	3,561	6,232	113
1999	4,680	4,471	4,107	4,063	7,153	160
500 m by 500 m (16.7 m spacing)						
1950	53,203	47,876	47,180	46,888	49,418	5,266
1955	48,958	47,580	46,737	45,920	48,994	3,275
1960	48,782	47,614	46,829	46,584	49,169	4,261
1965	48,846	47,678	46,942	46,382	49,303	4,116
1970	49,136	47,900	47,156	46,705	49,592	4,230
1975	48,541	46,864	46,303	45,838	48,449	3,207
1980	48,942	47,239	46,157	45,372	48,703	3,788
1985	48,501	46,847	46,234	45,628	48,333	3,676
1993	48,828	46,015	45,603	44,828	47,601	2,917
1996	48,690	46,933	46,009	45,271	48,427	2,886
1999	48,345	46,923	46,225	45,417	48,583	4,221

Table 3.3b shows the same data as presented in Table 3.3a but related to predictions for 1950.

TABLE 3.3b Maximum predicted ground level concentrations for 10 m stack (normalised to predictions for 1950)

	Percentile (averaging time)					
	1 hour				15 minute	Annual
Grid size/year	100	99.9	99.8	99.7	99.9	average
50 km by 50 km (1,667 m spacing)						
1950	1.00	1.00	1.00	1.00	1.00	1.00
1955	1.01	1.04	1.11	1.09	1.08	0.95
1960	1.00	0.93	0.95	0.96	0.86	0.60
1965	0.98	0.95	0.99	0.96	1.00	0.68
1970	0.99	0.94	1.00	1.02	0.96	0.80
1975	0.99	0.92	0.97	0.92	0.81	0.61
1980	1.00	0.94	1.00	1.00	0.89	0.65
1985	1.01	0.95	1.00	0.99	0.96	0.57
1993	1.02	0.94	0.95	0.91	0.85	0.54
1996	1.00	0.93	0.92	0.90	0.92	0.52
1999	0.98	1.00	1.00	1.03	1.06	0.74
500 m by 500 m (16.7 m spacing)						
1950	1.00	1.00	1.00	1.00	1.00	1.00
1955	0.92	0.99	0.99	0.98	0.99	0.62
1960	0.92	0.99	0.99	0.99	0.99	0.81
1965	0.92	1.00	0.99	0.99	1.00	0.78
1970	0.92	1.00	1.00	1.00	1.00	0.80
1975	0.91	0.98	0.98	0.98	0.98	0.61
1980	0.92	0.99	0.98	0.97	0.99	0.72
1985	0.91	0.98	0.98	0.97	0.98	0.70
1993	0.92	0.96	0.97	0.96	0.96	0.55
1996	0.92	0.98	0.98	0.97	0.98	0.55
1999	0.91	0.98	0.98	0.97	0.98	0.80

Table 3.3b shows that there are quite significant changes in the annual average concentrations over the years of meteorological data. The changes however for the percentiles are much smaller and quite possibly insignificant.

Figure 3.1 and Figure 3.2 are similar to those presented in the original study and are presented here to allow comparison with the study reported in NRPB-W3.

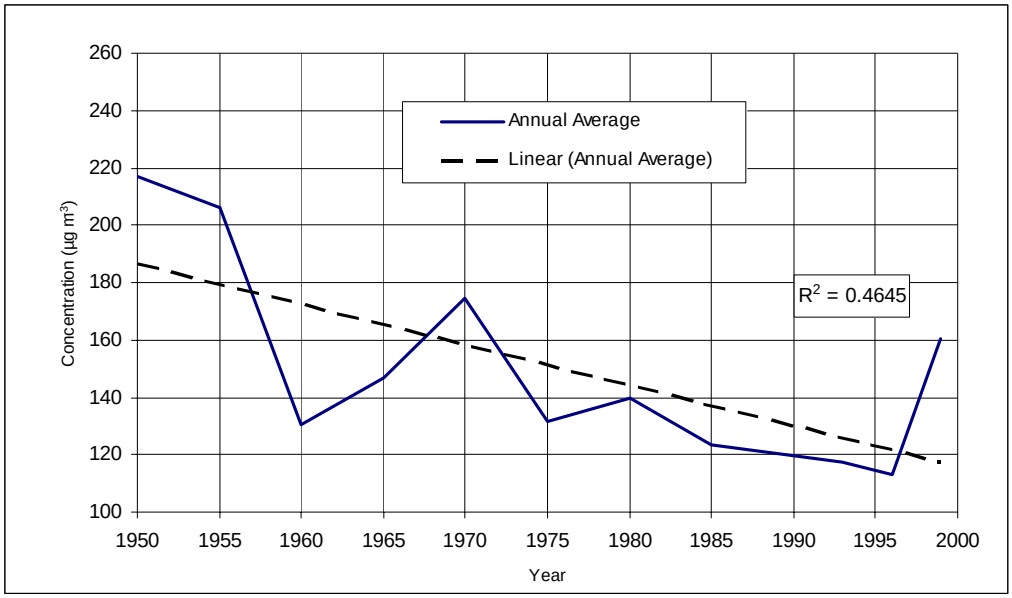

FIGURE 3.1 Maximum predicted annual average ground level concentration for 10 m source with 50 km by 50 km grid size (µg m^{-3})

Figure 3.1 is very similar to Figure A1 in the NRPB-W3 report and both show a downward trend in the maximum predicted annual average ground level concentrations with time. The dotted line shows the best fit straight line, the R^2 value of 0.46 suggests reasonable fit. An R^2 value of 1.0 suggests a perfect fit and R^2 of 0 suggests the data are random and no linear relationship exists.

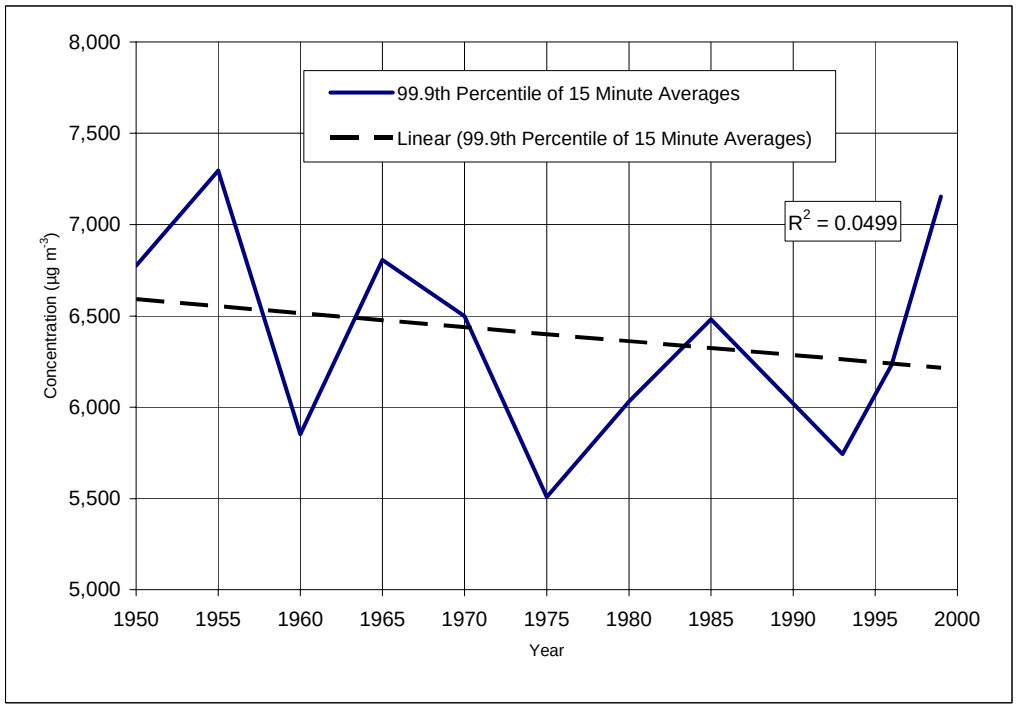

FIGURE 3.2 Maximum predicted 99.9th percentile of 15 minute average ground level concentration for 10 m source with 50 km by 50 km grid size (µg m^{-3})

Although similar in some respects to the Figure A2 presented in the study reported in NRPB-W3, the trend, if any, of maximum predicted concentrations with time is less clear than that of the original work. The R^2 correlation coefficient of 0.05 suggests no linear trend. The differences could be due to the different versions of ADMS used for the two studies, or other parameters such as roughness length that were not specified in the original work.

Using a 500 m by 500 m grid size, Figure 3.3 shows the maximum predicted annual average ground level concentration.

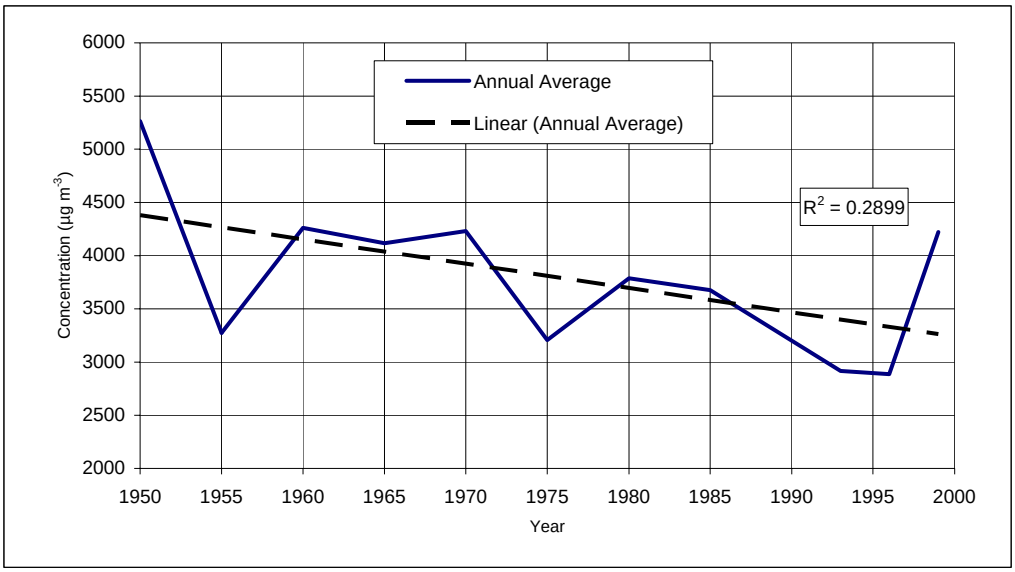

FIGURE 3.3 Maximum predicted annual average ground level concentration for 10 m source with 500 m by 500 m grid size (µg m^{-3})

The use of the small receptor spacing significantly increases the absolute values of the maximum concentrations, demonstrating that the peak concentrations lay in between the receptors modelled in the study reported in NRPB-W3. The trend in the maximum concentrations are however similar in both reports and the R^2 of 0.29 suggests some correlation to a straight line.

Figure 3.4a shows the maximum 99.9th percentile of 15 minute averages for the 10 m high source and 16.7 m spacing receptor grid. The figure shows a better correlation coefficient than that calculated for the larger grid and suggests a downward trend in maximum concentrations with time. Figure 3.4b has been included to illustrate that any downward trend in predictions is not large compared to the magnitude of the predicted concentrations.

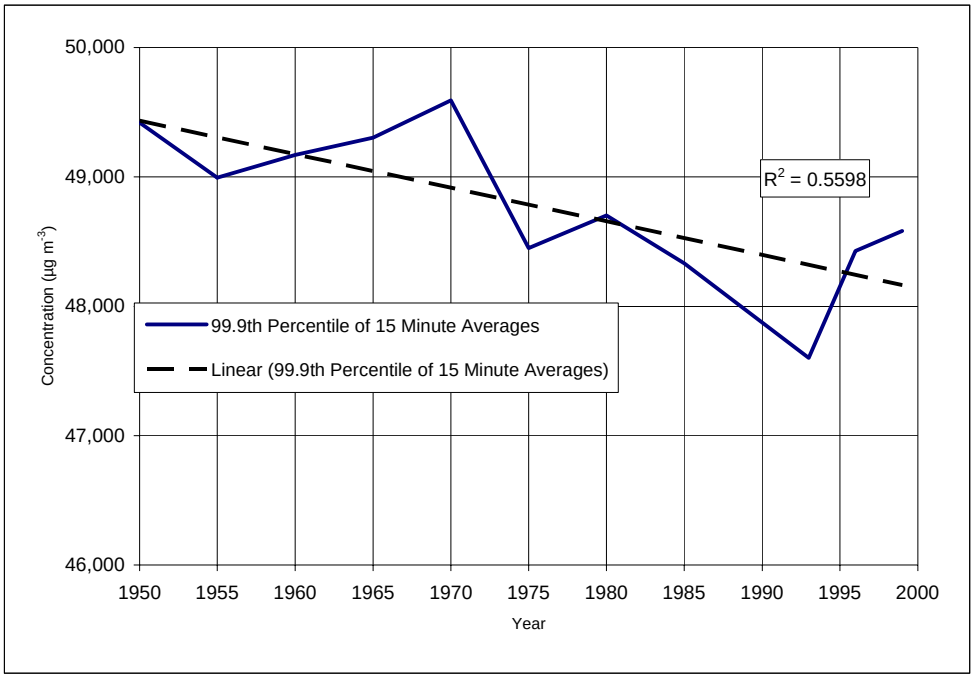

FIGURE 3.4a Maximum predicted 99.9th percentile of 15 minute average ground level concentration for 10 m buoyant source with 500 m by 500 m grid size (µg m^{-3})

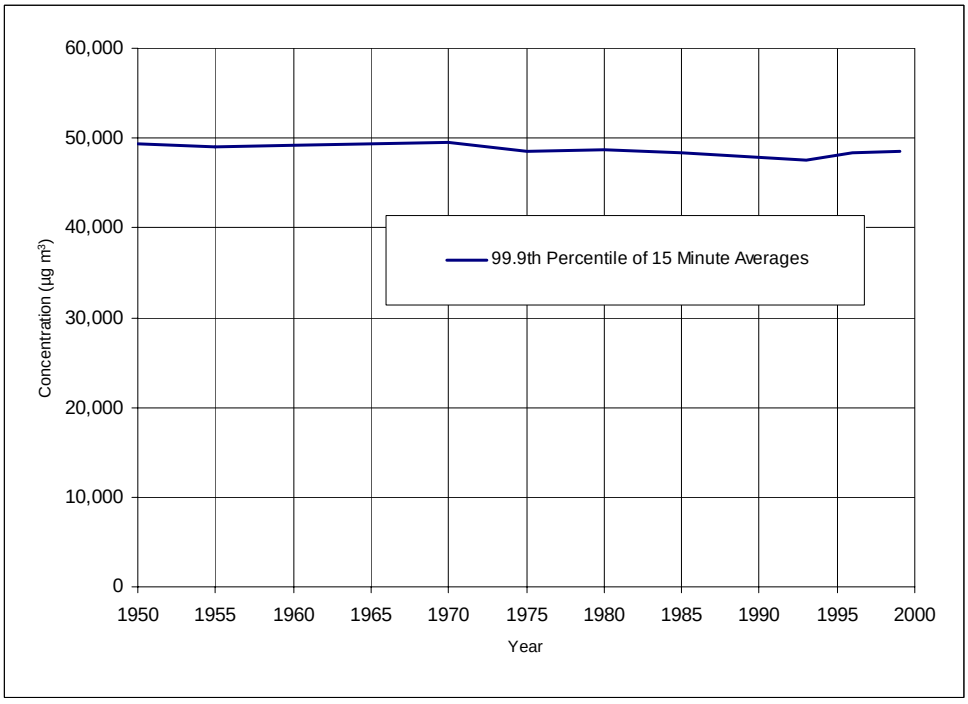

FIGURE 3.4b Maximum predicted 99.9th percentile of 15 minute average ground level concentration for 10 m buoyant source with 500 m by 500 m grid size (µg m^{-3})

Figure 3.5 illustrates that the 16.7 m spaced grid captures the maximum ground level concentration and is a suitable grid size for this source.

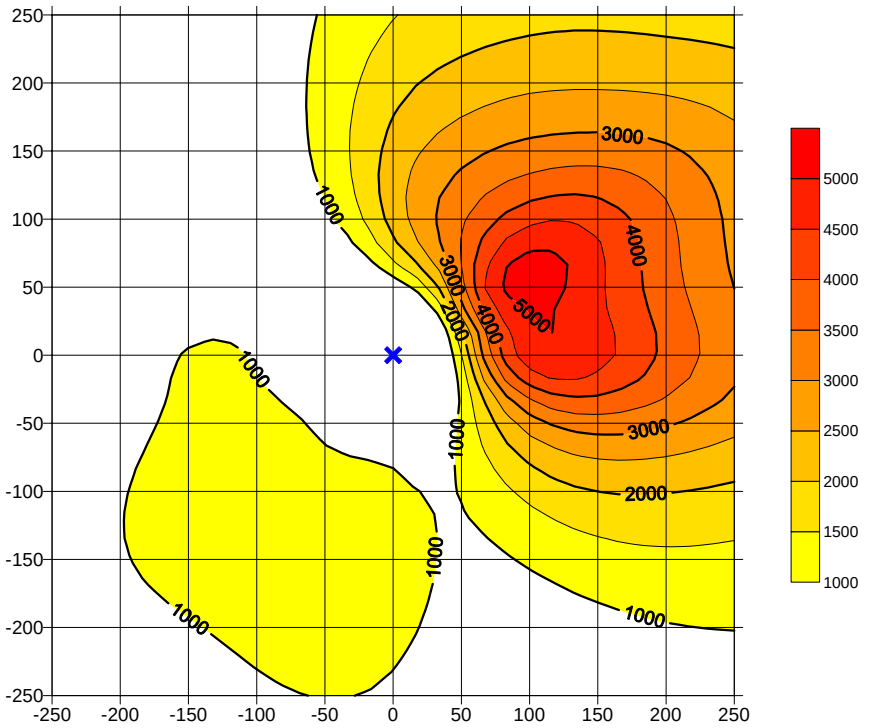

FIGURE 3.5 Maximum predicted annual average ground level concentration for 1950 meteorological data, 10 m high source and 500 m by 500 m grid (µg m^{-3})

Conclusion: For Source 1: (10 m, buoyant source) For the prediction of annual average impacts to maximum ground level concentrations Heathrow meteorological data does have a lifetime. However for statistics tending towards the maximum 1 hour (100^{th} percentile of hourly averages) there may be a statistically significant trend in the maximum predicted concentrations with time as the correlation coefficient (R^2) is 0.6 but this trend appears to be of insignificant practical importance because the year on year variation is small compared to the magnitude of the predicted concentrations.

The choice of a suitable stack height is usually driven by the impact of emissions to short term ground level concentrations (ie, maximum 99.8^{th} and 99.9^{th} percentiles). If these short term ground level concentrations are acceptable then long term (eg, annual averages) ground level concentrations are generally much smaller relative to the ambient air quality criteria. Since, for this type of source, there was no trend of practical importance in maximum predicted short term ground level concentrations the use of historical meteorological data would not have lead to an unsuitable stack height being selected.

3.4 40 m stack, no buoyancy

This section summarises the predictions for a 40 m stack with no buoyancy. To allow comparison with the predictions presented for the 10 m stack, predictions of annual average and 99.9th percentile of 15 minute averages are used to illustrate the effects of meteorological data.

Table 3.4a shows the maximum predicted concentrations for emission from the 40 m stack.

TABLE 3.4a Maximum predicted ground level concentrations for 40 m stack; 2 km by 2 km grid size (µg m^{-3})

	Percentile (averaging time)					
	Hour				15 Minute	Annual
Grid size/year	100	99.9	99.8	99.7	99.9	average
1950	63,774	27,970	19,605	17,121	29,166	868
1955	101,657	55,458	46,102	38,460	56,978	825
1960	71,535	49,984	37,133	31,450	50,825	747
1965	63,434	38,787	31,007	27,600	41,070	748
1970	91,214	38,886	32,257	26,537	40,645	821
1975	69,431	37,073	31,786	24,362	39,460	789
1980	87,437	43,415	38,255	32,343	45,400	874
1985	81,495	48,156	44,235	40,545	51,268	941
1993	94,355	73,268	58,051	54,850	75,924	929
1996	93,288	51,706	44,582	38,558	55,177	716
1999	128,996	62,435	54,848	49,229	65,364	1103

Table 3.4b shows the maximum predicted concentrations for emission from the 40 m stack, normalised to predictions for 1950.

TABLE 3.4b Maximum predicted ground level concentrations for 40 m stack; 2 km by 2 km grid size (normalised to predictions for 1950)

	Percentile (averaging time)					
	Hour				15 minute	Annual
Grid size/year	100	99.9	99.8	99.7	99.9	average
1950	1.00	1.00	1.00	1.00	1.00	1.00
1955	1.59	1.98	2.35	2.25	1.95	0.95
1960	1.12	1.79	1.89	1.84	1.74	0.86
1965	0.99	1.39	1.58	1.61	1.41	0.86
1970	1.43	1.39	1.65	1.55	1.39	0.95
1975	1.09	1.33	1.62	1.42	1.35	0.91
1980	1.37	1.55	1.95	1.89	1.56	1.01
1985	1.28	1.72	2.26	2.37	1.76	1.08
1993	1.48	2.62	2.96	3.20	2.60	1.07
1996	1.46	1.85	2.27	2.25	1.89	0.82
1999	2.02	2.23	2.80	2.88	2.24	1.27

Figure 3.6 shows the maximum predicted 99.9th percentile of 15 minute average and maximum annual average ground level concentrations for the 40 m high source and 2 km by 2 km grid (67 m receptor separation) for each year of meteorological data considered.

The predictions suggest that for the 40 m high non-buoyant source, the maximum ground level concentrations are increasing with time. This raises the possibility that the effect of urbanisation around Heathrow may have differing effects on dispersion depending on the nature of the source.

Figure 3.7 illustrates that the 2 km by 2 km grid (67 m receptor separation) captures the maximum ground level concentration and is a suitable grid size for this source. The separate areas of peak annual average concentrations are a function of the meteorological data and not the grid size. This has been checked by re running this condition with a 51 by 51 receptor grid (40 m spacing), the maximum predicted annual average concentration with a 51 by 51 grid was within 1% of the value for the 31 by 31 grid (67 m spacing).

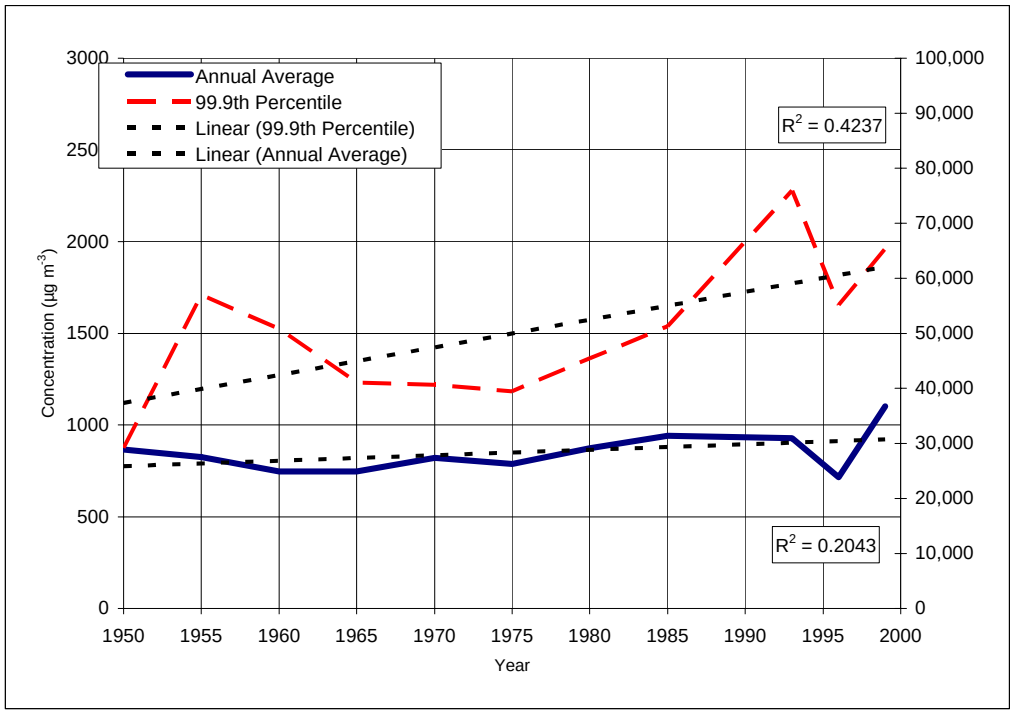

FIGURE 3.6 Maximum predicted 99.9th percentile of 15 minute average ground level concentration (right hand scale) and maximum annual average ground level concentrations (left hand scale) for 40 m non buoyant source with 2 km by 2 km grid size (µg m^{-3})

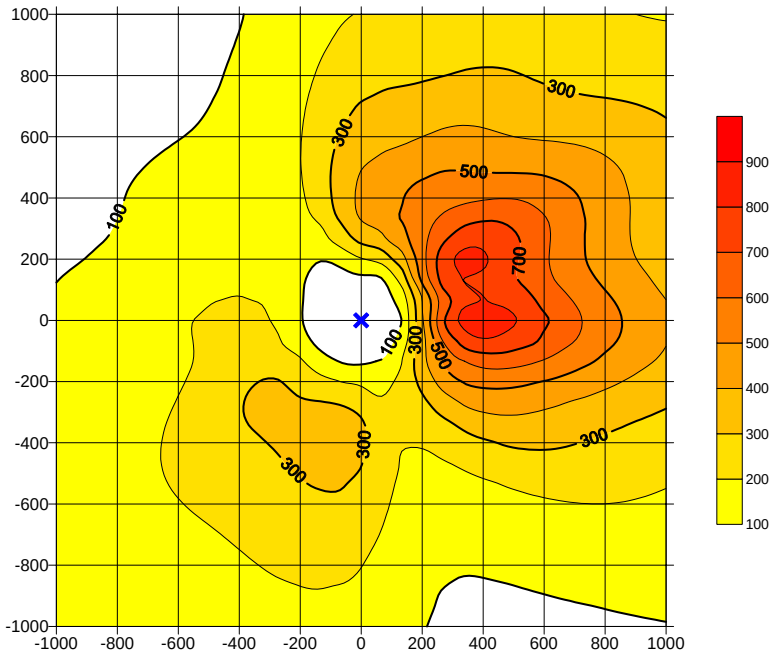

FIGURE 3.7 Maximum predicted annual average ground level concentration for 1950 meteorological data, 40 m high source and 2 km by 2 km grid (µg m^{-3})

Conclusion: For Source 2: (40 m non-buoyant source) For the prediction of impacts to maximum ground level concentrations, Heathrow meteorological data does have a lifetime for all statistics and the magnitude of the year to year change does appear to be of practical significance. All values tend to increase as more recent data are used. The trend is less marked for annual average than the maximum one hour average and higher percentiles

3.5 150 m stack, with buoyancy

This section summarises the predicted ground level concentrations for a 150 m stack with buoyancy. To allow comparison with the previous sections, annual average and 99.9th percentile of 15 minute averages are used to illustrate the effects of meteorological data.

Table 3.5a shows the maximum predicted concentrations for emission from the 150 m stack.

TABLE 3.5a Maximum predicted ground level concentrations for 150 m stack; 7.5 km by 7.5 km grid size, 250 m spacing (µg m^{-3})

	Percentile (averaging time)					
	Hour				15 minute	Annual
Grid size/year	100	99.9	99.8	99.7	99.9	average
1950	373	260	237	229	288	8.0
1955	436	283	252	235	304	5.4
1960	415	291	271	241	316	7.1
1965	386	261	231	223	293	6.4
1970	437	268	246	234	295	7.3
1975	437	273	255	240	296	5.0
1980	424	260	236	219	288	5.0
1985	443	288	255	237	311	5.4
1993	463	299	267	241	318	5.1
1996	392	276	243	223	303	4.2
1999	492	294	243	228	322	6.0

Table 3.5b shows the maximum predicted concentrations for emission from the 150 m stack normalised to those for 1950.

TABLE 3.5b Maximum predicted ground level concentrations for 150 m stack; 7.5 km by 7.5 km grid size, 250 m spacing (normalised to 1950)

	Percentile (averaging time)					
	Hour				15 minute	Annual
Grid size/year	100	99.9	99.8	99.7	99.9	average
1950	1.00	1.00	1.00	1.00	1.00	1.00
1955	1.17	1.09	1.06	1.03	1.06	0.68
1960	1.11	1.12	1.14	1.05	1.10	0.89
1965	1.03	1.00	0.97	0.97	1.02	0.80
1970	1.17	1.03	1.04	1.02	1.02	0.91
1975	1.17	1.05	1.08	1.05	1.03	0.63
1980	1.14	1.00	1.00	0.96	1.00	0.63
1985	1.19	1.11	1.08	1.03	1.08	0.68
1993	1.24	1.15	1.13	1.05	1.10	0.64
1996	1.05	1.06	1.03	0.97	1.05	0.53
1999	1.32	1.13	1.03	1.00	1.12	0.75

Figure 3.8 shows the maximum predicted 99.9th percentile of 15 minute average and maximum annual average ground level concentrations for the 150 m high source and 7.5 km by 7.5 km grid (250 m receptor separation) for each year of meteorological data considered.

Figure 3.9 illustrates that the 7.5 km by 7.5 km grid (250 m receptor separation) captures the maximum ground level concentration and is a suitable grid size for this source. The two lung shaped areas of peak annual average concentrations are a function of the meteorological data and not the grid size. This has been checked by re running this condition with a 51 by 51 receptor grid with receptor spacing of 150 m, equal to the stack height.

The predictions suggest that for the 150 m high buoyant source the maximum predicted annual average ground level concentration may be decreasing with time, whereas the 99.9th percentile of annual average ground level concentrations may be slightly increasing with time. This set of predictions casts further doubt on the trends in predicted ground level concentrations with time. It appears possible that a combination of stack height and source characteristics could be found that would show negligible change in maximum predicted ground level concentrations with time.

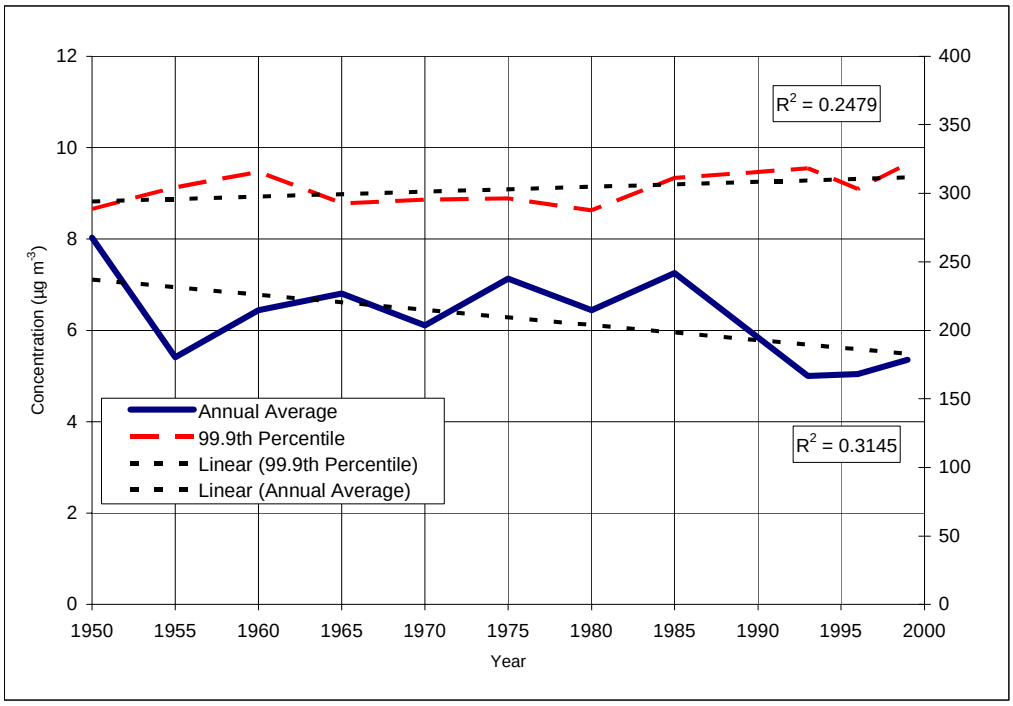

FIGURE 3.8 Maximum predicted 99.9th percentile of 15 minute average ground level concentration (right hand scale) and maximum annual average ground level concentrations (left hand scale) for 150 m buoyant source with 7.5 km by 7.5 km grid size, 250 m receptor spacing (µg m^{-3})

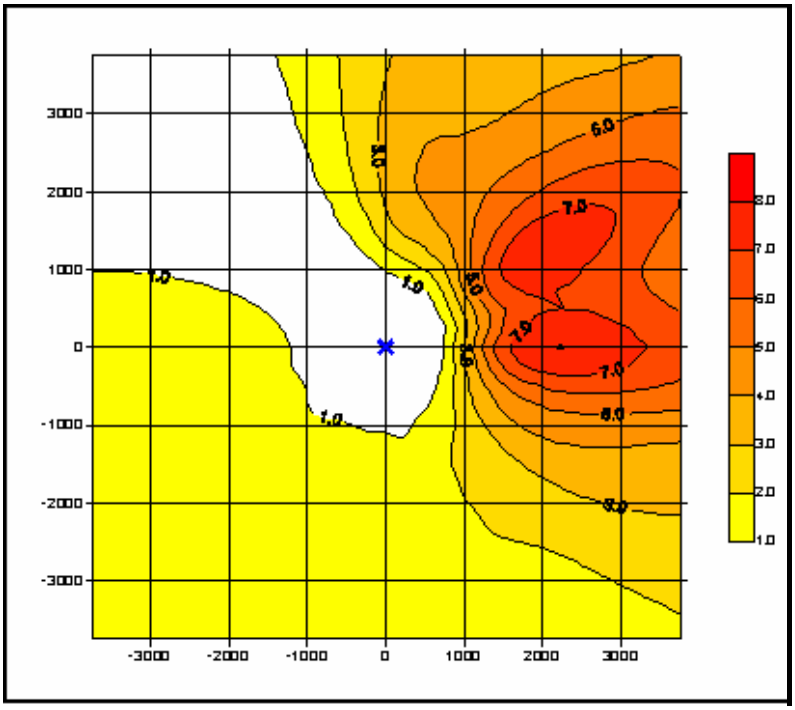

FIGURE 3.9 Maximum predicted annual average ground level concentration for 1950 meteorological data, 150 m high source and 7.5 km by 7.5 km grid (µg m^{-3})

Conclusion: For Source 3: (150 m buoyant source) For the prediction of impacts to maximum ground level concentrations Heathrow meteorological data does have a life time for all statistics. The predictions suggest the maximum predicted annual average ground level concentration may be decreasing with time, whereas the 99.9th percentile of hourly average ground level concentrations may be slightly increasing with time. The correlation coefficients for these trends are small and hence they may not be of statically significant. Also the trends are not large and therefore may not be of practical significance.

3.6 Summary of observed trends

Table 3.6 provides a summary of the observed trends in predicted ground level concentrations with time for each of the scenarios considered.

TABLE 3.6 Trends in maximum predicted ground level concentrations (correlation coefficient (R^2) in brackets)

Source	Annual average	99.9th Percentile of 15 minute averages
10 m Large Grid	↓ Down (0.5)	↓ Down (0.1)
10 m Small Grid	↓ Down (0.3)	↓ Down (0.7)
40 m Non Buoyant	↑ Up (0.2)	↑ Up (0.4)
150 m Buoyant	↓ Down (0.3)	↑ Up (0.2)

For the buoyant sources the trend in the maximum annual average ground level concentration is downwards as more recent meteorological data are used. For low level sources (10 m high) a similar trend is seen for short-tem stats (eg, 99.9th percentile). For the more elevated sources (40 m and 150 m) maximum ground level concentration for short term stats increase as more recent data are used.

4 EFFECT OF ROUGHNESS LENGTH

4.1 Introduction

This section explores the effects that roughness length can have on dispersion and predicted ground level concentrations. Also presented are details of the frequency of occurrences of low wind speeds.

4.2 Occurrences of low wind speeds at Heathrow observing station

Figure 4.1 (taken from the NRPB W3 report) shows the percentage of wind speeds less than 2 m s^{-1}, excluding calms. The figure shows there is an increase with time in occurrences of low wind speeds at the Heathrow site. This observed increase is in line with expectations as a consequence of the urbanisation of the land around Heathrow and corresponding increase in roughness length.

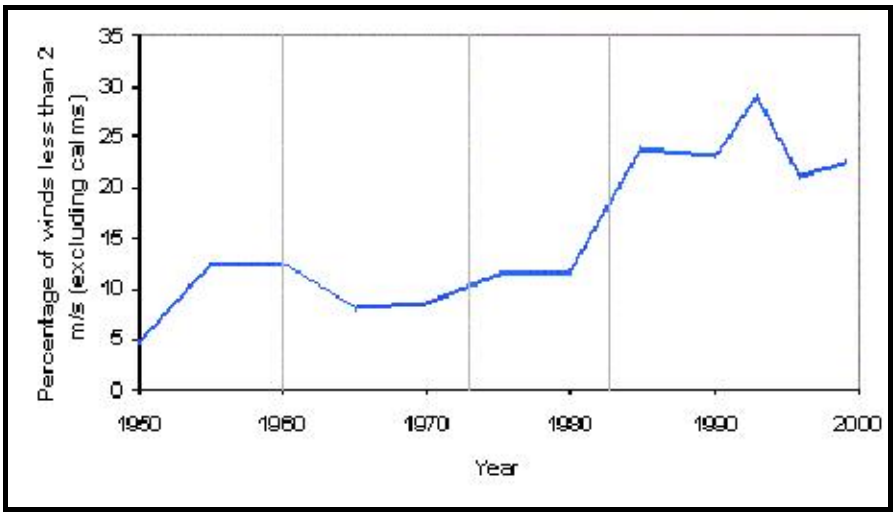

FIGURE 4.1 Percentage of observed wind speeds less than 2 m s^{-1}, excluding calms Heathrow observing station (%)

4.3 Predictions using a range of roughness lengths

The predictions presented in Section 3.2 suggest that changing land use may have affected the meteorology, which in turn may have an influence on predictions of ground level concentrations. The predictions also suggest that the change in land use may effect predicted ground level concentrations from different sources in differing ways.

To investigate this further, predictions of ground level concentrations have been made using a range of roughness lengths. The roughness lengths around Heathrow will have increased over the 50 years of meteorological observations. This change will be reflected in the meteorological data used in this study. Hence, if the same roughness length is used for all years the model will not be creating the vertical wind profile correctly. By combining the years of meteorological data with a more relevant roughness length, the dispersion is likely to reflect the actual conditions more accurately.

Although very difficult to estimate accurately, it is considered that the following are appropriate roughness lengths for Heathrow. It is possible the change in roughness length has been greater than the range suggested.

- 1950; 0.1 m
- 1980; 0.2 m
- 1996; 0.3 m

It should also be noted that roughness length will vary with wind angle and season of the year and the location of the observing station within the airport which is known to have moved several times since 1950.

The years chosen for examination were those considered being closest to the linear fit lines.

Predictions have been made for a range of roughness lengths for each of the three sources using 1999 meteorological data. Table 4.1 shows the maximum predicted ground level concentrations relative to predictions for 0.01 m roughness length.

TABLE 4.1 Predicted ground level concentrations for range of roughness lengths relative to predictions for roughness length of 0.01 m, 1999 meteorological data

Roughness length (m)/ source	Percentile (averaging time)					Annual average
	One hour				15 minute	
	100	99.9	99.8	99.7	99.9	
10 m Stack (buoyant)						
0.01	1.00	1.00	1.00	1.00	1.00	1.00
0.1	0.97	0.99	1.13	1.22	0.97	1.98
0.2	1.02	1.10	1.27	1.36	1.02	2.56
0.3	1.09	1.18	1.34	1.45	1.09	3.02
0.4	1.14	1.23	1.42	1.54	1.14	3.41
0.5	1.18	1.28	1.48	1.60	1.18	3.80
1.0	1.37	1.46	1.69	1.83	1.37	5.32
40 m Stack (no buoyancy)						
0.01	1.00	1.00	1.00	1.00	1.00	1.00
0.1	0.78	0.87	0.89	0.90	0.78	1.18
0.2	0.69	0.82	0.85	0.85	0.69	1.33
0.3	0.63	0.78	0.81	0.82	0.63	1.44
0.4	0.58	0.77	0.78	0.79	0.58	1.53
0.5	0.54	0.74	0.76	0.77	0.54	1.59
1.0	0.43	0.67	0.69	0.70	0.43	1.87
150 m Stack (buoyant)						

0.01	1.00	1.00	1.00	1.00	1.00	1.00
0.1	0.91	1.05	1.01	1.03	1.02	1.34
0.2	1.09	1.09	1.05	1.09	1.07	1.71
0.3	1.13	1.08	1.09	1.11	1.05	2.06
0.4	1.05	1.07	1.12	1.14	1.02	2.34
0.5	0.98	1.03	1.12	1.15	1.01	2.60
1.0	0.96	1.06	1.13	1.22	1.04	3.71

Figures 4.2, 4.3 and 4.4 show the effects of roughness length on maximum predicted ground level concentrations. For each of the three sources, the maximum annual average ground level concentration increases with roughness length. The effect of roughness on the predicted percentiles varies depending on the nature of the source. This finding supports the findings presented in Section 3.2 which also suggests that the nature of the source affected the trend in predicted ground level concentration with time.

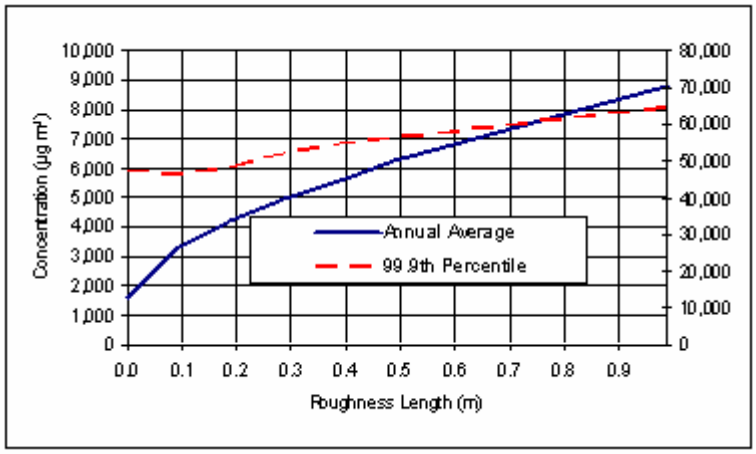

FIGURE 4.2 Maximum annual average ground level concentrations (left hand scale) and maximum predicted 99.9th percentile of 15 minute average ground level concentration (right hand scale) for 10 m buoyant source with 500 m by 500 m grid size (µg m^{-3})

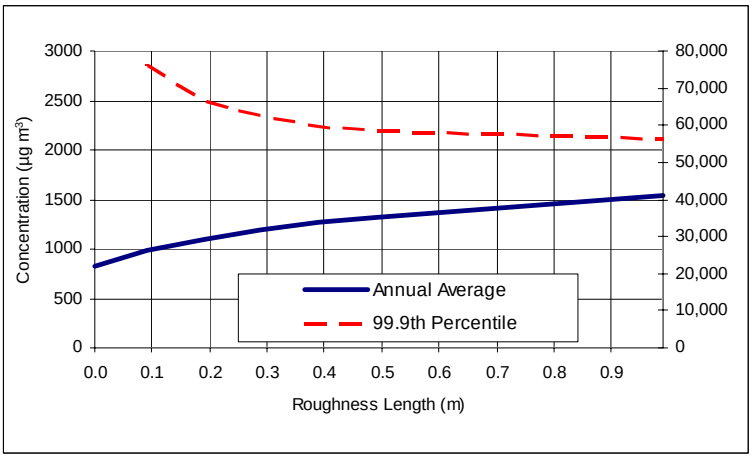

FIGURE 4.3 40 m Non buoyant source with 500 m by 500 m grid size (µg m^{-3})

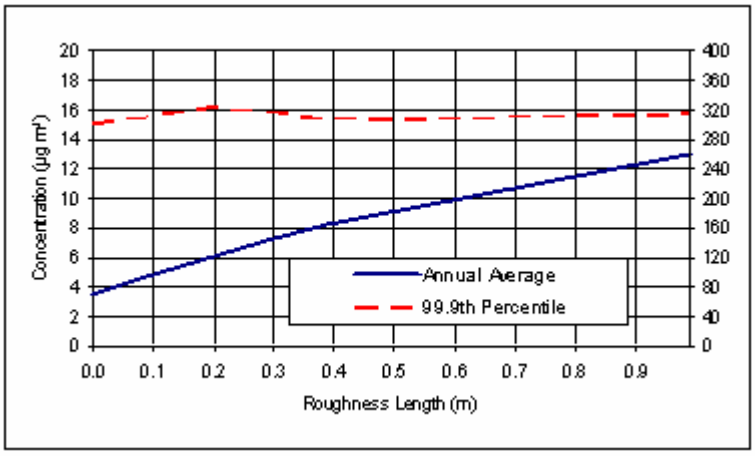

FIGURE 4.4 150 m Buoyant source with 500 m by 500 m grid size (µg m^{-3})

The figures show a clear trend of increasing maximum annual average concentrations with increasing roughness length. However the time series predictions generally show decreasing concentrations with time (ie, as the general roughness around Heathrow increases).

As Heathrow has become more developed the vertical wind speed and turbulence profile will have changed over time (1950-1999). These changes have not been directly accounted for in the modelling since the same roughness length (Zo = 0.2 m) was used for the time series modelling. Had more representative roughness lengths been used (ie those that increased over time) the trend in maximum annual average ground level concentrations may have been less negative or even positive with time.

It is interesting and possibly significant that the source that gave rise to the smallest increase in maximum predicted annual average ground level concentrations with increasing roughness (40 m non buoyant source) is also the only source that showed an increase with time series meteorological data.

If the trends in predicted concentrations can be explained by the effect that the change in land use has had on meteorological data, it may be possible to screen this out using ADMS. This is because ADMS has a utility to specify a different roughness length for the meteorological data site and the site around the source. Therefore, if observations were made at, for example a rural observing station (such as Heathrow in 1950), and predictions are required at an urban site (for example Heathrow in 1999); this can be allowed for in the model by specifying one roughness length for the observing site and one for the modelling site. Normally this feature is used where the two sites are separated by space but the effect is the same as here where the sites are separated by time.

In order to investigate this, predictions have been made with 1950, 1980 and 1996 meteorological data assuming that the roughness length is 0.3 m for the site around the source and that the observing station roughness lengths for each of the three years of data are 0.1 m for 1950, 0.2 m for 1980 and 0.3 m for 1996. The reason for selecting these years is that they are close to the linear best fit lines in predicted concentrations.

The reason for fixing the source roughness length at 0.3 m and varying the observing stations roughness length is simulating what one might do if wishing to model a new source at Heathrow with 'old' meteorological data.

The predictions made using these three years of data and the year dependent roughness lengths will show no trends with time if all three of the following are true;

- the selected roughness lengths are representative of the years; and
- it is just the change in roughness that is causing the observed trends in predicted concentrations with time; and
- the ADMS model algorithms are able to correctly compensate for difference in roughness lengths between the observing station and modelling site.

Table 4.2 shows the predicted concentrations for three years of observations with varying roughness lengths relative to predictions for a 0.1 m observing station roughness length.

TABLE 4.2 Maximum predicted ground level concentrations for range of roughness lengths (relative to 1950 and 0.1 m observing station roughness length)

Source	Percentile (averaging time)					
Year and observing station roughness length (m)	One hour				15 minute	Annual average
	100	99.9	99.8	99.7	99.9	
10 m Stack						
1950 / 0.1 m	1.00	1.00	1.00	1.00	1.00	1.00
1980 / 0.2 m	1.00	0.99	0.98	0.98	0.99	0.76
1996 / 0.3 m	0.99	0.99	0.99	0.98	0.99	0.61
40 m Stack						

1950 / 0.1 m	1.00	1.00	1.00	1.00	1.00	1.00
1980 / 0.2 m	1.24	1.21	1.66	1.68	1.26	0.96
1996 / 0.3 m	1.23	1.46	1.88	1.73	1.49	0.77
150 m Stack						
1950 / 0.1 m	1.00	1.00	1.00	1.00	1.00	1.00
1980 / 0.2 m	1.08	1.01	0.96	0.97	1.00	0.67
1996 / 0.3 m	0.98	1.03	0.96	0.95	1.01	0.61

Table 4.3 shows the predicted concentrations for three years of observations without varying roughness length of the observing station. Predictions are relative to those of 1950.

TABLE 4.3 Maximum predicted ground level concentrations for range of roughness lengths (relative to 1950)

Source	Percentile (averaging time)					
Year and observing station roughness length (m)	One hour				15 minute	Annual average
	100	99.9	99.8	99.7	99.9	
10 m Stack						
1950 / 0.2 m	1.00	1.00	1.00	1.00	1.00	1.00
1980 / 0.2 m	0.92	0.99	0.98	0.97	0.99	0.72
1996 / 0.2 m	0.92	0.98	0.98	0.97	0.98	0.55
40 m Stack						
1950 / 0.2 m	1.00	1.00	1.00	1.00	1.00	1.00
1980 / 0.2 m	1.37	1.55	1.95	1.89	1.56	1.01
1996 / 0.2 m	1.46	1.85	2.27	2.25	1.89	0.82
150 m Stack						
1950 / 0.2 m	1.00	1.00	1.00	1.00	1.00	1.00
1980 / 0.2 m	1.14	1.00	1.00	0.96	1.00	0.63
1996 / 0.2 m	1.05	1.06	1.03	0.97	1.05	0.53

By examination of the values presented in Table 4.1 and Table 4.2 the following conclusions may be drawn.

- For annual average concentrations, the effect of changing the observing station roughness length for both the 10 m and 150 m source has been to reduce the trend with time. This suggests that for these sources the trend in annual average concentrations with time has been reduced by varying the observing station's roughness length. It is possible that the trend could be completely eliminated by more substantial changes to the roughness length.
- For the 10 m and 150 m it appears that the effect of changing roughness length is not significant on the higher percentiles.

- For the 40 m non buoyant source, with the exception of predictions of annual average concentrations, it is possible that altering the observing stations roughness length range has reduced the change in predicted concentrations with time.

5 PREDICTED CONCENTRATIONS AND DISCUSSION; SPOT AND HOURLY AVERAGE DATA

5.1 Introduction

This section presents a comparison of predicted concentrations made using spot meteorological data (10 minute average wind speeds and directions) compared to hourly average data. Because of the shorter averaging period of the spot data, one would expect more extreme meteorological conditions than seen in the hourly data. One would however expect the 10 minute and hourly average annual averages to be similar.

Predictions are available for the following years for both spot and hourly average measurements and so results can be directly compared.

- 1960
- 1965
- 1985

5.2 Predicted concentration

Tables 5.1-5.3 show the maximum concentrations for the three sources considered where predictions are available for both 10 minute and hourly average meteorological data.

TABLE 5.1 Maximum predicted ground level concentrations for 10 minute and hourly average meteorological data for 10 m buoyant source, 500 m size grid (µg m^{-3})

	Percentile (averaging time)					
	One hour				15 minute	Annual
Met data year	100	99.9	99.8	99.7	99.9	average)
Spot (10 minute average)						
1960	48,818	47,669	46,734	46,576	49,234	4,105
1965	48,875	47,727	46,955	46,558	49,238	4,276
1985	48,877	47,181	46,754	46,078	48,797	4,158
1 hour average						

1960	48,782	47,614	46,829	46,584	49,169	4,261
1965	48,846	47,678	46,942	46,382	49,303	4,116
1985	48,501	46,847	46,234	45,628	48,333	3,676
Ratio: 10 minute average/1 hour average						
1960	1.00	1.00	1.00	1.00	1.00	0.96
1965	1.00	1.00	1.00	1.00	1.00	1.04
1985	1.01	1.01	1.01	1.01	1.01	1.13

TABLE 5.2 Maximum predicted ground level concentrations for 10 minute and hourly average meteorological data for 40 m non buoyant source (µg m^{-3})

	Percentile (averaging time)					
	One hour				15 minute	Annual
Met data year	100	99.9	99.8	99.7	99.9	average
Spot (10 minute average)						
1960	89,003	50,312	44,224	36,494	51,778	714
1965	78,841	61,650	54,806	39,803	63,819	772
1985	78,201	48,770	40,911	33,916	51,979	899
1 hour average						
1960	71,535	49,984	37,133	31,450	50,825	747
1965	63,434	38,787	31,007	27,600	41,070	748
1985	81,495	48,156	44,235	40,545	51,268	941
Ratio: 10 minute average/1 hour average						
1960	1.24	1.01	1.19	1.16	1.02	0.96
1965	1.24	1.59	1.77	1.44	1.55	1.03
1985	0.96	1.01	0.92	0.84	1.01	0.96

TABLE 5.3 Maximum predicted ground level concentrations for 10 minute and hourly average meteorological data for 150 m buoyant source (µg m^{-3})

	Percentile (averaging time)					
	One hour				15 minute	Annual
Met data year	100	99.9	99.8	99.7	99.9	average
Spot (10 minute average)						
1960	416	298	254	225	327	6.4
1965	473	275	237	222	290	6.8
1985	446	283	250	233	310	6.1
1 hour average						
1960	415	291	271	241	316	7.1
1965	386	261	231	223	293	6.4
1985	443	288	255	237	311	5.4
Ratio: 10 minute average/1 hour average						

1960	1.00	1.02	0.94	0.93	1.03	0.90
1965	1.23	1.05	1.03	1.00	0.99	1.06
1985	1.01	0.98	0.98	0.98	1.00	1.13

For the 10 m stack height there is no significant difference between maximum predicted concentrations made using 10 minute or hourly average meteorological data. For the 40 m stack the predictions made using hourly average meteorological data are generally lower than those made using 10 minute average data. In most cases, for the 150 m stack, the two sets of predictions are similar although there are some differences.

Conclusion: The predictions indicate that the use of 10 minute average meteorological data generally gives rise to either similar or higher ground level concentrations than those using hourly average data. This finding is in line with the expectation that the extremes would be higher with the 10 minute average data. The differences in the predicted annual average ground level concentration the 10 minute and hourly average meteorological data, which appear to be significant, suggests that the annual averages are significantly affected by a small number of large ground level concentrations.

The original Pasquill-Gifford dispersion parameters used by dispersion models for the rate of plume spread were derived from actual field measurements averaged over a period of 3 to 10 minutes. It may therefore be more appropriate to use spot (10 minute average) rather than hourly average meteorological data as these data more closely resemble the time period of the experimental data from which the equations were derived.

6 SUMMARY AND CONCLUSIONS

6.1 Summary

Atmospheric Dispersion Modelling (ADM) Ltd has been commissioned by the Atmospheric Dispersion Modelling Liaison Committee (ADMLC) to carry out an investigation into the effects of the urbanisation of the region around Heathrow on predicted ground level concentrations, using meteorological data from Heathrow. Twelve separate years of observations from Heathrow have been used in this assessment, spanning the years from 1950 to 1999.

This study follows earlier work undertaken by the Meteorological Office and reported in NRPB-W3 (NRPB, 2002) which concluded that meteorological data sets can have a lifetime, especially at sites such as Heathrow where there has been significant change in land use over the years.

The ADMS 3.1.2.0 (September 2001 release) dispersion model has been used to study the following three point sources;

- 10 m stack; with buoyancy
- 40 m stack; no buoyancy
- 150 m stack; with buoyancy

As well as presenting predictions of ground level concentrations with time for each of the three sources, modelling has been undertaken to examine the effect of changing roughness length on predictions. Also investigated is the difference between using 10 minute (spot) and hourly average meteorological data on predicted concentrations.

6.2 Conclusions

This study supports and strengthens the findings of the previous work that meteorological data can have a lifetime. For situations such as Heathrow, where there have been substantial changes in land use over the years, it is preferable to use a recent data set for dispersion modelling. It is suggested that data from the last five to ten years is preferable for observing stations where there has been significant changes in land use.

From the findings presented in this study it is not possible to determine what effect any long term trends in weather (ie global warming/climate change) is having of meteorological. This would require comparison with predictions made using observations from an observing station where there has been little or no change in land use over a long time period (eg, 50 years).

6.2.1 Time series of meteorological data

Table 6.1 provides a summary of the observed trends in predicted concentrations over the fifty years of observations.

TABLE 6.1 Trends in maximum predicted ground level concentrations (R^2 correlation coefficient in brackets)

Source	Annual average	99.9^{th} Percentile of 15 minute averages
10 m Large Grid	↓ Down (0.5)	↓ Down (0.1)
10 m Small Grid	↓ Down (0.3)	↓ Down (0.7)
40 m Non Buoyant	↑ Up (0.2)	↑ Up (0.4)
150 m Buoyant	↓ Down (0.3)	↑ Up (0.2)

Since many of the individual trends are quite clear, it is considered that there is sufficient evidence to suggest that the meteorological data for Heathrow is time limited. It also appears that the time varying meteorological data is exerting a different effect on the predictions, depending on which type of source is modelled.

Source 1; 10 m Buoyant Stack

For the prediction of annual average impacts to maximum ground level concentrations Heathrow meteorological data does have a lifetime. However for statistics tending towards the maximum 1 hour (100th percentile of hourly averages) there may be a statistically significant trend in the maximum predicted concentrations with time as the correlation coefficient (R^2) is 0.6 but this trend appears to be of insignificant practical importance because the year on year variation is small compared to the magnitude of the predicted concentrations.

The choice of a suitable stack height is usually driven by the impact of emissions to short term ground level concentrations (ie, maximum 99.8th and 99.9th percentiles). If these short term ground level concentrations are acceptable then long term (eg, annual averages) ground level concentrations are generally much smaller relative to the ambient air quality criteria. Since, for this type of source, there was no trend of practical importance in maximum predicted short term ground level concentrations the use of historical meteorological data would not have lead to an unsuitable stack height being selected.

Source 2; 40 m Non-Buoyant Stack

The predicted of impacts of emissions from the 40 m stack suggest that Heathrow meteorological data does have a lifetime for all statistics. All values tend to increase as more recent data are used. The trend is less marked for annual average than the maximum one hour average and higher percentiles

Source 3; 150 m Buoyant Stack

For the predictions of impacts to maximum ground level concentrations due to emissions from the 150 m high stack it does appear that the data does have a life time for all statistics. The predictions suggest the maximum predicted annual average ground level concentration may be decreasing with time, whereas the 99.9th percentile of hourly average ground level concentrations may be slightly increasing with time. The trend may however not be of statistical significance of or practical importance.

6.2.2 Roughness length

The investigation of the effects of roughness length on dispersion was only partly able to explain the trends in predicted concentrations.

6.2.3 Hourly average and 10 minute average meteorological data

The predictions indicate that the use of 10 minute average (spot) meteorological data generally gives rise to either similar or higher concentrations than those using hourly average data. Given a precautionary approach to dispersion modelling, it may be appropriate to use spot rather than hourly average meteorological data.

7 REFERENCES

LAQM (October 2002). Draft Review and Assessment Technical Guidance TG(02).

NRPB (2002). *Atmospheric Dispersion Modelling Liaison Committee Annual Report 2000/2001*. Chilton, NRPB-W3. ISBN 0 85951 471 4.

Personal communication between Linda Rigby (Met Office) and David Harvey (ADM Ltd)

R&D Technical Report P353: A review of dispersion model intercomparison studies using ISC, R91, AERMOD and ADMS (ISBN 1 85705 276 5) and R&D Technical Report P362: An intercomparison of the AERMOD, ADMS and ISC dispersion models for regulatory applications (ISBN 1 85705 340 0)

US Environmental Protection Agency (US EPA). Guideline on Air Quality Models Appendix W Part 51.